Geotechnical Engineering

Project Day 2022

Organised by the
SRI LANKAN GEOTECHNICAL SOCIETY

SLGS

PRESIDENT'S MESSAGE

Geotechnical Engineers help design structures that are either composed of soil or rock or are in contact with it. In essence, they engineer the interface between the natural and built environments. Research provides insight into the interaction and performance of structures with earth, such as bearing failures, settlement damage, and failures due to emergent processes such as landslides and liquefaction.

As the President of the Sri Lankan Geotechnical Society (SLGS), I am very pleased to send this message to the Proceedings of Project Day which will be held online on Thursday, 20th April 2023.

This annual event has been organized by SLGS since 2000 uninterruptedly with the objective of promoting research and enhancing the presentation skills of Civil Engineering students in Sri Lankan Universities. The event features a competition among final year undergraduates who have conducted research projects in Geotechnical Engineering. The best projects will be selected by a committee of distinguished Geotechnical Professionals appointed by SLGS, based on the written paper and the presentation.

This year, we are very much pleased to have 18 competitors from Sri Lankan Universities who have completed their undergraduate research projects on various Geotechnical Engineering aspects, including foundation design, ground settlement, slope stability, ground improvement, and rock mechanics. Competitors are expected to present their research objectives, procedure and findings in a four to six paged paper and to make a five-minute oral presentation. The best three competitors will receive cash awards and certificates.

Many winners in the past years have proceeded to do higher studies and subsequently established good carriers in the field of Geotechnical Engineering as both academics and practicing engineers.

I would like to thank all undergraduates and research supervisors for their interest and commitment for submitting papers and making presentations in this Project Day. Without their involvement and participation, this event would not have been a reality.

Also, I would like to thank the panel of evaluators namely, Dr. Manasi Wijerathna *(Geotechnical Engineer, Aurecon)*, Dr. Priyanath Ariyarathne *(Geotechnical Engineer, Transport for NSW)*, Dr. Chathuri Arachchige *(Postdoctoral Research Fellow, University of Technology Sydney)*, Dr. Avanthi Liyanage *(Geotechnical Engineer, Beca, Melbourne)*, Dr. Arivalagan Joseph *(Grad Geotechnical Engineer, Tonkin and Taylor)* and Dr. Subhani Medawela *(Postdoctoral Research Fellow, University of Technology Sydney)*, for submitting themselves on the difficult task of evaluating all the papers and presentations within a very short notice.

I am grateful to the members of the Organizing and the Executive Committees for being with me together offering their unstinting support to make this event successful. A special thanks goes to Dr. K H S M Sampath for his untiring effort in organizing and coordinating the Project Day this year. I lack words to thank Dr. Mark Ballouz, President of the International Society for Soil Mechanics and Geotechnical Engineering (ISSMGE) for his appreciations to SLGS for conducting this motivating event for the undergraduates. Let me also extend my sincere thanks to the key office bearers of South Asian Geotechnical Associations for their continuous support for SLGS activities.

I am certain that this Project Day will be another exciting and informative event by the Sri Lankan Geotechnical Society, and I wish everyone a very effective and fruitful Seminar.

This year also the Society has/will organize/d Geo-forum, our monthly short presentation event followed by a question-and-answer session, Design Workshops and an Annual Seminar to enhance the knowledge of the engineers and other professionals engaged in Geotechnical and Foundation Engineering related works. Also, we are planning to have our International Conference in 2025 in Colombo. I cordially invite all of you to participate in these events effectively to support SLGS in continuous and longstanding effort to enhance the knowledge in the field of Geotechnical and Foundation Engineering of fellow Engineers and other Professionals who are involved in the discipline.

Eng. K.L.S. Sahabandu
B.Sc.Eng.(Hons.), Pg. Dip.(Hyd.), M.Sc. (Struct.), C.Eng., M.I.C.E.(U.K.), M. Cons. E. (S.L.), F.I.E.(S.L.), Hon. F.S.S.E.(S.L.)
President,
Sri Lankan Geotechnical Society (SLGS)

SLGS EXECUTIVE COMMITTEE

Eng. K L S Sahabandu	President
Prof. H S Thilakasiri	Vice President
Prof. S A S Kulathilaka	Past President
Eng. K S Senanayake	Past President
Prof. U P Nawagamuwa	Hony. Secretary
Eng. (Mrs.) G DW N Galheana	Assistant Secretary
Eng. R M Rathnasiri	Treasurer
Eng. M D J P Wickramasooriya	Assistant Treasurer
Dr. N H Priyankara	Editor– Journal
Dr. K H S M Sampath	Editor– Newsletter
Dr. W A Karunawardena	Committee Member
Dr. J S M Fowze	Committee Member
Prof. L I N De Silva	Committee Member
Dr. S K Navaratnarajah	Committee Member
Eng. D Erandana	Committee Member

Content

Study of the influence of Construction sequence on Slope Rectification Projects

H.P.J Vimukthi, S.A.S. Kulathilaka
Department of Civil Engineering, University of Moratuwa, Sri Lanka

ABSTRACT: Rain-induced slope failures in Residual Soil Slopes has been identified as a major geotechnical hazard in Sri Lanka over the past few decades. Considering the damage they can do to the environment and society, it is necessary to take adequate remedial actions to prevent the activation of these slopes during rainfall periods. To achieve the required safety margin in these unstable slopes there are numerous stabilization measures available, such as surface & subsurface drainage improvement, construction of retaining walls, and reinforcement with soil nailing. However, the application of these rectification measures in the correct order is a critical factor during rectification, to keep the stability of slopes during the construction period. This paper discusses the importance of a proper construction sequence for slope rectification using two reported case histories. The study was done in a numerical approach using SEEP/ W & SLOPE/ W software packages, and the results illustrated how important the construction sequence in slope rectification to keep the slope stability during the period of construction.

KEYWORDS: Landslides, Slope Stability, Construction Sequence, Numerical Study, Slope rectification

1 INTRODUCTION

Landform variation of Sri Lanka has resulted in many steep slopes around the country, but more significantly in the central part of the country. Most of the slopes available in Sri Lanka are formed of residual soils, Colluvial soils, and rocks of different levels of weathering, which have very good shear strength under dry conditions due to prevailing matric suction. But during rainy periods due to infiltration, high matric suction gets reduced, which causes the reduction of shear strength and potential instability.

Reduction of soil shear strength during the rainy period has been identified as the major factor for the slope failures that Sri Lanka has been subjected in recent past. Many human lives have been lost in the country due to these rain-induced landslides. Geotechnical engineers are making a great effort to prevent these landslides before activation, or rectify the failed slopes to prevent further propagation of failures.

Numerous stabilization measures such as drainage improvement, construction of the retaining walls, and reinforcement with nailing have been adopted to rectify these failed slopes or enhance the stability of slopes with low safety margins. However, it is important to carefully plan the sequence of application of these stabilization measures to ensure the short-term stability of the slope during the period of construction.

The objective of the study presented in this research paper is to study how important the construction sequence is for slope rectification to maintain slope stability during the construction period.

2 METHODOLOGY

This study was performed using the data available from two reported case histories at Ginigathhena and Badulusirigama. Rectification designs were done by the National Building Research Organization (NBRO). Different slope stabilization measures have been adopted in these projects, and the impact of construction sequence on slope stability was evaluated using the Numerical simulation through GeoStudio 2018 software packages, SEEP/ W and SLOPE/ W.

2.1 *Data collection and Numerical Mode Development*

2.1.1 *Numerical Model Development*

Data required to conduct the study were gathered from reports prepared by NBRO and two M. Eng. research reports. Table 1.0 and Table 2.0 summarized the extracted data on the subsoil profile which was used to develop the numerical models.

Table 1. Properties of Sub–Soil Layers_Ginigathhena Slope

Parameter	Type of Soil			
	Top Soil Layer	Residual Soil Layer	Weathered Rock	Peat Layer
Material Model	Mohr coulomb	Mohr coulomb	Mohr coulomb	Mohr coulomb
Type of material Behaviour	Drained	Drained	Drained	Drained
Unit weights (kN/m^3	17	18.5	22	17
Cohesion (kN/m^2)	7	10	25	7
Friction angle	26^0	30^0	50^0	26^0
Sat. permeability(m/s)	8E-06	8E-06	1E-08	1E-08

Table 2. Properties of Sub-soil layers_Badulusirigama Slope

Parameter	Type of Soil Layer		
	Top Layer	Intermediate Layer	Bottom Layer
Material Model	Mohr coulomb	Mohr coulomb	Mohr coulomb
Type of material Behaviour	Drained	Drained	Drained
Unit weights (kN/m^3)	15	16	17
Cohesion (kN/m^2)	2	8	20
Friction angle	22^0	35^0	40^0
Saturated permeability (m/s)	9.95E-07	9.95E-08	8.6E-10

2.1.2 Rectification Design

Different rectification techniques which were adopted at Ginigathhena and Badulusirigama are listed below.

a. Slope stabilization measures for Ginigathhena Slope

1. Surface Drainage Improvement
   With upper slope surface drains, berm drains, and vegetation cover.
2. Subsurface drainage Improvement
3. Reinforcement with Soil Nailing
4. Slope geometry modification

There was a need to widen the road at the location of the failure, and the geometry modification was proposed as illustrated in Figure 1.0 with the allowance for the proposed widening

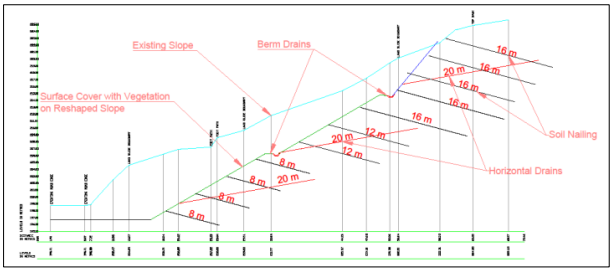

Fig. 1 Cross section of proposed mitigation measures

b. Slope stabilization measures for Badulusirigama Slope

1. Surface drainage improvement
2. Sub-surface drainage improvement

3 STUDY OF THE CONSTRUCTION SEQUENCE

Study of the construction sequence of each slope rectification project was done using numerical simulations through SEEP/ W and SLOPE/ W software. This section summarized the analysis details and the results obtained briefly.

3.1 *Construction sequence analysis – Ginigathhena Slope.*

The stability of the existing slope was evaluated initially before study about the sequence of stabilization measure application.

Since the existing slope stability under high water table conditions is not adequate (FoS = 0.947,

Fig.03) required stabilization methods had to be adopted.

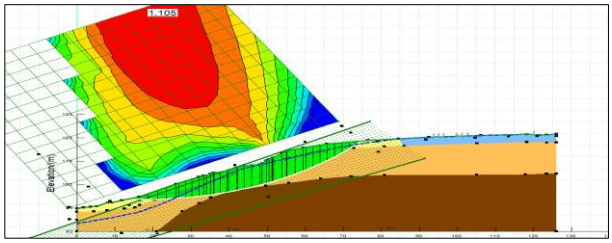

Fig. 2 Stability of Existing Slope [Under no-rainfall conditions]

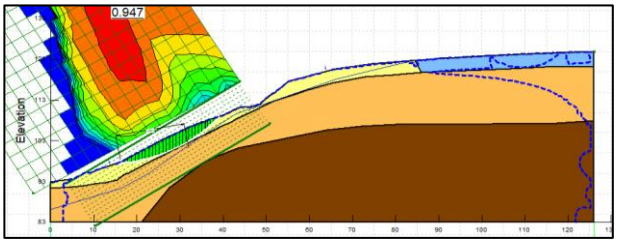

Fig.3 Stability of Existing Slope [Under Rainfall Conditions]

Upperslope surface drainage improvement as an initial consideration

As an initial measure drainage in the upper slope area was improved. This lowered the GWT level up to some extent and FoS was increased to 0.975 (Fig 4.0). With the application of the subsurface drainage, FoS was increased to 1.101 (Fig 5.0)

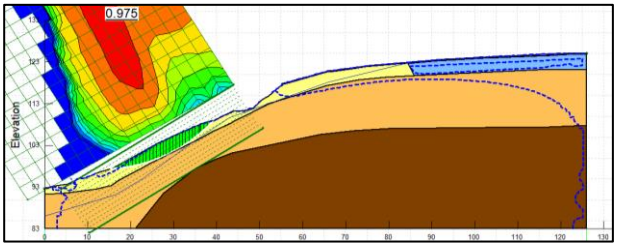

Fig. 4 Slope stability with Upperslope surface drainage improvement [Under Rainfall Conditions]

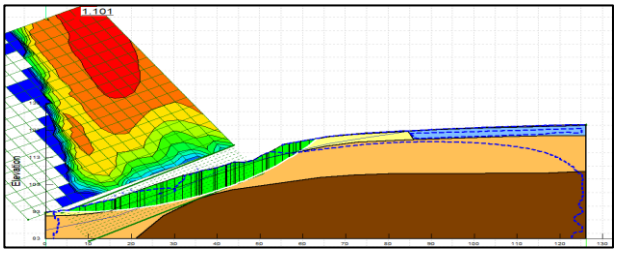

Figure 5.0: Slope stability with Upperslope surface drains & Temporary Sub drains [Under rainfall condition]

As resulted in this section the excavations were only possible after the lowering of the groundwater table.

<u>Geometry Modification as the second construction step</u>

Geometry modification can be implemented in two approaches; bottom – up and top–down construction approaches.

The possibility of each approach was checked using SLOPE/ W and analysis results are presented in Figure 6.0 and Figure 7.0.

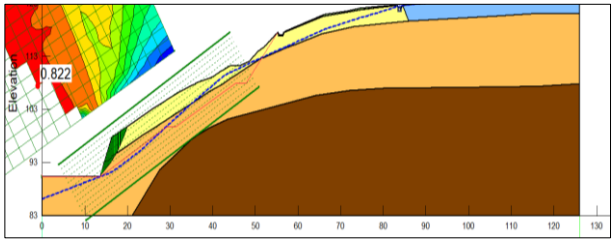

Fig. 6 Slope stability with bottom - up excavation

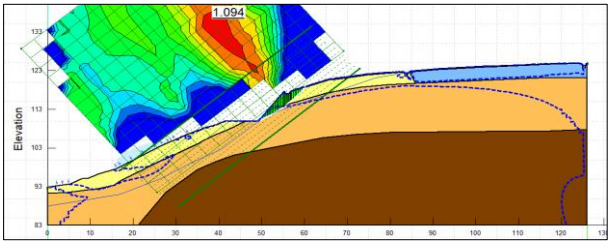

Fig. 7: Slope stability with top - down excavation

As resulted, Bottom – up construction approach was found to be not suitable for the construction and hence top – down approach has to be adopted. Initial unsupported excavation down to the first berm level resulted in a FoS of 0.949 (Fig 8.0) during a critical rainfall event and thus the initial excavation depth has to be further minimized.

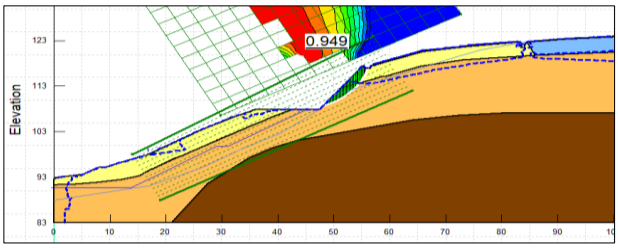

Fig. 8 Stability of Slope_Excavation to top berm level [Under rainfall conditions]

6.8m of vertical depth was found to be possible as the initial excavation depth with the FoS of 1.105 (Fig 9.0) during a critical rainfall event.

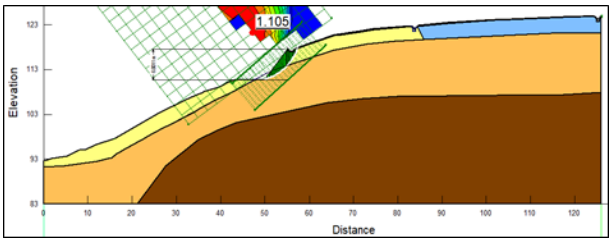

Fig. 9 Stability of Initial Excavation [Under rainfall conditions]

The stability of initial excavation is not adequate for long run and, as such soil nailing was introduced. When the soil nailing was introduced the FoS of initial excavation has increased to 1.924 (Fig 10.0). Under these existing conditions, the excavation down to the top berm level was possible and it resulted in an FoS of 1.259 (Fig 11.0)

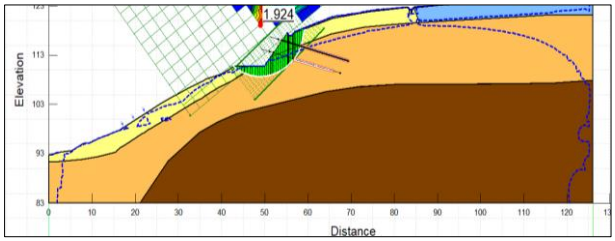

Fig. 10 Stability of Initial Excavation with soil nailing [Under rainfall conditions]

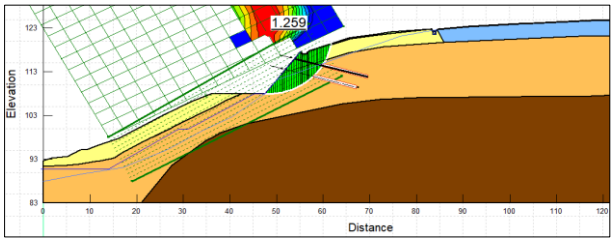

Fig. 11 Stability of Stage 01 Excavation with soil nailing [Under rainfall conditions]

The possibility of excavating the slope up to the mid berm level without any further improvements was studied and it resulted in an FoS of 0.959 (Fig 12.0) which was not adequate. As such remaining two soil nails were introduced to the excavation with Water table lowering by subsurface drains at the top berm level. With the adopted improvements FoS has increased to 1.200 (Fig 13.0) which is adequate in short-term conditions

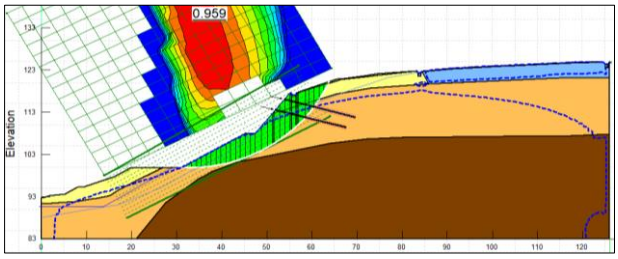

Fig. 12 Stability of excavation upto Stage 02 – Without further improvements [Under rainfall conditions]

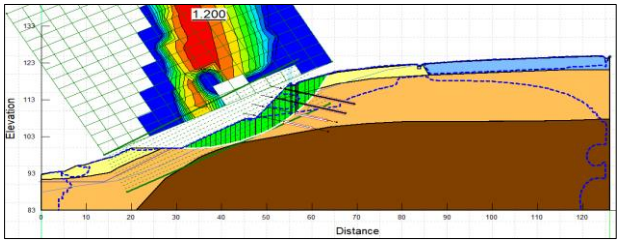

Fig. 13 Stability of excavation upto Stage_02-With stage 01 soil nails and subsurface drains [Under rainfall conditions]

Thereafter the possibility of excavation to bottom berm level was analysed without any further improvements and it resulted in a FoS of 1.076 (Fig 14.0) which was not adequate. As such soil nailing was introduced to the stage 02 excavation along with water table lowering by sub surface drains at the middle berm level, before starting the excavation of Stage 03. When the soil nailing and sub-surface drains were introduced, the FoS has increased to 1.230 (Fig 15.0) which is adequate for short term conditions.

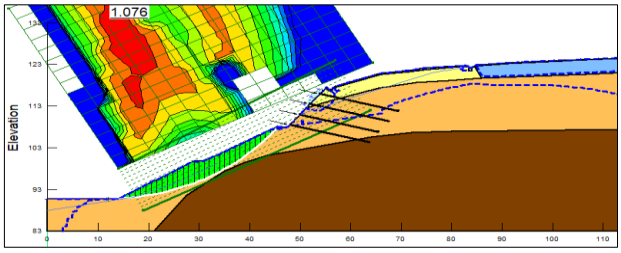

Figure 14.0: Stability of excavation upto Stage_03-Without any further improvements [Under rainfall conditions]

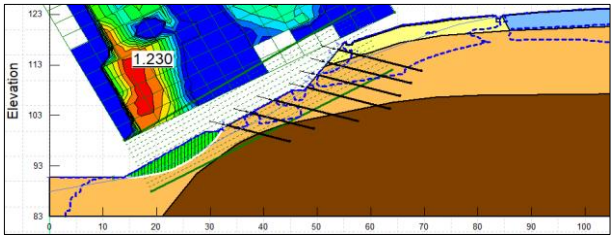

Figure 15.0: Stability of excavation upto Stage_03-With stage 02 soil nails and subsurface drains

Finally, all the remaining stabilization measures, including remaining soil nails, sub drains, and surface drains were introduced and it results in an FoS of 1.540 (Fig 16.0) which is adequate in long run.

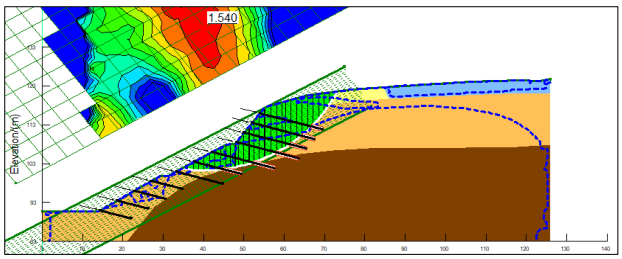

Figure 16.0: Stability of slope with all the stabilization measures [Under rainfall conditions]

3.2 *Construction Sequence Analysis – Badulusirigama Slope Rectification*

The stability of the existing slope was checked using SLOPE/ W and the FoS values obtained through the analysis are presented in Table 3.0. The field monitoring program of Badulusirigama Slope has identified the potential sliding mass of the slide as fully specified, with three separate slides namely, upper, middle, and lower. (Fig 17.0)

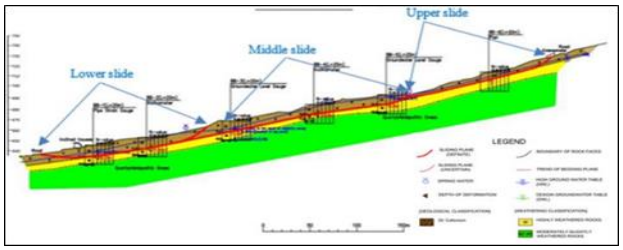

Figure 17.0: Potential Slip surfaces of the Slope (Japan International Cooperation agency, 2015)

Table 3. Existing Stability of Badulusirigama Slope

	Lower Slide	Middle Slide	Upper Slide
Under dry conditions	1.112	1.127	1.039
Under rainfall conditions	0.992	1.069	0.796

Rectification of the Badulusirigama Slide was done using surface drains, and subsurface drains. During the time of construction bottom–up construction approach was adopted.

The suitability of the adopted bottom–up construction approach was re – evaluated again using SEEP/ W and SLOPE/ W.

Bottom –Up construction approach – Under no rainfall condition

Drains were named as DF, DE, DD, DC, DB & DA from the bottom and the activation of drains was started from the bottom with Drain DF. Stability variation of all three slides with bottom–up drain installation, when there is no rain, is presented in Fig 18.0.

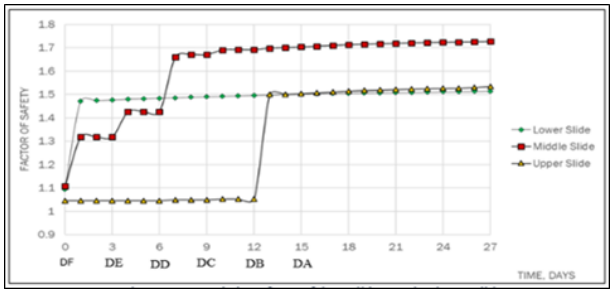

Fig. 18 Variation of FoS with Bottom – Up drain installation – Under dry conditions

Bottom-up construction approach – Under rainfall conditions

Thereafter the variation of FoS of the Slope with a Bottom – Up drain installation approach was again analysed under the presence of a critical rainfall that could occur in the region. Fig 19.0 presents the FoS variation of Slope under rainfall conditions.

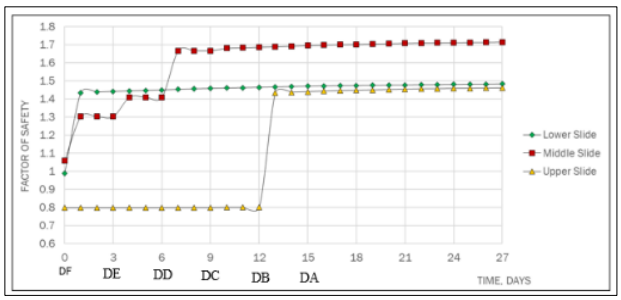

Fig. 19 Variation of FoS with Bottom – Up drain installation – Under rainfall conditions

Then, the slope stability with top–down drainage installation approach was analyzed under both no - rainfall conditions and in the presence of critical rainfall. The variation of FoS with drain installation are presented in Fig 20.0 and Fig 21.0.

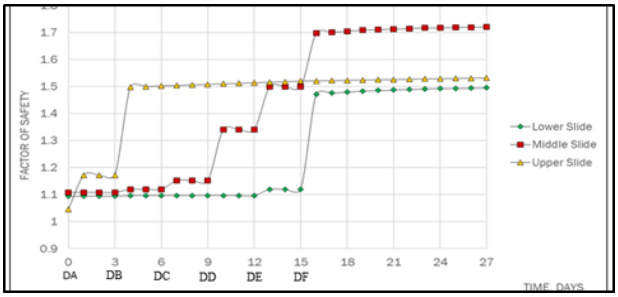

Fig. 20 Variation of FoS with Top - Down drain installation - Under dry conditions

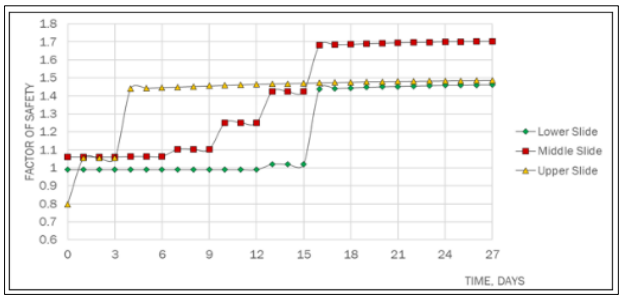

Fig. 21 Variation of FoS with Top - Down drain installation - Under rainfall condition

As per the above results both top–down and bottom–up construction sequences had some shortcomings.

Under the bottom-up construction approach, it will take at least 13 construction days to enhance the stability of the upper slide to a significant level. If rainfall occurred within that period the upper slide would have failed.

Similarly under top–down approach, it will take at least 16 construction days to enhance the stability of the lower slide up to a significant level. Thus, any

change in the groundwater table within that period can trigger a failure in the lower slide.

Due to these shortcomings of both bottom–up and top – down construction approaches another construction sequence was considered by activating the most critical drains in the first place. Previously conducted analyses for top–down and bottom–up construction approaches revealed that drains DF and DB as the most critical sub–surface drains among the adopted six drains. Thus another analysis was conducted by activating those two drains initially.

Analysis was conducted under saturated conditions [With the rainfall effect] to simulate the worst possible case scenario.

Fig 22.0 presents the variation of FoS of the three slides with this intermediate drain installation approach.

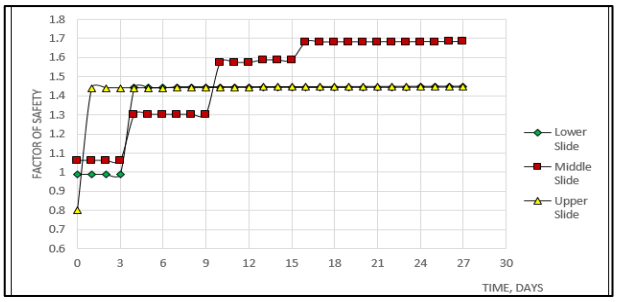

Fig. 22 Variation of FoS with intermediate drain installation approach

According to this analysis, the stability of all three slides can be increased upto a significant level within 3 construction days, even under the presence of a critical rainfall event.

4 CONCLUSIONS AND RECOMMENDATIONS

4.1 *Ginigathhena Slope Rectification Project*

Rising of ground water table during rainy season was identified as the major reason for the slope stability reduction and hence ground water table lowering was had to be considered as the initial construction step of the rectification measures. Thereafter geometry modification has to be conducted before commencing other rectification measures, because all the other stabilization measures had to be applied on the modified slope.

Top down construction sequence have to be adopted for the slope excavation and initial excavation depth have to be limited to a maximum value during the excavation. Thereafter further stabilization measures have to be applied on the slope in top – down approach by enhancing the stability of initial excavation using soil nails, berm drains and sub – surface drains.

The results indicated how important to follow a proper construction sequence to maintain the slope stability during the construction period, because according to the study results, following a different construction order during the rectification than stated in this paper could lead to slope instability during the construction.

4.2 *Badulusirigama Slope Rectification*

The drainage installation process of the Badulusirigama slope was evaluated under three construction approaches; top – down, bottom–up and intermediate.

The results of the analysis present that adaptation of a more suitable drainage installation approach is more appropriate than going for a conventional drain installation approach like top–down or bottom–up approaches.

ACKNOWLEDGMENT

Continuous support throughout the research by the Department of Civil Engineering, University of Moratuwa, and especially Prof. S.A.S. Kulathilaka is greatly appreciated.

REFERENCES

Amada, K., 2016. *Landslide Mitigation – The Badulusirigama, ,s.l.:*JICA

GEOSLOPE International Ltd. (2012a). *Seepage modelling with SEEP/ W*

GEOSLOPE International Ltd. (2012b). *Stability modelling with SLOPE/ W*

Japan International Coorperation agency. (2015). *"Proposal for rectification on landslide, slope failure and rock dall in pilot sites.*

Kankanamge, L.U.M & Kulathilke S.A.S (2020). *Improving the performance of Badulusirigama Landslide using subsurface drains: A numerical Study.*

Lakruwan, M. S., & Kulathilaka, S.A.S. (2019). *Enhancement of the stability at the site of an ancient lanslide in Road cutting with drainage and reinforcement - Case Histroy at Ginigathhena.*

National Building Research Organisation. (2014). *Mitigation of Landslide at Bridge No. 48/ 2 - Avissawella - Haton - Nuwara Eliya Road - Inital Proposal.* Colombo: Sri Lanka: Landslide Research and Risk Management Division, National Building Research Organisation

National Building Research Organization, 2016. *Rectification of unstable slope segments at bridge No. 48/2 on Avissawella – Hatton – NuwaraEliya road,* s.l.:n

Finite Element Analysis of Negative Skin Friction on a Single Pile on Soft Soil

F.S.A. Ansar, L.I.N. De Silva
Department of Civil Engineering, University of Moratuwa, Sri Lanka

ABSTRACT: This paper presents a study on mobilization of negative skin friction (NSF) through end bearing piles for two different soil profiles containing soft soils overlying a stiff residual soil and sandwiched between stiff residual soil layers. A commercially available finite element package PLAXIS 2D has been used for the analysis. The model has been validated using the results of a case study available in the literature. The position of neutral plane and magnitude of drag load is analyzed with the change of soil layer thickness for different pile diameters and axial loads. All the results were compared with an analytical method suggested in Sri Lankan guidelines. Pile settlement and axial shortening significantly affect the mobilization of NSF whereas magnitude of the axial load has no significant effect. It can be concluded that Finite element analysis can reasonably predict the mobilization of NSF on piles installed through layered soil profiles.

KEY WORDS: Finite Element Method; Negative Skin Friction; PLAXIS 2D; Residual soil; Soft soil;

1 INTRODUCTION

Negative Skin Friction (NSF) is induced whenever the soil settles more than the pile (Fellenius, 1984; Wong & Teh, 1996). Negative skin friction has two effects on the pile; The Drag load which is the additional compressive axial force and the Down drag which is the additional settlement (Chen et al., 2009). Drag load reduces the bearing capacity since it becomes an additional load to the pile. The drag load caused by NSF depends on location of the neutral plane and the distribution of NSF throughout the pile. Therefore, to estimate the NSF location of the neutral plane and the distribution of NSF throughout the pile should be analysed (Liu et al., 2012; Matyas & Santamarina, 1994). Neutral plane (NP) is the place where the relative settlement is zero. Above the neutral plane the skin friction is negative. NSF is a complex phenomenon which depends on several factors. Since NSF directly relates with soil settlement all the factors affecting consolidation affects NSF. According to past researchers it has been found that the relative settlement of even a few millimetres (2-5 mm) between soil and the pile would mobilize NSF (Chen et al., 2009; Kim & Mission, 2011; Matyas & Santamarina, 1994; Wong & Teh, 1996). Research had been done to evaluate the NSF of different soil types & on layered soil. Drag force and down drag would vary with soil profile (Comodromos & Bareka ,2005). Thus, it is important to investigate different type of soil profiles. When the soft soil layer is at the top of the soil profile, the depth to neutral plane increases when thickness of soft soil layer increases and the increase is significant for higher thickness of the soft soil layer (A. Hanna & Hoque, 2008). Though there are several research conducted for a case of soft soil layer at the top of the soil profile, a profile which is sandwiched is not well studied in literature. This research focuses on the variation of NSF with the variation of soft soil layer thickness for two different soil profiles.

2 METHODOLOGY

The variation of neutral point & magnitude of drag load was obtained by a numerical analysis. The model was first verified using the results of a case available in the literature. The parametric study was conducted for two different soil profiles. First a soil profile of soft soil overlying a stiff residual soil was considered (known as 'TOP' in latter parts). Then the soft soil was sandwiched between stiff residual soil layers (known as 'SANDWICH' in latter parts). Fig. 1 presents the summary of procedure adopted. Layer thicknesses used for scenario 01 and scenario 02 are presented in Table 1 and 2 respectively. The values obtained from model was compared with the method proposed by the ICTAD/DEV/15 (also known as CIDA) guidelines which is mostly used by the practitioners of Sri Lanka.

Table 1. Soil layer thicknesses used for scenario 01

Case	Layer Thickness (m)		
	Soft	Residual	Rock
1	5	20	2
2	7	18	
3	10	15	
4	12	13	
5	15	10	

Table 2. Soil layer thickness for scenario 02

Case	Layer Thickness (m)			
	T*	Soft	B*	Rock
1	8	5	12	2
2		7	10	
3		10	7	
4		12	5	
5		15	2	

*Top Residual *Bottom Residual

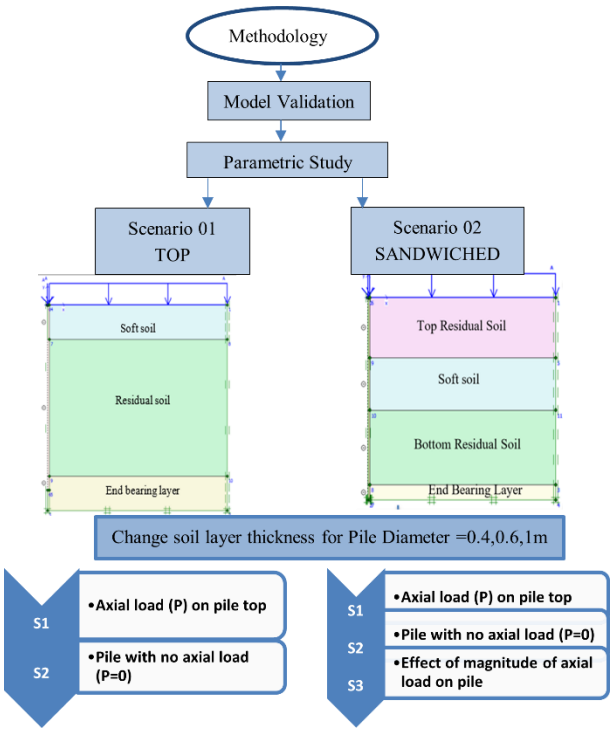

Fig. 1 Procedure followed in the research

3 MODEL VALIDATION

The verification of model was conducted using a known case by (Indraratna et al., 1992). This case was conducted for soft Bangkok clay. The subsoil was a thick clay layer overlying a sand layer. Clayey soils were categorized into three layers according to soil properties presented in Table 3 and 4. Finite element model was created using PLAXIS 2D software.

A circular pile of 400 mm diameter & 27m long has been used for the test. A 2m high embarkment has been raised as the surcharge. Density of embarkment material was 16.67 kNm-3 with 24×14 m base dimensions and side slopes of 2:1. A UDL of 33.35 kPa, with a radius of 7.4m was used as the surcharge in the model. The Mohr-Coulomb model was selected for validation.

Similar procedure was used by A. M. Hanna & Sharif, (2006) & Liu et al., (2012). The analysis results are presented in Fig. 2 and Table 5. The model results have a good agreement with the actual case. Therefore, the same modelling procedure has been used for the analysis of NSF of a single pile.

Table 3: Mohr-Coulomb parameters used in model validation (reprinted from (Liu et al., 2012))

Depth (m)	Material properties					
	γ (kN/m^3)	E (MPa)	υ	C (kPa)	φ	K (m/day)
0-4	17	4900	0.2	3	26	6.76E-04
4-10	17	4900	0.33	5.9	25	5.50E-05
10-20	17	4900	0.33	14.7	25	2.63E-05
20-24	17	6370	0.2	5.9	23	3.72E-05

Table 4. Material properties of end bearing layer & the pile (reprinted from (Liu et al., 2012))

Material	Material properties				
	Depth	γ	E	υ	K
End bearing	24-28	17	28	0.33	3.72E-05
Concrete	0-27	15	3.0E4	-	-

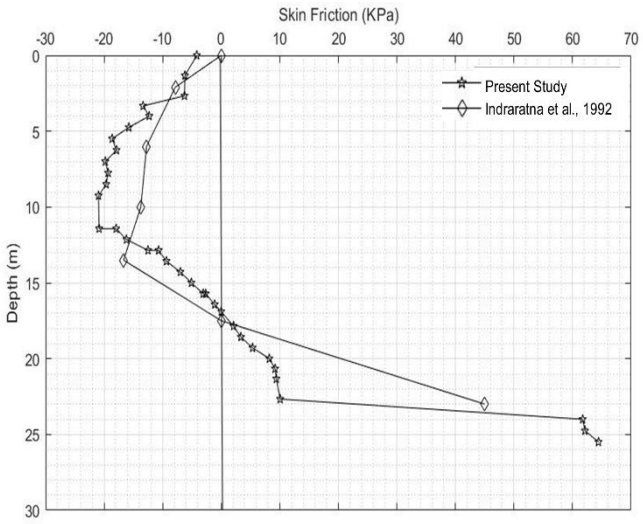

Fig. 2 Comparison of model results with field measurements

Table 5. Results of model validation

Parameter	Model Validation		
	*A	*P	*D
Max NSF (kN/m^2)	-17.64	-21	19%
Depth to Max. NSF (m)	13.5	10	26%
Neutral Point (m)	~17.5	~16.9	3.4%

*Actual((Indraratna et al., 1992)
*Present study
*Deviation of actual from model

4 PARAMETRIC STUDY

4.1 *Model details*

A numerical model was developed using PLAXIS 2D (version 8.2) software. A single pile was modelled as a volumetric element using axisymmetric model. A circular pile with diameters 0.4m,0.6m & 1m and length of 27m were modelled. The mesh was formed by 15-noded elements with 'medium' global coarseness. Ground water table was placed at the ground level. Surcharge on the ground was applied as a Uniformly Distributed Load of 33.5 kPa intensity.
The ultimate end bearing capacity of rock was assumed as 5000kPa. The load which could be withstood for this end bearing capacity was calculated and applied at the top of the pile (P). Consolidation analysis was conducted. As the first stage the loads and the interface were activated. All analysis results were obtained when P_{min} = 1 kPa. An interface friction coefficient (R_{inter}) value of 0.67 was used. Material properties used for models are presented in Table 6.

4.2 *NSF calculations*

The shear stress along the pile soil interface was obtained from the software and the neutral plane can be directly obtained from shear stress variation whereas the force was calculated as follows.

Total Drag Load= $\sum \Delta NSF$ (1)
$\Delta NSF = 2\pi R\, \Delta y\, \Delta\tau$ (2)

Where $\Delta \boldsymbol{y}$ is the distance between selected points, $\Delta \boldsymbol{\tau}$ is the Average pressure between selected points, $\boldsymbol{R}$ is the radius of pile.
The values obtained from model was compared with the method proposed by the ICTAD/DEV/15 guidelines which is mostly used by the practitioners of Sri Lanka. β method is proposed in this guideline.

$\tau_{neg} = \beta\, p(d)$ (3)

Where $\boldsymbol{\tau_{neg}}$ is the unit negative skin friction, $\boldsymbol{\beta}$ is the negative skin friction factor (proposed values are given in the guideline), $\boldsymbol{p(d)}$ is the vertical effective stress at the mid depth of layer that applies negative skin friction
Force due to NSF can be obtained by multiplying τ_{neg} with the associate pile area.

5 RESULTS AND DISUSSION

5.1 *Soft soil layer on top (Scenario 01: S1 and S2)*

First a load was applied on the pile and the variation of NSF was analyzed for a soil profile with soft soil layer at the top (Scenario 1). According to the analysis results the neutral point lies within the soft soil layer when a load is applied on the pile. Fig. 3 presents the range which NP & maximum NSF varies. Fig.4 presents the relationship between NP/T vs T. Here T, is the soft soil layer thickness. When the layer thickness increased the proportion of distribution of NSF within the soft soil layer was increasing. The deviation of the negative force with respect to the value obtained from CIDA is higher when the soft soil layer thickness is smaller. The deviation is in the range of 30 to 48%. Fig. 5 presents the percentage deviation.
The behavior of NSF was also analyzed when the pile is not loaded, and a surcharge is applied to the surrounding. In this case the NP was deep. The neutral plane didn't lie within the soft soil layer. Fig. 6 represents the variation of NSF with depth plotted according to the analysis results. The thickness of soft soil (T) is 10m. It can be observed that the variation is similar up to 75% of soft soil thickness in both the cases. The NP is within the soft soil layer when the load is applied on the pile. For P=0 case the NSF mobilizes through the stiff soil layer as well. Here P is the axial load applied on the pile.

5.2 *Soft soil layer on sandwiched (Scenario 02: S1, S2 and S3)*

When the pile is loaded NP was within the soft soil layer for each & every layer thickness. The position of NP did not significantly vary with the change of diameter of the pile for a particular layer thickness. The NP varies within 0.85T-1T. Here T, is the soft soil layer thickness. The deviation among the values predicted by the model & ICTAD calculated values were less than 20% in each case. Fig. 5 presents the percentage deviation.

Table 6. Material properties used in the model

Material	Material properties							
	Model	Analysis type	γ	E	υ	C	φ	K
Top Residual soil	MC	Drained	17	4.500E+04	0.2	5	31	1.00E-05
Soft clay	MC	Drained	15	1000	0.3	3	20	1.00E-08
Bottom Residual	MC	Drained	18	9.00E+04	0.2	8	33	1.00E-05
End bearing	LE	Drained	22	1.00E+06	0.2	-	-	1.00E-10
Concrete	LE	Drained	15	3.00E+07	0.3	-	-	-

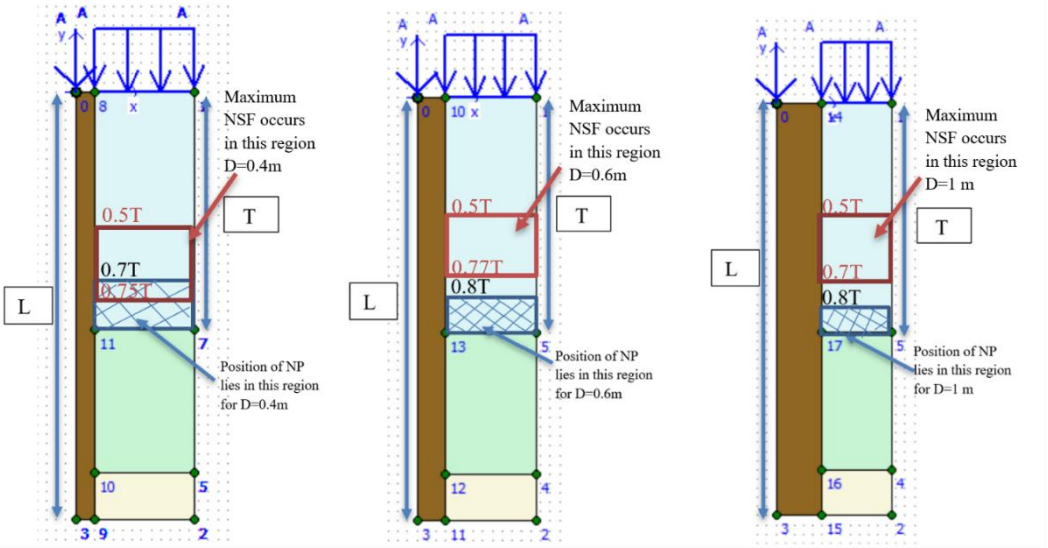

Fig. 3 Region which Neutral Point varies & maximum NSF occurs when P ≠0

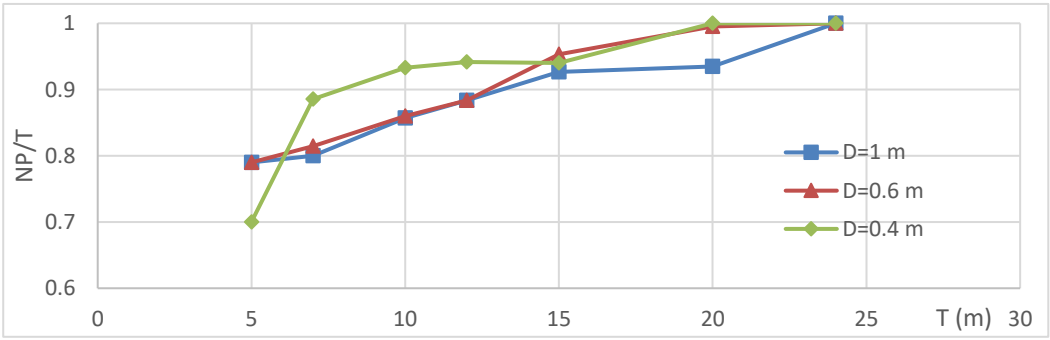

Fig. 4 Relationship between NP/T to T

`

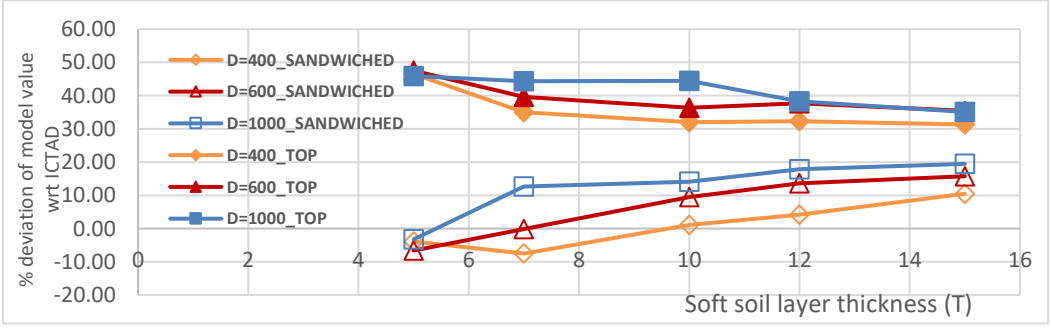

Fig. 5 Variation of percentage deviation of negative friction force with respect to CIDA values to soft soil thickness

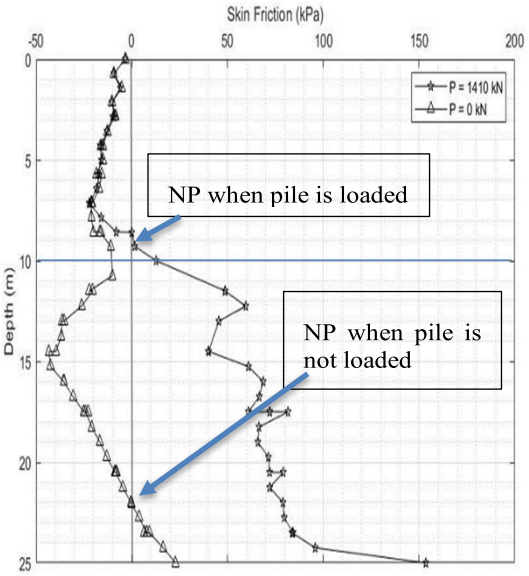

Fig. 7 Variation of NSF for T= 10m with and without an axial load on pile(D=600mm)

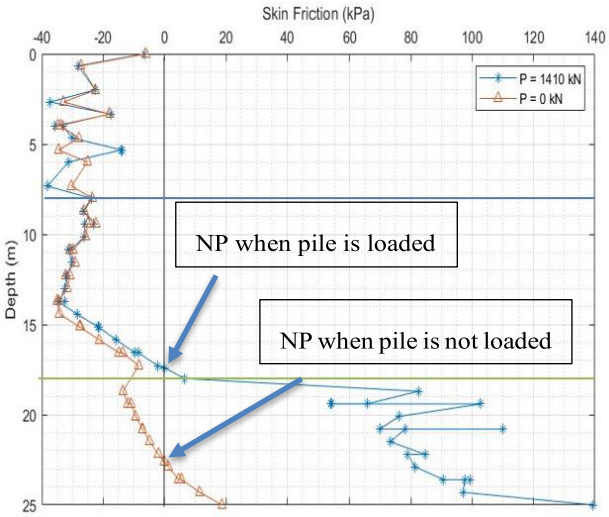

Fig. 6 Variation of NSF for T= 10m with and without an axial load on pile(D=600mm)

The behavior of NSF was also analyzed when the pile is not loaded, and a surcharge is applied to the surrounding. In this case the NSF was distributed with in the entire soft soil layer. For a particular soft soil layer thickness, the NP was deeper when the diameter is increased. To investigate the effect of axial load on the top of the pile, the load on the pile was varied for the 400 mm diameter pile. It was observed that the NP and the distribution of NSF doesn't have a significant effect with the change in the magnitude of the load applied if P≠0. Fig. 7 represents the variation of NSF with depth is plotted according to the analysis results for T=10m of pile diameter of 600mm.

6 CONCLUSION

When load is applied on the pile both the settlement and axial shortening of pile is significant compared to the settlement of residual soil layer. Therefore, the NP occurs within the soft soil layer. The settlement of the pile is smaller when a load is not applied on pile. Hence the settlement of soil is significant resulting in mobilization of NSF within the stiff residual layers as well. It can be stated that the FEM analysis can be used to predict the variation of NSF with a reasonable accuracy.

Volume elements simply means the pile is drawn as a soil cluster and pile properties are assigned as the material parameters. Though the pile installation process has an influence on NSF, pile is modelled as a wished-in-place pile. Therefore, any movements or changes in lateral earth and water pressures due to pile installation are not considered in the analysis. Further investigations should be done to accommodate the effect on pile installation. This study only focuses on variation of NSF for a particular soil profile. Hence using this data for another different soil profiles need to be analysed since the behaviour of NSF would depend on the soil profile.

7 REFERENCES

Chen, R. P., Zhou, W. H., & Chen, Y. M. (2009). Influences of soil consolidation and pile load on the development of negative skin friction of a pile. *Computers and Geotechnics*, *36*(8),1265–1271. https://doi.org/10.1016/j.compgeo.2009.05.011

Comodromos, E. M., & Bareka, S. V. (2005). Evaluation of negative skin friction effects in pile foundations using 3D nonlinear analysis. *Computers and Geotechnics*, *32*(3), 210–221. http://10.1016/j.compgeo.2005.01.006

Fellenius, B. H. (1984). Negative skin friction and settlement of piles. *Proceedings of the Second International Seminar, Pile Foundations, Nanyang Technological Institute, Singapore*, 18.

Guidelines for interpretation of site investigation data for estimating the carrying capacity of single piles for design of bored and cast in-situ reinforced concrete piles (second edition). (2011). Institute for Construction Training and Development (ICTAD).

Hanna, A., & Hoque, M. A. (2008). Coupled consolidation model for negative skin friction on piles in clay layers. *Geomechnics and Geoengineering*.

Hanna, A. M., & Sharif, A. (2006). Drag Force on Single Piles in Clay Subjected to Surcharge Loading. *International Journal of Geomechanics*, *6*(2), 89–96. https://doi.org/10.1061/(ASCE)1532-3641(2006)6:2(89)

Indraratna, B., Balasubramaniam, A. S., Phamvan, P., & Wong, Y. K. (1992). Development of negative skin friction on driven piles in soft bangkok clay. *Canadian Geotechnical Journal*.

Kim, H. J., & Mission, J. L. C. (2011). Development of negative skin friction on single piles: Uncoupled analysis based on

nonlinear consolidation theory with finite strain and the load-transfer method. *Canadian Geotechnical Journal*. https://doi.org/10.1139/t11-004

Liu, J., Gao, H., & Liu, H. (2012). Finite element analyses of negative skin friction on a single pile. *Acta Geotechnica*, *7*(3), 239–252. https://doi.org/10.1007/s11440-012-0163-x

Matyas, E. L., & Santamarina, J. C. (1994). Negative skin friction and the neutral plane. *Canadian Geotechnical Journal*. https://doi.org/10.1139/t94-069

Wong, K. S., & Teh, C. I. (1996). Negative skin friction on piles in layered soil deposits. *International Journal of Rock Mechanics and Mining Sciences & Geomechanics Abstracts*, *33*(3), A134–A135. https://10.1016/0148-9062(96)87149-X

Rice Husk Ash for soil stabilization: An analytical study

R.J.K.P.N. Ranathunga and K.H.S.M. Sampath
Department of Civil Engineering, University of Moratuwa, Sri Lanka

ABSTRACT: Rice Husk Ash (RHA) is one attractive alternative that is used as a full/partial replacement of cement/lime in problematic soil stabilization. This paper introduces statistical models; multiple regression analysis (MRA) and artificial neural network (ANN) for the prediction of Unconfined Compressive Strength (UCS), Soaked California Bearing Ratio (S-CBR), Maximum Dry Density (MDD), Optimum Moisture Content (OMC), and Plasticity Index (PI) of RHA-stabilized clayey soil. S-CBR and MDD of RHA-stabilized soil can be predicted with linear and non-linear MRA and UCS, OMC, and PI can be predicted with ANN models with prediction accuracy > 95%. In the validation process, all the proposed models express prediction errors < ±20%. A Parametric Analysis (PA) was performed to evaluate the variation of UCS with the input parameters. In general, the analysis suggests a 6-12% of RHA with a very little amount of cement (4-8%) or lime (3-6%) as the optimum mix proportion for soft soil stabilization.

KEY WORDS: Artificial Neural Network; geotechnical properties; Multiple Regression Analysis; Rice Husk Ash; soil stabilization

1 INTRODUCTION

Rapid urbanization and associated development activities have resulted in high demand for land plots to satisfy the growing construction demand. In most geotechnical-related projects, in-situ soil is not suitable for the intended application due to inadequate engineering properties of soil.

Soil stabilization is a technique that aims at improving the mechanical, physical, or chemical properties of problematic soils using stabilizing agents such that it meets the design requirements (Alhassan, 2008). It is the most convenient and rapid improvement technique from the point of strength, durability as well as the economy (Ramaji, 2012).

Recently, the use of industrial and agricultural waste materials as a full/partial replacement of traditional solidified materials (i.e., cement and lime) for soil stabilization has become widespread. The review of the literature shows that waste materials such as fly ash (Geliga & Ismail, 2010), blast furnace slag (Yadu & Tripathi, 2013), bottom ash (Güllü, 2014), and bagasse ash (Osinubi et al., 2009) can be effectively used in geotechnical applications.

Rice Husk Ash (RHA) is another promising waste material, which is already being used for the improvement of soft soil performance. RHA has been identified as good pozzolanic material, as it is comprised of more than 60% of silica and around 0.2-5% and 0.5% aluminium and iron oxides respectively, which are highly attributed to pozzolanic reaction (Muthadhi et al., 2007). Annually about 450.45 million tons of RHA is formed worldwide during the combustion of rice husk which is a by-product of rice processing (FAO, 2021; NGES, 2022). The lower production cost, superior performance, and convenient availability are strong motivators for expanding the use of RHA as an attractive additive.

This utilization practice is consistent with the United Nations Sustainable Development Goals: SDG 11 and 12 in terms of resource conservation, sustainable waste management through reduction, recycling, and reuse, substantially reducing environmental pollution and low carbon footprint (*The 17 Goals-Sustainable Development*, 2015).

For each soil stabilization application, an extensive series of experimental studies are required to investigate the enhancement of the geotechnical properties (i.e., strength characteristics, compaction characteristics, and plasticity) of stabilized soil and identify the optimum additives mixture. These engineering properties are related to the physical and chemical characteristics of natural soil and additives, the percentage replacement of soil with additives, and curing conditions (Pham et al., 2022).
Hence, the formation of viable inter-relationship among these parameters and engineering properties of RHA-based soil stabilization systems by adapting predictive techniques such as multiple regression analysis (MRA), support vector machine (SVM), and artificial neural network (ANN) would be beneficial as an indirect approach in the field of soft ground improvement.
Some scholars have already introduced statistical models that are only focused on the prediction of

strength characteristics i.e. UCS and CBR of RHA-stabilized soil systems (Ali et al., 2016; Rafizul & Roy, 2022; Tabarsa et al., 2021).

So far, no critical meta-analysis has been conducted introducing the prediction models for all the engineering properties pertinent to RHA-based soil stabilization such as strength characteristics (i.e., UCS, Soaked CBR), compaction characteristics (i.e., OMC, MDD), and plasticity (i.e., PI).

The present study focuses on addressing the above knowledge gap limiting to the evaluation of the post-stabilization behaviour of high plasticity clayey soil (CH) and low plasticity clayey soil (CL) classified based on the Unified Soil Classification System (USCS) which are stabilized using RHA as both full and partial replacement of cement or lime.

2 METHODOLOGY

2.1 *Data collection and processing*

For formulating the prediction models, the laboratory experimental data from an extensive literature review were used. Only the RHA samples with the summative composition of SiO_2, Al_2O_3, and Fe_2O_3 more than 70% were selected since they are regarded as good pozzolana as per ASTM C618-05 (2005).

For each prediction model, the geotechnical property of stabilized soil was selected as the output variable while using the respective property of natural soil and the contents of additives as input parameters both of which are highly influential for the resultant variations. Other appropriate independent variables which have a significant impact on each predictive property were selected based on the criteria specified in the literature and the availability of data. Table 1 presents the incorporated input parameters and the number of data sets utilized for developing each predictive model.

Table 1. Input parameters and number of data used for developing predictive models

Model	***Input parameters**	**No. of data**
Soaked CBR	*S-CBR$_o$, PI$_o$, MDD$_o$ RHA%, C%, L%*	34
MDD	*MDD$_o$, PI$_o$, Fine%, RHA%, C%, L%)*	90
UCS	*UCS$_o$, PI$_o$, OMC$_o$, D, RHA%, C%, L%*	137
OMC	*OMC$_o$, PI$_o$, Fine%, RHA%, C%, L%*	96
PI	*PI$_o$, SG$_o$, Fine%, RHA%, C%, L%*	67

**XXX$_o$*- Geotechnical properties of natural soil, *Fine%*- Percent finer of soil, *D*- Curing Period in days, *SG$_o$* – Specific gravity of natural soil, *RHA%*, *C%*, and *L%* – Percentage replacement of dry soil weight with RHA, cement or lime

In the analysis process, each dataset was randomly divided into two subsets covering the entire data range, 70% of the total data points for training and the remaining 30% for testing phases with validation practices.

2.2 *Modelling techniques*

Initially, Multiple Regression Analysis (MRA) was executed at a 95% confidence level to get the linear or non-linear relationships. Simple regression models are indeed helpful for interpreting data and attaining conclusions during pre-feasibility assessments, as there are no complex procedures to be followed to interpret the results.

When the models formulated with MRA give undesirable values for the Coefficient of determination due to complex interrelationships between independent and dependent parameters, as the next step, data were further processed with the artificial neural network (ANN) technique which is a more advanced analytical tool.

ANN is a subset of a computational learning system inspired by a simplification of neurons of a human brain. In the current study, multi-layer perceptrons (MLPs) that are trained with a feed-forward back-propagation algorithm (FFBP) with only one hidden layer were adopted to reduce the computational burden.

In ANN modelling, 'hyperbolic tangent sigmoid transfer function (tansig)' was selected as the activation function and the mean square error (MSE) was used as the performance function. The weight or bias change for a given neuron was calculated using LEARNGDM as the adaptive learning function. The most appropriate number of neurons in the hidden layer, training function, and epochs for the neural network of each model were determined through the hit-and-trial method to avoid under-fitting or over-fitting the data.

2.3 *Model performance evaluation*

In order to access the model performance in different aspects, four statistical indicators were selected: 1) coefficient of determination (R^2), 2) Nash–Sutcliffe efficiency (NSE), 3) normalized root mean square error (NRMSE), and 4) mean absolute percentage error (MAPE). Table 2 presents the statistical performance of developed predictive models.

R^2 is accounted as an indicator of the adequacy of the model when more than one input parameter is used and the R^2 values closer to 1, indicate a strong relationship.

The relative magnitude of the residual variance, compared to actual data variance is determined through the Nash–Sutcliffe model efficiency coefficient (E_f), which has an optimum value of 1, corresponding to the highest accuracy.

The root mean square error (RMSE) is utilized to measure the deviation in-between actual values and obtained values from a predictive model and it is more vulnerable toward outliers. Generally, the NRMSE facilitates the comparison of models and the NRMSE values closer to 0 suggests that the respective models are more perfect and promising.

The mean absolute percentage error (MAPE) gives an indication of model accuracy as a percentage. When the prediction performance of multiple models is analyzed, the model with the minimum MAPE is regarded as the best predictive model for the executed data set.

Table 2. Statistical performance of the developed models

Model	Analysis Method	R^2	E_f	NRMSE	MAPE
SCBR	**MRA**	**0.958**	**0.958**	**0.054**	**7.652**
MDD	**MRA**	**0.958**	**0.958**	**0.057**	**2.075**
UCS	**MRA**	**0.908**	**0.897**	**0.090**	**15.23**
	ANN	**0.999**	**0.999**	**0.039**	**0.017**
OMC	MRA	0.780	0.780	0.118	9.869
	ANN	**0.960**	**0.959**	**0.052**	**3.333**
PI	MRA	0.764	0.764	0.127	18.47
	ANN	**0.961**	**0.961**	**0.052**	**7.696**

Optimum results are distinguished by bold.

2.4 *Validation of the proposed models*

The efficiency of each proposed model was validated using the independent data sets (30% of total data points). As these sets of data are not used in developing the models, the error associated with these validation data is able to give a real indication of the prediction capability of the models.

3 RESULTS AND DISCUSSION

3.1 *Prediction of geotechnical properties of RHA-stabilized soil systems*

The statistical performance reveals that the soaked CBR and MDD of stabilized clayey soil is accurately foreseeable using regression analysis which gives both R^2 and E_f of more than 0.95, NRMSE of closer to 1, and MAPE of less than 10% (refer Table 2). Thus, a linear correlation; Eq. (1) and a non-linear correlation; Eq. (2) can be proposed for predicting those properties, respectively.

$$S\text{-}CBR = 2.0146S\text{-}CBR_o - 0.136PI_o + 0.0747OMC_o + 0.254RHA\% + 3.792C\% + 0.376L\% - 6.861 \quad (1)$$

$$ln(MDD) = 0.136MDD_o^2 - 0.56\left(\frac{PI_o}{100}\right)^2 + 0.002Fine\% - \left(\frac{7.6RHA\% - 2.5C\% + 12.8L\%}{1000}\right) - 0.0073 \quad (2)$$

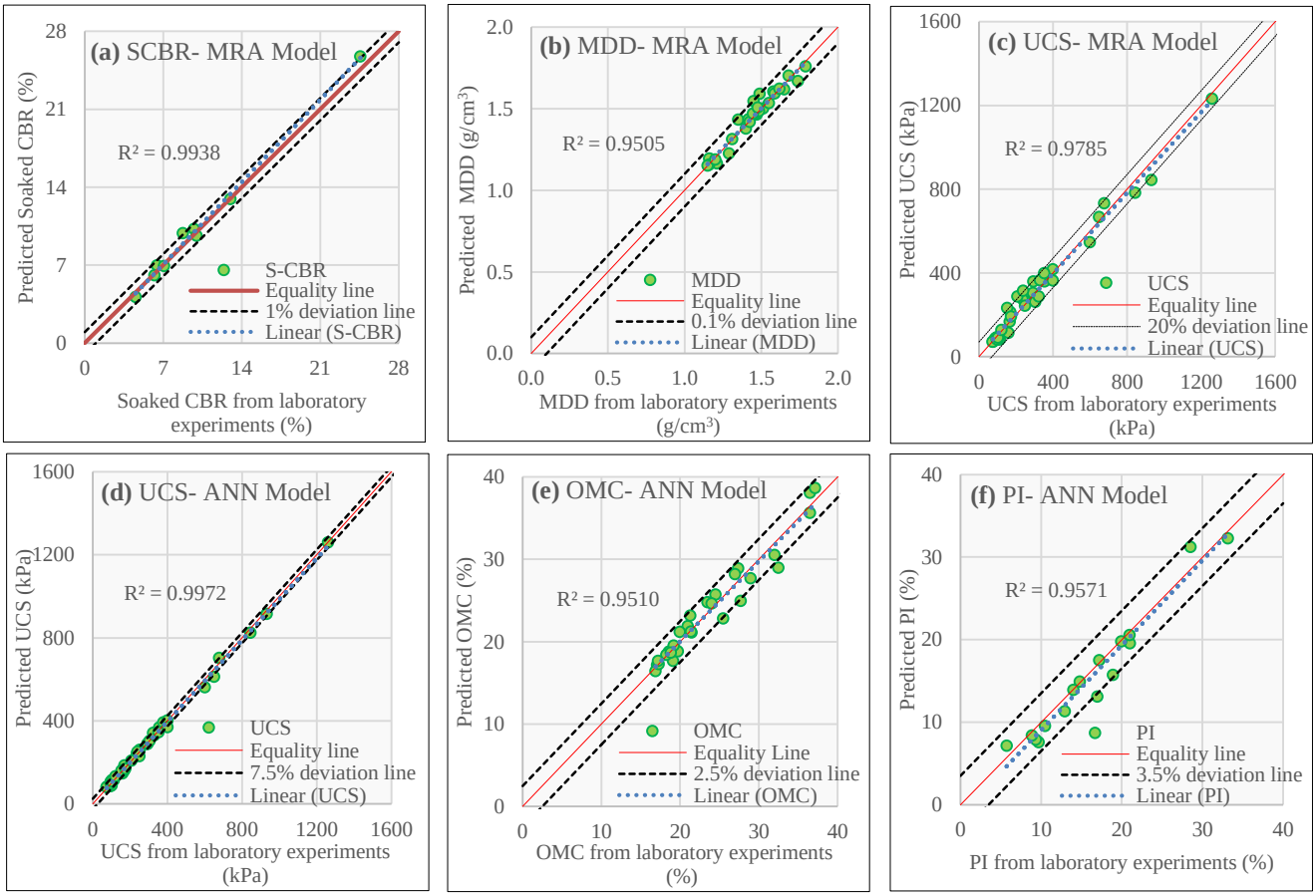

Fig. 1 Validation of the proposed models

The validation performance ensures that these formulae exhibit greater precision for predicting soaked CBR and MDD since predicted results are consequently ±1.0% and ±0.1% off the experimental results (see Fig. 1(a) and (b)).

These correlations are applicable for both full and partial replacement of cement/lime with RHA, as they are developed incorporating studies conducted on both conditions. For instance, in case of full replacement of RHA, the formula can be modified making C% = L% = 0.

For the prediction of UCS, a non-linear correlation was introduced in the form of Eq. (3) with a prediction accuracy of 90.77%. Since the MAPE of 15.23% confirms a less prediction capability, MRA can be used to reasonably predict the UCS. Considering the high importance of determining the UCS of stabilized soil in the design and construction of the ground improvement, ANN modelling was performed for a more reliable prediction.

$$ln(UCS) = \left(\frac{5.45UCS_o + 77.4PI_o - 71.4OMC_o}{1000}\right) + 0.003D + \left(\frac{3.77RHA\% + 18.52C\% + 3.85L\%}{100}\right) - 0.013\ [(RHA\%)^2 + (L\%)^2] + 3.465 \quad (3)$$

The prediction of UCS exhibits a maximum error of ±20.0% which was followed by an error of ±7.5%, respectively for the models formulated with regression analysis and ANN (see Fig. 1(c) and (d)).

Since the MRA fails to give efficient predictive models, ANN models with superior prediction performance are suggested to determine the OMC and PI of stabilized soil. Table 3 presents the details of the model parameters of those three ANN models.

The OMC and PI predictive models exhibit maximum prediction errors of ±2.5% and ±3.5% consequently confirming the robustness of ANN modeling (Fig. 1(e) and (f)).

Table 3. Model parameters and network architecture of formulated ANN prediction models

Parameter	UCS Model	OMC Model	PI Model
Network type	Feed-forward back-propagation		
Transfer function	TANSIG		
Performance function	MSE		
Adaptation learning function	LEARNGDM		
Number of input neurons	7	6	6
Number of output neurons	1	1	1
Number of hidden layers	1	1	1
Number of hidden neurons	10	6	7
Training function	TRAINLM		
Number of training epochs	1000		

3.2 *Parametric analysis for ANN-based UCS prediction model*

The UCS is regarded as the main influential geotechnical parameter for the determination of the optimum additives mixture with applicable amounts (Singh & Singh, 1991). Hence, a parametric analysis (PA) was performed to further examine the ANN-based UCS model. The objective of PA is to

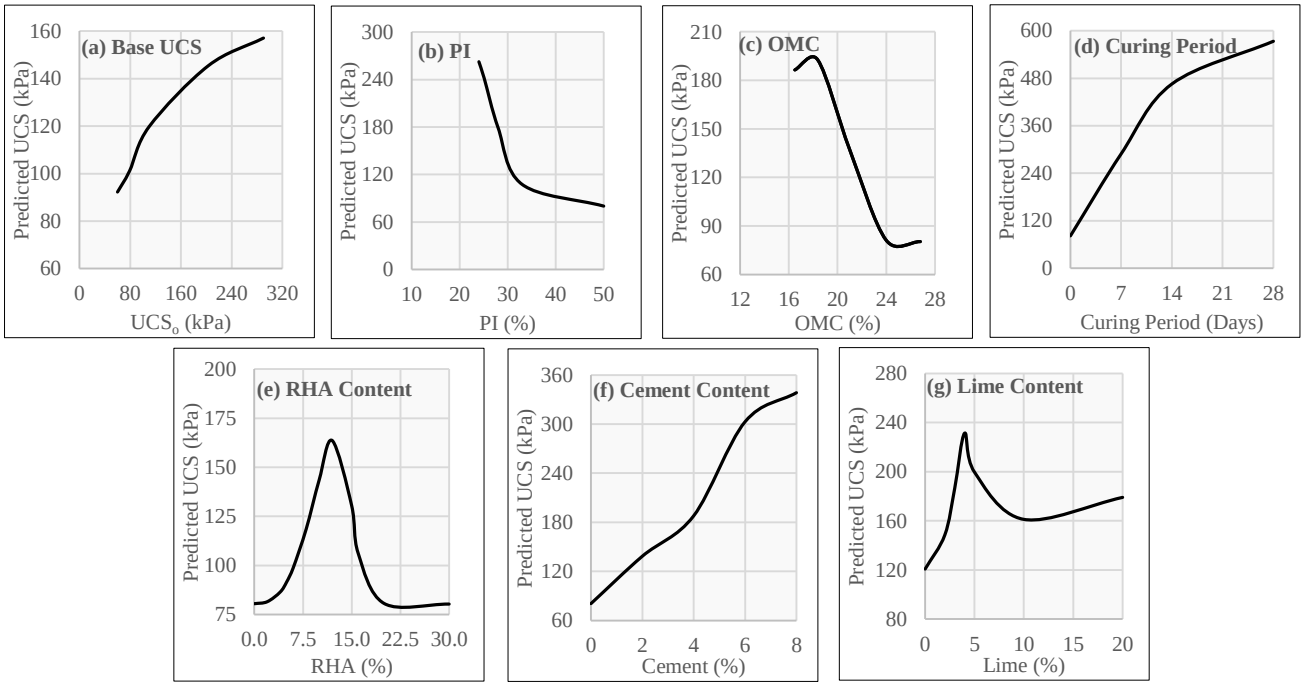

Fig. 2 Parametric Analysis of UCS predictive model for input parameters

evaluate the impact of each input parameter on the UCS of stabilized soil. The respective parameter is allowed to vary within its input range, while other input parameters are constant at the mean value of entire sets of data. Thus, the trend of UCS of stabilized soil with each input parameter is depicted in Fig. 2(a)-(g). Moreover, the indications of PA and their acceptance concerning the previous research findings are summarized in Table 4.

Overall, it is clear that the formulation results of PA are desired and compatible with previous research on soil stabilization with RHA as a full-partial replacement of cement-lime. It ensures that the proposed ANN-based UCS model is reliable and applicable.

3.3 *Recommendation for optimum additives combination for clayey soil stabilization*

The assessments on the microstructural mechanism of soil stabilization show that an optimum mixture of additives contributes to accelerating the hydration process and pozzolana reaction to form secondary cementitious compounds. These products are able to fill the pore space and bond the soil grains enhancing the strength of stabilized soil (Roy, 2014). However, any excessive amount of additives introduced to natural soil remains unreacted and leads to form weak bonds between the soil and cementitious compounds formed resulting in a drop in the strength of stabilized soil (Alhassan, 2008).

Hence, it is worth paying more attention to the selection of the optimum additives mixture as it is directly associated with the performance of stabilized soil as well as the financial aspects. Based on the results of PA that are consistent with previous findings, the application of 6- 12% RHA with a very little amount of cement (4-8%) or lime (3-6%) is suggested as the optimum mix of additives for stabilization of soil classified as CH and CL.

4 CONCLUSIONS

In terms of superior performance, material availability, financial aspects, and environmental impact, utilization of RHA as a full-partial replacement of cement-lime in soil stabilization is an attractive solution.

In the current study, MRA and ANN analyses were implemented to introduce the predictive models for RHA-stabilized clayey soil. The following conclusions can be derived with respect to the analytical results:

- For the prediction of soaked CBR, and MDD, regression analysis gives better correlations with prediction accuracy of more than 95%
- Since MRA does not provide satisfactory performance for the prediction of UCS, OMC, and PI, ANN models were introduced with R^2 of more than 0.95
- For ease of use, the UCS model developed with MRA which gives an R^2 of 0.9077 and MAPE of 15.2312% is recommended as a reasonable predictive model.

Table 4. Verification of parametric analysis results with the findings in the literature

Indications of PA	Verification Facts	Reference
UCS of stabilized soil positively correlates with the natural strength of soil (see Fig. 2(a))	• Although 5-20% of in-situ soil is replaced with a mixture of additives, a large portion is still covered by soil particles	Correia et al. (2013)
With the increment of PI, UCS of stabilized soil decreases (see Fig. 2(b))	• With a high PI, the stabilized soil tends towards ductile behaviour. • Thus, PI is negatively correlated with the UCS of treated soil.	Yao et al. (2020)
OMC has a remarkable negative impact on strength enhancement (see Fig. 2(c))	• High OMC considerably contributes to the growth of capillary pore size of stabilized soil resulting in a low level of crystalline structure • Thus, negative impact on the strength of stabilized soil	Horpibulsuk et al. (2005); Pham et al. (2022)
UCS of stabilized soil enhanced over the curing period (see Fig. 2(d))	• The microstructure analysis shows in the long term, a significant reduction of the volume of large pores and an increment of the volume of small pores can be observed. And also, cementitious compounds are formed with time. Overall soil strength is improved.	Pham et al. (2022); Yao et al. (2020)
The optimum mixture of additives is 6-12% RHA with a lesser amount of cement/ lime (see Fig. 2(e), (f), and (g))	• RHA-stabilized soil shows its best performance with the application of 6-12% of RHA • Only a lesser amount of cement (about 4-8%) or lime (about 3-6%) would be sufficient to obtain a good strength	Basha et al., (2005); Sabat (2012)
The strength gain rate with RHA is comparatively low compared to the cement or lime (see Fig. 2(e), (f), and (g))	• Use of RHA as a partial replacement by adding a very little amount of cement or lime would yield multiple enhancements of strength rather than using it solely as a soil stabilizer	(Basha et al., 2005; Hossain, 1986)

- All the predictive models express a good prediction capability with prediction error < ±20% and R^2 of more than 0.95
- Most results of the parametric study are in accordance with the experimental results of previous studies confirming the robustness of the proposed ANN-based UCS model

Hence, the proposed models are beneficial as an indirect approach to soil stabilization application.

For CH and CL soil stabilization, 6- 12% RHA in combination with a very little amount of cement (4-8%) or lime (3-6%) is recommended as the optimum binder mixture.

5 RECOMMENDATIONS FOR FUTURE EXPLORATIONS

The following recommendations are suggested for further improvement of the models to achieve more effective performance.

- Evaluation of the predictive performance with a greater number and more representative data sets from different countries around the world to exhibit the overall representation
- Further analysis on any type of soil treated with RHA-cement-lime and other possible waste material mixtures
- Formation of more accurate prediction models incorporating other influential factors that have a considerable impact on each predictive property
- Use of different statistical analysis techniques; i.e., support vector machine (SVM), adoptive neuro-fuzzy inference system (ANFIS) beyond MRA and ANN, and different ANN functions to obtain more reliable predictive models

Also needed is a robust assessment beyond the laboratory experiments in order to ensure the effectiveness of soil stabilization using RHA in field applications. These avenues of research would lead to a better understanding of the effective utilization of RHA in the field of soft ground improvement.

REFERENCES

Alhassan, M. (2008). Potentials of rice husk ash for soil stabilization. *Technical Report*, 5.

Ali, B., Rahman, A., & Rafizul, I. M. (2016). *Prediction of California Bearing Ratio of Stabilized Soil using Artificial Neural Network*. 11.

ASTM C618-05. (2005). *Standard Specification for coal fly ash and raw or calcined natural pozzolan for use as a mineral admixture in concrete*. American Society for Testing and Materials International, West Conshohocken Philadelphia.

Basha, E. A., Hashim, R., Mahmud, H. B., & Muntohar, A. S. (2005). Stabilization of residual soil with rice husk ash and cement. *Construction and Building Materials*, *19*(6), 448–453. https://doi.org/10.1016/j.conbuildmat.2004.08.001

Correia, A. A. S., Venda Oliveira, P., & Lemos, L. (2013). Prediction of the unconfined compressive strength in soft soil chemically stabilized. *Proc., 18th Int. Conf. on Soil Mechanics and Geotechnical Engineering*, 2457–2460.

FAO. (2021). *World Food and Agriculture – Statistical Yearbook 2021*. FAO. https://doi.org/10.4060/cb4477en

Geliga, E. A., & Ismail, D. S. A. (2010). Geotechnical properties of fly ash and its application on soft soil stabilization. *Journal of Civil Engineering, Science and Technology*, *1*(2), Article 2.

Horpibulsuk, S., Miura, N., & Nagaraj, T. S. (2005). Clay–water/ cement ratio identity for cement admixed soft clays. *Journal of Geotechnical and Geoenvironmental Engineering*, *131*(2), 187–192.

Hossain, A. S. M. M. (1986). *Cement and cement-rice husk ash stabilization of selected local alluvial soils*.

Kitazume, M., & Terashi, M. (2013). *The deep mixing method* (Vol. 21). CRC press London.

Muthadhi, A., Anitha, R., & Kothandaraman, S. (2007). Rice husk ash-properties and its uses: A review. *Journal of the Institution of Engineers. India. Civil Engineering Division*, *88*(5), 50–56.

NGES. (2022). *National Geographic Education Society: Staple Food Crops of the World*. https://education.nationalgeographic.org/resource/wbt-staple-food-crops-world

Osinubi, K. J., Bafyau, V., & Eberemu, A. O. (2009). Bagasse Ash Stabilization of Lateritic Soil. In E. K. Yanful (Ed.), *Appropriate Technologies for Environmental Protection in the Developing World* (pp. 271–280). Springer Netherlands. https://doi.org/10.1007/978-1-4020-9139-1_26

Pham, V.-N., Oh, E., & Ong, D. E. (2022). Effects of binder types and other significant variables on the unconfined compressive strength of chemical-stabilized clayey soil using gene-expression programming. *Neural Computing and Applications*, *34*(11), 9103–9121.

Rafizul, I. M., & Roy, A. C. (2022). Prediction of California Bearing Ratio of Fine- grained Soil Stabilized with Admixtures using Soft Computing Systems. *Journal of Civil Engineering, Science and Technology*. https://publisher.unimas.my/ojs/index.php/JCEST/article/view/2035

Ramaji, A. E. (2012). *A Review on the Soil Stabilization Using Low-Cost Methods*. 5.

Roy, A. (2014). *Soil Stabilization using Rice Husk Ash and Cement*. 6.

Sabat, A. K. (2012). *Effect of Polypropylene Fiber on Engineering Properties of Rice Husk Ash – Lime Stabilised Expansive Soil*. *17*, 11.

Singh, G., & Singh, J. (1991). *Highway engineering*. Standard Publishers Distributors.

Tabarsa, A., Latifi, N., Osouli, A., & Bagheri, Y. (2021). Unconfined compressive strength prediction of soils stabilized using artificial neural networks and support vector machines. *Frontiers of Structural and Civil Engineering*, *15*(2), 520–536. https://doi.org/10.1007/s11709-021-0689-9

The 17 Goals-Sustainable Development. (2015). https://sdgs.un.org/goals

Yadu, L., & Tripathi, R. K. (2013). Effects of granulated blast furnace slag in the engineering behaviour of stabilized soft soil. *Procedia Engineering*, *51*, 125–131. https://doi.org/10.1016/j.proeng.2013.01.019

Yao, K., Pan, Y., Jia, L., Yi, J. T., Hu, J., & Wu, C. (2020). Strength evaluation of marine clay stabilized by cementitious binder. *Marine Georesources & Geotechnology*, *38*(6), 730–743.

Prediction of geotechnical properties of soils stabilized with calcium carbide residue

D.M.T.U. Sandamali, K.H.S.M. Sampath
Department of Civil Engineering, University of Moratuwa, Sri Lanka

ABSTRACT: This research was conducted to study the applicability of calcium carbide residue (CCR) as a soil stabilizer with a comprehensive literature review and a statistical analysis. CCR can be identified as a promising stabilizer with significant improvements to the geotechnical properties of soils. With the experimental data available in literature, four models were developed to predict these improvements to facilitate the pre-feasibility stage of the practical application of CCR soil stabilization. This paper describes two such regression models which can predict the MDD, and OMC of CCR stabilized soils, with a prediction accuracy of ±5%. Also, an artificial neural network (ANN) model within an accuracy range of ±16% was developed to predict the UCS of CCR stabilized soils after 28 days of curing. In addition, a gaussian process regression (GPR) model was introduced to predict the plasticity index (PI) of CCR stabilized soil with a predictive accuracy of ±3%.

KEY WORDS: Artificial neural network; Calcium carbide residue; Regression analysis; Soil stabilization; Unconfined compressive strength

1 INTRODUCTION

Problematic soils such as clayey, silty and expansive soils can cause difficulties during constructions as a result of their lower strengths and higher compressibility characteristics. Furthermore, clay is a water sensitive soil that exhibits extreme volumetric changes with the absorption and evaporation of moisture. Therefore, using a soil stabilizer to improve the geotechnical properties has been a common practice in the construction field.

Many recent studies have focused on calcium carbide residue (CCR) as a stabilizer to replace cement due to the high costs and negative environmental impacts involving cement usage. CCR is a by-product of acetylene gas production process and can be identified as a $Ca(OH)_2$-rich material. When CCR is mixed with a soil, the cementitious products created as a result of pozzolanic reactions between $Ca(OH)_2$ from CCR and the natural pozzolanic materials such as alumina and silica in soil can strengthen the soil matrix (Latifi et al., 2018).

Addition of CCR as a soil stabilizer changes the properties of soils such as strength, compaction characteristics and index properties. In fact, addition of CCR decreases the maximum dry density (MDD) of soil while increasing the optimum moisture content (OMC) (Balarabe & Sharmila, 2018; Kumari et al., 2017; Mohammed et al., 2020; Mohammed et al., 2020; Varaprasad et al., 2020; Venkatesh et al., 2018, 2018, 2021).

Generally, the specific gravity of CCR is less than that of the soils. Therefore, the addition of CCR reduces the net specific gravity of the treated soil. This reduction of specific gravity and the aggregation of clay particles cause the decrement in MDD of the CCR treated clayey soils (Balarabe & Sharmila, 2018; Mohammed et al., 2020).

When the CCR is added to the soils, the natural pozzolanic material in soil such as silica and alumina react with $Ca(OH)_2$ from CCR. These pozzolanic reactions require water in which the requirement increases with the CCR dosage. Therefore, with the addition of CCR, the soil absorbs more water and hence the optimum moisture content of the CCR treated soils increases (Balarabe & Sharmila, 2018; Mohammed et al., 2020).

Generally, with the addition of CCR plasticity index (PI) tends to decrease until a certain CCR content and then becomes constant (Akinwumi et al., 2019; Joel & Edeh, 2013; Naveena et al., 2016). This particular CCR content is known as the "CCR fixation point". Absorption of Ca^{2+} ions during the cation exchange process results in flocculation of clay particles which cause the reduction of PI. At the fixation point, the Ca^{2+} ion absorption capacity reaches to a maximum and hence the change of PI becomes insignificant with CCR addition (Horpibulsuk et al., 2012).

With the increase in CCR content, UCS increases rapidly at first. Then after a certain CCR content, increment of UCS becomes insignificant with further addition of CCR. This certain amount of CCR coincides with the CCR fixation point and often identified as the "optimum CCR content". After reaching the fixation point, UCS tends to decrease with the increasing CCR content. This UCS drop can be clearly observed in clayey soils

stabilized with CCR (Akinwumi et al., 2019; Chindaprasirt et al., 2020; Joel & Edeh, 2013; Latifi et al., 2018). When all the natural pozzolanic materials present in soil are consumed for pozzolanic reactions, the remaining excess amount of $Ca(OH)_2$ causes unsoundness, resulting this strength reduction (Horpibulsuk et al., 2012).

The experimental studies over the years have shown the capability of CCR as a soil stabilizer. Also, it is important to know how the soil behaves after stabilizing with CCR, so that the CCR based soil stabilization to be utilized effectively with practical applications. But there are no studies to predict the change of behavior of CCR treated soils in terms of compaction properties, unconfined compressive strengths and plasticity to be found in the literature.

Therefore, main objective of this research was to conduct a comprehensive literature review and meta-analysis of the performance of geotechnical properties of clayey soil after stabilizing with CCR. Prediction models were developed to estimate MDD, OMC, UCS and PI of CCR stabilized soils using multivariate linear regression analysis, multivariate polynomial regression analysis, gaussian process regression (GPR) and artificial neural network (ANN).

The models developed to predict the geotechnical properties of the soils after stabilizing with CCR, can help in decision making in the prefeasibility stage by avoiding the requirement of large number of trial testing which minimize the time and cost for such investigations.

2 METHODOLOGY

The data required for training and validation of the models were collected through a systematic literature review. The collected data sets contain the properties of clayey, silty and expansive soils. Statistical tools available in Excel and MATLAB were used for the data analysis and the generation of relevant graphs.

Relevant independent variables for the models were selected considering the results from step-wise regression analysis and by following the recommendations of past research studies.

The best fit models were selected considering the R^2 value and standard error values of the regression analysis. This paper describes the models with highest R^2 values and the least standard error values. Several separate data sets were reserved for the validation of developed prediction models. These validation data were selected randomly to represent the entire data range used for training the models.

Table 1 summarizes the sources of data adopted for developing models. It should also be noted that the studies related to CCR soil stabilization is still limited. Hence the analysis was conducted using the limited numbers of data set available in the literature.

Table 01. Sources of data

Model	Data sources
MDD and OMC	Horpibulsuk et al., (2012), Latifi et al., (2018), Venkatesh et al., (2018), Mohammed et al., (2020), Mohammed et al., (2020), Venkatesh et al., (2018), Balarabe & Sharmila, (2018), Venkatesh et al., (2021), Varaprasad et al., (2020), Kumari et al., (2017)
PI	Horpibulsuk et al., (2012), Venkatesh et al., (2019), Venkatesh et al., (2018), Juneja & Shinde, (2019), Venkatesh et al., (2021), Ning-Jun Jiang et al., (2015)
UCS	Horpibulsuk et al., (2012), Latifi et al., (2018), Mohammed et al., (2020), Mohammed et al., (2020), Jiang et al., (2015), Quadri H.A et al., (2019)

3 DEVELOPED PREDICTION MODELS

3.1 *Prediction of Compaction Properties*

Using a database of 30 sets of data which is represented in Table 2, two regression models were developed to predict the compaction properties of CCR stabilized soil. MDD and the OMC of the soil stabilized with CCR were selected as the dependent variables. The compaction properties of natural soil and the CCR mix proportion were selected as the independent variables following a step-wise regression analysis.

Table 2. Parameters of the training data considered for the prediction of compaction properties

Parameters	**Units**	**Min**	**Max**	**Mean**	**Standard deviation**
$MDD_{(Soil)}$	kN/m^3	12.3	18.8	16.22	1.96
$OMC_{(Soil)}$	%	12	38	21.60	7.89
CCR%	%	2	30	8.3	5.91
$MDD_{(TS)}$	kN/m^3	11.51	18.3	15.30	2.02
$OMC_{(TS)}$	%	17.31	41.2	24.68	7.63

Model 01 was developed using multivariate linear regression analysis (MLR) to predict the MDD of CCR stabilized soils.

Model 01:

$$MDD_{(TS)} = 0.91545MDD_{(Soil)} - 0.06829CCR\% + 1.022403 \quad (1)$$

Model 01 has a R^2 value of 0.9027 which is close to 1 and the significance F for the model is way below 0.05. Also, the P-values for both selected

independent variables were less than 5%. Therefore, it can be seen that the developed model is an accurate and promising model. Also, the low p-values of independent variables show that the selected variables are suitable for the model.

In addition, the predictive curve of model 01 which was generated with MATLAB, is shown in Figure 1 and can be used for easy reference when the MDD of the natural soil and CCR dosages are available.

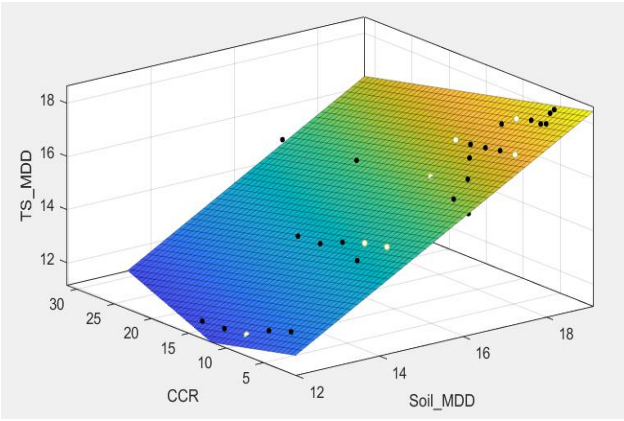

Fig. 1 MDD prediction curve

Model 02 is a third-degree polynomial function that can be used to predict the OMC of CCR stabilized soils. Multivariate polynomial regression analysis tool of MATLAB was used to derive the model.

Model 02:

$$OMC_{(TS)} = 46.13 - OMC_{(Soil)}\, CCR\% \left(0.03566 - 0.0007532\, OMC_{(Soil)} + \frac{4.946 - 0.2521\, OMC_{(Soil)} + 0.003365\, OMC^2_{(Soil)}}{CCR\%} - \frac{0.535}{OMC_{(Soil)}}\right) \quad (2)$$

This model has a R^2 value of 0.9862 and an adjusted R^2 value of 0.9826. Which shows model 02 is a promising model to predict OMC of clayey soils.

Also, a predictive curve for model 02 was generated using MATLAB, which is shown in Figure 2 and can be used for easy reference when the OMC of the natural soil and CCR dosages are available.

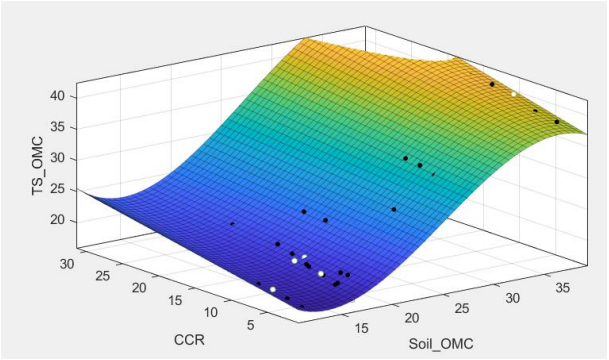

Fig. 2 OMC prediction curve

3.2 *Prediction of plasticity index*

A database containing 25 sets of data which is represented in Table 03 was used to develop prediction models for index properties. Three nonparametric models were developed to predict the liquid limit (LL), plasticity limit (PL) and plasticity index (PI) of CCR stabilized soils. However, the PI prediction model was selected as the best model to describe the plasticity characteristics of soil with the addition of CCR considering high accuracy.

Table 3. Parameters of the training data considered for the prediction of PI

Parameters	Units	Min	Max	Mean	Standard deviation
$PI_{(Soil)}$	%	17.9	41	32.19	9.75
CCR%	%	0	12	4.64	3.59
$PI_{(TS)}$	%	7.88	40.18	19.06	8.41
$Clay_{(Soil)}$	%	13.6	58	38.65	16.50

The PI prediction model is a gaussian process regression (GPR) model with the Matern 5/2 kernel function. This model use the PI of natural soil ($PI_{(Soil)}$), clay content of natural soil ($Clay_{(Soil)}$) and CCR% as model inputs. As indicated in Table 4 this model has a R^2 value of 0.98 indicating the capability of predicting PI of CCR stabilized soils. This GPR model can be reproduced with the training data summarized in Table 5.

Table 4. Details of PI prediction model

Dependent variable	Independent variables	Analysis technique	Model performance	
$PI_{(TS)}$	CCR% $PI_{(Soil)}$ $Clay_{(Soil)}$	GPR – Matern 5/2	R^2	0.98
			RMSE	1.35
			MSE	1.82
			MAE	1

Table 5. Training data for PI prediction model

Reference	UCSC	$Clay_{(Soil)}$ %	$PI_{(Soil)}$	CCR	$PI_{(TS)}$
Horpibulsuk et al., (2012)	CH	55	39	0	39.09
	CH	55	39	1	31.53
	CH	55	39	5	17.48
	CH	55	39	7	15.52
	CH	55	39	9	15.19
	CH	55	39	12	14.86
Venkatesh et al., (2019)	CH	29	41	0	41.0744
	CH	29	41	2	30.9504
	CH	29	41	4	23.1405
	CH	29	41	8	15.0413
	CH	29	41	10	14.1736
	CL	24	20	0	20

Venkatesh et al., (2018)	CL	24	20	2	14.0385
	CL	24	20	6	7.8846
	CL	24	20	8	7.8846
Juneja & Shinde, (2019)	CH	58	38	0	40.1826
	CH	58	38	2	23.7443
	CH	58	38	4	19.3607
	CH	58	38	6	18.2648
	CH	58	38	10	17.1689
Venkatesh et al., (2021)	CL	26	20	0	19.9231
	CL	26	20	4	10.0513
	CL	26	20	6	8.0769
Du et al., (2016)	CL	13.6	17.9	4	13.1
	CL	13.6	17.9	6	13.4

Generally, the optimum CCR content is determined by generating a PI vs CCR% plot using experimental data. The point where the reduction of PI become insignificant with CCR addition is selected as the optimum CCR content. This model can also be used to generate PI vs CCR% plot and hence can be used to determine the optimum CCR content without experimental trials when the clay content is given.

3.3 *Prediction of unconfined compressive strength*

A database containing 34 data sets which is represented by Table 6 was used to develop UCS prediction models. Two models to predict the UCS after 28 days of curing ($UCS_{(TS,28d)}$) were developed using artificial neural network (ANN) and gaussian process regression (GPR). However, the ANN model is described here considering comparatively high accuracy.

Table 6. Parameters of the training data considered for the prediction of UCS

Parameter	**Units**	**Min**	**Max**	**Mean**	**Standard deviation**
$UCS_{(Soil)}$	kN/m^2	19.2	1133.33	472.696	474.584
$UCS_{(TS,28d)}$	kN/m^2	44.3	6933.33	2263.911	2395.97
$Gs_{(Soil)}$	-	2.5	2.76	2.67	0.086
$Gs_{(CCR)}$	-	1.8	2.32	2.21	0.172
CCR%	%	0	50	9.206	9.923

The ANN model was developed adopting a feed-forward multilayer perceptron architecture with a single hidden layer as represented in Figure 3. With a trial-and-error process 10 neurons were selected as the optimum. This proposed model uses UCS of natural soil ($UCS_{(Soil)}$), specific gravity of natural soil ($Gs_{(Soil)}$), specific gravity of CCR ($Gs_{(CCR)}$) and the CCR% as inputs for the predictions and has a R^2 value of 0.99958 indicating this is a promising model to predict UCS of CCR stabilized soils. Table 7 indicates the model details including the adopted functions, weights and biases.

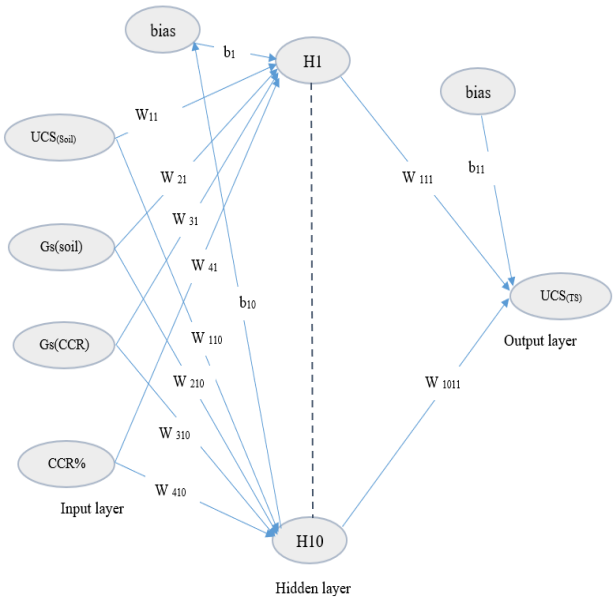

Fig. 3 ANN model architecture

Table 7. ANN model details

Training function	TRAINCGP
Adaption learning function	LEARNGDM
Performance function	MSE
Transfer function	TANSIG
Weights (Input layer to Hidden layer) (From W_{11} to W_{410})	[0.10244 -0.66157 2.7924 -2.2984; 2.3437 1.9791 0.76941 5.0114; -2.0565 -1.4843 -0.41489 0.80718; -1.1088 2.4557 -1.301 0.22012; -1.964 -0.82134 -1.4492 0.86674; 0.90099 -0.41182 0.96897 3.487; 3.0572 2.1068 0.54392 1.218; 1.1261 1.3329 1.964 0.59428; -0.75234 -3.084 0.61797 0.10909; -0.13046 4.3257 1.2134 -3.2212]
Weights (Hidden layer to output) (From W_{111} to W_{1011})	[1.7634 3.2878 1.4645 -1.2746 1.6511 -2.2109 2.2764 -0.3299 -0.8954 -1.8377]
Bias (b_1)	[1.1078; -1.1062; 1.2543; 0.48135; 0.36043; 0.19086; 1.1179; 1.2073; -1.9151; 1.719]
Bias (b_2)	[0.33396]

4 VALIDATION OF PREDICTION MODELS

Predictive capability of each developed model was assessed with model validation. Data for validation was selected to represent the entire data range adopts to train the models. An accurate idea of model performance was gathered with this validation process, since the validation data set did not used for training the model. Figure 4-7 shows the validation plots which indicates the correlation between experimented values vs the values predicted by the developed models.

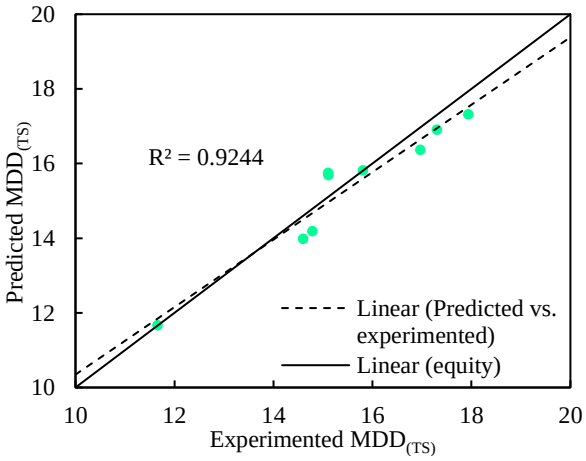

Fig. 4 MDD model validation plot

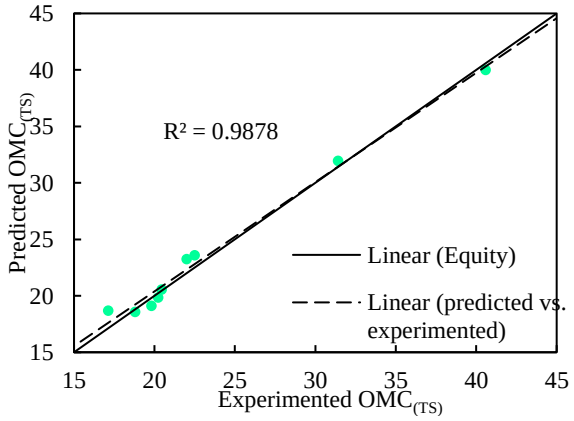

Fig. 5 OMC model validation plot

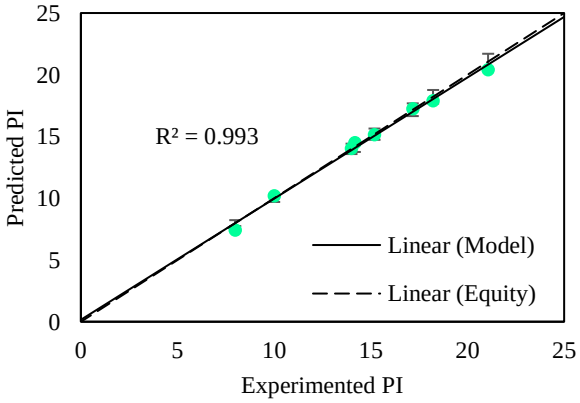

Fig. 6 PI model validation plot

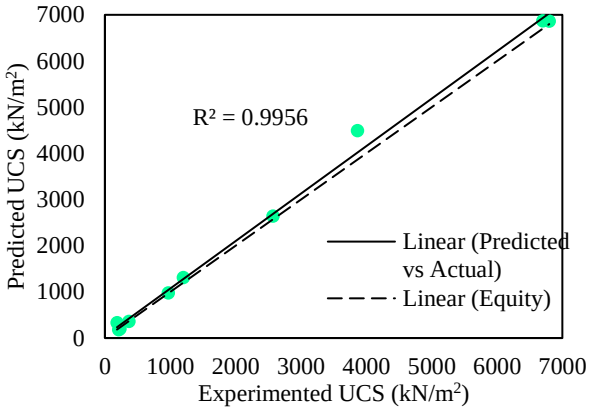

Fig. 7 UCS model validation plot

As shown in Figure 4-7, the trendlines generated for the validation plots are very close to the equity lines. And the trendlines have R^2 values close to 1, indicating a strong correlation between predicted and experimental results. Furthermore, according to the percentage error calculations developed models can predict the MDD, OMC, PI and UCS of CCR stabilized soils within accuracy ranges of ±5%, ±5%, ±3%, and ±16% respectively. Therefore, it can be concluded that the developed prediction models can predict the Geotechnical properties of CCR stabilized soils accurately.

5 CONCLUSIONS

According to past experimental studies, CCR can be successfully used for stabilization of problematic soils. The improvements to the soil profile can be predicted with the developed parametric and non-parametric models which are summarized below.

MDD of stabilized soils has a linear relationship with MDD of natural soil and CCR mix proportion. Model 1 has a R^2 value of 0.9027 and can predict the MDD of CCR stabilized soil within a prediction accuracy of ±5%.

OMC of stabilized soil can be described with a third-degree polynomial function of OMC of natural soil and CCR mix proportion. Model 2 has a R^2 value of 0.9862 and can predict the OMC of CCR stabilized soil within a prediction accuracy of ± 5%.

UCS of CCR stabilized soil is greatly influenced by the CCR mix proportion, Curing days, specific gravity of soil and specific gravity of CCR and the UCS of natural soil. Nonlinear models such as ANN and GPR can be used to predict the UCS of CCR stabilized soils. Proposed ANN model has a R^2 value of 0.99958 and can predict the UCS of CCR stabilized soil after 28 days of curing within an accuracy range of ±16%.

PI of CCR stabilized soil is mainly depend on the PI and clay content of natural soils. GPR (Matern 5/2) model has a R^2 value of 0.98 and can predict

the PI with CCR addition within an accuracy range of ±3%. This model can also be used to estimate the optimum CCR content.

REFERENCES

Akinwumi, I. I., Ajayi, O. O., Agarana, M. C., Ogbiye, A. S., Ojuri, O. O., & David, A. O. (2019). Investigation of Calcium Carbide Residue as a stabilizer for Tropical Sand used as pavement material. *WIT Transactions on The Built Environment*, *182*. https://doi.org/doi:10.2495/UT180261

Balarabe, W. I., & Sharmila, S. M. R. (2018). Soil Stabilization Using Calcium Carbide Residue and Coconut Shell Ash. *Journal of Basic and Applied Engineering Research*. http://www.krishisanskriti.org/jbaer.html

Chindaprasirt, P., Kampala, A., Jitsangiam, P., & Horpibulsuk, S. (2020). Performance and evaluation of calcium carbide residue stabilized lateritic soil for construction materials. *Case Studies in Construction Materials*, *13*. https://doi.org/10.1016/j.cscm.2020.e00389

Du, Y. J., Jiang, N.-J., Liu, S.-Y., Horpibulsuk, S., & Arulrajah, A. (2016). Field evaluation of soft highway subgrade soil stabilized with calcium carbide residue. *Soils and Foundations*, *56*(2), Article 2. https://doi.org/10.1016/j.sandf.2016.02.012

Horpibulsuk, S., Chayakrit, P., & Avirut, C. (2012). Soil Stabilization by calcium carbide residue and fly ash. *Journal of Materials in Civil Engineering*, *24*(2), Article 2. https://10.1061/(ASCE)MT.1943-5533.0000370

Joel, M., & Edeh, J. E. (2013). Soil Modification and Stabilization Potential of Calcium Carbide Waste. *Trans Tech*. https://doi.org/doi:10.4028/www.scientific.net/AMR.824.29

Juneja, A., & Shinde, S. T. (2019). Undrained Yielding of Black Cotton Soil Treated with Calcium Carbide Residue. *Indian Geotech J*. https://doi.org/10.1007/s40098-019-00380-8

Kumari, M. S., Kavya, B. V. S., & Vincent, G. J. (2017). A study on replacement of additives with CCR+FA to improve bearing capacity of soil. *Proceedings of National Conference on Recent Innovations in Civil Engineering*.

Latifi, N., Vahedifard, F., Ghazanfari, E., & A. Rashid, A. S. (2018). Sustainable Usage of Calcium Carbide Residue for Stabilization of Clays. *Journal of Materials in Civil Engineering*, *30*(6), Article 6. https://doi.org/10.1061/(ASCE)MT.1943-5533.0002313

Mohammed, I. K., Alhassan, M., & Alhaji, M. M. (2020). Improvement of Deficient Laterite Soil using Cement and Calcium Carbide Residue. *2 Nd International Civil Engineering Conference*.

Mohammed, S., Alhassan, M., & Alhaji, M. M. (2020). Stabilisation of Tropical Black Clay Using Calcium Carbide Residue and Cocunut Shell Ash. *Nigerian Institution of Civil Engineering*.

Naveena, P. C., Dinesh, S. V., Gowtham, B., & Umesh, T. S. (2016). Prediction of Strength Development in Black Cotton Soil Stabilised with Chemical Additives. *Indian Geotech*. https://doi.org/10.1007/s40098-016-0209-3

Varaprasad, B. J. S., Joga, J. R., & Joga, S. R. (2020). Remediation of expansive soils using mango kernel ash and calcium carbide residue. *Int. J. Environment and Waste Management*, *25*(2).

Venkatesh, N., Heera, L. M., & Rakesh, J. P. (2018a). Multi-scale laboratory investigation on black cotton soils stabilized with calcium carbide residue and fly ash. *Journal of Eng. Research*, *6*.

Venkatesh, N., Heera, L. M., & Rakesh, J. P. (2018b). Resilient modulus of clayey subgrade soils treated with calcium carbide residue. *International Journal of Geotechnical Engineering*. https://doi.org/10.1080/19386362.2018.1512230

Venkatesh, N., Heeralal, M., Rakesh, J. P., & Sudheer, K. Y. (2019). Permanent deformation behaviour of black cotton soil treated with calcium carbide residue. *Construction and Building Materials*. https://doi.org/10.1016/j.conbuildmat.2019.07.010

Venkatesh, N., Yewanth, P., Rama, V. P. C., Reddy, B. S. K., & Chaitanya, S. T. (2021). Evaluation of a Clayey Soil Stabilized by Calcium Carbide Residue as Pavement Subgrade. *Transportation Infrastructure Geotechnology*. https://doi.org/10.1007/s40515-021-00185-4

Finite Element Analysis on the Distribution of Stress through Layered Soils

T.I.P.K.M. Wijayarathne and L.I.N. de Silva
Department of Civil Engineering, University of Moratuwa, Sri Lanka

ABSTRACT: Evaluation of stress distribution through soil strata is one of the fundamentals of geotechnical analysis. Vertical stress is attributed to the loading intensity and geostatic stress. Even though many analytical methods have been developed idealizing the soil as a homogeneous, isotropic, and elastic material, the soil is multiphase in reality. In this study, stress distribution under a strip footing through a two-layered system consisting of sandy and clayey soils is analysed using the finite element method. Different cases are simulated by changing the soil properties, layer thicknesses, and the order of positioning of the soil types, and the results are compared with Boussinesq solutions. The results show that stress at a selected point is low when the soils are loose and soft compared to the soils which are dense and stiff. The lower the thickness of the sand layer higher the stress at a selected point. The cases with clay layers at the top show high stress at a particular depth when the thickness of the top layer is higher than the bottom layer while cases with sand layers at the top show high stress at the same depth when the thickness of the top layer is lower than the bottom layer. Vertical stress values of Boussinesq solutions agree with the finite element analysis values when moving away from the footing both in horizontal and vertical directions.

KEY WORDS: Stress Distribution; Two-layered soil system; Finite Element Analysis (FEA); Strip Footing

1 INTRODUCTION

Soil is a multiphase system in reality. Vertical stress is attributed to both loading intensity and geostatic stress. Hence, it is interesting to investigate the distribution of vertical stress through layered soils. When the stress propagates, the stress bulb gets distorted due to the nature of soils (Hanna, 1987).

It is an opportune need to simulate the field conditions using computer programs since the ideal conditions which are assumed in analytical methods are contradictory with what can be seen in the field.

Some have analysed the effect on a single soil medium (Sadek and Shahrour, 2007). On the other hand, it can be noted that the scarcity of the availability of relevant literature when it comes to simulating the distribution of vertical stress through layered soils using the finite element software.

In this study, the stress distribution from a strip footing through a two-layered soil system consisting of pure clayey soil and sandy soil will be investigated using numerical models of PLAXIS 2D geotechnical software. It is achieved in the following objectives.

- Objective 1 - Study the vertical stress distribution variation by changing the properties of soils (sand layer over clay layer)
- Objective 2 - Study the vertical stress distribution variation by changing the thicknesses of soil layers (sand layer over clay layer)
- Objective 3 - Study the vertical stress distribution variation by interchanging the position of soil type (clay layer over sand layer)

The findings of this study will be useful for accurate estimation of stress distribution in two-layered soil systems which is to estimate the settlement and load-displacement behaviour of structures. In addition, it gives an idea about the influence zone depths, which is useful in identifying appropriate ground improvements for foundations.

2 LITERATURE REVIEW

Boussinesq's (1885) equations are widely used in determining the intensity of vertical load in a soil system generated from an applied load. They have been derived assuming that the soil behaves as a homogeneous and elastic material. Westergaard's (1938) theory assumes that thin sheets of a negligible thickness of rigid material are sandwiched in a homogeneous soil mass. These thin sheets are closely spaced and are of infinite rigidity which results in incompressible nature. These thin sheets permit only downward deformation of the soil mass without lateral deformation.

Burmister (1945a, 1945b, 1945c) developed equations for calculating the stress in two-layered and three-layered soils at the top level, interface, and bottom level according to elastic theory. The accuracy of the equations has been proven by equalizing the elastic properties in both layers; a homogeneous deposit

throughout. Equations had been reduced to Boussinesq equations. Jones (1962) developed tables to calculate the vertical stress distribution through a three-layered soil system at the interfaces with the aid of a digital computer. Peattie (1962) developed graphical charts to calculate the vertical stress factors through three-layered soils at interfaces using Jones tables. Applied loading stress is multiplied by the factor obtained from the chart to estimate the vertical stress. Influence diagrams for stresses in two-layer systems have been computed by Burmister (1965) with aid of a computer covering suitable ranges of the basic two-layer system parameters.

Analytical theories themselves do not provide a correct estimation of how the stress is distributed through the soil system and there could be disagreements between experimental methods, numerical methods, and analytical methods. An experimental study conducted by Kögler and Scheidig (1927; as cited in Akai et al., 1971) has shown that vertical pressure under the footing has been less spreader than the Boussinesq's solutions, and also there exists a zone of zero stress. This experiment has proven that the basic assumption of linear stress distribution under a loading plate could not apply to the actual situations and Fröhlich (1934; as cited in Akai et al., 1971) confirmed the research results by Kogler-Scheidig.

Since a great deal of time and effort had gone into the development of rational design methods, it was considered important to check the validity of this theory by experimentation. Akai et al. (1971) conducted a detailed investigation to study the stress distribution through two-layered soils. It can be seen that there is much deviation in experimental results with Boussinesq solutions at shallow depths while there is reasonable agreement at higher depths.

The finite element method (FEM) is a numerical method for solving partial differential equations in a continuum which is idealized as an assemblage of finite elements with specified nodes. Required accuracy is obtained by meshing and partial differential equations are transformed into a linear equation with the help of matrices.

Sadek and Shahrour (2007) conducted finite element analyses regarding elastoplastic states for both cohesive and frictional soils using FEA. From this study, it can be understood that the Boussinesq solutions underestimate the stresses in an area that corresponds to the plasticity state. Keller et al. (2016) studied soil stress under a rolling wheel using finite element analysis for three-layered soil. It can be understood that the soil deformation is elastic and reversible up to yield stress and beyond that, soil deforms plastically and irreversibly. Silva et al. (2018) conducted FEA to model the compaction of soil by presenting the changes in the initial stress condition due to vehicle traffic in the sugar cane industry. It is noted that the soils with higher moisture can propagate the stress to deeper layers and the concentration of vertical stresses immediately below the tires and slight overlap in the stress bulb at the latter parts.

3 METHODOLOGY

Computer models were developed by changing the strength and stiffness properties of soils, layer thicknesses of soils, and the position of soil layers.

4 MODEL VALIDATION

An experimental study on stress distribution that has been conducted for a single-layer system of sand by Akai et al (1971) is chosen for the model validation.

Normalized stress vs r/a charts have been plotted for four z/a values where the r is the horizontal distance from the center of the circular footing, a is the radius of the footing and z is the depth measured from the footing. Experimental normalized stresses are obtained from the charts and numerical normalized stress are obtained from the numerical model developed using PLAXIS 2D. Model validation results are presented in Fig. 1.

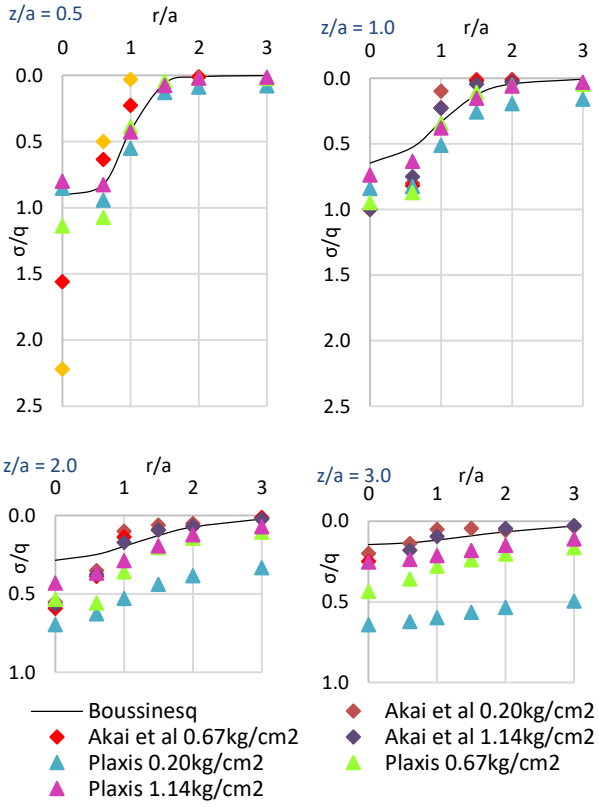

Fig.1 Results of model validation

5 NUMERICAL ANALYSIS

5.1 *Effect of soil properties on stress distribution*

Computer models were developed by changing soil properties of sandy and clayey soils and nine different combinations were obtained. Soil properties are shown in Table 1. All the cases were analysed by placing 5 m of sandy soil as the top layer (h_1) and 3 m of clayey soil as the bottom layer (h_2) as shown in Fig. 2.

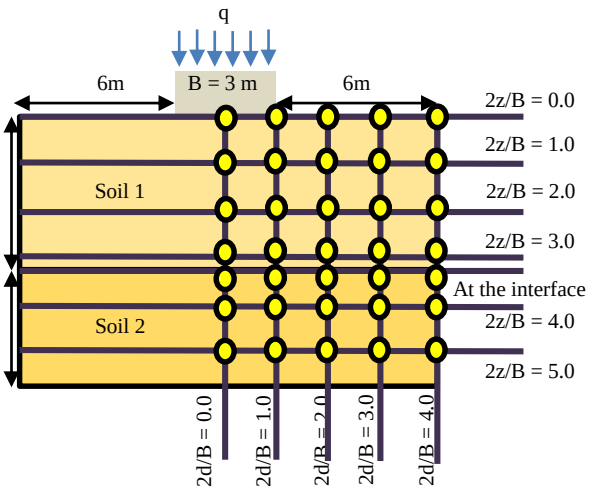

Fig. 2 Numerical model

A 3 m wide 0.6 m thick concrete strip footing is proposed for the study where the Elastic modulus (E) is 30 Gpa, Poisson's ratio (ν) is 0.15 and the density of the concrete is 25 kN/m^3. Elastic properties which need to be fed into the computer model were calculated as in Eq. (1), (2), and (3).

$$EA = 30{,}000{,}000 \text{ kN/m}^2 \times 0.6\text{m} = 1.8 \times 10^7 \text{ kN/m} \quad (1)$$

$$EI = (30{,}000{,}000 \text{ kN/m}^2 \times (0.6\text{m})^3)/12 = 5.4 \times 10^5 \text{ kN/m}^2\text{/m} \quad (2)$$

$$W = 25 \text{ kN/m}^3 \times 0.6\text{m} = 15 \text{ kN/m/m} \quad (3)$$

Half of the model was analysed using plain strain idealization. The water table was assumed to be located at the ground level and the Mohr-Coulomb model was selected to represent the soil properties. Drained behaviour and undrained behaviour were assumed for sandy soil and clayey soil respectively. The model was analysed using consolidation analysis and the simulation was divided into two phases where the first phase is to apply the foundation with load and specify a construction time of 1day and the second phase is to wait for the end of consolidation until the excess pore water pressure is less than 5 kPa.

A static load is applied with an intensity of 100 kN/m^2 and 15 kN/m^2 of the load is contributed by the self-weight of the footing. Hence the total load applied to the soil system is 115 kN/m^2.

Vertical stresses for horizontal distance from the center of the footing/radius (r/a) = 0, 1.0, 2.0, 3.0 to 4.0 at depth/radius of the footing (z/a) of 0.0, 1.0, 2.0, 3.0, 4.0, 5.0 and at interface are obtained. Vertical stress values were obtained for the locations which are marked in yellow circles in Fig. 2.

Normalized stress (σ/q) vs depth/width of the analysed portion of the footing (2z/B) are plotted at five different ratios of horizontal distance/ width of the analysed portion of the footing (2d/B). Since the Plaxis values are attributed to both the loading intensity and the geostatic stress, geostatic stress resulting from the dense sand and stiff clay was added to the Boussinesq solutions for a reasonable comparison. Fig. 3 includes the graphs plotted at 2d/B = 0, 1 and 2.

At shallow depths under the center of the footing, the cases where the dense sand at the top shows lower stress while loose sand shows higher stress at a selected point. When moving horizontally and vertically away from the footing, stresses at a particular depth show a better agreement with all the soil combinations as well as with Boussinesq solutions. Stress distribution of cases where there are similar sand types has nearly the same vertical stress at a particular depth and form sets when moving vertically and horizontally away from the footing as shown in Fig. 3.

5.2 *Effect of thickness of soil layers on stress distribution*

Computer models were developed by changing layer thicknesses for loose sand overlying stiff clay and dense sand overlying soft clay. Soil properties are shown in Table 1. Three cases were analysed by placing 5 m, 3 m, and 1 m of sandy soil as the top layer (h_1) and 3 m, 5 m, and 7m of clayey soil as the bottom layer (h_2) as shown in Fig. 2 and for each case, two soil combinations were used.

Static load (q) is applied with an intensity of 100 kN/m^2 for soil thickness in case 1, 75 kN/m^2 for case 2, and 50 kN/m^2 for case 3. 15 kN/m^2 of the load is contributed by the self-weight of the footing. Hence the total load applied to the soil system is q + 15 kN/m^2.

Geostatic stress resulting from each case was added to the Boussinesq solutions for a reasonable comparison. Fig. 4 includes the graphs plotted at 2d/B = 0, 1, and 2 for loose sand overlying stiff clay and dense sand overlying soft clay.

Table 1: Soil Properties

	Clay 1 Soft clay	Clay 2 Medium clay	Clay 3 Stiff clay	Sand 1 Loose sand	Sand 2 Medium sand	Sand 3 Dense sand
γ_{unsat} (kN/m^3)	15	16	18	15	17	19
γ_{sat} (kN/m^3)	17	18.5	20	16	18.5	20
kx (m/s)	1 x 10^{-6}	1 x 10^{-6}	1 x 10^{-6}	1 x 10^{-4}	1 x 10^{-4}	1 x 10^{-4}
ky (m/s)	1 x 10^{-6}	1 x 10^{-6}	1 x 10^{-6}	1 x 10^{-4}	1 x 10^{-4}	1 x 10^{-4}
Elastic modulus (kN/m^2)	3000	11000	35000	12000	30000	50000
Poisson's ratio	0.35	0.3	0.3	0.35	0.3	0.3
Cohesion (kN/m^2)	15	55	175	-	-	-
Friction angle (°)	-	-	-	25	30	35
Dilatancy angle (°)	-	-	-	-	-	5

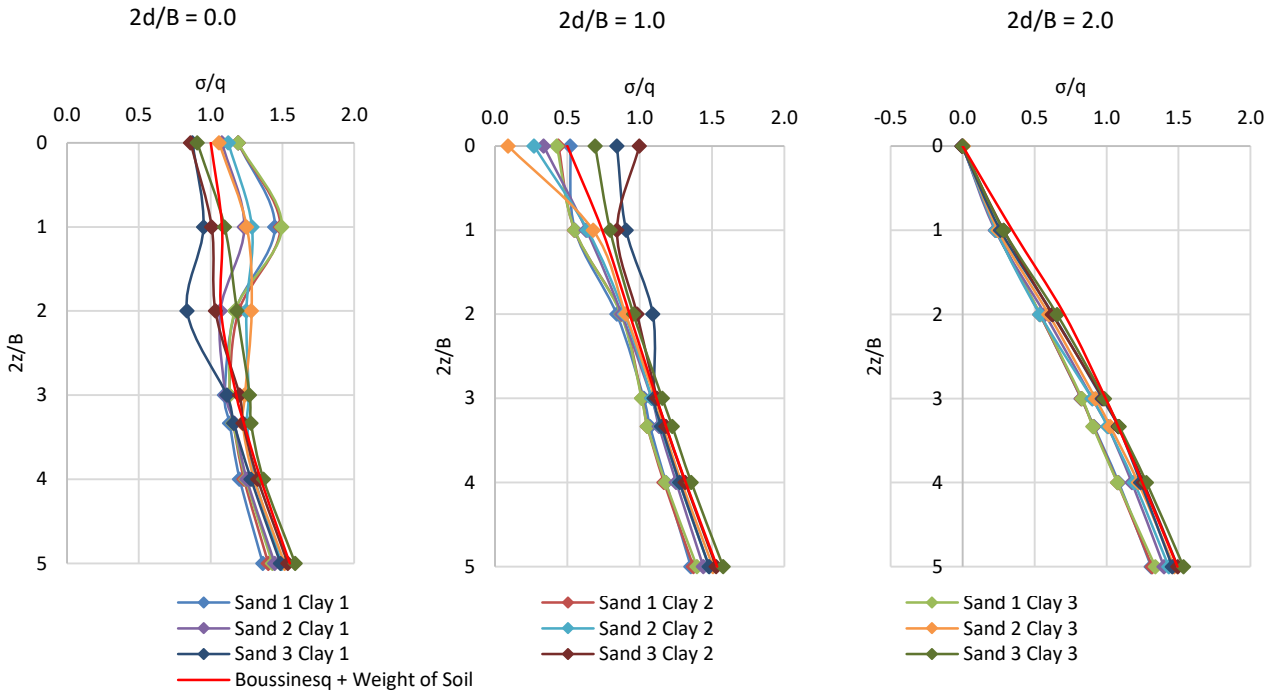

Fig. 3 Normalized stress vs depth with the variation of soil properties

For loose sand overlaying stiff clay, At shallow depths under the center of the footing, higher stress is acting on the soil when the layer thickness of the sand is increasing. The lower the sand thickness higher the stress acting on a particular point at greater depths. At the edge of the footing, the lowest stress value belongs to the case where the thickness of the sand layer is 3m and the clay layer is 5m. When moving away from the footing, normalized stress is similar at shallow depth for all the cases. Higher the depth lower the stress when the thickness of the sand is higher. Upward stress is generated in sand 1m clay 7m case at the surface level. Numerical values and Boussinesq values agree well when moving horizontally and vertically away from the footing.

For dense sand overlying soft clay, When the thickness of the sand layer is smaller, it initially gets lower stress compared to other cases under the center of the footing. The greater the depth greater the stress that would be taken by the case with the lowest thickness of sand. At greater depth, Boussinesq solutions agree with the FEA values. Stress propagation is lower compared to loose sand overlying stiff clay. At the edge of the footing, the lowest stress value belongs to the case where the thickness of the sand layer is 3m and the clay layer is 5m. Upward stress is generated in all the cases; sand 5m clay 3m, sand 3m clay 5m, and sand 1m clay 7m at the surface level. Plaxis values and Boussinesq values agree well when moving horizontally and vertically away from the footing.

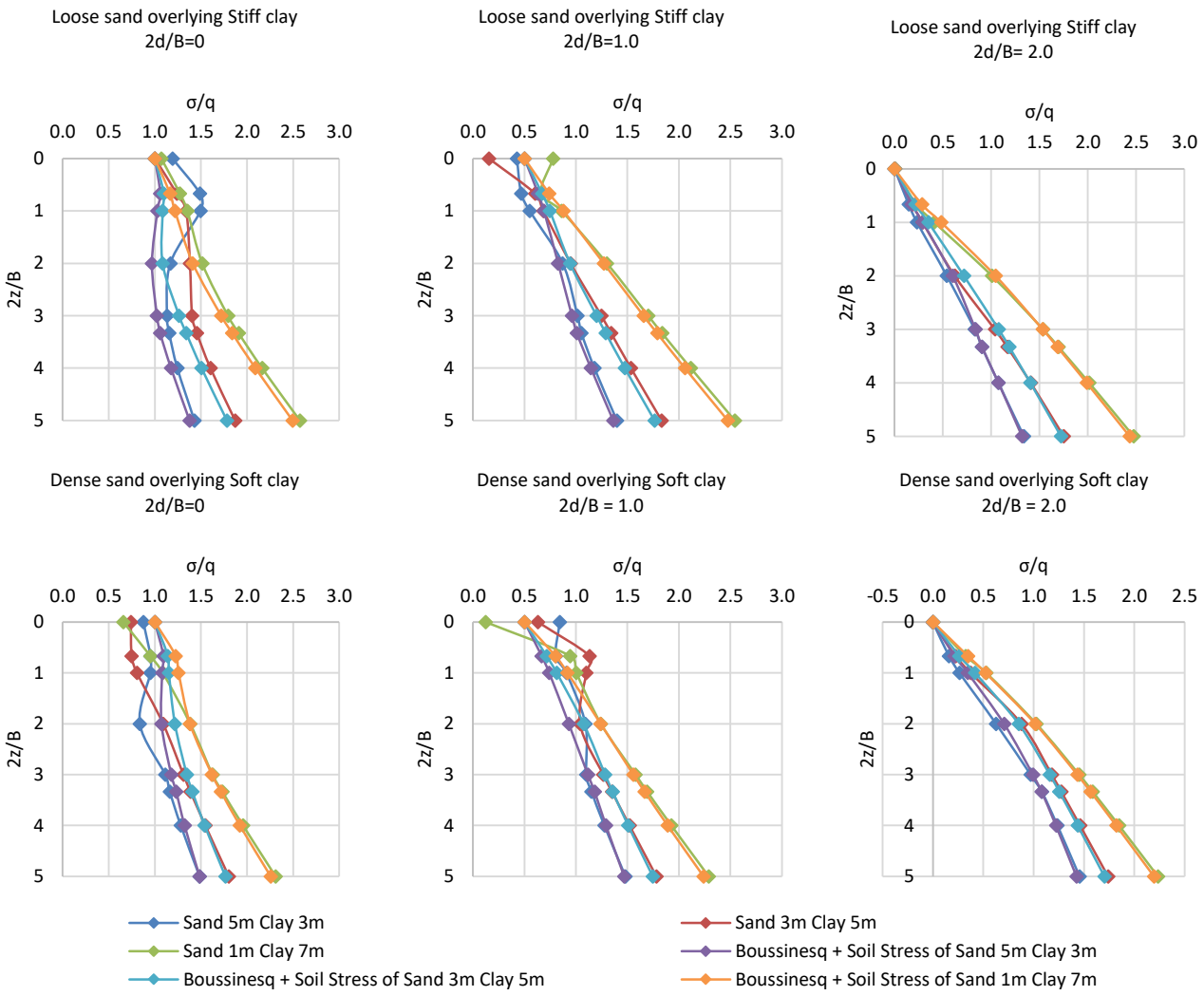

Fig. 4 Normalized stress vs depth with the variation of thicknesses of soil layers

5.3 *Effect of the position of soil layers on stress distribution*

Computer models were developed for loose sand overlying stiff clay, stiff clay overlying loose sand, dense sand overlying soft clay, and soft clay overlying dense sand and. Soil properties are shown in Table 1. Twelve cases were analysed for different soil combinations by placing 5 m, 3 m, and 1 m as the top layer (h_1) and 3 m, 5 m, and 7m as the bottom layer (h_2) as shown in Figure 2. Geodetic stress resulting from each case was added to the Boussinesq solutions for a reasonable comparison. Fig. 5 includes the graphs plotted at 2d/B = 0 for the sets described below.

For the cases where the top layer thickness is 5 m and the bottom layer is 3 m (set 1), the larger stress at a selected point is taken by the case with the stiff clay at the top. The stress at a selected point is low when the top layer is sand and further it is lower for the loose sand. Boussinesq solutions yield closer to FEA values when the top layer is clay and when moving away from the footing. Cases with dense sand at the top and stiff clay at the top show upward stress at the surface level.

For the cases where the top layer thickness is 3 m and the bottom layer is 5 m (set 2), lower stress at a selected point is taken by the cases where sand is at the top. The case with loose sand at the top shows higher stress at a selected point. It is contradictory when compared to set 1. All the curves converge closer with the depth and distance. This set shows less deviation of stress than other sets (set 1 and set 3)

For the cases where the top layer thickness is 1 m and the bottom layer is 7 m (set 3), larger stress is taken by the cases where sand is at the top. The highest stress at a selected point is shown by the case where the loose sand is at the top and stiff clay at the bottom. FEA values agree with the Boussinesq values when moving horizontally and vertically away from the footing.

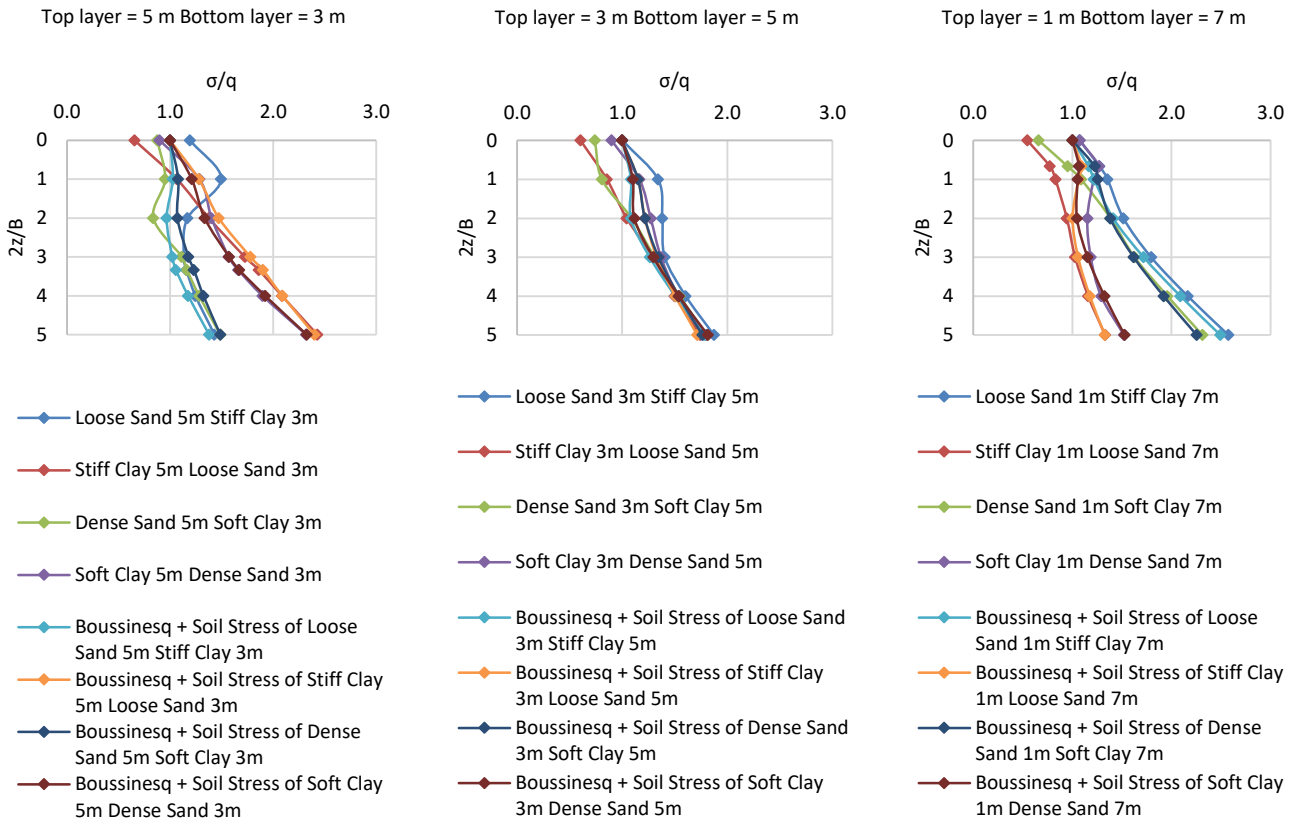

Fig. 5 Normalized stress vs depth with the variation of position of soil layers

6 CONCLUSION

Vertical stress at a selected point in soft and loose soil combination is smaller when compared to dense and stiff soil combination mainly due to the geostatic stress. The lower the thickness of the sand layer is higher the stress at a selected point. Dense sand overlying soft clay gives lower vertical stress compared to the loose sand overlying stiff clay. The top layer with clayey soil shows higher stress at a selected point when the top layer thickness is higher than the bottom layer thickness and stiff clay at the top shows the highest stress. Top layers with sandy soil show higher stress at a selected point when the top layer thickness is lower than the bottom layer thickness and loose sand at the top shows the highest stress. Boussinesq solutions provide a stress distribution reasonably close to the distribution obtained through FEA when moving away from the footing in both horizontal and vertical directions.

REFERENCES

Akai, K., Shiomi, S., & Kiuchi, T. (1971). Model studies on the stress distribution in layered soil systems. *Proceedings of the japan society of civil engineers*, *1971*(185), 83–94. https://doi.org/10.2208/jscej1969.1971.83

Boussinesq, J. (1885). Applications des potentiels à l'étude de l'équilibre et mouvement des solides elastiques, Gauthier–Villard, Paris

Bowles, J. E. (1988). *Foundation analysis and design*.

Brown, S. F. (1967). *Stresses and deformations in flexible layered pavement systems subjected to dynamic loads* (Doctoral dissertation, University of Nottingham). http://eprints.nottingham.ac.uk/id/eprint/11667

Burmister, D. M. (1945). The general theory of stresses and displacements in layered systems. I. *Journal of applied physics*, *16*(2), 89–94. https://doi.org/10.1063/1.1707558

Burmister, D. M. (1945a). The general theory of stresses and displacements in layered soil systems. II. *Journal of applied physics*, *16*(3), 126–127. https://doi.org/10.1063/1.1707562

Burmister, D. M. (1945b). The general theory of stresses and displacements in layered soil systems. III. *Journal of applied physics*, *16*(5), 296–302. https://doi.org/10.1063/1.1707590

Burmister, D. M. (1958). Evaluation of pavement systems of the WASHO road test by layered system methods. *Highway Research Board Bulletin*, (177). http://onlinepubs.trb.org/Onlinepubs/hrbbulletin/177/177-003.pdf

Burmister, D. M. (1965). *Influence diagrams for stresses and displacements in a two-layer pavement system for airfields. Part 1*. Columbia univ new york dept of civil engineering and engineering mechanics. Https://apps.dtic.mil/sti/pdfs/ad0614693.pdf

Das, B. M. (2017). Shallow Foundations: Bearing Capacity and Settlement, Third Edition (3rd ed.). CRC Press.

Hanna, A. M. (1987). Finite element analysis of footings on layered soils. *Mathematical modelling*, *9*(11), 813–819. https://doi.org/10.1016/0270-0255(87)90501-x

Jones, A. (1962). Tables of stresses in three-layer elastic systems. *Highway research board bulletin*, (342). http://onlinepubs.trb.org/Onlinepubs/hrbbulletin/342/342-008.pdf

Keller, T., Ruiz, S., Stettler, M., & Berli, M. (2016). Determining soil stress beneath a tire: Measurements and Simulations. *Soil science society of america journal*, *80*(3), 541–553. https://doi.org/10.2136/sssaj2015.07.0252

Murthy, V. N. S. (2002). By V.N.S. Murthy – Geotechnical Engineering: Principles and Practices of Soil Mechanics and Foundation Engineering (1st Edition) (9/25/02). Taylor & Francis Inc.

Peattie, K. R. (1962). Stress and strain factors for three-layer elastic systems. *Highway Research Board Bulletin*, (342).

Establishment of Threshold Rainfall Intensities for Critical Slopes in Sri Lanka

V. R Panagoda, Prof. S. A. S Kulathilaka

Department of Civil Engineering, University of Moratuwa, Sri Lanka

ABSTRACT: Most of the landslides are triggered by excessive rainfall. Sloping grounds in Sri Lanka are made of colluvial soils, residual soils, and rocks (metamorphic) at different levels of weathering. Groundwater table is low and high matric suctions prevail during dry periods. But with rainwater infiltration, matric suction would be lost, perched water table may develop, or groundwater table may rise developing instability. Susceptibility to landslide in hilly terrain was assessed by National Building Research Organization considering six terrain factors, and four levels of susceptibility were established. The threshold rainfall values triggering failure in these four regions would be different. Ideally, that should be obtained by proper modelling of infiltration and computing the resulting reduction of factor of safety. In the absence of such an analysis, threshold values based on experience are currently used in issuing warnings. The process should be improved by identifying site-specific threshold values. In this research, initially, a parametric study was conducted by applying different rainfall intensities for a typical high slope. The study was then extended to three actual landslides using GeoStudio 2018 software.

KEY WORDS: Landslides; Rainfall Threshold; Unsaturated Soil; Matric Suction; Infiltration

1 INTRODUCTION

The threshold values were introduced by studying the correlation between the landslide occurrences in Sri Lanka and the daily rainfall before the events (Bandara, 2008). A generalised form of thresholds has been used for the most landslide susceptibility areas in Sri Lanka at present. There is a need, to identify specific threshold value rather than the standard limits for intensities, to make decisions on early warning and evacuation in a more reliable manner. Therefore, three sites; Pinnawala, Badulusirigama and Ginigaththhena were considered in this research paper.

1.1 *Methodology*

First, a parametric analysis was conducted for a typically high cut slope with berms to identify the influence of; shear strength parameters, matric suction, rainfall intensity and duration on the rainfall threshold values. Then a recent landslide (Pinnawala) where rainfall records were available was back analysed to calibrate the process. Finally, the threshold rainfall values for two recently rectified critical slopes (Badulusirigama and Ginigathhena) were established, and the enhancement achieved with the rectification measures was studied. Infiltration and stability analyses were done through GeoStudio 2018 package.

2 PARAMETRIC STUDY

Parametric analysis for a typical high slope with berms was conducted to illustrate the influence of several parameters; shear strength parameters, rainfall intensity, duration, and matric suction on the rainfall threshold values. The complex weathering profiles were simplified in Figures 1 (a) and (b), with a uniform residual soil layer and a layer of residual soil overlying a weathered rock. The uniform slope was given a saturated soil permeability of 1×10^{-5} m/s and a saturated volumetric water content of 0.5. The permeability of the upper and lower layer in the two-layered slope is considered 1×10^{-5} m/s and 1×10^{-8} m/s, respectively.

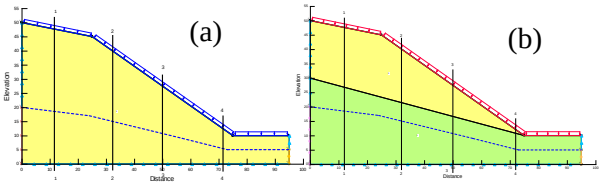

Fig. 1 Geometry of the Parametric Slopes

The water tables of the slopes are given in Figure 1. It was kept well below as the groundwater table in the dry season is quite deep from surface level. The continuous and intermittent rainfall intensities (5 mm/hr, 10 mm/hr, 20 mm/hr and 40 mm/hr) were applied on the ground surface for infiltration analysis.

Boundary conditions for infiltration analysis (Figure 1) were utilized, as explained in Kulathilaka and Sujeewan (2011). The upper bound for the matric suction of the unsaturated zone was introduced as 100 kPa. The slope stability was then analysed by the limit equilibrium approach using Spencer's method. The parameters varied in the analysis are presented in figure 2.

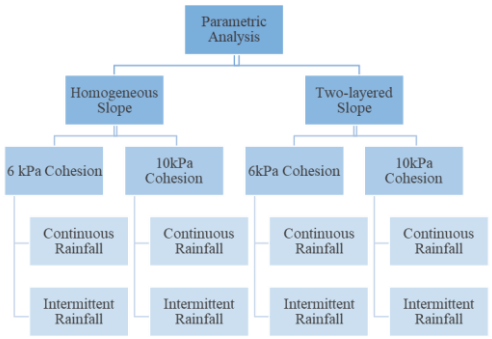

Fig. 2 Methodology of the Parametric Analysis

2.1 *Key findings*

2.1.1 *Effect of rainfall intensity*

As rainfall progresses, the matric suction reduces from its maximum value to zero at the near-surface of the slope. Development of the perched water zones is also notable at shallow depths when the rainfall intensity is larger (Figure 3(b)). Also, the rise of the groundwater table is prominent towards the toe. It may be due to the lateral flow from upper levels of the slope (Figure 3 (a)).

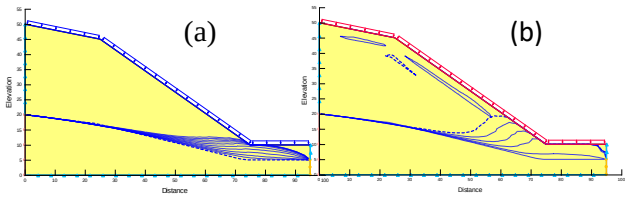

Fig. 3 The rise of GWT in homogenous slope for (a) 5 mm/hr and (b) 20 mm/hr Rainfall

The higher the rainfall intensity, the lesser the time required for failure as it reduces the near-surface suction when water infiltrates. Those slopes failed due to the advancing of the wetting front. When comparing the pore water pressure profiles of two slopes, the reduction of matric suction is rapid when there is a hard layer underneath. As the wetting front progresses, the matric suction is lost near the surface as rainfall continues. Due to the lower permeability of the hard layer, there is a stagnation of water and increase of porewater pressure closer to the boundary. Factor of Safety (FoS) reduces more rapidly under these conditions. The variation of FoS with time under different conditions is presented in Figure 4.

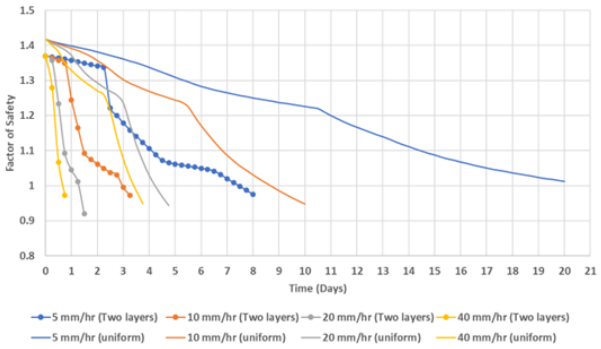

Fig. 4 Comparison of FOS variation between uniform and two-layered slope with 6 kPa cohesion that experience continuous rainfalls of different intensities

2.1.2 *Effect of intermittent rainfall*

Slopes that are subjected to intermittent rainfalls (with no rain on the alternate days) are stable for a longer duration of low-intensity rains. Even for 20mm/hr intermittent rainfall, pore water pressure just becomes zero, while continuous rain induces positive pore water pressure near the surface. Hence these slopes are stable for a longer period.

2.1.3 *Effect of cohesion*

When considering slopes with different cohesion, it is quite evident that slopes with lower cohesion become unstable quicker than those with greater cohesion (Figure 5).

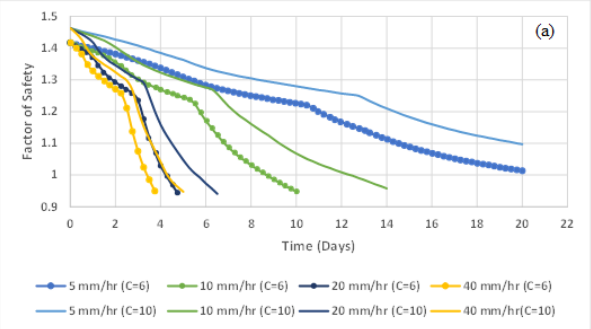

Fig. 5 FoS variation for homogeneous slope with cohesion of 6 kPa and 10 kPa for continuous rainfall

2.1.4 *Effect of matric suction*

The matric suction closer to the surface could have an upper limit (100 kN/m^2- Case 1) based on the characteristics of the soil, or it can follow the same gradient as hydrostatic (Case 2). The comparison of FoS variation under different rainfall intensities for the two cases of matric suction is shown in Figure

6. Case 2 has a high initial FoS, always higher than Case 1. Also, the development of a significant perched zone could be observed only for case 2.

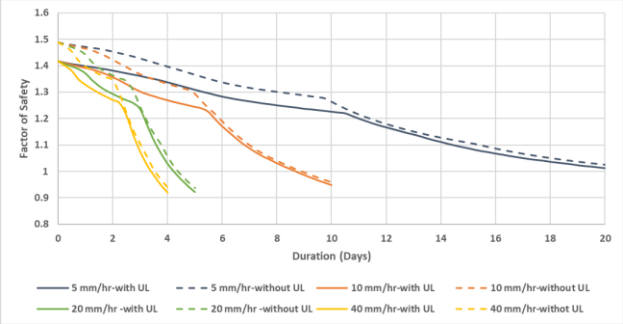

Fig. 6 Comparison of FOS Variation between With and Without Upper Limit for Matric Suction

2.2 *Summary on parametric study*

The threshold rainfalls were obtained under different initial conditions (cohesion and matric suction) for uniform and two-layered slopes. The relationships established between rainfall intensity and duration show a strong correlation ($R^2 \sim 0.9$) and are quite different to each other, as summarized in Figure 7. Results show that the low-intensity rains require more duration to trigger a failure. When the low permeable layer underlies the topsoil, the slope fails within a shorter duration. The slopes with a greater cohesive top soil layer are stable for a longer period. This variation in the response indicates the importance of site-specific threshold values for slope instability. Hence, this paper focuses on three actual landslides in different regions of Sri Lanka.

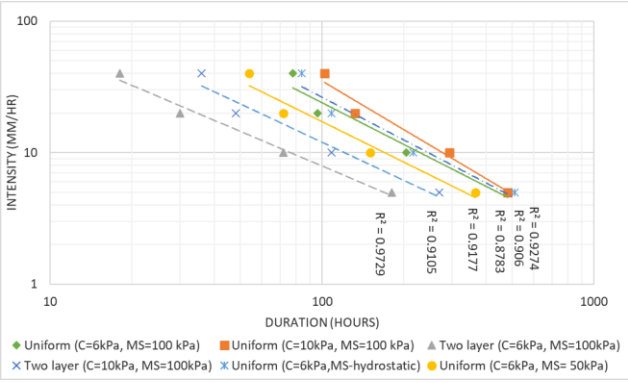

Fig. 7 Rainfall intensity-duration correlation for Slope with uniform residual soil and Slope with residual soil and rock layer

3 BACK ANALYSIS OF PINNAWALA LANDSLIDE

3.1 *Background*

Pinnawala landslide is in the Balangoda DS division in the Rathnapura district. The landslide was initiated in December 2013. A crack has appeared at the crest and propagated towards the toe. A complete catastrophic failure has not happened. According to the landslide susceptibility maps of NBRO, landslides are to be expected in this region. The slope stability was improved with surface drains in 2016 to minimize the possibility of further slope movements. The initiation of failure was back analysed to calibrate the process as the records of rainfall that triggered the failure are available. Subsoil data were established from investigations done during the rectification.

3.2 *Geology and Soil Properties*

During the investigation, three boreholes were drilled. The subsoil layers were mainly sandy silt and silty sand, which have a depth of 5.5 m to 7 m from the ground surface. And it is underlaid by highly weathered rock and the bedrock formed of Charnockitic gneiss. According to the information gathered in the boreholes, a 2D model was developed, as shown in Figure 8. The material parameters of the top layer were deduced based on laboratory test results. The other layers were assigned properties based on the description in borehole logs, SPT N values, and literature on similar soils. The assigned shear strength and hydraulic properties are given in Table 1.

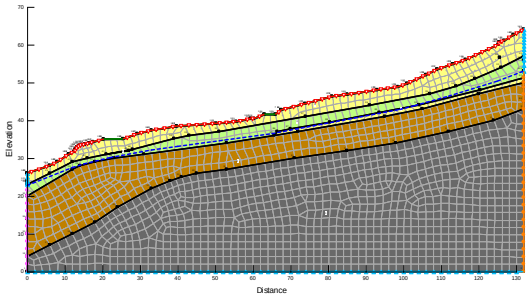

Fig. 8 Geometry, initial water table and boundary conditions of Pinnawala slope

As the initial water level before failure was not known, it was determined by a trial-and-error approach. As the rainfall event at failure is known, the slope was back analysed with different initial water levels to achieve the state of failure. The water table was first taken to be at a lower level and lifted gradually. When the water level is near the interface of 'Loose-medium silty sand' and 'Medium-dense silty sand', the slope reaches the marginal stability (FoS of 1.049) as given in Figure 9.

Table 1. Hydraulic characteristics and Shear Strength parameters of slope

Soil type	K_s (m/s)	Θ_{Sat}	γ(kN/m^3)	C (kPa)	ϕ
Loose-medium silty sand	1×10^{-5}	0.45	16	3	20º
Medium-dense silty sand	1×10^{-6}	0.5	17	6	18º
HWR	1×10^{-10}	0.4	18	10	30º
MWR	1×10^{-14}	Saturated	20	40	40º

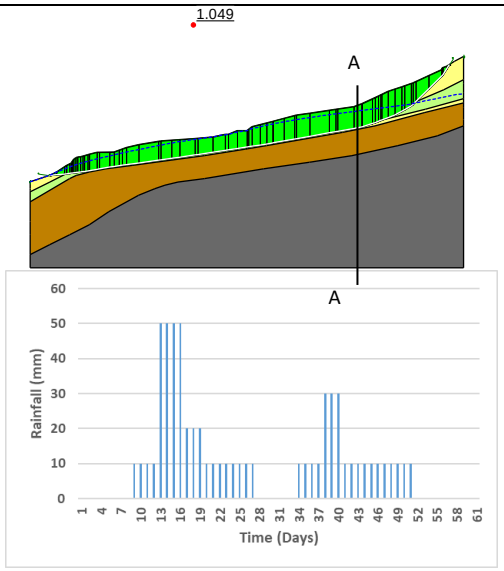

Fig. 9 FoS at failure of Pinnawala slope and Rainfall event at failure

3.3 *Rainfall event at failure*

The monthly rainfall data for the location in 2013 was obtained from National Building and Research Organization (NBRO). As the antecedent rainfall plays a great role in triggering a failure, the daily rainfall intensities are also essential. Hence the daily rainfall pattern presented in Figure 9 is assumed based on the total accumulated rainfall (620 mm) over November and December

3.4 *Interpretation of Results*

The slope was stable with a high safety factor (1.613) initially due to the high matric suction (nearly 50 kPa) resulting from low groundwater levels. But the water table moves upward with prolonged rainfall over 60 days. The water table rise was prominent towards the toe of the slope. The safety factor reduces vastly when the water table reaches the surface. The most critical failure surface obtained had a factor of safety of 1.049 (Figure 9) on the 40th day, simulating the actual failure in December.

3.5 *Effect of Rectification measures*

The slope was rectified with surface drainage measures in 2016. Surface drainage measures were modelled with the SEEP/W by incorporating a 50 mm thick low permeable layer over the slope surface to simulate the concrete drains and the vegetation cover. A parametric study was conducted by applying values of 10^{-6} m/s and 10^{-7} m/s for permeability. Comparison of the pore pressure profile changes due to the applied rainfall, with and without drainage measures, are given in Figure 10 (for section A-A in figure 9). Results show that the rise of the groundwater table is low when the surface drains are implemented. Because the low permeable upper layer restricts some amount of infiltration into the soil. Hence it is evident that drains can effectively prevent the rise of the GWT.

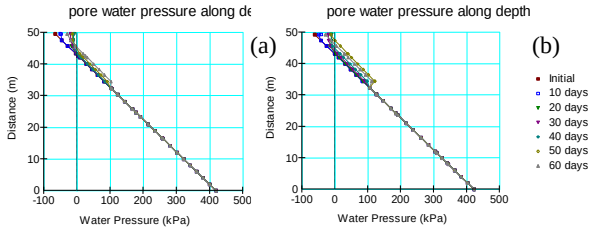

Fig. 10 Pore pressure profiles at section A-A (a) with and (b) without drainage measures

A comparison of variation in FoS values for slope with and without drainage measures is presented in Figure 11. Though the recorded minimum FOS of the slope without rectification is 1.05, it has improved to 1.08 and 1.21 with surface drainage measures (For assigned permeabilities of 10^{-6} m/s and 10^{-7} m/s). The percentage increase of FoS is about 9% and 30.4%. Hence, the results indicate that by improving the surface drainage – increasing runoff and reducing the infiltration (modelled here by reducing the permeability of a thin layer near surface) the lowering of FoS of a critical slope during a rainfall can be prevented to some extent.

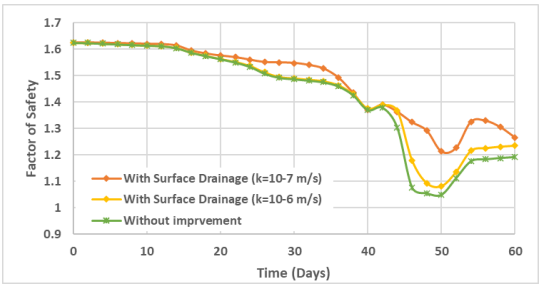

Fig. 11 Comparison of variation in FoS values for slope with and without drainage measures

4 THRESHOLD RAINFALL INTENSITIES FOR TWO RECTIFIED SLOPES

4.1 *Introduction*

Specific rectification measures are introduced to improve the stability of sites of critical importance. Those rectified slopes must be able to withstand a much heavier rainfall. Hence the threshold rainfall value of the slope should increase after the rectification. To validate the above aspect, two rectified slopes, Badulusirigama and Ginigathhena, were studied in this research. The analyses were conducted to assess prevailing conditions and behaviour after implementing the rectification measures.

4.2 *Analysis of Badulusirigama Slope*

Badulusirigama slope in the Badulla District was rectified mainly with surface and sub-surface drains. The bedrock of the site constitutes of Gneiss. On top of it, layers of highly weathered rock and colluvium soil are present. The shear strength parameters, hydraulic characteristics and the initial water level was obtained from (Kankanmge et al., 2020). The stability analysis was conducted with and without rectification measures under actual rainfall events in December 2014 and constant continuous rainfall of intensities 5 mm/hr, 10 mm/hr, 20 mm/hr and 40 mm/hr.

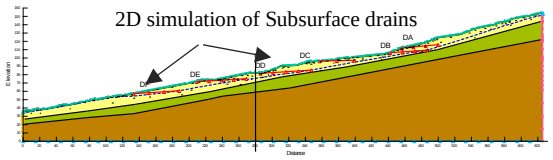

Fig. 12 Geometry and the simulation of subsurface drains of Badulusirigama slope

The continuous rainfall intensities (5 mm/hr to 40 mm/hr) were plotted against the duration it takes to fail before rectification. A strong correlation between rainfall intensities and duration was observed for all slip surfaces. Hence, if the rainfall intensity is known, the time taken for instability can be estimated more reliably.

Another set of analyses was carried out after the rectification to identify the effect on stability. Figure 13 compares factor safety before and after the rectification under actual rainfall events in December 2014. A significant improvement in the FOS of three slides was observed even after the heavy rainfall on the 65th day. Before rectification, the slope has a high groundwater table and little unsaturated zone. But after implementing the subsurface drains, a significant lowering in the water table can be seen even after the critical rainfall event. Even though the initial water table is high, it has reduced because subsurface drains drain out the water already on the slope, creating an unsaturated upper layer of considerable thickness.

The slides are stable and maintain a higher FOS for days throughout the designed continuous rainfall after rectification. A sudden increase in FOS (Figure 14) may be due to a rapid drainage path through the installed drains when water infiltrates the soil. The results indicate that the factor of safety values for any slide did not reach marginal stability when the subsurface drains were implemented. A rectified slope can withstand more heavy rainfall –the threshold rainfall will increase due to the rectification measures. This increased value could be used as a measure of the adequacy of the rectification process.

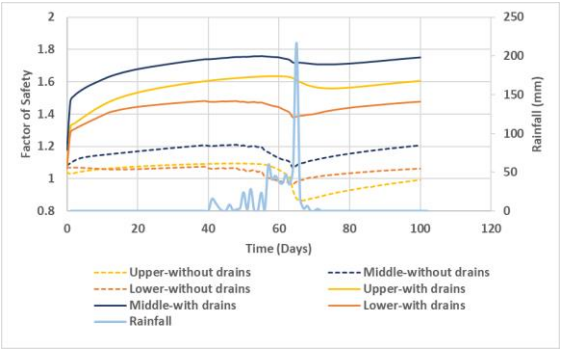

Fig. 13 Comparison of FoS variation of slope before and after rectification under rainfall events in December 2014

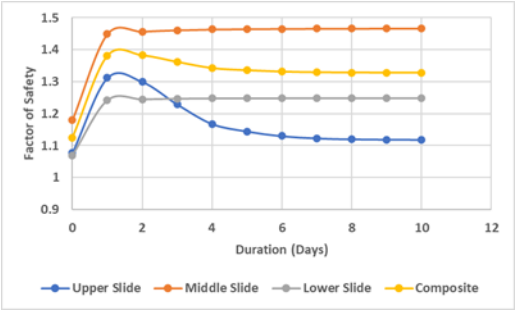

Fig. 14 FoS variation for 20 mm/hr rainfall after rectification of Badulusirigama slope

4.3 *Analysis of Ginigathhena slope*

The Ginigathhena slope was rectified with the surface drainage, subsurface drainage, and reinforcement by soil nailing. The initial water table, hydraulic characteristics, and shear strength parameters were applied as indicated in 'Evaluation of the Performance of Landslide Mitigation Measures at Ginigahthena' (Lakruwan & Kulathilaka, 2020).

A 5 mm/hr, 10 mm/hr, 20 mm/hr, and 40 mm/hr rainfall were applied on the slope with various drainage arrangements such as 'No Drains', 'Only Surface Drains' and 'Both Surface and Subsurface Drains' for 'With Nails' and 'Without Nails' conditions. The response of stability analysis is given in Figure 15.

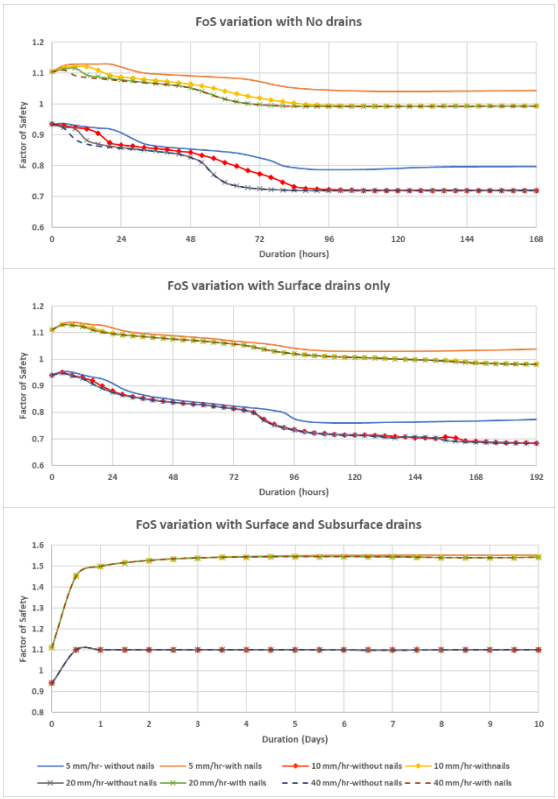

Fig. 15 FoS variation of slope with (a) No drains, (b) only surface drains and (c) surface and subsurface drains

When summarising the results obtained,

- The 'No drain' and 'Surface drain only' conditions without nails are always unstable for all selected rainfall intensities.
- Each drainage condition with nails, experiencing the 5mm/hr rainfall always have FoS greater than unity. For other rainfall intensities, threshold rainfall is very much greater.
- For every rainfall event, the slope with surface and sub-surface drainage are always stable.

The threshold rainfall values and the stability of the Ginigathhena slope for designed rainfall intensities are given in Figure 16.

Intensity (mm/hr)	Threshold rainfall (mm)					
	No drains		Surface drains		Surface & sub-surface drains	
	Without nails	With nails	Without nails	With nails	Without nails	With nails
5	Always Fos < 1.0	Fos > 1.0	Always Fos < 1.0	Fos > 1.0	Always Fos is around 1.1	Always Fos > 1.5
10		840		1440		
20		1360		2640		
40		1360		2640		

Fig. 16 Hydraulic characteristics and Shear Strength parameters of slope

5 CONCLUSION

As landslides are triggered mainly by heavy rainfall, it is important to identify the threshold rainfall intensities which cause sliding to prevent disasters. In the absence of critical rainfall intensity for a particular slope, currently in Sri Lanka, it is determined by previous experience. Hence, proper modelling of rainfall infiltration and the subsequent reduction of safety factors on slopes is essential. In this paper, a typical long infinite slope and three actual landslides were considered. A clear indication of an increase in threshold rainfall values was established. Hence, these slopes would be able to withstand intense rainfalls that may fall due to climate changes. And that will be important to take remedial measures and make decisions on early warning more reliable.

The slopes with varied rectification techniques reveal that subsurface drains, which lower the water table and partially desaturate the topsoil, more efficiently increase stability than surface drains. The surface drains are only effective while raining to facilitate runoff before infiltration. Though excessive rainfall is considered as the governing factor for slope instability, geology, geomorphology, physical processes, manmade processes, etc., also impact susceptibility to failure. Hence, these other factors also need to be incorporated depending on the scenario while making decisions on stability.

REFERENCES

Bandara, R.M.S.,(2008), Landslide Early Warning in Sri Lanka,Regional seminar on experience of geotechnical investigations and mitigation for landslides, Bangkok, Thailand , 13-14 October, 2008

Lakruwan, S. O. A. D. M., & Kulathilaka, S. A. S. (2021). Economising Soil Nailing Design by Drainage Improvement—Case History at Ginigathhena. In V. Vilímek, F. Wang, A. Strom, K. Sassa, P. T. Bobrowsky, & K. Takara (Eds.), *Understanding and Reducing Landslide Disaster Risk* (pp. 331–339). Springer International Publishing. https://doi.org/10.1007/978-3-030-60319-9_37

Kankanamge, L., Kulathilaka, S. A. S., Ganepola, G. A. C., & Nawagamuwa, U. P. (2020). Improving the performance of Badulusirigama Landslide using subsurface drains: A numerical study.

Kulathilaka, S. A. S., & Sujeevan, V. (2011). Rain triggered slope failures in unsaturated residual soils. *Geotechnical Journal, Journal of the Sri Lankan Geotechnical Society*, *6*, 20–26.

Sujeevan, V., & Kulathilaka, S. A. S. (2011). Rainfall infiltration analysis in unsaturated residual soil slopes. *Geotechnical Journal, Journal of the Sri Lankan Geotechnical Society*, *6*, 9–19.

Strength characteristics in fly ash- mixed Sri Lankan dredged clays in early curing

A.M.D. Rathnayaka and Dr. W.M.N.R. Weerakoon

Department of Civil Engineering, University of Sri Jayewardenepura, Sri Lanka

ABSTRACT: Dredged clay utilization for construction activities can be seen in several countries as a sustainable approach. Strength characteristics need to be studied to identify the potential for reuse. Fly ash is a highly available and cost-effective binding material. This study focuses on the strength characteristics of fly ash mixed with Sri Lankan dredged clays in early curing. Non-marine dredged clay from Bellanwilla and fly ash from Norochcholai power station were mixed as a volume-based ratio of 5%, 10%, 15%, and 20% of fly ash contents. Undrained shear strength was obtained by direct shear test (DST) and unconfined compression test (UCT). The pH measurements were taken to observe the alkalinity of the mixture during the curing time. Results show the strength improvement with increasing fly ash content and curing time. Undrained shear strengths from the DSTs and the UCTs were well compared and low undrained shear strengths for UCTs were observed in all testing.

KEY WORDS: Dredged clay, fly ash, strength characteristics, early curing, Portlandite

1 INTRODUCTION

Dredged clay (DC) is a material excavated in the dredging process to remove the materials deposited on the bottom or side surfaces of the water bodies. In Sri Lanka, the maintenance and development of ports, land reclamation, and coastal construction activities produce a high volume of dredged clays. Maintenance of reservoirs, construction of flood control structures, and wetland development activities produced non-marine dredged clays. Disposal of DC affects the marine ecology and survival of marine flora and fauna. Therefore, the reuse of dredged clay is important to avoid negative environmental impacts and get economic benefits. Fly ash (FA) is produced in thermal power plants and industrial boilers by the combustion of pulverized coal, as waste material. Since Sri Lanka annually produces 150,000 tons of fly ash as a residue from coal burning, it has the potential to use as a binder for solidification Gimhan, et al (2017). The chemical composition of fly ash has the potential to increase strength by forming bonds. Therefore, several studies suggest binding with fly ash Phetchuay et al (2016); Jamsawang et al (2020). ASTM D 5239 provides the standard practice for FA use as a soil stabilizer. The pozzolanic reaction produces CSH gel which has cementitious properties.

According to past studies, dredged soil can be mixed with different binders such as cement, lime, fly ash, steel slag, cement kiln dust, ground granulated blast furnace slag, and quarry dust. Some studies have been done to identify the strength improvement and factors that influence the strength gain when treated with cement Kang, et al (2015); Xiao, et al (2014). Consequently, some studies have done dredged soil mixed with steel slag to identify strength mobilization and factors that affect strength development Toda et al (2018); Weerakoon (2018). There are many coastal construction activities in Sri Lanka, and dredged clay can be effectively utilized for backfilling, road sub-base construction, land reclamation, and other activities. Despite some studies based on the reuse of DC and FA still, a lack of complete and detailed studies about the strength characteristics of FA mixed with Sri Lankan DC. The main objectives of this study are listed below.

(i) To identify the variation of strength characteristics with curing time.
(ii) To identify the variation of strength characteristics with fly ash content.
(iii) To identify the pH variation in the mixture from immediately after mixing to 7 days of curing.
(iv) To compare the results obtained from the direct shear test (DST) and unconfined compression test (UCT) curing period ranging from 3 days to 28 days.

2 METHODOLOGY

2.1 *Materials*

Non-marine dredged clay was collected from the dredging operations in Bellanwilla, Sri Lanka. Initially, the sample was sieved through 2 mm mesh (No.10) to remove coarser materials. ASTM D4318 was followed to determine the Atterberg limits. ASTM D6913 and ASTM D7928 were followed for determining the gradation.

Table 1. Physical properties of dredged clay

Plastic limit (%)	Liquid limit (%)	Plasticity index	Wet Bulk density (g/cm^3)
33.3	46.0	12.7	1.90

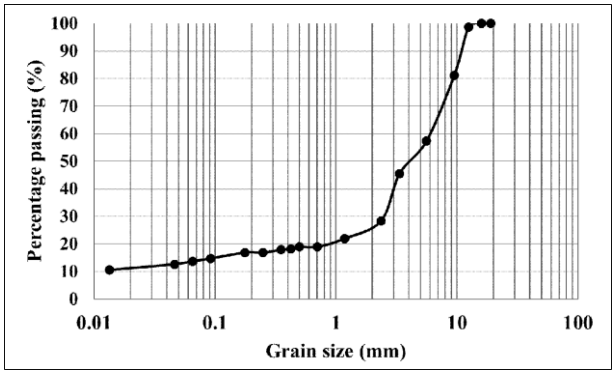

Fig. 1: Particle size distribution of dredged clay

Sri Lankan FA produced in Norochcholai was used in laboratory testing. It was carefully collected and stored to avoid any moisture.

Table 2: Physical properties of fly ash

Bulk density (g/cm^3)	Specific gravity (G_s)	Moisture content (%)
1.16	2.10	0.7

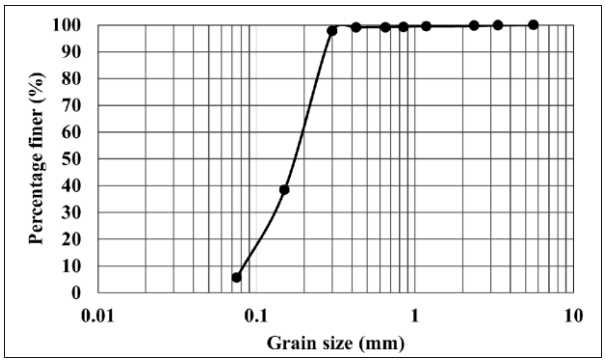

Fig. 2: Particle size distribution of fly ash

2.2 *Sample preparation*

The specimens for the laboratory testing were prepared in a volume-based ratio by mixing dredged clay with four different mixed proportions of fly ash. Fly ash content, α, is defined in the following Eq. (1).

$$\alpha = \frac{v_f}{v_f + v_c} \times 100\% \qquad (1)$$

Where v_f and v_c are the volumes of fly ash and volume of dredged clay respectively. The α values for this study were selected as 5%, 10%, 15%, and 20%. The water content of a dredged clay sample was first increased to 1.5 times its liquid limit by adding distilled water and, the sample was thoroughly mixed for about 3 minutes using a spatula.

Table 3: Summary of sample preparation

Test	Number of samples				Total
	5% FA+95% DC	10% FA+90% DC	15% FA+85% DC	20% FA+80% DC	
DST	10	10	10	10	40
UCT	12	12	12	12	48
pH	7	7	7	7	28
					116

2.3 *Mechanical testing methods*

2.4 *Direct shear test (DST)*

Direct shear apparatus was used to measure the shear strength of soil, and here the strain-controlled test was used. A motorized and floor-mounted automatic direct–residual shear test machine (UTS-2060.SMPR) was used. The test series was performed in accordance with ASTM D3080. 1 kPa vertical stress and the shearing rate of 2 mm/min were applied in this test series.

2.5 *Unconfined compression test (UCT)*

Testometric M350-CT10 electro-mechanical tensile testing machine in compression state was used in the test series. ASTM D2166 was followed, and the test series was performed under the 2% per minute strain rate. The unconfined compressive strength (q_u) is defined as the maximum stress during the testing.

2.6 *pH measurements*

The pH meter was calibrated before the use according to the manufacturer's guidelines. ASTM D 4972 – 01 (2007) was followed to find the pH changes.

3 RESULTS AND DISCUSSION

3.1 *Evaluation of shear strength characteristics*

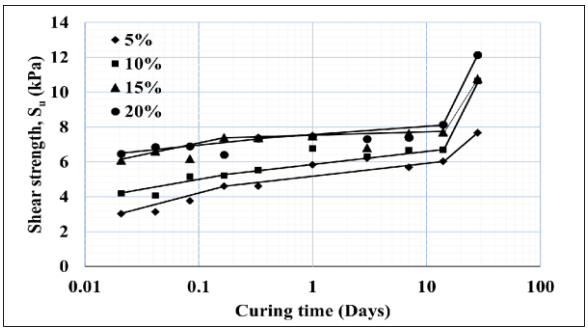

Fig. 3: The relationship between shear strength and curing time with trend lines in semi-log scale.

DST was performed for all mix proportions at the curing period starting from 0.5 hours to 28 days. According to the variation in each series, strength improvement can be divided into three different stages. In 5%, 10%, and 15% mix proportions, the first stage shows significant strength improvement, curing period ranging from 0.5 hours to 4 hours. However, the 20% mix proportion shows relatively low strength improvement in the first stage, lasting from 0.5 hours to 8 hours. Further diffusion and dissolution of fly ash in the mixture are continued at this stage. Between 4 hours and 14 days curing period can be observed as the second stage of 5%, 10%, and 15% samples, while 8 hours to 14 days in 20% sample. The third stage was observed from 14 days to 28 days of curing time, which shows a relatively higher strength improvement than the other two stages.

All the test results in each curing period have proved that S_u was increasing with curing time and FA content. Fig. 4 also illustrates that the 28 days samples have achieved relatively higher shear strength than other mix proportions. An increase in the potential of C-S-H bond formation can be expected by increasing FA concentration.

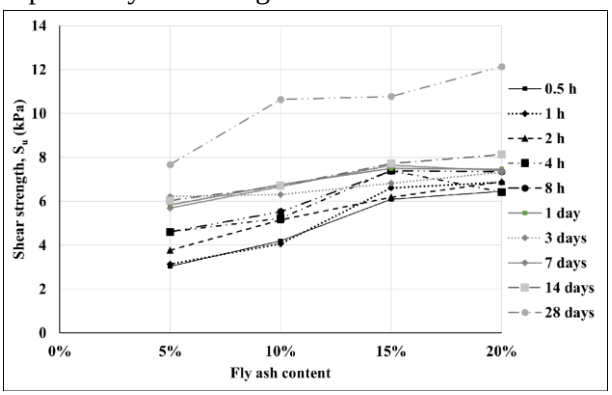

Fig. 4: Relationship between S_u and fly ash content

3.2 *Variation of unconfined compressive strength*

Table 4: Unconfined compression test results

	Curing day (Days)	5%	10%	15%	20%
Mean (kPa)	3	2.06	3.56	5.48	5.67
	7	2.55	4.73	5.99	7.01
	14	3.65	5.21	5.88	8.13
	28	7.95	11.82	13.49	12.26
Range (Max-Min) (kPa)	3	0.98	0.52	1.04	0.58
	7	0.69	1.62	1.21	0.28
	14	1.44	3.17	1.09	1.85
	28	1.61	1.96	5.08	3.06
Coefficient of variation (%)	3	24.48	8.00	10.19	5.63
	7	14.52	17.26	14.82	16.17
	14	19.73	30.53	9.60	11.38
	28	10.20	8.33	19.19	13.46

The unconfined compressive strength (UCS) was defined at the state of the maximum load acting on the specimen and stress value at this state. Since the 3 days after the curing, it had to withstand itself, UCS values were obtained for 3 days, 7 days, 14 days, and 28 days. Table 4 represents the mean, range between maximum and minimum test results, and coefficient of variation with respect to three independent tests. Since UCS is varied in the range of 0-25 kPa the soil can be classified as very soft clay according to the general relationship between consistency and UCS of clays DAS (2009). All the mixed proportions illustrate an increasing trend of UCS with respect to the curing period, and a significant difference in the rate of strength increment can be observed in 15% samples.

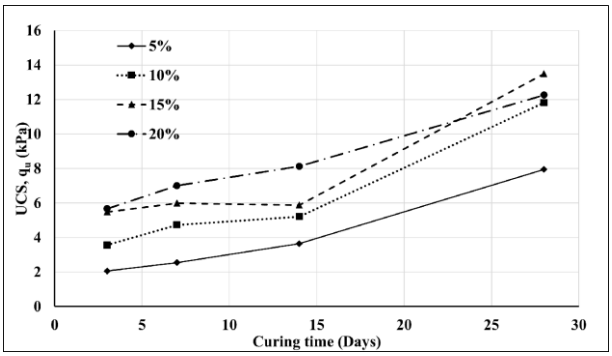

Fig. 5: Variation of q_u with curing time

Fig. 6 has proved that q_u increases with the FA content of the sample. Samples in 3, 7, and 14 days show a relatively similar trend of q_u improvement while 28 days showed another variation.

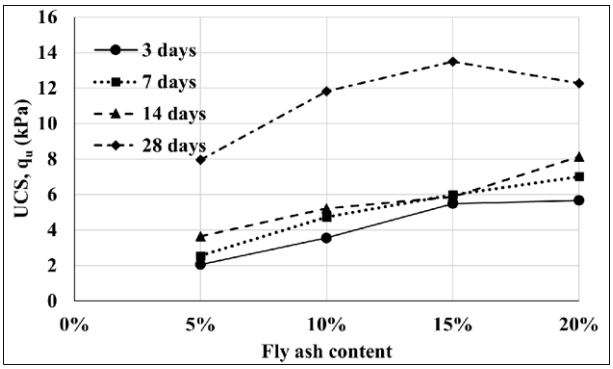

Fig. 6: Variation of unconfined compressive strength q_u with the fly ash content

3.3 *Comparison of direct shear test results and unconfined compression test results*

Dredged clay mixes with 5%, 10%, 15%, and 20% of FA samples at curing periods ranging from 3 days to 28 days were considered for the comparison of strength values obtained by DST and UCT. Fig. 7 illustrates the comparison and deviation from the 1:1 ratio.

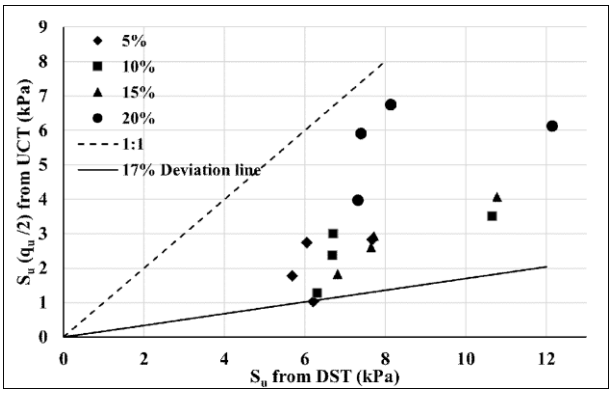

Fig. 7: Correlation between shear strength obtained by direct shear test and unconfined compressive strength obtained by unconfined compression test.

All the data points have shown that S_u obtained by UCT is lower than S_u obtained by DST. 17% maximum deviation line was introduced where the point showing the most significant variance intersects. 5% sample at 3 day curing period showed the 5.18 kPa (16.58%) maximum deviation. Low hardening characteristics due to low FA content and low curing period can cause that. 20% of fly ash samples show a relatively low percentage of variation with the 1:1 line, which means UCT test results tend to achieve a 1:1 relationship with the strength improvement. Since all the test results are below 13 kPa and DST results are higher values, DST results are the most reliable.

Since the sample was fully covered until the testing, it remained in the soft state. A horizontal failure plane exists in DST, while failure planes along the vertical direction can be observed in UCT. The plane of the specimen failure may not be the weakest plane of the specimen, which results in the variation of results. The heterogeneous nature of the materials, unidentified constituents in the materials, improper mixing, instrumental errors, anisotropic nature of the rate of loading, and human errors may be affected to slight deviations. Environmental factors such as temperature and humidity can be affected because all the samples for the same combination were not prepared at once.

3.4 *pH variation in fly ash – clay mixture*

The values range between 8.1 and 10.4, which shows a decreasing pattern. Samples with high FA content show a high pH value due to the oxides present in FA creating an alkaline nature. 5%, 10%, 15%, and 20% FA content samples have 8.3, 8.8, 9.6, and 9.9 initial pH values after the 1 hour. This is a relatively low capacity for the pozzolanic reaction and that proves the low strength observed in the DST and UCT series.

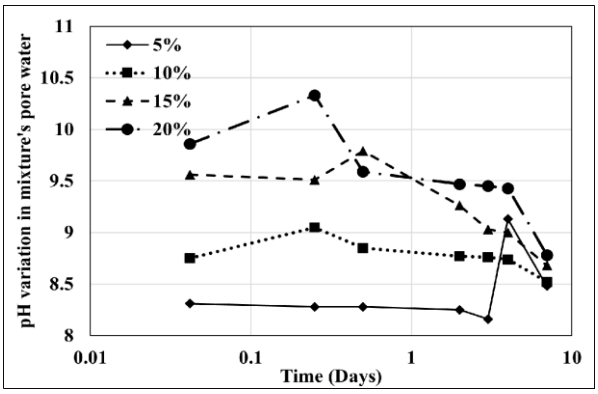

Fig. 8: pH variation in fly ash-dredged clay mixtures' pore water with curing time

Organic content and acids present in the mixture interrupt the pH rise in the mixture. Also, the increase in organic matters hinders strength improvement and increases the strength loss. A study of four DC and one non-marine DC mixed with 30% steel slag has identified a decreasing trend in pH during the curing period ranging from immediately after mixing to 91 days (Weerakoon, 2018). Accordingly, relatively high initial pH readings and high strengths have been observed. This also shows the deviation with different DC. A further drop in pH after the 7 days can be expected with further strength improvement.

4 CONCLUSIONS

This study focused on the strength characteristics of fly ash mixed with Sri Lankan dredged clay in early curing based on laboratory mechanical test series. One non-marine dredged clay was mixed with four fly ash combinations as 5%, 10%, 15%, and 20%. The changes in the properties were observed in short to medium curing times ranging from 0.5 hours to 28 days. The strength characteristics were analyzed using a direct shear test (DST) and an unconfined compression test (UCT). pH variation in each combination was observed initially after mixing to 7 days of curing.

(i) Shear strength increment can be divided into three different stages, 0.5 hours to 4 hours, 4 hours to 14 days, and 14 days to 28 days. The third stage shows a higher strength gain.

(ii) Test results revealed that strength increases with fly ash content and curing time. The 12.14 kPa of maximum shear strength, which was approximately doubled the initial shear strength, was obtained in 20% of fly ash content at 28 days of curing time.

(iii) The increasing trend was observed in unconfined compressive strength concerning time and fly ash content. The 13.49 kPa maximum value was observed in 15% of fly ash content at 28 days of curing time.

(iv) When comparing test results of both tests, DST results are always higher than half of the UCT results.

(v) The pH value increases with the fly ash content due to the oxides present in FA creating an alkaline nature and the decreasing trend of pH was also observed with the strength improvement of the sample.

Further tests and investigations can be done with different clay types, fly ash contents, water contents, environmental conditions, and adding other binder materials. In addition to strength tests loss on ignition, XRD test, and morphological analysis can be performed.

ACKNOWLEDGEMENTS

I would like to extend my gratitude to the Department of Civil Engineering, Faculty of Engineering, University of Sri Jayewardenepura for giving me the opportunity to do this research project.

REFERENCES

DAS, B. M., 2009. Principles of Geotechnical Engineering. Seventh Edition ed. Stamford: Cengage Learning.

Gimhan, P., Dissanayaka, J. & Nasvi, M., 2017. Suitability of Fly Ash Produced at Lakvijaya Coal Power Plant as a Light Weight Embankment Material.

Jamsawang, . P. et al., 2020. Mechanical and microstructural properties of dredged sediments treated with cement and fly ash for use as road materials. Road Materials and Pavement Design.

Kang, . G., Tsuchida, . T. & Athapaththu, A. M., 2015. Strength mobilization of cement-treated dredged clay during the early stages of curing. Soils and Foundations, 55(2), pp. 375-392.

Phetchuay, C. et al., 2016. Strength development in soft marine clay stabilized by fly ash and calcium carbide residue based geopolymer. Applied Clay Science.

Weerakoon, N. R., 2018. Characteristics of stiffness and strength mobilization in steel slag-mixed dredged clays from immediately after mixing.

Xiao, H. W., Lee, F. H. & Chin, K. G., 2014. Yielding of cement-treated marine clay. Soils and Foundations, 54(3), pp. 488-501.

Toda, K. et al., 2018. Key factors affecting strength development of steel slag-dredged soil mixtures. Minerals, 8(5), pp. 1-16.

Numerical Modeling of Gravel Compaction Piles in Soft Soil under Drain Condition

T.K.S. Fernando and N.H. Priyankara
Department of Civil and Environmental Engineering, University of Ruhuna, Sri Lanka

ABSTRACT: Soft soil has become a major problem in the field of Civil Engineering. The solution that discussed in this paper is the improvement of soft ground using Gravel Compaction Piles (GCP). However, the knowledge on the behaviour of GCP improved ground under drain condition is less. Therefore, a numerical analysis was done using PLAXIS-2D software to study the effect of drainage on the stability of GCP improved ground. The 3D condition was modelled in to 2D using the parameter conversion method. The effect of permeability of GCP material was studied by considering the permeability ratio between GCP and surrounding soft soil. Based on the analysis, it was identified that, when the permeability ratio is more than 100, it increases the stability of the GCP improved ground. The effect of stiffnesses of surrounding soil was found for different permeability ratios too. The effect of encasement for the composite ground has also discussed in this paper. Finally, the critical length of the GCP was found as 15 m.

KEY WORDS: Gravel Compaction Piles, Numerical Modeling, Parametric Study, Smear Zones

1 INTRODUCTION

Every section in the world develops with time including the construction field as well. The first stage of every construction is to investigate the ground condition as most of the structures are made on the ground. Ground condition is highly dependent on the available soil layers at that particular place. Some soils are capable of bearing the load of the structures, while some do not. The reason behind that incapability may be the characteristics of a particular soil element. Due to low shear strength, high compressibility, or position of the water table, failure can occur. The structure may settle unevenly or collapse due to the unsuitable soil structure. Therefore, it was the method in earlier to abandon those places containing weaker soil (soft soil) when constructing structures. But because of the increase in population and development, places with suitable soil conditions have become limited. To fulfill human requirements, soft soil has become a problem to overcome. One reason to overcome that problem was limited suitable land area requirement, and the other one is it won't be economical to pass the unstable grounds while constructing, especially roads, bridges, and embankments. Scientists and engineers proposed different methods to overcome that matter. Two of the best solutions were to improve the ground condition to withstand the load or transfer the load to the underlying hard stratum through piles.

However, transfer the structural load to underlaying hard stratum through piles is not an economical option for roads that occupy a large plan area and moderately loaded buildings. As the load transferring method is not possible everywhere, ground improving techniques have become the most preferable method.

Under the ground improvement techniques, columnar inclusion plays a major role. Many columnar inclusion methods are practicing in the construction field. For this study, the method that discussed is the Gravel Compaction Piles (GCP). Two main roles are performed by GCP in the field. First is, it increases the bearing capacity of the soft soil since a stiffer material is used as the GCP material. The other role is, it acts as a drainage path. Since the GCP material is a highly permeable material, pore water can flow through the GCP. Therefore, the rate of consolidation increases in the GCP improved soft ground. However, drainage behaviour of the GCP is very rarely discussed.

One of the most common soft soil types in Sri Lanka is the peaty clay. Peaty clay has a problematic nature due to its high-water content, high compressibility and very low shear strength. Those factors are not favorable factors for constructions. On the same time, the most commonly used GCP material in Sri Lanka is Aggregate Base Course (ABC). Since it is a well graded material, after the compaction, the permeability of the GCP material is considerably low. Due to large horizontal permeability of peaty clay, pore water flows towards the GCP and through the GCP, water flows out vertically. However, due to low permeability of GCP material (ABC), the performance of the GCP is questionable.

Even though GCPs have been successfully applied in many expressway projects in Sri Lanka, it

was failed in the Southern Expressway Extension Project section-1 from Matara – Beliatta. This clearly implies that, there is less knowledge on the behavior of GCP. Since this is an underground improvement method, the best way of analyzing its behavior is using the Finite Element Methods (FEM).

There are very limited studies on the behaviour of GCP in Sri Lankan peaty clay using FEM analysis. As such, this research study was carried out to identify the behaviour of GCP improved composite ground in Sri Lankan peaty clay using PLAXIS-2D analysis. In order to achieve this aim, first numerical model was developed and validated using the available field data, Then, the behaviour of the GCP improved ground was investigated by varying the drainage condition, surrounding pressure and GCP length.

2 LITERATURE REVIEW

Since the real data are available for the 3D condition, it is necessary to convert 3D condition in to 2D condition for the PLAXIS-2D analysis. To convert from axisymmetric mode (3D condition) to plane strain mode (2D condition), two methods were introduced by Tan et al., (2008), namely Parameter matching scheme and Geometry matching scheme. In the parameter matching scheme, only parameters are changed while geometry has kept as it is. Geometry means the column diameters and drainage zones. Converting parameters are stiffness of the column material and permeability of soft soil. In the geometry matching scheme, only geometry has changed while keeping material parameters constant. This method is established based on the equivalent drainage capacity of the column in the axisymmetric and plane strain condition (Tan et al., 2008). This concept is originally developed for conversion of vertical drain system to equivalent plane strain drain walls (Indraratna & Redana 1997). Therefore, geometry has converted while parameters have kept as it is. For this research study, both the methods have been used.

3 METHODOLOGY

In order to find the behaviour of GCP improved composite ground, following procedure was carried out.

3.1 *Development of the model*

In order to validate the model, all material parameters were taken from the actual data of Outer Circular Highway Northern Section-1 (OCH-NS1) Project (Karunawardana et al., 2017). The Developed models using both conversion methods are described in the following section.

3.1.1 Geometry conversion method

Geometry has to be converted from 3D case to 2D case as this model is following the parameter constant method. A row of actual GCP is represented by a trench in the plain strain (2D) method. In this conversion, the volume of gravel material in the row of GCP is equal to the volume of the trench. For this analysis, whole area around the GCP was considered as smear (disturbed) zone.

As such, there is no any undisturbed area around the GCP. The margin of the smear zone was taken as 0.64 m away from last GCP. The model considered for the analysis is shown in Figure 1.

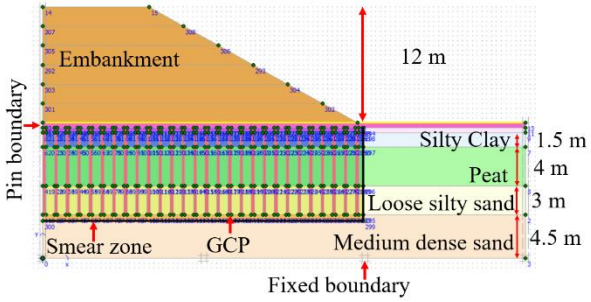

Fig. 1 Developed model

The original parameters were used for geometry conversion method as shown in Table 1. For other parameters, certain values were assumed based on the literature review. Horizontal permeability of the smear zone was taken as one third of the original value (Indraratna & Redana 2000).

Table. 1 Soil properties used in geometry conversion method (Karunawardana et al., 2017)

Parameter	Unit	Embankment	GCP	Silty clay	Peat	Medium dense sand
Material model		Mohr-coulomb	Mohr-coulomb	Mohr-coulomb	Soft soil	Mohr-coulomb
Type of behavior		Drained	Drained	Undrained	Undrained	Drained
Unit weight	kN/m^3	18	19	17	11	17
Horizontal permeability	m/day	1	19.2	0.03	0.0003	0.5
Vertical permeability	m/day	1	19.2	0.01	0.0001	0.5
Youngs modulus	kN/m^2	50 000	30 000	25 000		81 000
Poisson ratio		0.3	0.3	0.3		0.3
Cohesion	kN/m^2	5	1	3	1	1
Friction angle	deg	32	36	20	16	45
Dilatancy angle	deg	0	0	0	0	0
Modified compression index	Cc'				0.075	
Modified swelling index	Cs'				0.012	

3.1.2 Parameter conversion method

In parameter conversion method, there is no need to change the geometry. Therefore, actual diameter and spacing values can be used for modelling. According to Webber et al., 2006 diameter of the smear zone is estimated as two times the column diameter.

As in the geometric conversion method, smear zones of two piles are intersected. As such, whole area around the GCP was considered as smear zone. Hence, there is no any undisturbed area around GCP. The margin of the smear zone was taken as 0.7 m away from last GCP. The material parameters used for the analysis was same as the geometric conversion method as depicted in Table 1 except stiffness of GCP and permeability of peat layer. Material parameters were converted according to the method proposed by Indraratna and Redana (2000). Based on above conversion, stiffness of the peat was taken as 14,333 kPa while horizontal and vertical permeability of peat were taken as 0.000333 m/s and 0.000111 m/s respectively for the analysis.

3.2 *Validation of the model*

Validation procedure was done based on the actual field data of the Outer Circular Highway Northern Section-1 (OCH-NS1) Project mentioned in Karunawardana et al. 2017. Settlement versus time relationship was used for the validation purpose.

3.3 *Parametric analysis*

Parametric analysis has been performed by changing only one parameter at a particular time and keeping rest of the parameters as constants. The effect of drainage on settlement and stability has analyzed. Factors that affect the drainage condition are permeability of GCP material, stiffness of GCP material and column clogging (Pal & Deb, 2018). The behavior of GCP has also investigated for different pile lengths as well. The effect of surrounding confining pressure of in-situ soil on the stability of GCP improved ground has also observed. Factors that affect the surrounding confining pressure are stiffness of surrounding soil, cohesion of surrounding soil and stiffness of geotextile encasement (Guetif et al., 2007). When considering the above factors, it can be noted that key parameter on the GCP stability is the stiffness of surrounding soft soil. However, in the validated model, soft soil model has been used for the peat clay, then the effect of stiffness of surrounding soil cannot be measured. Because, the soft soil model doesn't contain the parameter of stiffness for soft soil. Therefore, that validated model cannot be used for this analysis. Hence, a different unit cell model was used and validated in order to study the effect of stiffness of surrounding soft soil on GCP stability.

3.4 *Development of the unit cell*

The unit cell was modelled, using the data presented by Alkhorshid et al., 2018. To model the soft soil layer, hardening soil model was used. Hardening soil model is a hyperbolic model of the elastoplastic kind and was developed within the context of friction hardening plasticity. To represent irreversible soil compaction under main compression, the model also incorporates compression hardening. The behavior of sands, gravel, and softer soil types like clays and silts may all be predicted using this second-order model. Therefore, it can be used as the model for soft soil (Brinkgreve 2002). Hardening model consist of stiffness values. Then the effect of stiffness on GCP stability can be easily analyzed. The developed unit cell model and the used parameters are shown in Figure 2 and Table 2 respectively.

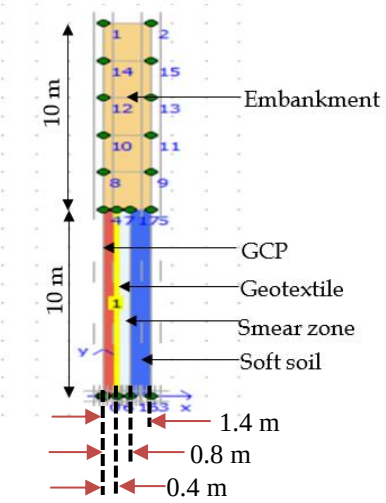

Fig. 2 Developed unit cell model

Table. 2 Soil properties used in unit cell model (Alkhorshid et al., 2018)

Material Property	Unit	Soft clay	GCP	Embankment
		Hardening Soil	Mohr-coulomb	Mohr-coulomb
γ_{sat}	kN/m^3	16	19	22
E'	kPa		45000	42000
ϕ'	deg	23	39	35
ψ	deg	0	5	0
c'	kPa	7	0	6
v'		0.2	0.3	0.33
E_{50}^{ref}	kPa	2313		
E_{oed}^{ref}	kPa	1850		
E_{ur}^{ref}	kPa	6938		
K_0		0.6	0.37	0.43
m	power	1		
P^{ref}	kPa	100		
OCR		1		

3.5 *Validation of the unit cell*

Developed unit cell was validated using the data presented by Alkhorshid et.al, 2018. Settlement versus embankment height data were concerned in the validation procedure.

4 RESULTS AND DISCUSSION

After successfully modelling the GCP improved ground and the Unit cell, a parametric study has performed. The obtained results are presented in this section.

4.1 *Validated results*

Settlement versus time graphs were obtained for both conversion methods and the results were compared with the actual data as shown in Figure 3.

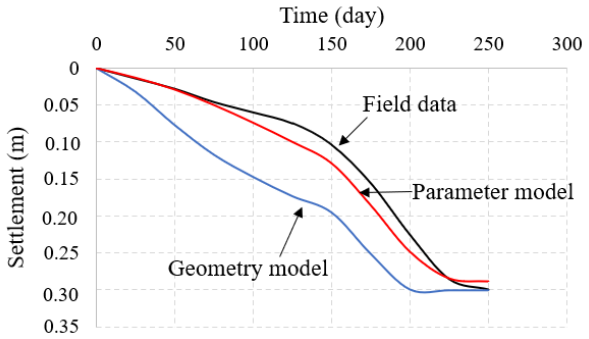

Fig. 3 Comparison of field data and GCP model

The Root Mean Square Error (RMSE) value of Geometry conversion method is 0.0658 while for Parameter conversion method it is 0.0197. The validity gets higher when the RMSE value is closer to zero. When considering the shape and the RMSE values, it can be concluded that parameter conversion method is more accurate. Therefore, for further analysis, the model developed using parameter conversion is used.

The unit cell was validated using the data presented by Alkhorshid et al., 2018. In this analysis, only the parameter conversion method was used. The comparison of the field data and model results are presented in Table 3. The settlement at top of the GCP over embankment is presented in the table.

Table. 3 Results of the unit cell models

Embankment height (m)	Alkhorshid et al, 2018	Unit cell
2	0.200	0.200
6	0.515	0.514
8	0.637	0.637
10	0.747	0.742

It can be noted that the root mean square (RMS) value for settlement of Alkhorshid et.al, 2018 is 0.56325 while that of developed unit cell is 0.56137. Since those values are almost equal, it is clear that the developed unit cell has validated successfully.

4.2 *Effect of drainage on stability of the GCP improved ground*

The effect of drainage on stability of GCP improved ground has been studied by analyzing the variation of pore water pressure versus time for different permeability ratios as shown in Figure 4. The permeability ratio is defined as permeability of GCP over permeability of soft soil. In order to study the effect of drainage, permeability ratio was varied from 10 to 1000 while keeping other factors constant.

It can be seen that irrespective of the permeability ratio, maximum excess pore water pressure generated at the end of embankment construction. Further, it can be noted that with the increment of permeability ratio, excess pore water pressure development has been decreased. In lower permeability ratios, high pore pressure development can be observed due to low rate of consolidation. If the permeability ratio is more than 100, maximum excess pore water pressure can be reduced by 75%. This clearly indicates, stability of GCP improved ground increases with the increment of permeability ratio.

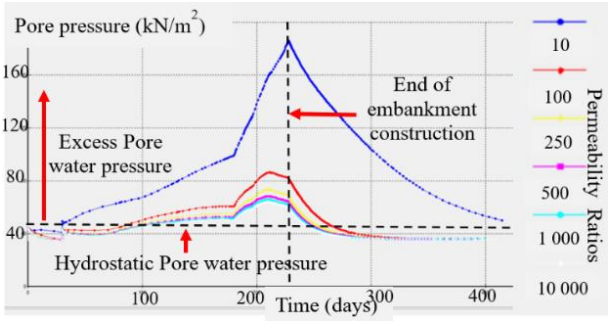

Fig. 4 Variation of porewater pressure versus time for different permeability ratios

4.3 *Effect of surrounding confining pressure on stability of the GCP improved ground*

The effect of surrounding confining pressure on stability of the GCP improved ground was studied by performing analysis on unit cell model. The effect of surrounding confining pressure was analyzed with respect to stiffness ratio. The stiffness ratio is defined as stiffness of GCP to that of surrounding soft soil. The variation of pore water pressure with respect to different stiffness ratios and different permeability ratios is illustrated in Figure 5. The stiffness ratios vary from 10 to 25.

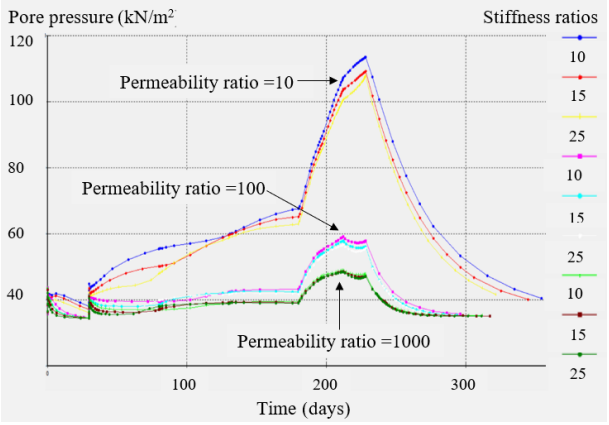

Fig. 5 variation of pore pressure versus time for different stiffness ratios

It can be seen that the effect of stiffness ratio on the development of pore water pressure is insignificant when compared with that of permeability ratio. Even though, there is a slight change in pore water pressure with respect to stiffness ratio under low permeability ratio, there is no such variation in stability. This behaviour clearly indicated that permeability of GCP is more significant than the stiffness of GCP material. However, when a stone column has poor drainage capacity owing to lesser permeability, its stiffness greatly enhances that capacity, and the decrease of excess pore pressure ratio value becomes more important (Pal & Deb, 2018).

The performance of the geotextile encased GCP was analyzed with respect to lateral displacement of GCP improved ground as illustrated in Figure 6. The effect of stiffness of geotextile on lateral displacement is presented in the same figure.

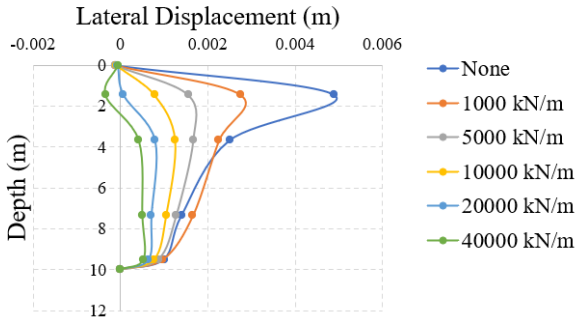

Fig. 6 Lateral displacement over depth for different geotextile stiffnesses

It can be seen that there is a significant reduction in lateral displacement at shallow depth (twice as the column diameter) when GCPs are encased with geotextile. The reason for this is that the geotextile encasement serves as the GCP's radial confining reinforcement. It acts as a barrier to lateral soil movement. At shallow depths, it exhibits a negative lateral displacement as the stiffness of the geotextile encasement increases (becoming larger than the stiffness of the GCP material). It is thus because, according to Murugesan et al., (2006), increasing the stiffness of the geosynthetic encasement mobilizes more lateral stresses in the GCP. However, the use of geotextile encasement greatly decreased lateral movement and enhanced the ground stability.

4.4 *Behavior with different GCP lengths*

GCP lengths were varied from 6 – 21 m and results were analysed to find the critical GCP length as depicted in Figure 7.

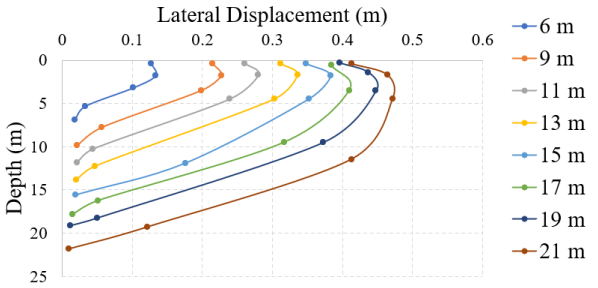

Fig. 7 Lateral displacement over depth for different GCP lengths

The data presented in the figure is corresponding to the lateral displacement at the end of preloading period. For a particular depth, the highest lateral displacement is recorded in the highest GCP length. Irrespective of the GCP length, maximum lateral displacement is recorded between 0-5 m. Also, it can be observed that when GCP length is increasing, depth to the maximum lateral displacement point is also slightly increasing. By considering that fact, maximum lateral displacement versus GCP length can be plotted as illustrated in Figure 8.

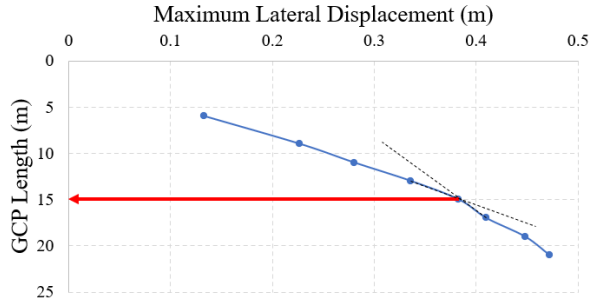

Fig. 8 Maximum lateral displacement over GCP length

It can be identified that until GCP length comes to 15 m, the gradient is approximately constant. However, when the GCP length is more than 15 m, there is a significant increment in gradient compared to low GCP lengths.

5 CONCLUSIONS

Based on above analysis, following conclusions can be drawn;

- The parametric conversion method is more realistic when converting 3D condition in to 2D.
- Higher the permeability of GCP material, more the stability of GCP improved ground.
- When installing GCP in the soft ground, it is very much effective to set the permeability ratio more than 100.
- The permeability is more significant than the stiffness when consider the stability of the GCP improved ground.
- The lateral displacement of the GCP improved ground can be significantly reduced when GCPs are encased with geotextile.
- The critical GCP length can be recommended as 15 m.

6 REFERENCES

Alkhorshid, N., Araújo, G. and Palmeira, E., 2018. Behavior of Geosynthetic-Encased Stone Columns in Soft Clay: Numerical and Analytical Evaluations. *Soils and Rocks*, 41(3), pp.333-343.

Brinkgreve, R., 2002. *Plaxis version 8 Material Models Manual*. Netherlands: A.A. Balkema publishers, pp.6 – 10

Guetif, Z., Bouassida, M. and Debats, J., 2007. Improved soft clay characteristics due to stone column installation. *Computers and Geotechnics*, 34(2), pp.104-111.

Indraratna, B. and Redana, I., 2000. Numerical modeling of vertical drains with smear and well resistance installed in soft clay. *Canadian Geotechnical Journal*, 37(1), pp.132-145.

Karunawardana, A., Ooka, A. & Nithiwana, W., 2017. Improvement of Sri Lankan peaty clay using the gravel compaction pile method for the construction of a highway embankment. *19th International Conference on Soil Mechanics and Geotechnical Engineering*.

Murugesan, S. and Rajagopal, K. (2006) "Geosynthetic-encased stone columns: Numerical Evaluation," *Geotextiles and Geomembranes*, 24(6), pp. 349–358. Available at: https://doi.org/10.1016/j.geotexmem.2006.05.001.

Pal, S. and Deb, K., 2018. Effect of Stiffness of Stone Column on Drainage Capacity during Soil Liquefaction. *International Journal of Geomechanics*, 18(3).

Tan, S., Tjahyono, S. and Oo, K., 2008. Simplified Plane-Strain Modeling of Stone-Column Reinforced Ground. *Journal of Geotechnical and Geoenvironmental Engineering*, 134(2), pp.185-194.

Weber, T.M., Laue, J. & Springman, S.M. 2006. Centrifuge modelling of sand compaction piles in soft clay under embankment load. VI International Conference on Physical Modelling in Geotechnics. (Eds Ng et al.) Hong Kong. Taylor & Francis Group, London. (1): 603–608.

Failure of Gravel Compaction Pile Improved Embankment – Case study

T. Nekasiny and N.H. Priyankara
Department of Civil and Environmental Engineering, University of Ruhuna, Hapugala, Galle, Sri Lanka

ABSTRACT: Due to scarcity of suitable lands, it becomes necessary to utilize the marshy lands consist of soft soil for infrastructure development. The soft soil has a problematic nature due to its high moisture content, high compressibility, and very low shear strength. To overcome this problematic nature, several ground improvement techniques can be adopted. This research study aims to identify the causes of failure of the Gravel Compaction Pile (GCP) improved trial embankment in Section 1 of the Southern Expressway Extension Project in Sri Lanka. Here, the slope stability of the embankment during the construction was analyzed using Matsuo and Kawamura's method and GEOSLOPE SLOPE/W software. According to this study, the main causes of the failure are improper site investigation, improper field monitoring, and stabilizing techniques provided were insufficient for the high thickness soft soil layer. In order to avoid these failures in the future, possible stabilizing techniques and recommendations are also discussed in this study.

KEY WORDS: Gravel Compaction Pile, Peaty soil, Slope stability, Stabilizing techniques

1 INTRODUCTION

The rapid development and population growth of a country would make the land very scarce by raising the demand for a substantial number of infrastructures. The scarcity of suitable lands for construction encourages the widespread use of areas underlined by weak soil deposits that are considered either marginal or inappropriate. Due to the scarcity of good lands, a considerable percentage of the number of infrastructure development projects in Sri Lanka such as the Colombo – Katunayake expressway, Southern Expressway, and Central expressway passes through flood plains and marshy terrain made up of extremely soft peat, organic soils, and clay.

The road embankment construction over peat deposits is quite challenging because of the poor peaty soil properties such as high moisture content, high compressibility, and very low shear strength. Kulathilaka and Madhusanka (2015) reported that Sri Lankan peaty soil has high moisture content of about 300 %, low shear strength of about 0.99 kN/m^2, and compression index (C_c) of 1.510. As such, peaty soil does not provide favourable conditions for construction on them. The primary consolidation of the peat is very high, with significant secondary compression. Therefore, geotechnical engineers face many challenges because the peaty soil cannot support high loading and construction can result in excessive settlement. In order to overcome these challenges, there are two ways, namely transfer the structural load to underlying hard stratum through piles or improve the engineering properties of soft soil. However, the transferring of load through piles to the hard stratum is not an economical solution for roads occupying a large plan area and moderately loaded buildings. Improving engineering properties of soft soil is the most economical option and it is a responsibility of the geotechnical engineers to find appropriate ground improvement technique/s based on the subsurface soil conditions.

Gravel Compaction Pile (GCP) is one of the soft ground improvement techniques, that aims to increase load-bearing capacity, and reduce settlement by densification of subsoil. GCPs are formed by forcibly injecting gravel into the in-situ soft clay via a casing. The subsequent injection of gravel will lead to a cavity-expansion type displacement and introduce some "setup" in the strength of the soft soil (Figure 1). Generally, 40 cm diameter casing is used to construct 70 cm diameter GCP.

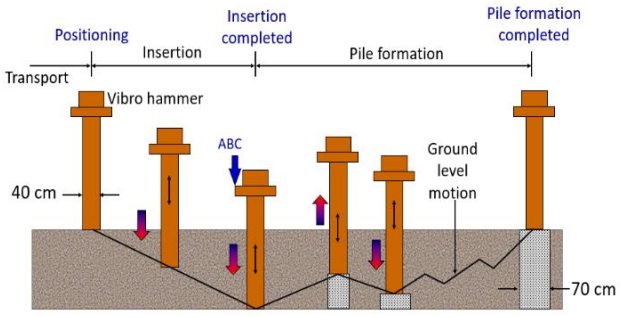

Fig.1 GCP construction procedure

Section 1 of the Southern Expressway Extension Project connecting Matara to Beliatta is mainly going through the Nilwala flood plain. In Section 1, trial embankment section was constructed on the soft ground consisting of peat and soft clay deposits which was improved by the Gravel Compaction Pile (GCP) technique. According to the initial site investigation, the thickness of the soft peaty clay layer was about 6 m to 15 m. However, during the GCP installation, it was realized that the soft soil layer thickness is more than 15 m on the Right-Hand Side (RHS) of the embankment; in some locations, it is about 18 m. Soon after the GCP installation, embankment construction was started and, during the soil filling, it was noted that the embankment was sliding towards the right-hand side leading to reduce the slope stability of the embankment. Precaution activities have been done and they also failed. Then the construction has been abandoned and caused a huge financial loss. Therefore, this study aimed to identify the causes of failure in the GCP improved trial embankment section to prevent such failures in the future.

2 METHODOLOGY

2.1 *Development of subsurface soil profile at the GCP trial embankment section*

Subsurface soil profile was developed using the borehole data and GCP records, to identify the variation of the soft soil layer thickness from Left Hand Side (LHS) to Right Hand Side (RHS).

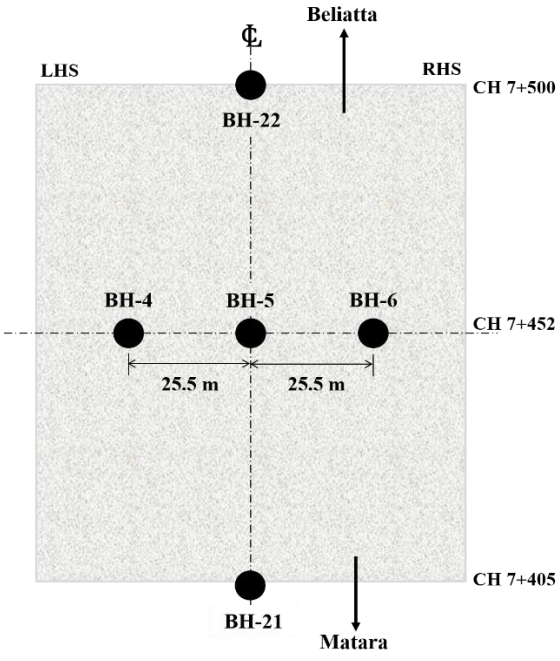

Fig.2 Borehole locations within the GCP trial embankment section

Two boreholes namely BH-21 and BH-22 were done in the initial stage of the project at the center line at the chainages Ch.7+405, and Ch.7+500 respectively, and three boreholes namely BH-04, BH-05, and BH-06 were done at Ch.7+452 covering the entire cross-section. The borehole locations at the trial embankment section are shown in Figure 2.

Due to variation of the subsurface soil profile with the distance, the GCP installation field records were used to develop the variation of soft soil thickness within the GCP trial section. Generally, GCPs are installed up to the medium stiff or stiff stratum. As such, GCP length approximately indicates the soft soil layer thickness at that particular location. Further, to develop the 2D and 3D subsurface soil profile, VisLog software was used.

2.2 *Geotechnical design parameters of subsurface soil*

Geotechnical parameters were obtained to identify the characteristics of the subsurface soil based on the laboratory and field tests data. Undisturbed (UD) samples were collected from every borehole where the soft clay was encountered within the range of drilling depths. Compressibility and shear strength parameters of the soft soil were obtained through the oedometer test and Consolidated Undrained (CU) triaxial test respectively.

2.3 *Variations of slope stability of trial embankment at different stages of construction*

After the installation of GCP, during the construction of the embankment, the field behaviour was monitored using the settlement plates, piezometers, inclinometers, and surface stakes. Field instrumentation arrangement is shown in Figure 3. Settlement plates were used to measure the settlement of the soil underneath the embankment, while piezometers and inclinometers were used to measure the variation of the pore water pressure and lateral displacement of the ground respectively. In addition, surface stakes were used to monitor the lateral movement of the ground.

Based on the observed lateral displacement and settlement records, the slope stability of the embankment was evaluated using the graphical method proposed by Matsuo and Kawamura (Matsuo & Kawamura, 1977). Further, stability of the embankment was analyzed using GEOSLOPE SLOPE/W software.

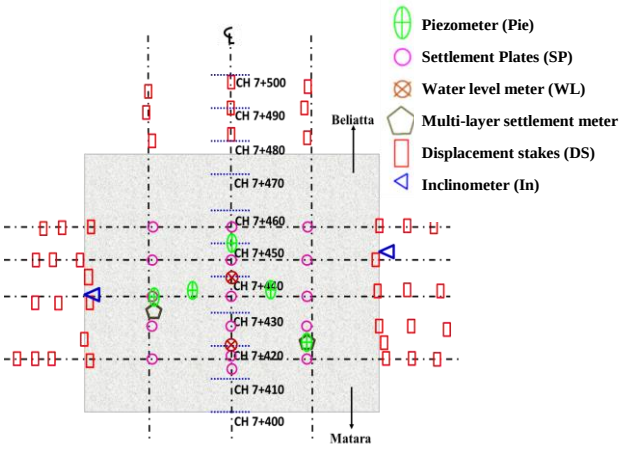

Fig.3 Instrumentations in the GCP trial section

2.3.1 Matsuo and Kawamura (1977) method

The method proposed by Matsuo and Kawamura (1977) to estimate the Factor of Safety (FOS) and slope failure based on field monitoring data is presented in Figure 4. Each curve in the Figure 4 is corresponding to a different Factor of Safety (FOS) from 1.0 to 1.67. The graph indicates a relationship between settlement and ratio of lateral displacement to settlement.

Then, based on the observed data, maximum embankment settlement versus the ratio of incremental changes of maximum lateral displacement to settlement was plotted in the Matsuo and Kawamura's diagram, to verify the variation of factor safety at different depths during different stages of the embankment construction.

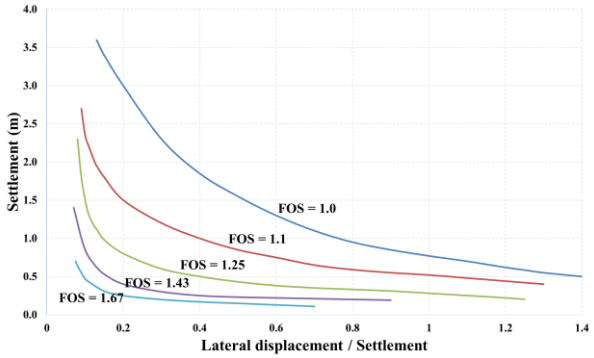

Fig.4 Matsuo and Kawamura's diagram

3 RESULTS AND DISCUSSION

3.1 *Subsurface soil profile at GCP improved trial embankment section*

Based on borehole logs, subsurface soil profile across the chainage 7+452 can be idealized as shown in Figure 5. It can be seen that soft soil thickness significantly varied from left to right, where soft soil thickness in Left Hand Side (LHS) is about 4.0 m where as that of Right Hand Side (RHS) is about 16.0 m. In addition, GCP installation records were used to identify the soft soil thickness variation. Figure 6 illustrates the GCP installation records at Ch. 7+460. Both methods illustrated that soft soil thickness is more in RHS when compared to LHS. By combining borehole logs and GCP installation records, variation of soft soil thickness within the trial embankment section can be idealized as shown in Figure 7.

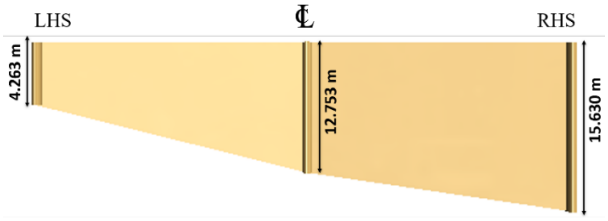

Fig.5 Variation of soft soil layer at Ch. 7+452

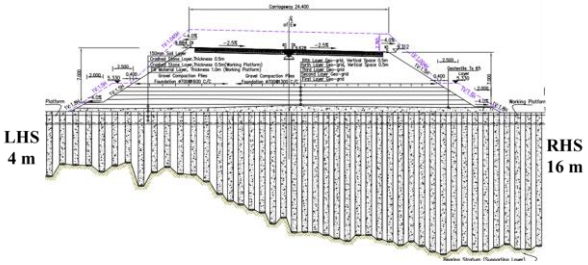

Fig.6 GCP installation records at Ch. 7+460

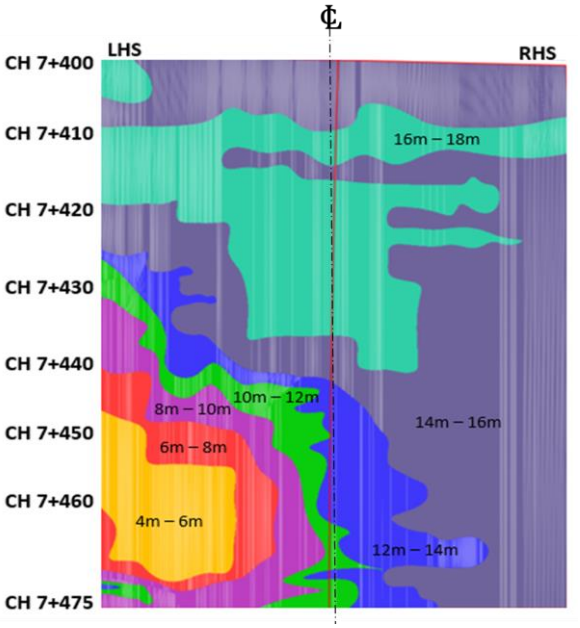

Fig.7 Subsurface soil contour map

Based on this idealization, it can be seen that soft soil thickness in RHS is varied from 12 m to 18 m. However, in the LHS, basically it is 4 m to 10 m. Especially, in chainage 7+400 to 7+420, even in LHS soft soil thickness is varied from 16 m to 18 m.

This clearly illustrates the heterogeneous nature of the subsurface.

3.2 *Geotechnical parameters of subsurface soil*

The physical and engineering properties of the very soft peaty clay available in the subsurface are summarized in Table 1.

Table 1. Properties of peaty clay

Property	Value
Natural moisture content (%)	107 – 150
Unit weight (kN/m^3)	11.38 – 12.85
Coefficient of consolidation (C_v) (m^2/year)	1.0 – 1.5
Pre-consolidation pressure (C_c') (kN/m^2)	68 – 74
Compression Index (C_c)	0.997 – 1.14
Initial void ratio (e_0)	2.4 – 2.62
Modified Compression Index $C_c' = \frac{C_c}{1+e_0}$	0.28 – 0.33
Modified Secondary Compression Index (C_α')	0.08 – 0.1
Drained friction angle ($\emptyset'$) (degree)	19 – 23
Drained cohesion (C') (kPa)	1.9 – 6.3
Undrained friction angle ($\emptyset_u$) (degree)	16.8 – 20.5
Undrained cohesion (C_u) (kPa)	0

Based on the data presented in Table 1, it can be noted that peaty clay consists of higher moisture content and very low shear strength. The undrained cohesion (C_u) equal zero indicates that soil is normally consolidated. Further, oedometer test results indicated that peaty clay is highly compressible. The in-situ undrained shear strength (C_u) of very soft peaty clay was found as 3.0 kPa, based on the vane shear test.

3.3 *Quality of GCP material*

The quality of the GCP material was investigated at thirteen (13) GCP locations by conducting Dynamic Cone Penetration Test (DCPT) at center of the GCP. Then, the measured DCPT – M values were converted into SPT – N values using the correlation as shown in Equation 1.

$$\text{SPT} - \text{N} = \frac{\text{DCPT}-\text{M}}{1.5} \quad (1)$$

The variation of SPT-N values over depth at different chainages are presented in Figure 8.

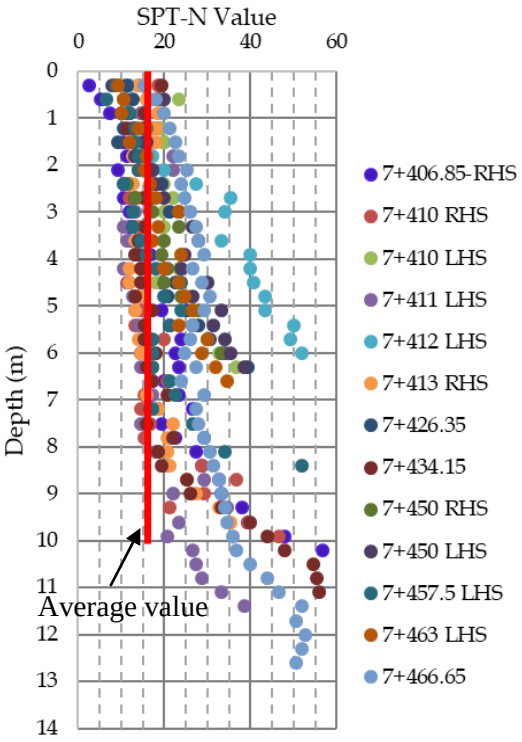

Fig.8 SPT-N value over depth at GCP locations

It can be clearly seen that the SPT – N values are gradually increased with the depth due to overburden pressure. Even though SPT-N values were increased with depth, when the overburden correction was applied to the measured SPT-N value, the corrected SPT-N values are around 40 – 50. This implies GCP was properly compacted.

Then friction angle of the compacted GCP materials were estimated using Equation 2.

$$\emptyset = 0.3N + 27 \quad (2)$$

Where $\emptyset$ is the friction angle and N is the field measured SPT-N value. By taking average SPT-N value of 16 as indicated in Figure 8, it can be concluded that friction angle of the GCP material is about 32^o.

3.4 *Variation of slope stability of the embankment*

The summary of the trial embankment construction is illustrated in Table 2. The graphical presentation of the embankment construction is shown in Figure 9.

Table 2. Summary of embankment construction

Phase	Details	Duration (days)
0	Platform construction after GCP installation	20
1	Embankment construction	100
2	Waiting period	89
3	Berm construction	40
4	Embankment construction	48

It can be noted that embankment construction has been started soon after the GCP installation without allowing any time for pore water pressure dissipation.

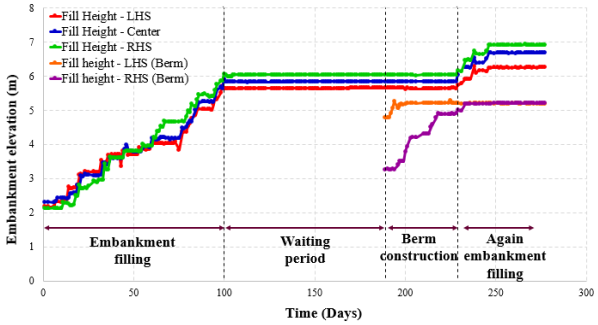

Fig.9 Variation of embankment elevation over time at Ch. 7+455

The settlement of the subsurface soft ground due to embankment construction is presented in Figure 10. The variation of lateral displacement over depth at different time intervals is illustrated in Figure 11.

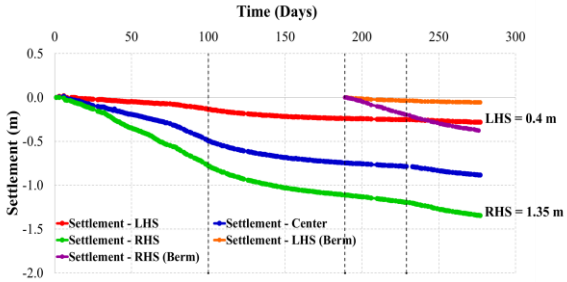

Fig.10 Settlement over time at Ch. 7+455

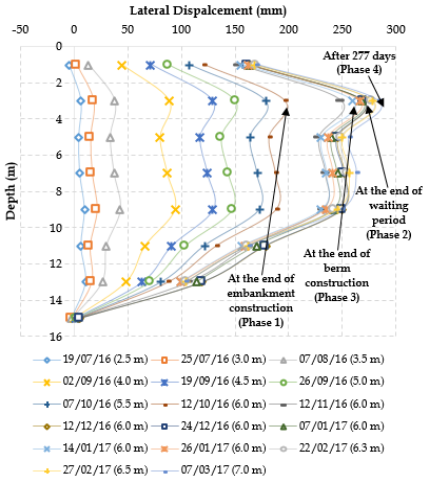

Fig.11 Variation of lateral displacement over depth at different phases

The variation of Factor of Safety (FOS) during the embankment construction is shown in Figure 12. It can be clearly seen that FOS gradually decreases with the increase of embankment height due to huge lateral displacement in RHS.

It can be clearly seen that at the end of phase 1, FOS is about 1.24. Further, it can be noted that rate of lateral displacement has been significantly increased. Then, embankment filling was stopped as indicated in Figure 9 (waiting period) expecting a FOS improvement, however, there is no considerable improvement in FOS (FOS = 1.20). Further, it can be noted that rate of lateral displacement has been significantly decreased (Figure 11). Then, the berm was constructed to reduce the lateral displacement and Matsuo and Kawamura's curve was moved to the left indicating a slight improvement in the stability. However, when the filling was started again, the FOS reduced up to 1.1 which is less than the required minimum FOS of 1.20 for short term stability (ICTAD, 2009). Therefore, it clearly shows that the embankment is unstable at this stage.

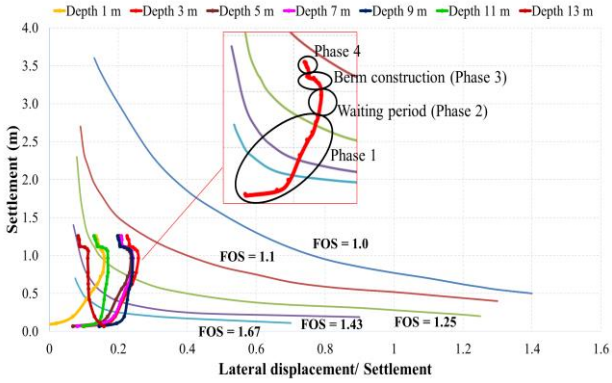

Fig.12 Variation of FOS in RHS of the embankment using Matsuo & Kawamura Method at Ch. 7+455

The above embankment condition was numerically modelled using Geoslope SLOPE/W software as shown in Figure 13.

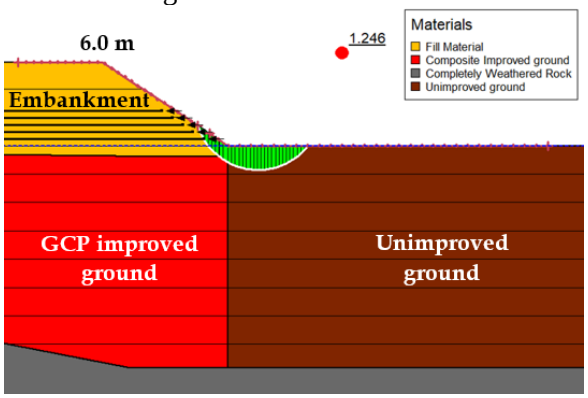

Fig.13 Slope stability analysis using Geoslope SLOPE/W software at the end of phase 1

The stability of the slope was evaluated using 'Spencer's method' and slip surfaces were generated using 'Entry and Exit' method.

In this analysis, assuming that FOS obtained through Matsuo and Kawamura method is correct, composite shear strength parameters of the GCP improved ground were obtained. The shear strength parameters obtained through back analysis is shown in Table 3.

Table 3. Back analysis results

Embankment height (m)	FOS		Shear strength parameters	
	Matsuo & Kawamura	SLOPE/W	Cohesion (kPa)	Friction angle (°)
2.5	1.92	1.941	7.2	19.5
3.0	1.80	1.795	6.0	19.0
3.5	1.68	1.676	5.3	17.0
4.0	1.43	1.428	3.3	12.0
4.5	1.34	1.359	2.3	9.0
5.0	1.30	1.312	1.8	6.0
5.5	1.25	1.249	0.3	4.0
6.0	1.24	1.246	0.0	1.2

Based on the results presented in Table 3, it can be noted that shear strength parameters gradually decreased with the increment of the embankment height. The decrement in shear strength parameters clearly stated that the ground improvement technique - GCP method, adopted was failed.

3.5 *Possible stabilizing techniques*

Berm construction and/or extension of GCP without any reinforcement, from the toe of the embankment is not sufficient to provide lateral support, when the soft soil thickness is about 18 m. Then, the model was analyzed with the installation of precast concrete piles at the toe, and realized FOS was increased significantly as shown in Figure 14. Therefore, this study concludes that in order to stabilize the embankment on huge soft soil layer thickness, the most possible stabilizing technique is to provide a lateral support with reinforcement. And also, if the soft soil layer thickness is more than 13 m to 15 m, it is not a good choice to use GCP improvement technique.

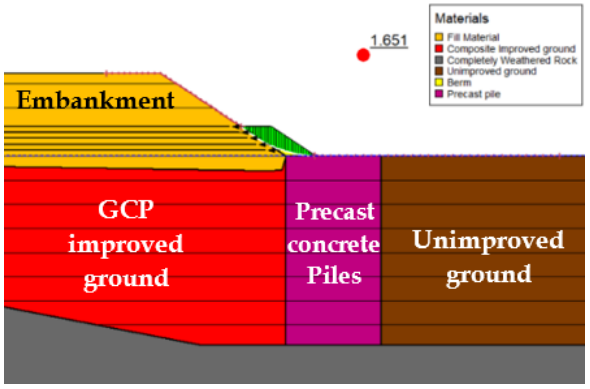

Fig.14 Slope stability analysis with the installation of precast concrete piles at the toe of the embankment

4 CONCLUSIONS

Based on this research study, the following conclusions can be drawn;

- This study implies the importance of proper site investigation prior to start the GCP construction. The applicability of the GCP in higher soft soil thickness is not effective.
- Even though, higher soft soil thickness was realized during the GCP installation which was more than the design value, necessary precautions were not taken to revise the GCP spacing or design.
- Embankment construction was started immediately after the GCP installation, without allowing for excess pore water pressure to dissipate, which may result in the subsurface shear failure during the embankment construction.
- Even though, toe support has been provided, lateral movement of the embankment was not controlled considerably. Since, subsurface has already failed due to excess pore water pressure, with providing toe support it couldn't control the lateral movement due to embankment load.
- In order to achieve the slope stability during high embankment construction in thick soft soil layers, it is recommended to provide some kind of toe support before starting the embankment filling, by installing precast concrete piles to a certain distance beyond the embankment edge.

REFERENCES

ICTAD Publication No. – SCA/5, (2009). Standard specifications for construction and maintenance of roads and bridges. 66.

Kulathilaka, S.A.S., & Madhusanka, K.A.C., (2015). Possible use of Paddy Husk Ash in Improvement of Engineering Characteristics of Peaty Clay. 408–410.

Matsuo, M., & Kawamura, K. (1977). Diagram for construction control of embankment on soft ground. 37–52.

Optimization of end bearing capacity of bored piles on rock based on field measurements

B.A.C Danushka, N.H. Priyankara, A.M.N. Alagiyawanna and K. Senevirathe
Department of Civil and Environmental Engineering, University of Ruhuna, Sri Lanka.

ABSTRACT: Bored piles are one of the famous deep foundation techniques which are practiced all over the world. Most of the bored piles are socketed into the bedrock to gain higher bearing capacity. However, estimation of end bearing capacity for rock socketed bored pile is questionable. There are a lot of theoretical and empirical methods have already been developed to estimate the end bearing capacity of bored piles on rock and there is no any clear indication about the accuracy of those methods to apply into Sri Lankan context. Therefore, designers use different methods based on their experiences which may result the overestimated designs. As such, in this research study, different empirical and theoretical methods were compared with the pile load test results in Sri Lanka and concluded the most reliable method/s to estimate the end bearing capacity of rock socketed bored piles in Sri Lankan context.

KEY WORDS: Bored piles, End Bearing Capacity, Rock Socketed, Sri Lankan Context, Most Reliable Method

1 INTRODUCTION

Many Civil Engineering Projects, such as highway viaducts and other heavy structures cannot rely on shallow foundations for their stability due to presence of weak subsurface as shallow depth. Therefore, deep foundations, especially bored piles are used to transfer the structural load to underlying hard stratum. Most of the bored piles are socked into the bed rock to achieve higher end bearing resistance.

There are some reasons to go for the pile foundation as the deep foundation. One of them is, when the water table is high, it may be a problem for the stability of the structure. Also soil at shallow depth may be compressible. So, it cannot carry the load of large structure. Since water table is high near to riverbed and coastal areas, usually trying to go for a piling construction. Sometimes difficulties are raised during excavating the subsurface soil. because it may not be possible, and collapsing may be occurred while excavating. In such situations, usual recommendation is to go for a pile foundation. The basic mechanism of a pile is to transfer the load of the super structure through hard stratum or rock strata. Pile foundation can be categorized into two ways such as based on the basic design function and based on the method of construction (Poulos and Davis, 1981). Based on the load transfer mechanism, mainly piles can be divided into two parts such as end bearing piles and friction piles. Sometime combination of both functions of piles (Fig. 1)are used in the field as well based on the situation and the ground conditions. Piles can also be categorized according to the construction method such as displacement (driven) piles and replacement (bored) piles (Gould, 1981). Because of the minimal disturbances to the surrounding due to the vibration and subsurface soils, bord piles are very often than the driven piles.

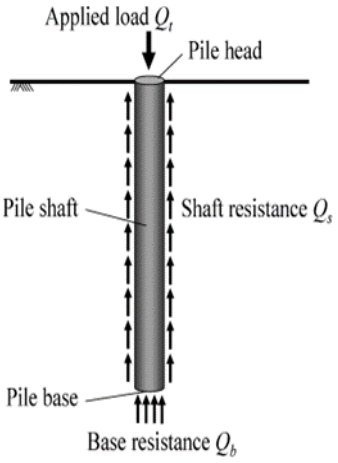

Fig. 1. Components of resistance of a pile

The End Bearing Capacity (EBC) of a bored pile in socketed rock is depended on many external, internal conditions and rock parameters. They may vary depend on the rock type, method of test,

equipment, and mechanism as well. Therefore, a lot of relationships have been developed to compute the EBC by researchers.

Generally, bored pile foundations are designed based on the data gathered from the sub surface through boreholes, inspecting the soil/rock samples and laboratory test results to ensure that its bearing characteristics conform to those deduced from the results of exploratory boreholes and soil/rock tests (Poulos and Davis, 1981).Usual practice is to verify the load bearing capacity of the piles in the field using a Static pile load test (SLT/MLT) or Pile Dynamic Analysis (PDA/DLT). It is difficult to conduct field pile load tests for small scale projects due to economic constraints. As such, it is a need of the hour to select the most reliable theoretical and/or empirical method/s to precisely estimate the End Bearing Capacity (EBC)of the bored piles. Although, many theoretical and empirical methods have been developed by many researchers to estimate carrying capacity of bored piles, studies on the reliability of these methods based on the field measurements are limited. Only very few researches have been carried out to verify the reliability of these proposed methods based on field load test results for their local contexts (Sharudin *et al.*, 2016). Applicability of these methods for Sri Lankan context is questionable and reliability of the existing methods for Sri Lankan context needs to be investigated.

Due to unavailability of reliable methods to estimate end bearing capacity of bored piles in Sri Lankan context, most designers adopt the method of Institution for Construction Training and Development (ICTAD) to estimate carrying capacity(ICTAD, 2017). However, it was reported that field measurements are much higher than of design values, which are obtained using ICTAD method, leading to overdesign the bored piles. As such, some designers use thumb rules based on their experience to estimate the end bearing capacity of bored piles, which may lead to adopt low factor of safety on bored pile design. Then one of the most burning issues in the construction industry can be solved by the results of this research study.

2 LITREATURE REVIEW

Initially, seventeen (17) number of Theoretical/Empirical methods were found through a comprehensive literature review. Although, there are lot of methods to evaluate end bearing capacity in theoretically, all methods cannot be used for evaluation. Because there are some possible reasons to rejection. Due to limitations of rock quality parameters in equations, constraints of dimensions of piles, locations and terminated conditions of pile, accuracy of assumed parameters and Limitations of access to some of the rock parameters, only nine (09) number of methods were selected for determining the ultimate end bearing capacity (q_{max}).

(i) Kulhaway and Goodman (1987)

$$q_{max} = \sigma_c \frac{(N_\emptyset + 1)}{F} \quad (1)$$

$$N_\emptyset = \tan(45 + \frac{\varphi}{2})^2 \quad (2)$$

Where σ_c is Uniaxial Compressive Strength (UCS) of rock, φ is drained friction angle and F is a recommended safety factor.

(ii) Tomlinson (1993)

$$q_{max} = 0.33\sigma_c \quad (3)$$

(iii) Zhang and Einstein (1998)

$$q_{max} = 4.83\ {\sigma_c}^{0.51} \quad (4)$$

(iv) Vipulanandan et al. (2007)

$$q_{max} = 4.66\ {\sigma_c}^{0.56} \quad (5)$$

(v) Bishnoi (1968)

$$q_{max} = J.C.N_{cr} \quad (6)$$

$$N_{cr} = 2\tan(45 + \frac{\varphi}{2}) \quad (7)$$

Where J is a correction factor depend on the nature of discontinuities, C is the cohesion of rock mass and N_{cr} is the modified bearing capacity factor.

(vi) ICTAD guidelines (1997)

Institution for Construction Training and Development (ICTAD) guidelines recommend a graphical method (Ref: BS2004, 1986) to estimate the end bearing capacity on rock which is related to UCS

value and Rock Quality Designation (RQD) value as shown in Fig. 3.

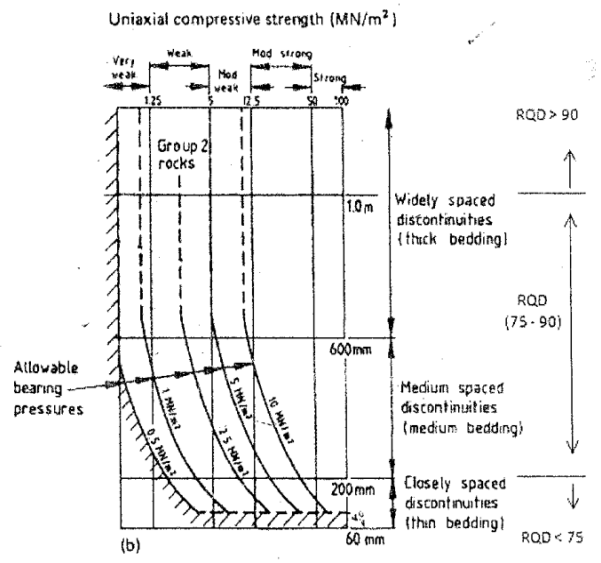

Fig. 3. ICTAD Method (Source BS2004,1986)

(vii) RMR Method

Based on the Rock Mass Rating (RMR), which was proposed by Bieniawskin in 1989, allowable end bearing capacity can be determined as Table 1**.**

Table 1:RMR Method

Parameters	RMR value			
	<40	50	70	88
Allowable bearing capacity(kPa)	3000	5000	10000	14500

*Note: Recommended safety factor 3.0 and interpolation is allowed.

(viii) Hong Kong guidelines

Hongkong guidelines refer to the code of practice for foundation (BD2004a) to estimate the end bearing capacity on rock which has four regions based on the UCS value, Core Recovery (CR) value and the nature of the rock material.

(ix) Peck et al. (1974)

Peck et al (1974) suggested a semi-empirical correlation between allowable bearing pressure and Rock Quality Designation (RQD) directly as shown in Fig. 2**.** safety factor of 3.0 is recommended for the compressions of semi-empirical methods.

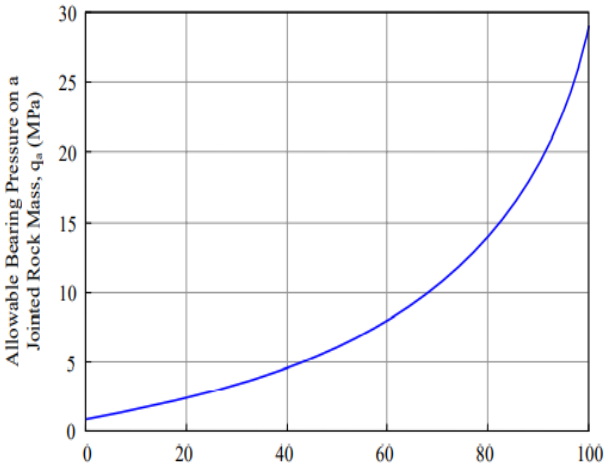

Fig. 2. Peck et al. Method

3 METHODOLOGY

Methodology of the study can be presented in a flow diagram as shown in Fig. 4**.**

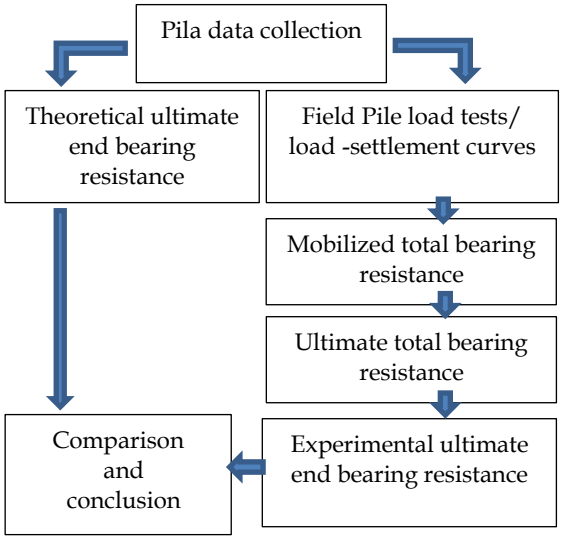

Fig. 4. Flow of Methodology

3.1 Collection of Pile Data

Initially, 12 pile load tests were collected including 7- static load tests (SLT) and 5- dynamic load tests (DLT). But some piles did not have required data to evaluate the theoretical end bearing capacities due to the limitations of the accessibility to the data. Finally, seven (07) number of pile tests were selected from different construction projects in Sri Lanka as shown in Table 2.

Table 2: Details of selected piles

Project Name / City	Test Pile No.	Type of load test
Port Access Elevated Highway (PAEH) project (Colombo)	TP-39	SLT
	TP-70A	SLT
	TP-70A	DLT
New Kelani Bridge Project (Kelaniya)	DEMA-BR1-7	DLT
Proposed housing project (Orugodawatta)	P-19	DLT
	P-76	DLT
	P-224	DLT

*Note: SLT-static load test, DLT- dynamic load test

3.2 Field Load Tests to Estimate the EBC

Generally, piles are tested for 1.5 times or 2.0 times the design load to check for the mobilized capacity without reach to the failure point. To identify the mobilized bearing capacity of a bored pile, there are two methods used in the field. They are Static Load Test (SLT) / Maintained Load Test (MLT) and Dynamic Load Test (DLT) /Pile Dynamic Analysis (PDA).

In static load test, the pile top is loaded using heavy concrete cubes.In Pile Dynamic Analysis (PDA) test, the constant weight is dropped from a certain height while it hit the pile top according to the standard way.

Since most of the theoretical/Empirical methods predict the ultimate end bearing capacity. Therefore, mobilized end bearing capacity wanted to be interpreted into ultimate for the comparison. For interpretation of the ultimate capacity from the mobilized capacity, it was performed using well established graphical methods. Out of seven (07) graphical methods (Davisson method (1973), Double tangent method, Brinch Hansen 80% method (1963), Chin-Konder method (1971), Fuller and Hoy method (1977), Hirany and Kulaay Method (1989), Slope -tangent method), only three (03) accurate graphical methods were selected based on the failure load test (According to the ICTAD guidelines: Either the settlement for design load exceeds 6mm or settlement for 1.5 times design load exceeds 12mm, pile is said to be almost failed) results which was conducted in New Maternity hospital project, Karapitiya, Galle, Sri Lanka as shown in Fig. 5.Total ultimate bearing capacities were calculated based on graphical methods. Ultimate skin friction needed to be separated from the total pile capacity

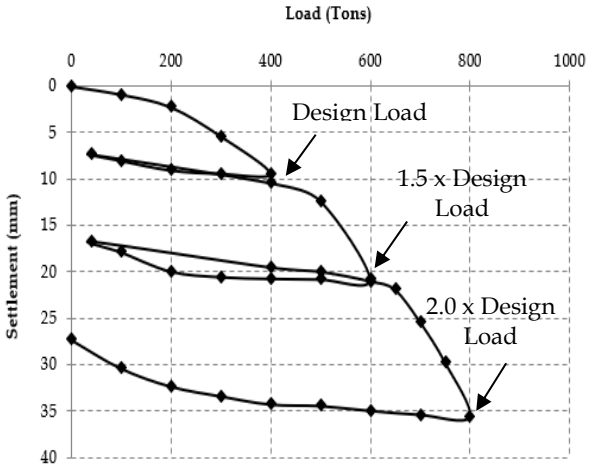

Fig. 5. Failure Load -Settlement Curve

There are two Graphical methods were found for separating the Skin friction through the Literature. They are Van weele method (1957) and Chin's Method (1978).

3.2.1 Van Weele method (1957)

Van weele suggested that when a pile is loaded, the load is initially carried mostly by the skin friction until the shaft slip is sufficient to mobilize the ultimate skin friction. This behavior is represented by the initial straight-line segment of the load settlement curve, when the ultimate skin friction mobilized; the load is carried by the ultimate skin friction plus mobilized end bearing.

3.2.2 Chin's Method (1978)

According to the Chin (1978), the inverse of the slope of the second segment yields the total ultimate carrying capacity while the inverse of slope of the first segment gives the ultimate skin friction capacity (Celestial, and Lanka, 1996).

Comparing the load settlement curve of pile load test results and some literature the most accurate method was selected to separate the ultimate skin friction of pile. After separation the ultimate friction, ultimate end bearing capacity was calculated for selected pile load tests (Table 2).

3.3 Comparison of theoretical and experimental end bearing resistance

After evaluating the theoretical ultimate end bearing resistance and experimental end bearing resistance, Comparison was done based on the type of the load tests including SLT and DLTs.

4 RESULTS AND DISCUSSION

4.1 Interpretation of Ultimate End Bearing Resistance

Based on the failure pile load test, ultimate end bearing resistances were interpreted using seven graphical methods to identify the most reliable graphical method/s.

Table 3: Selection of Interpretation Method

Method	Predicted ultimate bearing resistance (tons)	Actual ultimate bearing resistance (tons)
Davisson Method (1973)	340	(450-600)
Double-Tangent Method	420	(450-600)
Brinch Hansen 80% Method (1963)	503	(450-600)
Chin-Konder Method (1971)	1296	(450-600)
Fuller and Hoy Method (1977)	590	(450-600)
Hirany and Kulhaway Method (1989)	Not satisfied	(450-600)
Slope-Tangent Method	280	(450-600)

* Note: Range of (450-600 tons) is based on the shape of the failure pile load test (Fig. 5)

According to the analysis, double tangent method, Brinch Hansen 80% (1963) method and Fuller and Hoy (1977) methods were selected as the most reliable graphical methods to interpret the ultimate total bearing resistance. Because other graphical methods predict more deviated ultimate total bearing resistance than actual ultimate total bearing resistance (450-600 tons) of failure pile load test.

4.2 Separation of Ultimate Skin Friction

Separation of the ultimate skin frictionas performed graphically using Van weele method and Chin method for each pile load tests.Based on the analysis and the literature ,Chin method was unable to predict the ultimate end bearing resistance due to the graphical matters for most of the cases .Therefore, Van weele method (1957) was nominated for the separation of ultimate skin friction from the total resistance.

4.3 Overall Comparison

Theoretical ultimate end bearing resistance was determined using nine (09) methods. Double tangent, Brinch-Hansen 80% and fuller and Hoy method were nominated for interpretation the ultimate total bearing resistance from mobilized resistance from load- settlement curve. By reducing the skin friction using Van Weele method (1957), experimental ultimate end bearing resistance was calculated as shown in Table 4**.**

Table 4: Overall Comparison

Pile No	END BEARING RESISTANCEE (kN)													
	Theoretical Methods										Experimental Methods (SFS.-Van Weele Method)			
	Kulhaway and Goodma	Tomlinson	Zhang and Einstein	Vipilan andan et al.	Bishnoi	ICTAD guide lines	RMR Method	Hong kong guide lines	Peck et al.	Double tangent	Brinch Hansen 80%	Fuller and Hoy
TP-39 (SLT)	14500	6718	23855	26594	5089	33929	33930	25447	57680	12500	13495	-
TP-70A (SLT)	12082	5598	21737	24013	4241	11875	20358	16965	15262	18000	24963	-
DEMA-BR1	10516	4873	16938	18924	4430	9425	7069	11781	15315	2900	1330	2100
P-19 (DLT)	10343	4792	20080	22011	3630	10857	10179	10179	10179	4500	12810	11000
P-76 (DLT)	19920	9230	28051	31772	6992	16965	13572	16965	16965	2400	5330	3700
P-224 (DLT)	17072	7910	19559	22625	7990	13360	13360	9543	9924	13100	19500	21000
P-70A (DLT)	12080	5598	21737	24013	4241	11875	20358	10179	16289	14000	20497	-

*Note: SFS-Skin Friction Separation

Fig. 6 shows the overall comparison for selected piles. Red colour symbols represent the theoretical values while blue colour symbols indicate the experimental values.

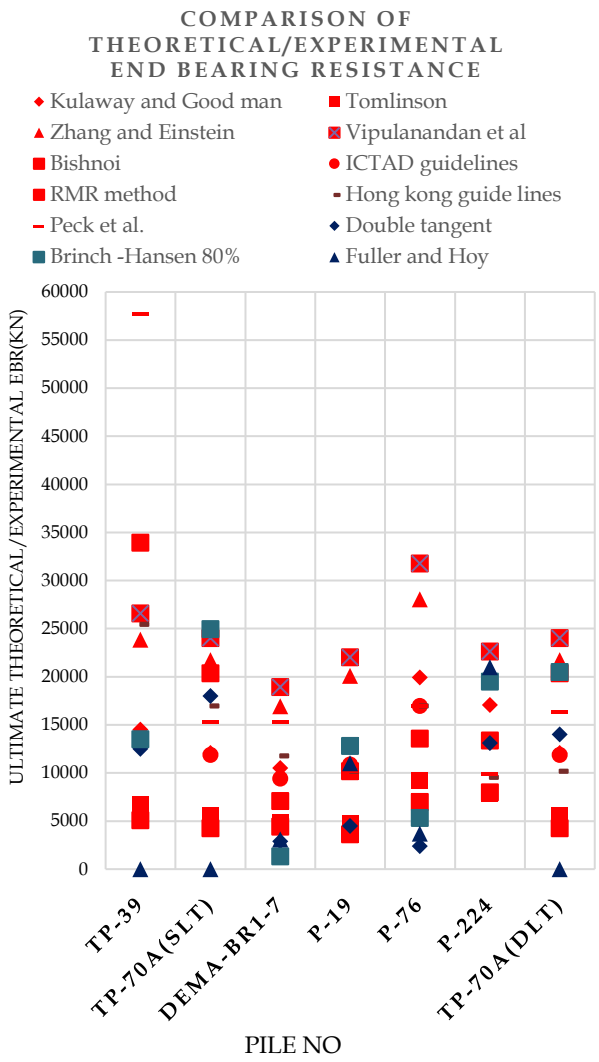

Fig. 6. Comparison of Theoretical and experimental ultimate end bearing resistance

5 CONCLUSIONS

According to the results basically it shows staggered relationships. Both SLT and DLT give closer mobilized resistance. The EBR which was estimated using Zhang and Einstein (1996), Vipulanandan et al. (2007) and Kulaway and Goodman (1987), were well agreed with the SLT results. Similary, Zhang and Einstein (1996), Hong Kong guidelins, ICTAD guidelines and RMR method give much closer values to DLT results. According to the overall results, for any type of load test (SLT or DLT), Zhang and Einstein (1996) and RMR method can be recommended as the most reliable methods to estimate the end bearing capacity on rock in Sri Lankan context.

If there were enough failure load test results with required rock parameters, experimental ultimate end bearing capacity can be found directly and the recommended methods would be validated detailly. Since there were very limited failure load tests which have been conducted in field, accessibility to those failure load tests was a challenge. Therefore, it will be a part to be covered in the future.

6 ACKNOWLEDGEMENT

We would like to acknowledge Prof. Sudeera de Silva, Head of the department of Civil and Environmental Engineering, Faculty of Engineering, University of Ruhuna for giving all the facilities to conduct the undergraduate research project. Moreover, we are very great full to Eng. Mrs. Bihani Madushika from Engineering & Laboratory Services (Pvt) Ltd, for her unconditional helps and guidance on this research study.

7 REFERENCES

Zhang, L. (2010) 'Prediction of end-bearing capacity of rocksocketed shafts considering rock quality designation (RQD)', Canadian Geotechnical Journal, 47(10), pp. 1071–1084.

Poulos and Davis (1981) Pile foundation analysis and design, International Journal of Rock Mechanics and Mining Sciences & Geomechanics Abstracts. doi:10.1016/0148-9062(81)90191-1.

Sharudin, E.S. et al. (2016) 'Rock bearing resistance of bored piles socketed into rock', Jurnal Teknologi, 78(8–6), pp. 45–51. doi:10.11113/jt.v78.9638.

ICTAD (2017) Guidelines for interpritation of site investigation data for Estimating the carrying capacity of single piles for design of bored and cast in-situ reinforced cocrete piles. First. ICTAD/DEV/15.

Serrano, A., Olalla, C. And Galindo, R.A. (2014) 'INVE_MEM_2014_196869.pdf', International Journal of Rock Mechanics and Mining Sciences, pp. 83–90.

Thilakasiri, I. Et al. (2015) 'International society for soil mechanics and foundation engineering', Geotextiles and Geomembranes, 1(2), pp. 161–162. Doi:10.1016/0266-1144(84)90012-8.

Federation of Piling Specialists (2006) 'Handbook on Pile Load Testing', Handbook, (February), p. 47.

Numerical Analysis on Deformation Behavior of Soil – Cement Column Supported Pipes

D.P.L.N.Y.M. Perera and N.H. Priyankara
Department of Civil and Environmental Engineering, University of Ruhuna, Sri Lanka

ABSTRACT: Micro Tunneling (MT) has been used globally to lay pipes to overcome the inconveniences caused when using the Open Cut method. The major problem faced during MT in soft soil is the settlement of the Tunnel Boring Machine (TBM) head. Therefore, it is necessary to improve the soft soil below the proposed bedding level of the pipe. As an economical ground improvement method Soil Cement Columns (SCCs) can be used but the behavior of the SCC under pipe loading has not been studied. In this research the analytical methods available to calculate the vertical earth loads acting on buried pipes were reviewed and the long-term consolidation behavior of SCCs under pipe loading was studied. Furthermore, the lateral deformation behavior of the SCCs was studied during the MT process and PLAXIS 2D software was used for the numerical modelling. Results obtained revealed that numerical modelling of buried pipes can be done to obtain accurate results matching the analytical equations. The cohesion of the soil above the crown of the pipe has a significant impact on the vertical soil load on the pipe in trenchless conditions and the sensitivity of the horizontal jacking force for lateral behavior of SCCs was high compared to the length of the SCCs.

KEY WORDS: PLAXIS 2D, Micro tunnelling, Soil Cement Column (SCC), Long term consolidation, Lateral deformation

1 INTRODUCTION

The transportation of water has always been an important concern in the field of Civil engineering. The main and the most conventional mode for transporting water is by using pipes. Pipes made up of various materials with different lengths and diameters are used to convey water to residential areas, convey stormwater, collect and transport wastewater from domestic, agricultural, commercial and industrial sectors to wastewater treatment plants. These are the most frequent applications in Sri Lanka. Additionally, pipes are also used in many countries for the transportation of refined petroleum fuels across long distances directly to industrial facilities.

Although Open Trench method is the most commonly used method globally to lay pipes, the need for trenchless piping techniques have raised. This is due to heavy traffic caused during the construction and repair work of pipelines when using the Open Trench method. The concept of Micro Tunneling (MT) as a trenchless alternative for laying pipes is used as a sustainable solution for the above problem. It involves the use of a remotely handled, guided pipe jacking process using a Tunnel Boring Machine (TBM) where the excavations are done only at the starting and the ending positions of the pipe. The pipe is driven underground between these two locations using a pipe jacking process. The disturbances in the day-to-day activities of the public, traffic jams, the high CO2 emission and the cost and time consumption due to digging up and refilling large sections of land during the Open Trench method can be minimized by using the concept of MT.

One of the major issues faced when using the MT technique was the settlement of the TBM head during the tunnel operation, especially in soft soil (Lee, et al., 1992). And the pipes are subjected to earth loads due to backfilling material and surcharge loads during the operation stage, which may cause differential settlement of the pipes, thereby the expected conveyance efficiency of the pipes may be hindered. The safety of buried pipes under different loading conditions depends highly on the safe material and geometric design of them. This cannot be achieved unless their actual behavior is well understood. As a significant portion of the pipeline is buried in the ground the soil pipe interaction is important as a part of the stress analysis. As such it is important to study the vertical loads due to the soil overburden and the surcharge loads acting on the ground surface.

Even though there is a huge technological advancement in the field of Geotechnical engineering, engineers are facing difficulties in monitoring the pressure variation on top of buried pipelines acting due to soil loads and surcharge loads especially at the service stage. Therefore, no field measurements of earth pressure have been reported to validate the calculation methods found in the literature. To

overcome these issues, available commercial finite element software can be used to simulate the field conditions of buried pipelines and use the data obtained from analytical methods for validation purpose.

Due to settlement issues faced during the MT process, ground improvement techniques such as Soil Cement Columns (SCCs) can be used to improve the ground, but the behavior of SCC improved ground has not been fully understood. Many studies have been done on settling of the TBM head and ground surface settlements using various geotechnical finite element software like Flac 2D, Abacus, Plaxis 2D etc. during and after the Micro tunnelling process, (Duan, 2001, Tamagnini,et al.) but very few studies have been done on developing a method to reduce the settlement using ground improvement techniques. Even though the behavior of deep mixing cement improved grounds have been studied in the past, only very limited research has been conducted to study the behavior of SCC supported pipes. As such, in this research study behavior of buried pipes in SCC improved ground was studied.

2 METHODOLOGY

In order to study the behavior of buried pipes, the vertical load on the buried pipes were analyzed using 4 analytical methods, namely, Marston, GB, ASTM and EN (Shao, et al., 2016). A comparison was then done on these identified standards to investigate any unconformities or discrepancies. To validate the analytical results a buried pipe was modelled using PLAXIS 2D software with relevant soil and pipe parameters.

2.1 *GB standard*

The Chinese National standard GB50332 has defined the calculating method of soil pressure installed by trenchless technologies based on Terzaghi Soil Arching Theory and the related parameters have been simplified. Here the cohesion of the soil is totally disregarded. The used equations are Eq. (1), (2) and (3).

$$B = D[1+\tan(45-\Phi/2)] \quad (1)$$

$$k = (1-e^{-}(2K_a\mu h/B)) /(2K_a\mu h/B) \quad (2)$$

$$q = kYh \quad (3)$$

Where, Φ = Friction angle of soil, K_a = Active earth pressure coefficient, μ = Friction coefficient of the sliding surfaces, D = Diameter of the drilling hole, B = Silo width, k = Soil arching factor, Υ = unit weight of soil, q = Soil pressure.

2.2 *EN standard*

EN standard uses 2 different methods for calculating the soil earth pressure acting on trenchless pipelines, for granular soils and compressible soils as the arching effect in these 2 groups of soils are obviously different. For granular soils a better arching effect is formed while in compressible soils the consolidation effect tends to diminish the arching effect. The Eq. (4), (5), (6) and (7) are relative to the granular soils.

$$K = 1 - \sin(\Phi) \quad (4)$$

$$B = D [1 + 2\tan(45-\Phi/2)] \quad (5)$$

$$k=[1-(2c)/(\Upsilon B)][B(1-e^{-(2K h\tan\Phi/B)}]/[2Kh\tan\Phi] \quad (6)$$

$$q = k\Upsilon h \quad (7)$$

Where, Φ = Friction angle of soil, K = Earth pressure coefficient at rest, h = Cover depth, c = Cohesion strength, D = Diameter of the drilling hole, B = Silo width, k = Soil arching factor, Y = Unit weight of soil, q = Soil pressure.

2.3 *ASTM standard*

ASTM F1962 proposed a modified version of the Terzaghi Soil Arching Theory for the calculation of vertical soil loads on pipes installed under trenchless conditions. The cohesion of the soil is totally disregarded. The used equations are given in Eq (8), (9), (10), (11), (12), (13).

$$\delta = \Phi/2 \quad (8)$$

$$B = 1.5D \quad (9)$$

h_{min} = 5D (to guarantee the development of the soil arching) (10)

$$K_a = [\tan(45 - \Phi/2)]^2 \quad (11)$$

$$k = (1-e^{-}(2K_a h\tan\delta/B)) /(2K_a h\tan\delta/B) \quad (12)$$

$$q = k\Upsilon h \quad (13)$$

Where, δ = Friction angle mobilized in the sliding surfaces, Φ = Friction angle of soil, Ka = Active earth pressure coefficient at rest, h = Cover depth, D = Diameter of the drilling hole, B = Silo width, k = Soil arching factor, Y = Unit weight of soil, q = Soil pressure.

2.4 *Marston's method*

Marston's theory estimates the load on a buried pipe as equal to the weight of the prism of soil directly

over it, plus or minus the frictional shearing forces transferred to that prism by the adjacent prism of soil. The used equations are given in Eq (14), (15) and (16).

$$W = CwBd^2 \quad (14)$$

$$C = (1\text{-}e - (2K_aH\mu'/B_d)) /(2K\mu'/Bd^2) \quad (15)$$

$$k = (1\text{-}\sin\Phi)/(1+\sin\Phi) \quad (16)$$

Where, W = Vertical load on pipe, w = Density of backfill material, Bd = Width of the trench on top of pipe, Ka = Active lateral earth pressure, H=Height of the backfill material above the pipe, μ'=Coefficient of friction between the fill material and the sides of the trenches, Φ = Friction angle of soil.

To study the long-term consolidation behavior of the SCC improved ground under pipe and traffic loading, a numerical model was established using PLAXIS 2D software. The pipe settlement data available at the Greater Colombo Water and Wastewater Management Improvement Investment Project was used to validate the numerical model. Further, parametric analysis was done to study the effect of the length of Soil Cement Columns and horizontal jacking force on the lateral deformation of SCCs.

2.5 *Modelling of Soil Cement Column improved ground*

The geometric modelling, material modelling and pipe loading were the main components considered in establishing the numerical model. The subsurface soil profile considered for this analysis is shown in Figure 1. The subsurface mainly consists of 1.2m thick soil fill followed by 12.1m thick soft soil layer. Completely weathered rock is 13.3m below the ground surface. Further, water table is at the ground surface.

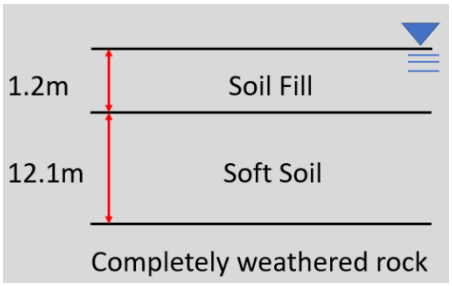

Fig. 1 Soil profile used for the analysis

Soil Cement Columns (SCC) were used to support the pipe as shown in Figure 2. SCCs were placed at 1.0m spacing both longitudinal and transverse directions as depicted in Figure 2 (a). Diameter of the SCC is 1.2m. SCCs were installed up to the completely weathered rock layer. The pipe is supported by two SCCs as illustrated in Figure 2 (b). 1.2m diameter pipe was placed at a depth of 3.5m from the ground surface and supported by 2 numbers of SCCs at a particular cross-section. [Figure 2 (b)].

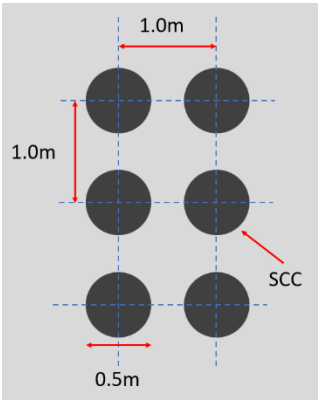

(a) Plan

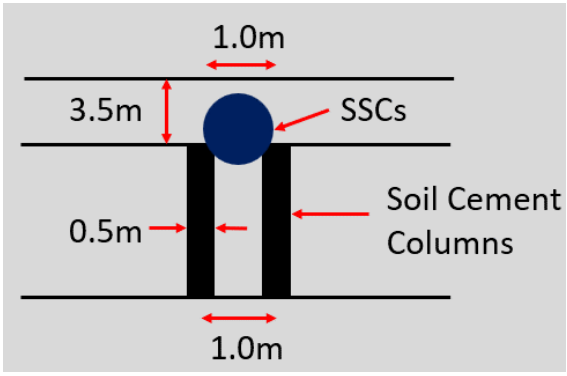

(b) Elevation

Fig. 2 SCCs arrangement

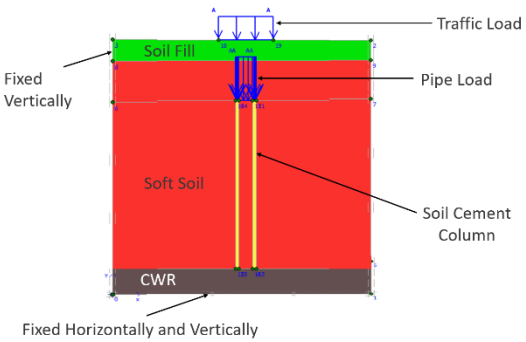

Fig. 3 PLAXIS 2D model

The numerical model used for the analysis is presented in Figure 3.

Fixed supports and roller supports were considered at the bottom and vertical boundaries respectively. At the interface between the SCC and soft clay,

interface elements were used. The length (L) and the height (h) of the model were 50m and 16m respectively. To convert the 3D Soil Cement Columns into plain strain conditions, the equivalent strip was used as shown in Figure 4. The area replacement ratio (as), which is calculated as the total area of SCCs divided by the original area of unreinforced ground, was considered assuming columns are arranged in a square pattern.

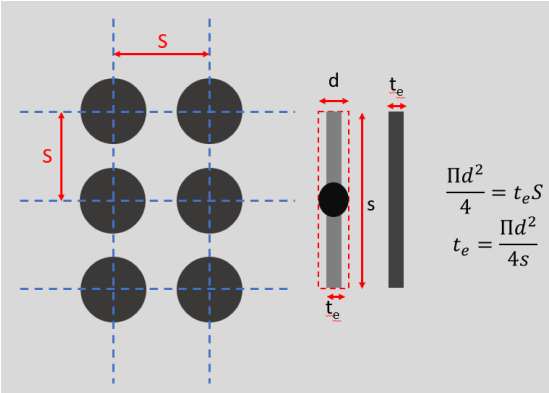

Fig 4 Equivalent strip to convert 3D SCC to plain strain conditions

Soft clay, SCC and pipe properties were obtained from the ongoing MT project in Colombo Municipal Council (CMC). Material properties for the soil layers and the SCC obtained from the soil investigation done at the site are given in Table 1. The pipe loading calculations were done under 2 separate stages, i) During the operational stage and ii) During the construction stage. The operational stage is when the installed pipe is under service and the pipe is delivering its intended purpose. During the operational stage the loads acting on the SCCs are; i) The load due to the overburden soil, ii) Self weight of the pipe and iii) Weight of the sewage in the pipe per meter run. The geometric model used in the analysis is shown in Figure 5. 15 nodded elements were considered to generate the mesh of the model and the mesh coarseness was assigned as fine.

MC – Mohr – Coulomb, C – cohesion, Φ – Friction angle, C_u – Interface cohesion, E – Young's Modulus, ν – Poisson ratio, k_x – coefficient of permeability in horizontal direction, k_y – coefficient of permeability in vertical direction.

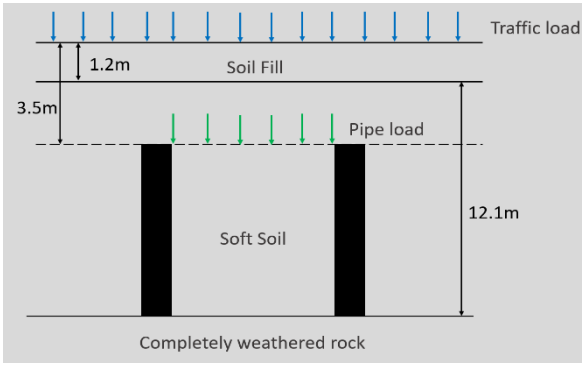

Fig 5 Geometric model used for the Plaxis analysis

To study the lateral deformation behavior of SCC composite ground during the MT process, the MT operation was modelled using FEM analysis using PLAXIS 2D. Due to the practical difficulty of obtaining lateral deformation values of the SCCs during the MT operation, there was no field data to validate the numerical model. Therefore, the validated PLAXIS model which was established to model the operation stage of the buried pipe on SCC improved ground was used to study the lateral deformation behavior of SCC composite ground during the MT process. During the construction stage the vertical loads acting on the SCCs are; i) The load due to overburden soil, ii) Self weight of the pipe, iii) Weight of the machine (TBM) and iv) Lateral force exerted during the MT process. A schematic diagram indicating the loads acting on the model ground is shown in Figure 6.

Table 1 : Material properties

Material	**Material model**	**Material type**	**Strength parameters**			**Compressibility properties**		**Permeability**		**Dry unit weight**	**Wet unit weight**
			C' (kPa)	Φ (kPa)	C_u (kPa)	E (kPa)	ν	k_x (m/d)	k_y (m/d)	Y_{unsat} (kN/m^3)	Y_{sat} (kN/m^3)
Soil fill	MC	Drained		30	25	750	0.4	1.5×10^{-4}	1.5×10^{-4}	15	17
Soft Soil	MC	Drained		30	25	750	0.4	1.5×10^{-4}	1.5×10^{-4}	11	14
Completely weathered rock	MC	Drained	10	38		40000	0.25	1.5×10^{-4}	1.5×10^{-4}	20	22
SCCs	MC	Drained		35	450	172500	0.25	1.5×10^{-4}	1.5×10^{-4}	14	14

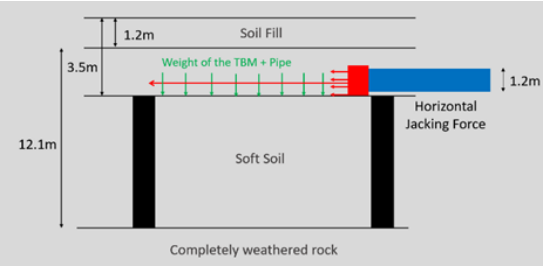

Fig. 6 Schematic diagram of the loads

3 RESULTS AND DISCUSSION

Terzaghi's Soil Arching Theory is considered as the basic principle on which the calculation of vertical loads on buried pipes depends (Shao, et al., 2016). The comparison of the vertical load on buried pipes calculated using the available 4 different analytical methods are summarized in Table 2. The results of the numerical model (PLAXIS 2D) are also presented in the same table. It can be seen that the Marston's method, GB method and the ASTM method gives identical solution for the load while the EN method shows a deviation. The results obtained from PLAXIS 2D are close to the results of the first 3 analytical methods.

Table 2: The results from analytical and numerical methods

	Marston's method	GB method	ASTM method	EN method	PLAXIS 2D
Vertical load at the crown of the pipe (kN/m)	73.74	73.74	73.74	56.51	73.94

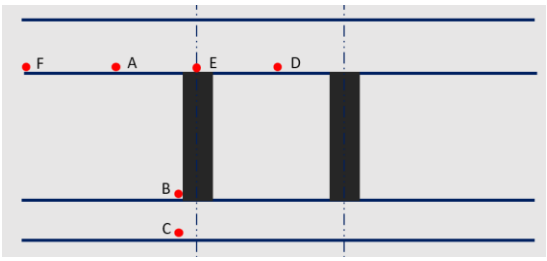

Fig. 7 Points considered for settlement comparison

The numerical model was validated using the settlement records obtained from Greater Colombo Water and Wastewater Management Improvement Project. Six points were considered for the settlement comparison as illustrated in Figure 7. "E" represents a point on the Soil Cement Column where as "D" represents a point in between Soil Cement Columns. Points "A" & "F" are away from the pipe loading. Point "B" is on the completely weathered rock layer while point "C" is within the completely weathered rock layer. The variation of settlement overtime at points A to F is illustrated in Figure 8.

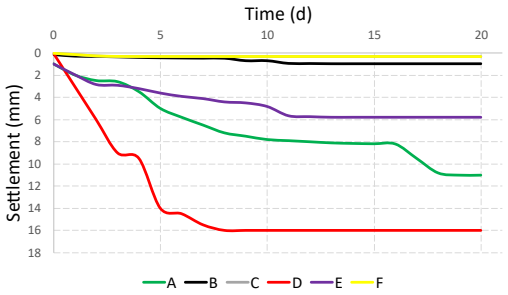

Fig. 8 Variation of settlement over time (numerical analysis)

Since completely weathered rock is very stiff there is no any settlement at points B and C. The point "D" which is at the middle of the SCC improved ground gives the maximum settlement. The settlement records at Colombo Municipal Council pipe project is shown in Figure 8. The ultimate settlement obtained from the field records was about 17mm as we can obtain from the difference of initial and final settlement values in Figure 9. The maximum settlement given by numerical model at point D is about 16mm as shown in the Figure 10. As such, it can be concluded that the results obtained from the numerical model is almost close to the field records.

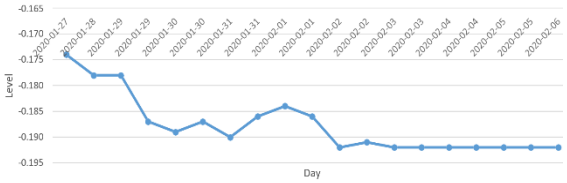

Fig. 9 Settlement records in the field

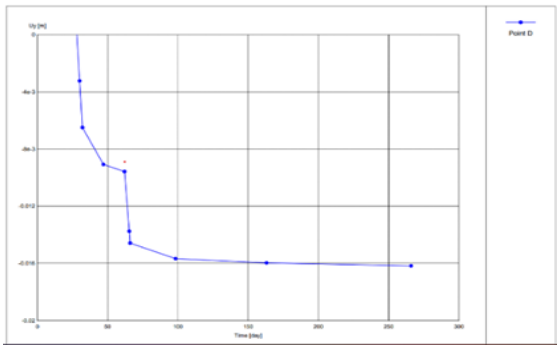

Fig. 10 Numerical settlement values

Due to practical difficulties of obtaining the settlement on top of SCCs (point E) in the site, there were no available settlement records. Therefore, to validate the settlement on top of SCCs the analytical Equation (15) was used. Where S = settlement, F = Force on the SCC.

Total force on SCC at operational stage (F) = self-weight of the pipe ($2\Pi\times0.6\times0.12\times25$) + weight of the sewerage in the pipe ($\Pi\times(1.2\text{-}0.24)^2\times9.81/4$ =11.31+7.1 = 18.41 kN/m),

L = length of the SCC (9.8m),

A = Cross sectional area of SCC ($\Pi\times0.5^2/4$= $0.196m^2$)

E = Young's modulus of SCC (1.72×105 kN/m^2).

$S=FL/AE= (18.41\times9.8)/(0.196\times1.72\times10^5)=5.4mm$ (15)

The above completed settlement was compared with the settlement at point E obtained from the numerical model which was 5.7mm. Thereby, it can be concluded that the settlement on top of SCCs obtained from PLAXIS 2D is validated analytically.

To compare the lateral deformation of the SCCs during the MT process, a normalized ratio J/L was considered where J is the jacking force and L is the SCC length. The variation of the lateral deformation of the SCCs are plotted against the J/L ratio under 2 conditions; i) varying the horizontal jacking force keeping the length of the SCC constant, and ii) varying the length of the SCC keeping the horizontal jacking force constant. The graphical representation of the obtained results is illustrated in Figure 11 and Figure 12. Based on Figure 11, it can be seen that the horizontal deformation of SCC gradually increases with the increase of jacking force. On the other hand, lateral deformation decreases when the SCC pile length decreases.

To study the sensitivity of the 2 parameters namely L (length of the SCC) and J (Horizontal jacking force) the results were plotted in the same graph as shown in Figure 13. It can be noted that when the J/L ratio increases from 10 to 28, lateral deformation has been significantly increased under constant SCC length and varying jacking force. Conversely, when the J/L ratio increases from 10 to 28, lateral deformation has slightly decreased under constant jacking force and varying SCC length. As such, it can be concluded that the most sensitive parameter on lateral deformation is horizontal jacking force than that of SCC length.

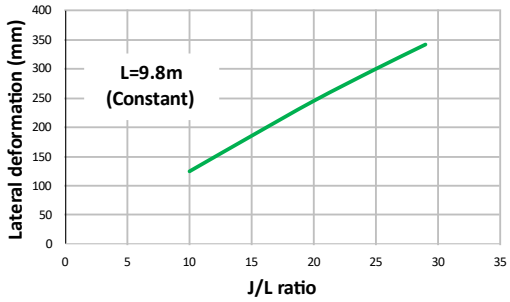

Fig. 11 Variation of lateral deformation over horizontal jacking force

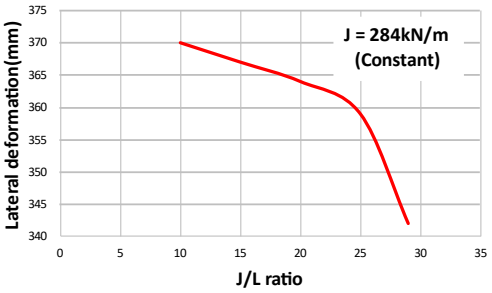

Fig. 12 Variation of lateral deformation over SCC length

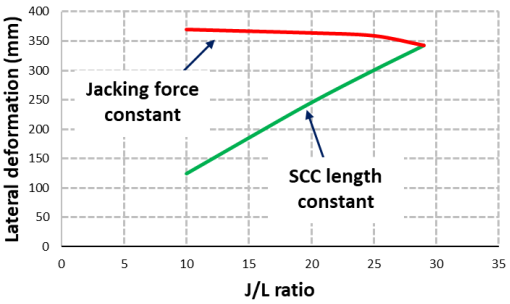

Fig. 13 Sensitivity analysis

4 CONCLUSION

One of the major issues faced by engineers when it comes to pipeline design is the absence of a clear methodology to estimate the vertical loads acting on buried pipes due to overburden pressure and surcharge loads. It was realized that the Terzaghi soil arching theory is the basis for all most all methods available for the calculation of vertical loads on a buried pipe. 4 methods namely; Marston's method, ASTM method, GB method and EN method were studied in the research. Out of the above 4 methods Marston's method, ASTM method and the GB method gave similar results while the EN method showed a slight deviation. The numerical study which was done using PLAXIS - 2D to calculate the vertical soil loads on buried pipes implies that the

results obtained were close to the values obtained from the Marston's, ASTM and GB methods. The long – term deformation behavior of SCC improved ground was studied numerically. The ground settlement records from the ongoing MT project in the CMC was used for validation purposes. It can be noted that the settlement of SCC improved ground consolidated under pipe loads and comes to a constant value. To study the lateral deformation behavior of SCCs during the construction stage of the MT process the validated model based on the long-term settlement records was used. The lateral deformation behavior of SCCs was studied considering 2 parameters namely, horizontal jacking force and the length of the SCCs. When the horizontal jacking force was increased the lateral deformation of SCCs increased. When the length of the SCCs was decreased the lateral deformation of the SCCs decreased. The sensitivity analysis illustrated that horizontal jacking force was the more dominant factor in lateral deformation of SCC than the length of SCC.

5 REFERENCES

Shao, L., Zhou, X. & Zeng, H., 2016. Comparison of Soil Pressure Calculating Methods Based on Terzaghi Model in Different Standards. The Open Civil Engineering Journal, Volume 10, pp. 481-488.

Duan, Z., 2001. Ground movement associated with microtunneling.

Lee, K. M., Rowe, K. R. & Lo, K. Y., 1992. Subsidence owing to tunnelling. Estimating the gap parameter. Canadian Geotech, pp. 929-940.

The prediction of settlement of organic soils due to increase in stresses

C.O Welikala, H.S Thilakasiri
Department of Civil Engineering, Sri Lanka Institute of Information Technology.

ABSTRACT: The analysis of primary and secondary consolidation on organic soil is significant, because of the complex nature of the soil due to the high amount of water content and void ratio. Even though surcharging has been carried out, organic soils tend to settle with a reduced rate of secondary consolidation with time after initial primary consolidation. Therefore, researchers have established empirical correlations to predict the secondary consolidation settlement. However, the established methods predict less accurate results on Sri Lankan organic soils due to its unique organic matter and microstructure. Therefore, laboratory tests were conducted on organic soil samples to obtain the behaviour of post-surcharge secondary consolidation with time. The observations suggest that Sri Lankan organic soils consume more time than predicted by empirical correlations to create a reasonable impact from post-surcharge secondary consolidation. The results were compared with the actual secondary consolidation settlement monitoring data of the Colombo-Katunayake Expressway (CKE) project as well.

KEY WORDS: Secondary consolidation, Organic soil, Surcharge, Post surcharge secondary consolidation, Microstructure

1 INTRODUCTION

Organic soil is an important soil type, formed by the accumulation of partially or fully decomposed organic matter, such as animal and plant residues. Generally, organic soils have a high amount of moisture contents, high compressibility, and a high rate of creep behaviour properties that result in catastrophic settlements due to increased stresses compared to the other types of soils. Because of these properties, organic soils create various problems for infrastructure development. Such as slip failure, difficulty in sampling, localized sinking, shrinkage, and change in material. (Edil and Haan (1994), Haan (2006), Huat (2006))

The secondary consolidation settlement is defined as the increase of the settlement due to the reorientation of soil particles under constant effective stress. The primary and secondary consolidation settlements could take place at the same time, but for convenience, it is assumed that only after the completion of the primary consolidation settlement the secondary consolidation settlement begins. Even though the secondary settlement is approximately negligible for sandy and gravel soils, according to Mesri et al (1997), secondary consolidation settlement is significant for organic soils.

Most of the construction built on an underlying organic soil layer, subject to soil improvements such as preloading along with sand compaction piles, crushed stone piles, etc to minimize the impact of primary and secondary consolidation. Also, preloading increases the shear strength of the soil, by densification and consolidation of the soil, which is followed by a decrease in the natural moisture content (Bowles, 1997). After removal of the surcharge (preloading), organic soil undergoes an expansion considerably higher than clayey soils. However, the impact of secondary consolidation is minimized by the soil improvements, organic soil tends to settle under applied design load under time-dependent secondary consolidation that occur due to rearrangement of the microstructure of the organic matter. Therefore, the time-dependent (post-surcharge secondary consolidation) is a critical aspect with respect to the organic soils and it will be significant to predict that settlement before construction commenced on top of organic layers.

Therefore, Mesri et al. (1997) proposed a method for the prediction of secondary consolidation settlement after surcharge removal based on series of oedometer test results on undisturbed samples of Middleton peat. Mesri et al. (1997) considered several terms for their study. Such as the post-surcharge secondary compression index (C'_α) and post-surcharge secondary compression index after time t_l that will vary with the time(C''_α). Based on the laboratory test results, he proposed a relationship for the behaviour of the C''_α/C_α (C_α – Coefficient of secondary consolidation in the normally consolidated soil) versus the function of $t/\ t_l$ (Where t_l is time to reappear the secondary consolidation and t is the time considered) for different surcharge ratios as shown in Fig 1. Like Mesri et al (1997), Ladd (1989) proposed a method to predict the secondary consolidation of cohesive soils with the assumption the

rate of secondary compression is linear when plotted in a semi-log plot. Under Ladd's method, two parameters are considered, C'_α – Secondary compression that undergoes when soil is over-consolidated and aged under the surcharge load and C_α – Secondary compression that undergoes when soil is not surcharged and unaged. With respect to the aging of the soil under surcharging stress, Ladd has proposed a relationship between C'_α / C_α as a function of AAOS (Adjusted amount of surcharge) and AOS (Amount of surcharge) Bartlett et al (2020).

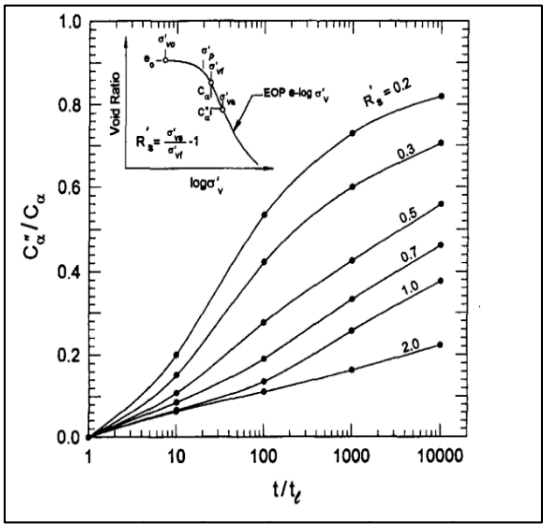

Fig 1. C''_α / C_α variation with t/t_l for Middleton peat (Mesri et al. 1997)

Similar to Mesri et al. (1997), Aljouni et al. (2001), Feng (1991), Mesri and Feng (1991) obtained a relationship of C''_α / C_α versus t/t_l for organic soil samples from James Bay peat and an inorganic soft clay samples. Those observations suggest that based on geological properties the relationship of C''_α / C_α versus t/t_l may vary from location to location. The Colombo Katunayake Expressway project (CKE) is an expressway built underlying peat layers up to 11m in thickness. Therefore, the above-mentioned secondary consolidation prediction methods are utilized to predict secondary consolidation after the surcharge removal during the defect liability period of the project. However, the obtained results deviate from the actual settlement results due to several limitations of the Mesri et al. (1997) method.

There is a lack of certainty on whether the Mesri et al. (1997) method is suited for the organic soils in Sri Lanka to predict the secondary compression behavior with the C''_α / C_α vs t/t_l as shown in Fig. 1. Therefore, a proper study should be carried out to analyze the applicability of the Mesri et al. (1997) method on the organic soil presence in Sri Lanka consistent with low to medium-range organic content. This study intends to reproduce the C''_α / C_α ratio with t/t_l and analyze the results with Mesri's results using the available data from the CKE project and deposit in the southern province of Sri Lanka and compare the accuracy of the secondary consolidation settlements obtained by Hyperbolic, Mesri et al. (1997) and Ladd (1989) methods on Sri Lankan organic soils.

2 METHODOLOGY

In contrast to clay and sandy soils, organic soil has a unique behaviour in secondary consolidation with time due to the presence of organic matter. Therefore, the settlement takes place in a complex manner. In this study, the accuracy of the above-mentioned methods will be assessed, and improvements will be suggested for the C''_α / C_α variation with t/t_l that will be suited to the condition of Sri Lankan organic soils. The methodology that has been followed to achieve the objectives and aims mentioned above is described in the following section.

2.1 *Available data*

Special Oedometer test results for organic soil samples from the Colombo Katunayake Expressway project with organic content variation within 10% to 90%. (However, only the samples in the range of 10% to 30% organic content will be used for the computations)

Special oedometer tests (As described in section 2.2) were carried out for the CKE project under the over-consolidate stage, and the results were analyzed to obtain the variation of C''_α / C_α ratio with time. Further, organic soil samples from the southern deposits were tested in the laboratory under a special oedometer testing procedure described in section 2.2, and analyzed the test results to obtain the behaviour C''_α / C_α ratio with t/t_l.

2.2 *Special oedometer test*

Settlement readings were taken at 0, 0.125, 0.25, 0.5, 1, 2, 5, 10, 15, 30, 60, 120, 240, 480 & 1440 mins for each loading that is equivalent to the applied stresses of 9,18,36,72,144 and 288kPa. Within the loading stage of the test, the pre-consolidation pressure of each soil sample was calculated using Casagrande's construction based on the estimated void ratios data for each load increment. The major difference between the special oedometer testing from the conventional method is the soil samples were subjected to a sequence of loading, unloading, and reloading stages to simulate the post-surcharge condition similar to the field condition of expressway construction. Within an expressway, preloading is carried out to minimize the impact of the settlement of the soil and then, remove it up to the design load, and then the traffic load will apply on the embankment after the defect liability period of the expressway. The unloading stage proceeded 3-4

days after the maximum load increment had been loaded. The loading, unloading, and reloading sequence of the testing is mentioned in following Table 1. The reloading increment within the procedure is called as "Surcharge ratio".

Effective Surcharge ratio (R_s) = $(\sigma'_{vs})/(\sigma'_{zf}) - 1$ (1)

Where σ'_{vs} = Effective surcharge stress (kN/m^2)
σ'_{zf} = Effective final stress (kN/m^2)

Table 1. The sequence of unloading and reloading of the special oedometer test for the R_s value of 0.3

Stage	Method
Loading	Based on the selected load increments, samples were loaded up to 8kg by doubling the previous load. The samples were kept for 24 hours at each load increment and recorded the settlements.
Unloading	The maximum load that has been subjected under the loading stage is removed from 8kg to 4kg, 4kg to 3kg, and 3kg to 2kg.
Reloading	Thereafter, the reloading the soil sample proceeded. First, the sample was subjected to the first reloading increment of 2kg to 5kg and the sample was kept for 7 days under the maximum load to obtain time-dependent secondary consolidation. Then, the remaining reload increments of 5.5kg and 6kg were placed on the existing load and kept for 7 days at the maximum load at each reload increment.

Along with the estimation of the void ratios, the time to end the primary consolidation was estimated for each load increment as well as in reload increments of each organic soil sample using the square root time method to obtain the time to reappear the secondary consolidation. Based on the void ratio versus log time graph plotted under the loading stage (normally consolidated stage), the secondary compression index (C_α) was estimated for each soil sample by obtaining the gradient of the linear part after the completion of primary consolidation. The $C'_\alpha$was estimated based on the void ratio versus the log time graph for reloading stages of the samples by obtaining several gradients along the graph after the time t_l. With the use of C'_α and C_α, the reduction of the secondary compression index was obtained. The variation of the C'_α / C_α versus t/t_l reproduced to compare with behaviour predicted by Mesri et al (1997).

3 RESULTS

3.1 *Determination of moisture content, specific gravity, and initial void ratios*

Table 2. shows the moisture contents, specific gravity, and initial void ratios estimated using the observations from the special oedometer test. Pre-consolidation pressure gives an overall idea about the soil's past overburden pressure it has been subjected to. This data has been utilized to arrange the load sequences for the special oedometer test to achieve the study's objectives. Also, it gives the idea that soil is in the over-consolidated or normally consolidated stage. The Table 2. only represents the selected samples from the CKE project and the results from the southern deposits that have been utilized to achieve the objective of the study.

Table 2. Specific gravity, organic content, and initial void ratio of the samples which were subjected to special oedometer tests from the CKE project

Parameter/ Samples	Organic content %	Specific gravity	e_0	C_α
A	27.2	2.484	3.927	0.055
B	27.2	2.484	3.925	0.056
T1	15.9	2.229	1.578	0.0258
T8	15.8	2.295	2.396	0.028
T4	22.7	2.378	2.233	0.0615
T5	26	2.278	1.595	0.0342

3.2 *The behaviour of secondary consolidation at the reloading stage (Removal of surcharge)*

In parallel to special oedometer testing, void ratio variation with the time has been observed with respect to the settlement readings in each load increment. A resultant void ratio versus log time graph at the reloading stage of the test is shown in Fig 2.

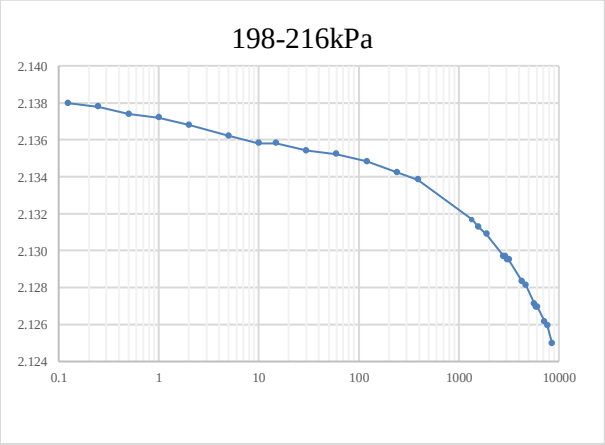

Fig 2. Post-surcharge secondary consolidation behaviour under R_s=0.3

According to the study, the post-surcharge secondary consolidation variation was analyzed to investigate the behaviour of organic soil samples in Sri Lanka based on the observed settlement results. It was noted that for each surcharge ratio of the soil sample, the variation of the ratio between C''_α / C_α slightly increased for a considerable time before starting to increase rapidly with time. Fig 3. represents the C''_α / C_α versus time function for all samples tested from the Southern deposit and CKE compared with the behaviour proposed by Mesri et al. (1997).

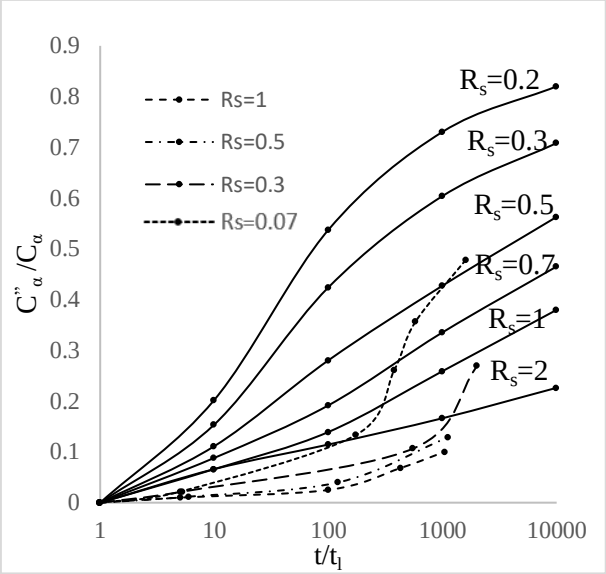

Fig 3. C''_α / C_α versus t/t_l for different surcharge ratios

4 DISCUSSION

The modified secondary consolidation is time-dependent, and it will be influenced by the microstructure of organic matter present within the soil. In 1997, Mesri et al. (1997) proposed a method to assess the modified coefficient of secondary consolidation (C''_α) by considering the time function (t/t_l). However, his findings were done on peat samples (Extract from Middleton, USA) with a high amount of organic content (around 95%). Therefore, there is a concern about applying this method to predict the modified secondary consolidation for the organic soils in Sri Lanka. Because in Sri Lanka organic soils consist of a range of low to medium organic content. Therefore, the impact of the time-dependent secondary consolidation of organic soils in Sri Lanka may vary, and the prediction accuracy will be less. Therefore, in this study, the accuracy of secondary settlement prediction methods and applicability of the methods on organic soils in Sri Lanka have been assessed using the ground investigating results and field monitoring data of the CKE project and Southern organic soil deposit. Mesri et al. (1997) suggest that the C''_α / C_α of organic soil will increase with the elapsed time, and it will vary with the surcharge ratio of the soil. The above conclusion has been further verified by Mesri et al (1997) in a similar study on soil samples of "James Bay peat" that has an organic content in the range of 96% (Ajlouni et al (2001)). However, the observed results from James Bay peat suggest an incremental trend on C''_α / C_α with time and are not similar to the results from Middleton peat. It suggests the C''_α / C_α vs t/t_l can vary with the geological formation based on the characteristics of organic soil.

Even though the C''_α / C_α will increase from the initial stage, the results obtained through the study on Sri Lanka organic soil showed a different behaviour from the findings of Mesri et al (1997) and Aljouni et al.(2001). It indicates that the C''_α / C_α variation is almost negligible to a considerable elapsed time and starts to increase. But the behavior may shift upward or downward based on the reload increment (Surcharge ratio – R_s) applied on the soil sample (like the findings of Mesri et al (1997)). However, in Mesri's proposed graphs the rate of increasing C''_α / C_α reduced in the latter part, but for the Sri Lankan organic soils, the latter part behavior suggests an incremental trend and may achieve a maximum reduction C''_α / C_α with the time pass. The reason will be the microstructure of the organic matter and the percentage of organic content present within the soil in Sri Lanka that has a significant variation from the Middleton peat and James Bay peat. According to Karunawardane (2010), the microstructure of Sri Lankan organic soil doesn't contain fibrous materials than Middleton and James Bay peat and it has decomposed more than the above-mentioned peats. Therefore, it is fair to obtain a behaviour of secondary consolidation mentioned above.

To check the accuracy of these methods to predict the secondary consolidation of organic soil deposits, actual settlement measured in the CKE project was compared with different prediction methods, Mesri et al., (1997), Ladd (1989) and the Hyperbolic method proposed by Tan et al. (1991). The study suggests that the secondary consolidation settlement prediction using the hyperbolic method is more satisfactory than the other two methods; the Ladd method and Mesri et al. (1997) method as shown in Fig 4. Because the hyperbolic prediction is mainly based on the field monitoring data and not based on any empirical correlation. It can be stated that irrespective of the stress applied to the soil layer, the hyperbolic predictions go on par with the field settlement data during the service period. In Ladd's (1989) method, a relationship has been developed to estimate the reduction of secondary compression under normally consolidated and over consolidated conditions.

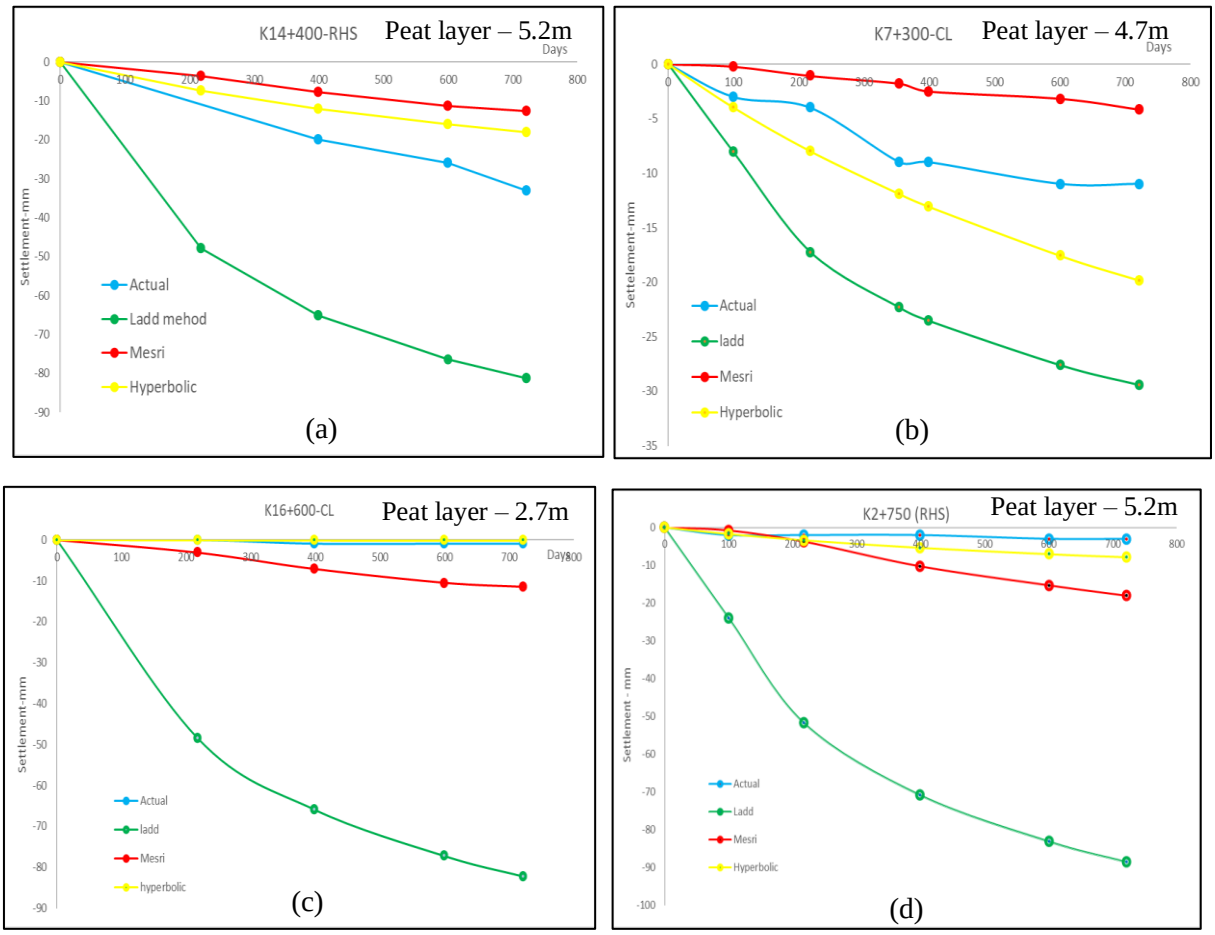

Fig 4. Settlement prediction by secondary consolidation prediction methods along CKE project

However, Ladd (1989) does not show any variation of the post-surcharge secondary compression with the time function and Ladd suggests a specific reduction value of secondary compression for a specific adjusted amount of surcharge (AAOS) and amount of surcharge (AOS). However, the reduction of secondary compression considerably influences the aging of the soil (elapsed time) and the condition of the soil (Sri Lankan organic soil contains low and medium organic content in contrast with organic soils in other countries). Therefore, the estimation of settlement from Ladd's (1989) method may predict over-estimated results for the Sri Lankan organic soils as shown in Fig 4. (a), (b), (c) & (d). Fig 4. (c) & (d) shows the increasing of the secondary consolidation more than the prediction by Mesri et al. (1997) method.

In the study, the time is affected heavily at the reloading stage of the special oedometer test to obtain a substantially comprehensive response on the reduction rate of C''_α / C_α. Therefore, as a future recommendation, more satisfactory results can be obtained on the reduction rate of secondary compression by considering the time duration kept at its reloading increment. Considering the results and discussion of the study, Sri Lankan organic soil has a unique variation of C''_α / C_α with respect to the proposed Mesri et al. (1997) variation. Therefore, it suggests that Sri Lankan organic soil has less increment in C''_α / C_α at the initial stage and start to increase with a rapid rate at the latter stage of the post surcharge secondary consolidation.

5 CONCLUSION

Assessing the secondary consolidation behaviour of organic soil is a critical aspect of geotechnical engineering because, with time, organic soils may undergo excessive settlements that will be hard to rehabilitate again. However, the behavior of secondary consolidation with time has been assessed by Mesri et al. (1997) using a peat sample of Middleton, the final outcomes from the proposed method estimate less accurate prediction for the Sri Lankan organic soils. Therefore, within the study, the accuracy of the Mesri et al method and the remaining prediction methods (Ladd and Hyperbolic methods) were assessed, and improvements were suggested for C''_α / C_α with the time under the

applicability of Mesri method for the Sri Lankan organic soils.

Special consolidation tests with a sequence of loading, unloading, and reloading stages were performed to assess the time-dependent secondary consolidation of organic soils as outlined in Table 3. Target reloading increments were preformed to achieve a substantially comprehensive variation for C''_{α}/ C_{α} with time. With respect to the obtained results, the reduction of C''_{α}/ C_{α} with time will initially begin with a lower rate (almost constant) to a considerable time and start to increase rapidly with time. Due to the time limitations of the special oedometer test, it is not reasonable to predict the full spectrum of the variation. The obtained results clearly showed that more time will be required to create a significant impact from the modified secondary consolidation. Therefore, the structures already constructed or planned to construct on organic soil layer may subjected to excessive settlements in its lifetime (The impact will affect the structure after a considerable elapsed time from the time of the finish of construction). In conclusion, future studies assessing the behaviour of time to reappear the modified secondary consolidation with respect to the organic matter present and its microstructure can be carried out along with methods to improve the organic soils to minimize the impact of the post-surcharge secondary consolidation.

6 REFERENCES

Bartlett, S. F., Lawton, E. C., & Gibbs, Z. M. (2020). Evaluation of Secondary Consolidation Settlement Associated with Embankment Construction for Fast-paced Transportation Projects [Research Report – MPC Publications]. University of Utah.

Bowles, J., 1997. Foundation Analysis and Design. 5th ed. Singapore: McGraw-Hill.Chu, J., Bo, M. W. & Choa, V., 2004. Practical considerations for using vertical drains in soil improvement projects. Geotextiles and Geomembranes, Volume 22, pp. 101-117.

Den Haan EJ, Kruse GAM (2006) Characterization and engineering properties of Dutch peats. Proc. 2nd Int. Workshop on Characterization and Engineering Properties of Natural Soils, Singapore.

Edil TN, Den Haan EJ (1994) Settlement of peats and organic soils. Proc. Settlement'94 Vol 2, ASCE, New York. 1543–1572.

Feng, T.W. 1991. Compressibility and permeability of natural soft clays and surcharging to reduce settlements. Ph.D. Thesis, University of Illinois at Urbana-Champaign, Urbana, Illinois

Gholamreza Mesri, Timothy D. Stark, M. A. Ajlouni, & C. S. Chen. (1997). Secondary Compression of Peat with or without Surcharging. Journal of Geotechnical and Geoenvironmental Engineering, 123(5), 411–421.

Huat BBK (2006) Deformation and shear strength characteristics of some tropical peat and organic soil, Pertanika. J. Sci. & Technol. 14(1&2):61-74.

Mesri G., Ajlouni M.A., Feng T.W. and Lo, D.O.K. 2001. Surcharging of soft ground to reduce secondary settlement. Proc. of the 3rd International Conference on Soft Soil Engineering, Swets & Zeitlinger, Hong Kong, 55-65.

Mesri, G., and Feng, T.W. 1991. Surcharging to reduce secondary settlements. Proc. International Conference on Geotechnical Engineering for Coastal Development, 1, Yokohama: 359-364.

Tan, T., Inoue, T. and Lee, S., 1991. Hyperbolic Method for Consolidation Analysis. Journal of Geotechnical Engineering, 117(11), pp.1723-1737.

NOVEL ANALYTICAL METHOD TO PREDICT THE GEOTECHNICAL ENGINEERING PROPERTIES OF CLAYEY SOIL STABILIZED WITH FLY ASH

K. Kowsikan and S. Jayalakshan

Department of Civil Engineering, University of Peradeniya, Sri Lanka

ABSTRACT: The study aims to develop predictive models to determine the geotechnical properties (Optimum Moisture Content (OMC), Maximum Dry Density (MDD), and Unconfined Compressive Strength (UCS)) of clay soil stabilized with fly ash (FA). For this purpose, many data were collected from relevant literature and predictive models were developed using ANN. Models were developed for OMC, MDD, and UCS of Fly ash stabilized clayey soil stabilized clayey soil. The developed models were validated with independent sets of data obtained from the literature and experimental results. It was verified that three proposed models (OMC model, MDD model and UCS_7d model) were successfully trained and validated. Therefore, these three models can be used to predict the OMC, MDD, and USC_7d of clayey soil stabilized with fly ash.

KEY WORDS: Artificial Neural Network, Fly ash, clay soil, Geotechnical properties

1 INTRODUCTION

Civil engineering project located in areas with inappropriate soils is one of the major problems in the world. Different methods can be selected for soil improvement such as hydraulic, mechanical, dynamical, physical, and chemical methods. However, Chemical soil stabilization has been used for several years to render the problematic soils capable of meeting the requirements of specific engineering projects (Kolias et al., 2005). Chemical soil stabilization is the most used by adding mineral additives to the clayey soil such as lime, silica, natural pozzolana, cement, slag, and fly ash. It is one of the suitable and economical methods for reducing both compressibility and plasticity but increasing both durability and strength.

Several laboratory investigations were provided to assess the effect of mineral additives on the geotechnical properties of soils. These laboratory studies are very beneficial for geotechnical engineers to obtain better practical results. But laboratory tests are costly and take a long time for each study. For these reasons, analytical techniques are used to predict geotechnical properties. Analytical tools can be used to develop models to predict different physical and mechanical properties of soils and consequently the reduction of both the time consumption and cost. In addition, the analytical models have been applied as an effective approach with high performance compared with the statistical models.

There are several analytical tools and techniques are in the literature, such as artificial neural networks (ANNs) (Hanandeh et al., 2020; Leong et al., 2018) multivariable regression (MVR) (Adhikari et al., 2019; Ahmed et al., 2018), genetic programming (Hanandeh et al., 2020; Leong et al., 2018), etc. Among these techniques, ANN reflects the behaviour of the human brain, it allows computer programs to recognize patterns and solve common problems in the fields of machine learning and deep learning.

There are very limited studies focusing on computer-based models for predicting the geotechnical properties of stabilized clayey soils whereas the previous studies showed the capacity of ANNs models in the prediction of different soil characteristics. This research will use the ANN machine learning toolbox in MATLAB to develop correlations to predict the geotechnical properties of clayey soil stabilized with fly ash. The required parameters for the model including Atterberg limits, MDD, OMC, UCS, CBR, etc will be collected from the literature. Data sets will be used to develop independent model for fly ash stabilized clayey soil. The developed ANN model will be validated by performing laboratory experiments for clayey samples stabilized with the above cementitious binder.

2 MATERIALS AND METHODS

2.1 *Data collection and treatment*

In this research, the data bases consist of results collected from several experimental studies of different types of soil stabilized by using fly ash published worldwide in literature. The data of stabilized clayey soil by using fly ash were gathered and compiled from a higher number of research projects to establish the three data bases (30 research projects carried out on the effect of fly ash on geotechnical properties: MDD, OMC and UCS). The database used for the development of ANNs models makeup a total of 27 and 18 types of soil respectively with the compaction characteristics models (MDD-ANNs and OMC-ANNs) and UCS-ANNs model. Table 3.1 shows the number of data sets collected for each ANNs model. These data were used to check the reliability of the model for predicting of OMC, MDD, UCS-7days and UCS-28 days of clayey soils stabilized with different contents of fly ash.

According to the literature data, percentage of fly ash, CaO percentage, PI (%), MDD_0 were chosen as input parameters for MDD model, percentage of fly ash, CaO percentage , PI (%), OMC_0 were chosen as input parameters for OMC model and percentage of fly ash, CaO percentage , PI (%), UCS_0 were chosen as input parameters for UCS _7d and UCS _28d models in fly ash stabilized clayey soil.

There are many techniques to remove outliers from a dataset. According to Dagmar Blatná.,2006 least median of squares (LMS) procedure and the least trimmed squares (LTS) regression are good for simple outliers and on the other hand Cook's Distance method and the robust distance are used mainly for multivariate outliers. One method that is often used in regression settings is Cook's Distance (C.Gunasekera et al.,2020). Cook's distance method was used to detect and remove the outliers to improve the dataset for machine learning modelling.

2.2 *ANN model Development*

The performance of ANN models depends on many parameters as the network topology and the learning parameters such as number of input and output, number of hidden layers, number of neurons in hidden layer, transfer function in hidden layer, maximum error, and number of learning cycles. There were no common rules to define the number of hidden layers and number of neurons in each hidden layer. Trial and error method was used to develop the model depending on the number of neurons in the hidden layer.

The models were developed by using the Levenberg – Marquardt algorithm as training function. It was proved as the fastest training algorithm for multilayer perception (Ismen et al., 2017). LM is most robust than the Gauss-Newton (GN) and it is faster to converge than either the GN or gradient decent on its own (Nelles, 2001). It was decided to use a three-layer feed forward – back propagating network with a tan-sigmoid function as the hidden layer transfer function and mean square error as the performance function. The best ANN model was determined by using trial and error method. It was preferred to use simple architecture of one hidden layer with limited number of neurons. Limited number of neurons were selected according to the better performance of the ANN model.

To check the efficiency of trained ANNs models, it is important to test their ability to generalize forecasting beyond the training data and to perform well when it was nominated with stranger data sets, inside the range of the input parameters was used in the training. Therefore, the capacity of proposed ANNs models were developed for check the geotechnical properties of new data which were obtained by other results from other research excluded from the training data must be validated. Regression value R and mean square error (MSE) and mean absolute percentage error (MAPE) were used to check the efficiency of ANNs models. Mean square error is the average squared difference between output and target. Lower values are better, zero means no error. Regression R values measured the correlation between outputs and targets. R value 1 means close relationship, 0 means random relationship.

To check the efficiency of trained ANN models, it is important to test their ability to generalize forecasting beyond the training data and to perform well when it was nominated with new independent data sets, inside the range of the input parameters used in the training. Therefore, the ability of the proposed ANN models were checked using a new set of data obtained by other results from other research.

Regression value R, mean square error (MSE) and mean absolute percentage error (MAPE) were used to check the efficiency of ANNs models. Mean square error is the average squared difference between output and target. Lower values are better, zero means no error.

3 MODEL VALIDATION THROUGH EXPERIMENTS

3.1 *Materials*

Raw expansive soil was collected from Hettipola Hospital site. Atterberg limit test was conducted, and PI value was obtained as 23%. As it difficult to find expansive soils having a wide range of PI values, different percentages of bentonite were mixed with the raw expansive soil sample to prepare the expansive soil with required PI value. Based on the trial mixers it was found that 7% and 15% of bentonite mixed soil satisfied the required PI (25% - 50%) range for the expansive soil.

Table 1. Composition of Class F fly ash (Dissanayake et al.2017)

Constituents	Percentage Composition / (%)
SiO_2	52.03
Al_2O_3	32.31
Fe_2O_3	7.04
CaO	5.55
MgO	1.3
SO_3	0.07
K_2O	0.68
Cl	1

7% and 15% bentonite mixed two soil samples were prepared. According to the ranges of soil properties in the data collection, two different percentage of fly ash (15% and 25%) were mixed with the two samples. Then the natural soil samples and fly ash stabilized samples were used for the experimental procedure.

3.2 *Proctor compaction test (BS1377- 4: 1990)*

Standard Proctor compaction test was carried out for the natural soil sample and fly ash stabilized soil sample to find the MDD and OMC. Soil and water were mixed until the mixture becomes a uniform colour. This mixture was placed in three equal layers in the cylindrical compaction mould with internal diameter of 100 mm, height 127 mm and volume of 1000 cm^3. Each layer was compacted using 4.5 kg rammer dropped freely 27 blows on the sample from the height of 450 mm. Then, extension collar was removed, strike off excess soil and level the surface of the compacted soil to the top of the mould using the straight edge. The weight of the sample with mould was measured to the nearest gram. The soil samples were taken from top and bottom of the removed sample to determine the water content. Then the removed sample was broken and mixed with the suitable increment of water, and the procedure was repeated until the mould weight reaches maximum and then starts to decrease. Moisture content versus dry density graph was plotted and OMC and MDD were determined from the graph.

3.3 *Unconfined compression test (BS1377: Part 7: 1990)*

This test was carried out to determine the UCS of the soil samples. Cylindrical specimens were prepared using Standard mould (38mm diameter and 76mm height) to test UCS by load frame method. The specimen was placed centrally on the pedestal of the compression machine between the upper and lower platens. Contact between the specimen, upper platen and the force measuring device was made by adjusting the machine. Set the axial deformation gauge to read zero. Initial readings of the force and compression gauges were taken. 1 mm/min axial deformation rate was 33 used for the UCS test. Simultaneous readings of the force measuring device and the axial deformation gauges at regular intervals of compression were recorded. Final reading of the force measuring gauge was recorded after removing the load. The specimen was removed from the apparatus for the determination of its moisture content. Axial strain applied force and axial compressive stress was calculated to plot the graph of compressive stress Vs corresponding values of strain, and the point on the graph representing the failure condition and young's modulus of each sample mixtures was found.

4 RESULTS AND DISCUSSION

4.1 *MDD model*

The architecture of one hidden layer constituted of 14 neurons makes the better performance model for predicting the MDD. According to Figure 4.1, the training data set has high performance compare than validation and target data sets. The regression value (R) of all data for MDD model was approximately 0.9759.

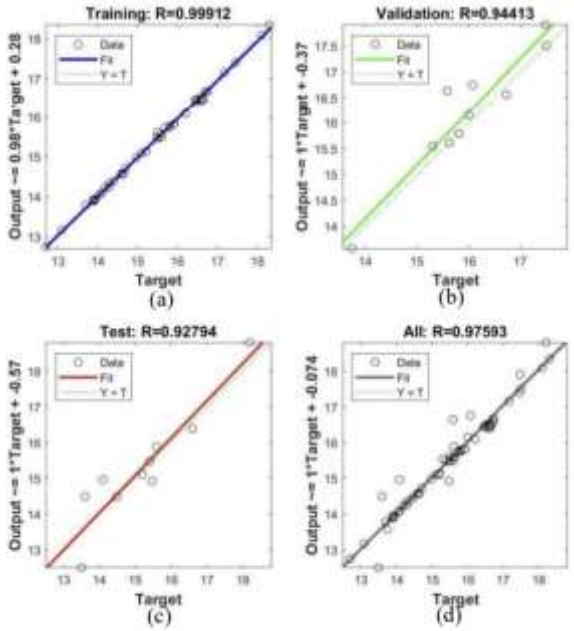

Fig. 1 Regression values of MDD – ANN model (a)Training,(b) Validation ,(c) Testing and (d) Overall

4.2 *OMC model*

The architecture of one hidden layer constituted of 19 neurons makes the better performance model for predicting the MDD. The training data set has high performance compare than validation and target data sets. The regression value of all data for OMC model was approximately 0.9739.

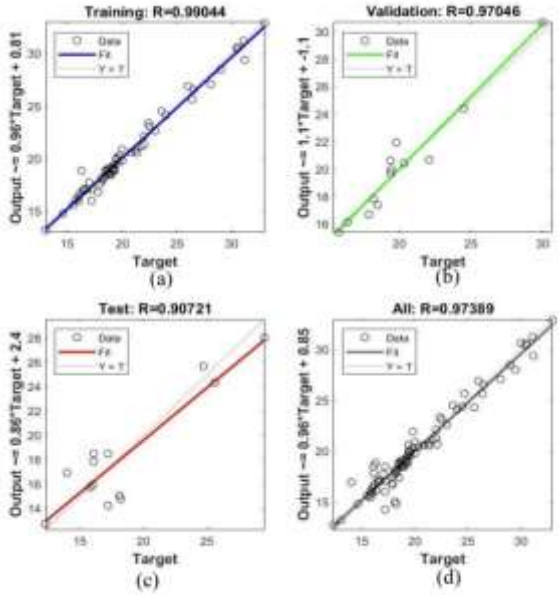

Fig. 2 Regression values of OMC – ANN model (a)Training, (b) Validation, (c) Testing and (d) Overall

4.3 *UCS-7days model*

The architecture of one hidden layer constituted of 14 neurons makes the better performance model for predicting the MDD. As shown in figure 4.3, the training data set has high performance compare than validation and target data sets. The regression value of all data for UCS_7d model was approximately 0.9835.

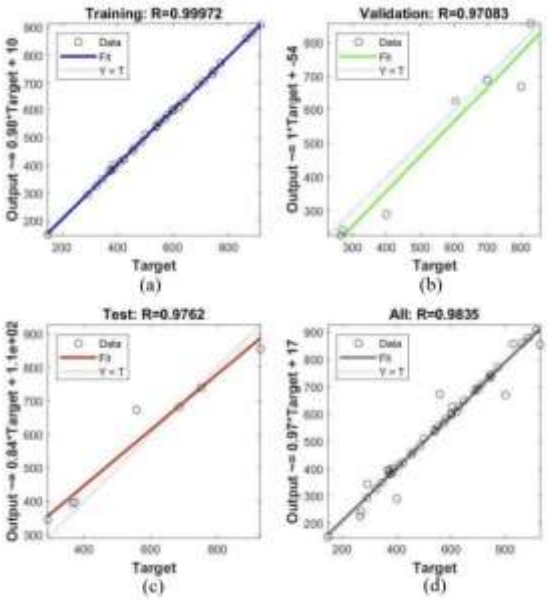

Fig. 3 Regression values of UCS_7d – ANN model (a)Training, (b) Validation ,(c) Testing and (d) Overall

4.4 *UCS-28days model*

The architecture of one hidden layer constituted of 15 neurons makes the better performance model for predicting the MDD. As shown in figure 4.4, the training data set has high performance compare than validation and target data sets. The regression value of all data for UCS_28d model was approximately 0.9888.

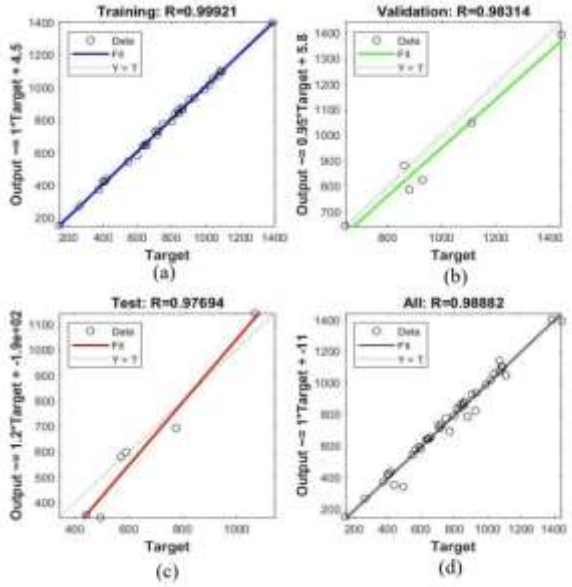

Fig. 4 Regression values of UCS_28d – ANN model (a)Training, (b) Validation, (c) Testing and (d) Overall

4.5 *Sensitive analysis*

The relative influence of input parameters cannot be readily observed in an ANN model. Hence the connection weight approach was used as suggested by Leong et al (2018) to find the variable contribution to the model. This approach ranks OMC of the natural soil as the most important parameter followed by Fly ash content, PI % and CaO% for OMC model. In MDD model, MDD of the natural soil as the most important parameter followed by CaO%, PI% and Fly ash content. In UCS_7d model and UCS_28d model, fly ash % as the most important parameter followed by CaO%, PI% and UCS of the natural soil.

4.6 *Model validation via experiment*

Results got from laboratory experiments were used to test the validation of the model previously obtained. Obtained results were added into the model and got further regression value and model was validated. Comparatively OMC model has high regression value than the other three models and UCS_28d model has low regression value than the other three models. For the OMC-ANNs model we used comparatively large data sets to develop the model so that the model accuracy is high for that and for UCS_28d model we used comparatively small amount of data sets to develop the model, so that the model accuracy is low for that. From this validation we can conclude that using more data to develop the model gives better accurate model than less used data models.

5 CONCLUSION

This study was made to develop ANNs models used for predicting geotechnical properties of fly ash stabilized clayey soils. This study carried out in this work showed the feasibility of using a simple ANNs to predict the MDD, OMC and UCS of clayey soil stabilized with fly ash. The advantages of the artificial neural over traditional regression analysis as applied to stabilization have been highlighted in the foregoing sections. In a typical field stabilization project, to improve the properties of expansive clays, experimental data are usually generated from several field and laboratory tests to monitor and ascertain the progress made in terms of improvement. These procedures are expensive and time-consuming and may be reduced to a minimum using ANN to predict the field response of the soils. The methods used in this study can easily be applied to study other types of cementitious binders stabilized with clayey soil, based on obtained results, the following conclusion can be drawn.

- Artificial Neural Network (ANN) can be used to predict the unconfined compressive strength (UCS), maximum dry density (MDD) and optimum moisture content (OMC) of the expansive stabilized with fly ash.
- It was verified that all proposed models were successfully trained and validated where the obtained results showed that the statistical analysis of geotechnical data is one of the most suitable techniques for developing new statistical model which can present the best understanding of problematic soils behaviour.
- Sensitivity analysis shows that OMC and MDD of the natural soil most influenced the OMC model and

MDD model respectively. For UCS models, fly ash content as the most influenced parameter.
- The regression values of the validation studies via experiments showed a better accurate of the three constructed models for predicting the studied geotechnical properties of fly ash stabilized clayey soil. (MDD, OMC and UCS_7d).
- It was verified that from this validation we concluded that using more data to develop the model gives better accurate model than less used data models.

ACKNOWLEDGMENTS

Our research study becomes a reality with the kind support of and help of many individuals. We would like to extend our sincere thanks to all of them. Foremost, we are highly indebted to our supervisor Dr. M. C. M. Nasvi for his valuable guidance and constant supervision in progressing this endeavour. Furthermore, we would like to express our gratitude to distinguished members of the panel, Dr. S. K. Navaratnarajah and Dr. A. M. R. G. Athapaththu for their advice and guidance during progress presentations. On top of that, we extend our gratitude to the department of civil engineering not only for the encouragement provided by conducting the research project as a part of the degree program but also for the laboratory facilities. Finally, our thanks and appreciations also go to all individuals in and out of the faculty who have willingly helped us out with their abilities.

REFERENCES

Ashraf, Ali, Sadek S Rahman, Omar Faruk and Abul Bashar. "Determination of Optimum Cement Content for Stabilization of Soft Soil and Durability Analysis of Soil Stabilized with Cement" Am J Civ Eng 6 (2018): 39-43.

Blatná, D., 2006. Outliers in regression. *Trutnov*, *30*, pp.1-6.

Cokca, E., (2001). Use of class c fly ashes for the stabilization of an expansive soil. *Journal of Geotechnical and Geoenvironmental Engineering*, *127*(7), pp.568-573.

Das, S.K., Samui, P., Sabat, A.K. and Sitharam, T.G., (2010). Prediction of swelling pressure of soil using artificial intelligence techniques. *Environmental Earth Sciences*, *61*(2), pp.393-403.

Deepak, M.S., Rohini, S., Harini, B.S. and Ananthi, G.B.G., (2021). Influence of fly-ash on the engineering characteristics of stabilized clay soil. *Materials Today: Proceedings*, *37*, pp.2014-2018.

Gunasekara, C., Lokuge, W., Keskic, M., Raj, N., Law, D.W. and Setunge, S., (2020). Design of Alkali-Activated Slag-Fly Ash Concrete Mixtures Using Machine Learning. Materials Journal, 117(5), pp.263-278.

Hossein Alavi, A., Hossein Gandomi, A., Mollahassani, A., Akbar Heshmati, A. and Rashed, A., (2010). Modeling of maximum dry density and optimum moisture content of stabilized soil using artificial neural networks. *Journal of Plant Nutrition and Soil Science*, *173*(3), pp.368-379.

Jalal, F.E., Xu, Y., Iqbal, M., Javed, M.F. and Jamhiri, B., (2021). Predictive modeling of swell-strength of expansive soils using artificial intelligence approaches: ANN, ANFIS and GEP. *Journal of Environmental Management*, *289*, p.112420.

Leong, H.Y., Ong, D.E.L., Sanjayan, J.G., Nazari, A. and Kueh, S.M., (2018). Effects of significant variables on compressive strength of soil-fly ash geopolymer: Variable analytical approach based on neural networks and genetic programming. Journal of Materials in Civil Engineering, 30(7), p.04018129.

Ling, Y., Wang, K., Wang, X. and Li, W., (2021). Prediction of engineering properties of fly ash-based geopolymer using artificial neural networks. *Neural Computing and Applications*, *33*(1), pp.85-105.

Mahajan, S.M. and Parbat, D.K., (2015). Effects of fly ash on engineering properties of BC soil. *Int J Eng Sci Res*, *1*.

Mir, B.A. and Sridharan, A., (2013). Physical and compaction behaviour of clay soil–fly ash mixtures. *Geotechnical and Geological engineering*, *31*(4), pp.1059-1072.

Mozumder, R.A. and Laskar, A.I., (2015). Prediction of unconfined compressive strength of geopolymer stabilized clayey soil using artificial neural network. *Computers and Geotechnics*, *69*, pp.291-300.

Naderpour, H., Rafiean, A.H. and Fakharian, P., (2018). Compressive strength prediction of environmentally friendly concrete using artificial neural networks. *Journal of Building Engineering*, *16*, pp.213-219.

Obianigwe, Njideka and Ben U Ngene. "Soil Stabilization for Road Construction: Comparative Analysis of a Three-Prong Approach" Mater Sci Eng 413 (2018).

Owamah, H.I., Atikpo, E., Oluwatuyi, O. and Oluwatomisin, A.M., (2017). Geotechnical properties of clayey soil stabilized with cement-sawdust ash for highway construction. *Journal of Applied Sciences and Environmental Management*, *21*(7), pp.1378-1381.

Numerical Simulation of Under Sleeper Pads Using Hyper-Elastic Material Models for Railway Applications

D. Panneerselvam, K. Ratnavel and S.K. Navaratnarajah
Department of Civil Engineering, University of Peradeniya, Sri Lanka

ABSTRACT: Railway transportation is one of the popular modes of transportation in most countries. The application of Under Sleeper Pads (USPs) in ballasted tracks is becoming popular to improve track performance while reducing track deterioration. Predicting the non-linear behavior of USPs under train loading is beneficial in the numerical simulation of train track models. Hence, this study focuses on numerical simulation of the non-linear behavior of USPs under the static loading condition by employing hyper-elastic material models. A numerical model of static load test on USP was developed using the Finite Element Method (FEM) and validated with the experimental data from the literature. Then a parametric study was carried out to investigate the effect of USP thickness on its static stiffness. The results of the parametric study revealed that the static stiffness increases when the USP thickness reduces.

KEYWORDS: Ballasted track, Under Sleeper Pad, Hyper-elastic materials, Numerical simulation

1 INTRODUCTION

The rail networks in many countries play a prominent role in the conveyance of bulk freight and commuter transport. The rapid growth in population, urbanization, as well as increasing congestion in highway transport and growing demand for energy is forcing rail industries to implement heavier and faster railway corridors to achieve efficient and cost-effective services. Many researchers have proposed that the inclusion of energy-absorbing rubber pads with appropriate properties could reduce the maintenance cost while increasing the life cycle of a track. There are mainly three types of energy-absorbing rubber pads being used in the track system: Rail Pad (RP), Under Sleeper Pad (USP), and Under Ballast Mat (UBM). The application of USP is an established practice in many railway networks worldwide due to their influence on enhancing track performance.

Finite Element Method (FEM) is one of the major approaches used in many numerical studies for railway applications. FEM has been successfully used to capture ballast layer stress, vertical and horizontal deformations of ballast, sleeper stress, and so on. In terms of simulating the behavior of USPs, few numerical studies have modeled them as a 3-D solid element with linear elastic material properties in FEM simulation of large-scale laboratory tests (Navaratnarajah et al., 2018; Ngamkhanong and Kaewunruen, 2020). Since the USP is made of a rubber-like material, it exhibits non-linear stress-strain behavior under excessive loading. Many studies have incorporated hyper-elastic material models to predict the non-linear behavior of rubber-like materials (Arachchi et al.,2021). However, studies on the application of hyper-elastic material models to simulate energy-absorbing rubber pads using FEM are very limited.

The static bedding modulus is the main characteristic parameter of an energy-absorbing rubber pad which can be evaluated using the static load test in the laboratory. In this study, numerical models were developed to simulate the static load test of a USP using the FEM approach. The USP was modeled in FEM employing hyper-elastic material properties to capture the non-linear behavior of rubber. The models were validated using experimental data from Navaratnarajah (2017) for quasi-static load conditions. Then a parametric study was done by changing the thickness of the rubber pad to capture the variation of static bedding modulus of the rubber pad.

2 HYPER-ELASTIC MATERIAL MODELS IN ABAQUS

The most attractive property of rubbers is their ability to experience large deformation under small loads and to retain initial configuration without considerable permanent deformation after the load is removed. Their stress-strain behavior is highly non-linear. Hyper-elastic materials are commonly used to capture the nonlinear stress-strain behavior of rubber when subjected to large deformations. In this study, a hyper-elastic material model is adopted to capture the behavior of the USP using ABAQUS 6.14/CAE commercial FEM software. ABAQUS software has many forms of hyper-elastic material

models. They are Moony-Rivlin model, Neo-Hookean model, Yeoh model, Ogden model, Reduced Polynomial model, Full Polynomial model, and Arruda-Boyce model, among others. All of these material models are having own strain energy functions to describe the behavior of rubber-like materials.

It is important to select the best suit hyper-elastic material model to accurately predict the behavior of a particular rubber pad having specific material properties. To select the best-suited material model, it is required at least one set of test data from the uniaxial test, biaxial test, volumetric test, and planer test (Arachchi et al., 2021). The curve fitting approach in ABAQUS facilitates the user to evaluate these test data and determines the stable hyper-elastic material models together with corresponding coefficient values to represent each material model. An error calculation with respect to test data can be done to compare the stable material models by using three selected statistical indexes such as Mean Absolute Percentage Error (MAPE), Mean Absolute Deviation (MAD), and Mean Squared Deviation (MSD).

$$MAPE = \frac{\sum_{t=1}^{n}\left|\frac{y_t-\hat{y}}{y_t}\right|}{n} * 100\% \quad (1)$$

$$MAD = \frac{\sum_{t=1}^{n}|y_t-\hat{y}|}{n} \quad (2)$$

$$MSD = \frac{\sum_{t=1}^{n}|y_t-\hat{y}|^2}{n} \quad (3)$$

Here the test data values (Y_t) and obtained stress values ($\bar{Y}$)

3 NUMERICAL SIMULATION OF STATIC LOAD TEST ON USP

3.1 *Selection of best suite hyper-elastic material model*

The curve fitting approach was used to evaluate the uniaxial compression data and volumetric test data of a rubber pad obtained from Navaratnarajah (2017). Ogden N=1, Reduced polynomial N=1, Reduced polynomial N =3 and Arruda-Boyce models were obtained as the stable material models from the curve fitting approach, and the accuracy of the models was assessed using statistical error indices. The statistical error index values for the stable material models are shown in Table 1.

Table 1. Statistical index values

Error indexes	Stable Hyper-Elastic models			
	Ogden N=1	Reduced polynomial N=1	Reduced polyno-mial N=3	Arruda Boyce
MAPE	4.9299	4.4200	4.4835	4.4199
MSD	7.1E+6	9.6E+6	4.1E+6	9.7E+6
MAD	2374.0	2208.70	1744.9	2214.01

It is clear from the error measurements, the Arruda Boyce material model shows the minimum values for the statistical indexes and provides a good curve fit with experimental test data as shown in Fig. 1. Therefore, the Arruda Boyce model was taken as the best-fitted material model, and the material coefficients were obtained from the results of the material evaluation as shown in Table 2 below.

Table 2. Material coefficients of Arruda Boyce model

Coefficients (Pa)	μ	μ_o	λ_m	D
Values	593558.548	600965.531	7.002	3.756

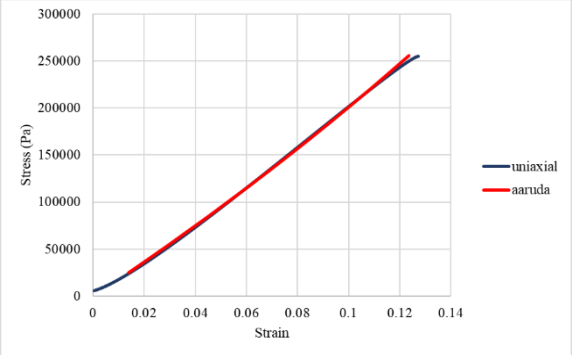

Fig. 1 The comparison of the uniaxial compression test data and Arruda Boyce material model results evaluated in ABAQUS 6.14/CAE

3.2 *Development of the USP model*

A model of the static load test (as per DIN 45673-5) on USP was developed in ABAQUS 6.14/CAE. The experimental data for the validation of the numerical simulation of the static load test on the sleeper pad was taken from Navaratnarajah (2017). According to the standard, the rubber pad was placed on a strong base plate and the load was applied on top of the rubber pad using the loading plate. The experimental setup is shown in Fig. 2 and the load to be applied on the top loading plate is shown in Fig. 3.

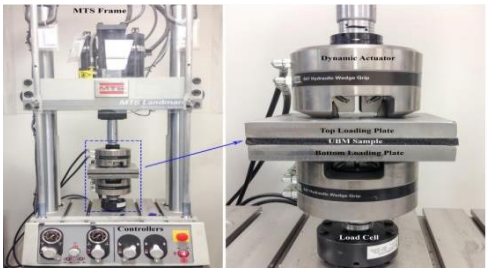

Fig. 2 MTS high performance servo hydraulic testing apparatus (Navaratnarajah, 2017)

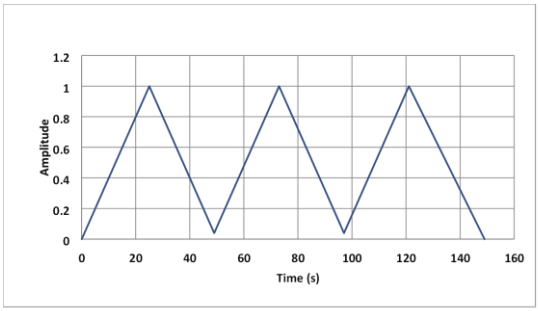

Fig. 3 Amplitude curve of quasi-static loading

The USP was developed as a 3-D deformable solid element having the dimensions of 200×200×10 mm. Two 3D discrete shell planar rigid plates were introduced to the top (loading plate) and bottom (base plate) of the USP surfaces. Fig. 4 shows the developed model of USP with top and bottom plates. The density of USP was used as 420 kg/m^3(Navaratnarajah 2017). The hyper-elastic material properties given in Table 2 were assigned to USP to capture the non-linear behavior.

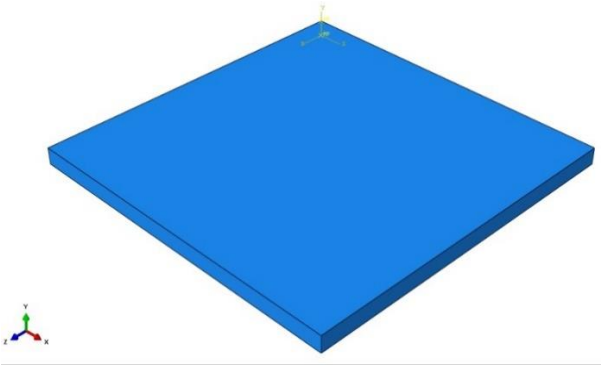

Fig. 4 The modelled sleeper pad with rigid plates

The viscoelastic property of rubber material helps it to return to its original shape after the deformation. To enhance the material model towards the real scenario, viscoelastic properties are incorporated. It can be analyzed under the time domain or frequency domain. Here time domain, Prony series was used for the viscoelastic constants. The constants used in this study are shown in Table 3.

Table 3. Viscoelastic properties used in the simulation

g	k	μ
0.15	0	5.76
0.08	0	220.41

The surface-to-surface interaction with frictional penalty condition with frictional co-efficient μ = 0.85 between sleeper pad and rigid bodies was introduced in the numerical model. The model was restrained using two boundary conditions where the bottom rigid plate was fixed while the top rigid plate was only unrestrained for vertical motion. Dynamic implicit analysis was used for the quasi-static loading. The applied load is 0.25 MPa as shown in Fig. 3.

3.3 *Meshing and mesh sensitivity analysis*

The mesh was assigned from the standard element library of a family of 3D stress. The 8-node linear brick, reduced integration with hourglass control, hybrid with constant pressure (C3D8RH) elements were adopted for modeling the sleeper pad. In contrast, the two rigid bodies were meshed with R3D4 elements, which is a 4-node 3D bilinear rigid quadrilateral from discrete rigid element family. The appropriate meshing size of the elements should be determined since coarser elements consume lesser computation time. However, to get realistic results in displacements and stress distribution, optimum size should be determined through mesh convergence study (Navaratnarajah, 2017).

Variation of the maximum stress on the sleeper pad with mesh density was analyzed in the mesh sensitivity analysis. The mesh density, where the results were shown to be converging was selected as the converged mesh density. The obtained converged mesh density was 13600 as shown in Fig. 5.

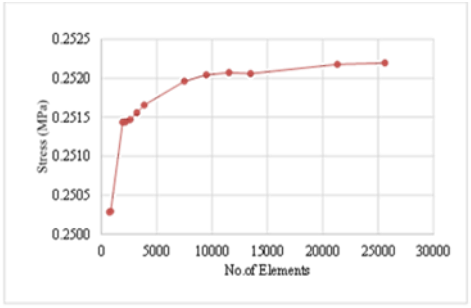

Fig. 5 Variation of maximum stress in sleeper pad with mesh density

3.4 *Validation*

The validation of the numerical model of the static load test on USP was done by comparing the numerical results with the experimental results from Navaratnarajah (2017). Variation of vertical stress with

vertical strain was considered in the comparison process. Obtained variation of stress vs strain for three load cycles is given in Fig. 6. The comparison of the experimental and numerical results for the third load cycle is shown in Fig. 7.

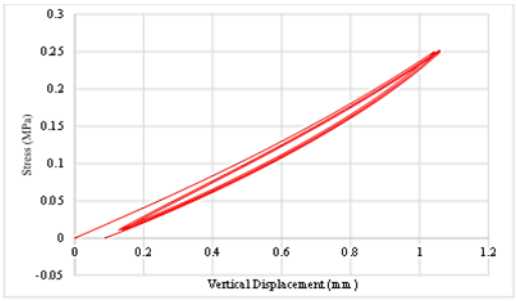

Fig. 6 Variation of vertical stress with vertical displacement

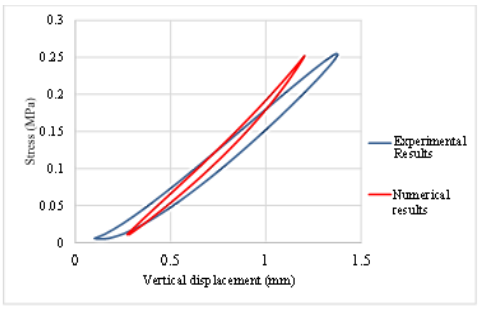

Fig. 7 Comparison of FEM results and Experimental results (Navaratnarajah 2017) for the 3rd cycle

3.5 *Parametric study*

The validated numerical model with the 10 mm thick Under Sleeper Pad was used to investigate the effect of USP thickness on its static bedding modulus values under the parametric study. For that, 3 different numerical models of static load test were developed with 8 mm, 12 mm, and 14 mm thick USPs. The variation of vertical stress with vertical displacement for 8 mm, 10 mm, 12 mm, and 14 mm thick USPs under the third load cycle is shown in Fig. 8.

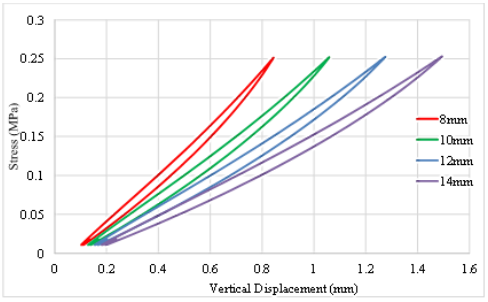

Fig. 8 Variation of vertical stress with vertical displacement for the third load cycle for various thicknesses

4 RESULTS AND DISCUSSIONS

Following the DIN 45673-5 specification, for the static analysis, the calculated static bedding modulus (C_{stat}) values based on the gradients of stress-displacement curves are shown in Fig. 9. The experimental and numerical bedding modulus values are 0.20 N/mm^3 and 0.25 N/mm^3, respectively and the variation between them is about 25%. Therefore, the developed FE model incorporating hyper-elastic material models can be used to predict the static bedding modulus of USP.

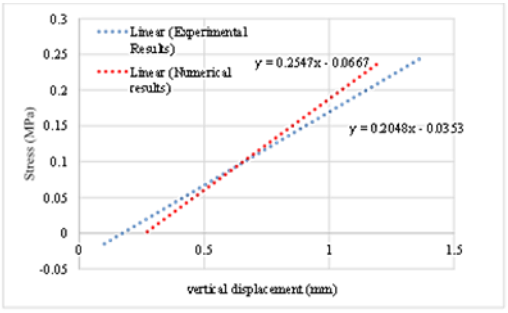

Fig. 9 Gradients of stress-displacement curves and calculated static bedding modulus value

The static bedding modulus values of each thickness are obtained from the gradients of the stress displacement curves which are shown in Fig. 10. Here results clearly show that the static bedding modulus of the USP increases as the thickness decreases. Therefore, the developed numerical models in FEM can be successfully used for the simulation of train-track models where USPs are employed.

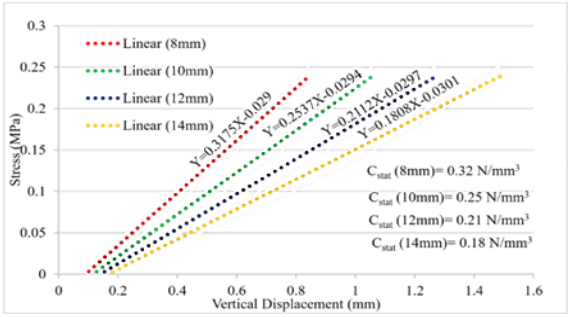

Fig. 10 Gradients of stress-displacement curves and calculated static bedding modulus values

5 CONCLUSIONS

This study aims to simulate the non-linear behavior of USPs for static responses using hyper-elastic material models in FEM. The static load test on USP was numerically modeled and validated with the experimental data from the literature. From the validated numerical model, a parametric study was done for different thicknesses of USP. It is identified that

static stiffness is significantly varied with the thickness of the USP. The static stiffness increases when the thickness of the USP decreases. The developed numerical model of USP can be successfully used in numerical simulations of ballasted rail tracks.

ACKNOWLEDGMENTS

Our sincere thanks to the Head of the Department of the Civil Engineering University of Peradeniya, who has given immense support to conduct the study.

REFERENCES

Arachchi, N.M.L.W., Abegunasekara, C.D., Premarathna, W.A.A.S., Jayasinghe, J.A.S.C., Bandara, C.S. and Ranathunga, R.R.M.S.K., 2021. Finite Element Modeling and Simulation of Rubber Based Products: Application to Solid Resilient Tire. In ICSECM 2019 (pp. 517-531). Springer, Singapore.

DIN 45673-5:2010-08 Mechanical vibration. Resilient elements used in railway tracks. Part 5: Laboratory test procedures for under-ballast mats.

Ferreira, P.A. and López-Pita, A., 2013. Numerical modeling of high-speed train/track system to assess track vibrations and settlement prediction. *Journal of transportation engineering*, *139*(3), pp.330-337.

Gent, A.N., 2012. Engineering with rubber: how to design rubber components. Carl Hanser Verlag GmbH Co KG.

Indraratna, B. and Nimbalkar, S., 2013. Stress-strain degradation response of railway ballast stabilized with geosynthetics. *Journal of geotechnical and geoenvironmental engineering*, *139*(5), pp.684-700.

Jayasuriya, C., Indraratna, B. and Ngo, T.N., 2019. Experimental study to examine the role of under sleeper pads for improved performance of ballast under cyclic loading. *Transportation Geotechnics*, *19*, pp.61-73.

Krishnamoorthy, R.R., Saleheen, Z., Effendy, A., Alisibramulisi, A. and Awaludin, A., 2018, October. The effect of rubber pads on the stress distribution for concrete railway sleepers. In *IOP Conference Series: Materials Science and Engineering* (Vol. 431, No. 11, p. 112007). IOP Publishing.

Mayuranga, H.G.S., Navaratnarajah, S.K., Bandara, C.S. and Jayasinghe, J.A.S.C., (2019) A STATE OF THE ART REVIEW OF THE INFLUENCE OF RUBBER INCLUSIONS IN RAILWAY TRACKS.

Mayuranka H.G.S, Navaratnarajah S.K, Bandara C.S, Jayasinghe J.A.S.C, (2021), Numerical Simulation of Energy Absorbing Rubber Pads Using FEM And DEM Approaches (A Comparative Study), ICSECM2021-159, pp.

Navaratnarajah, S. K. (2017), 'Application of rubber inclusions to enhance the stability of ballasted rail track under cyclic loading' Faculty of Engineering and Information Sciences.

Navaratnarajah, S.K., Indraratna, B. and Ngo, N.T.,2018. Influence of under sleeper pads on ballast behavior under cyclic loading: experimental and numerical studies. *Journal of Geotechnical and Geoenvironmental Engineering*, *144*(9), p.04018068.

Ngamkhanong, C. and Kaewunruen, S. (2020). "Effects of under sleeper pads on dynamic responses of railway prestressed concrete sleepers subjected to high intensity impact loads." Engineering Structures, 214, 110604.

Shahzad, M., Kamran, A., Siddiqui, M.Z. and Farhan, M., (2015). Mechanical characterization and FE modeling of a hyperelastic material. Materials Research, 18, pp.918-924.

Sun, Q., Indraratna, B. and Grant, J., 2020. Numerical simulation of the dynamic response of ballasted track overlying a tire-reinforced capping layer. *Frontiers in Built Environment*, p.6.

Zbiciak, A., Kraśkiewicz, C., Sabouni-Zawadzka, A., Pełczyński, J. and Dudziak, S., 2020. A novel approach to the analysis of under sleeper pads (USP) applied in the ballasted track structures. *Materials*, *13*(11), p.2438.

Sol-Sánchez, M., Moreno-Navarro, F. and Rubio-Gámez, M.C., 2014. Viability of using endof-life tire pads as under sleeper pads in railway. *Construction and Building Materials*, *64*, pp.150-156.

Setsobhonkul, S., Kaewunruen, S. and Sussman, J.M., 2017. Lifecycle assessments of railway bridge transitions exposed to extreme climate events. Frontiers in built environment, 3, p.35.

Assessment of Shear Strenght Properties of Dredged Sand

P.L. Punchihewa, R.J.K.B.C. Ranathunga and A.M.R.G. Athapaththu

Department of Civil Engineering, University of Peradeniya, Sri Lanka

ABSTRACT: Cohesion and friction angle generally represent the shear strength parameters of soils. The linear Mohr-Coulomb envelope has been extensively used to explain the theoretical concept of the shear strength parameters of soil. However, the Mohr-Coulomb envelope deviates from the linear behavior because of elements like confining pressure, relative density, mineralogy, particle crushing, particle size distribution, etc. Also, the relative density of the dredged sand affects to the geotechnical properties of soil directly. Therefore, in this research, the variation of dredged sand shear strength parameters with relative density was assessed, and a series of direct shear tests were used to evaluate the non-linear stress variation with an increase in normal stress. Using the findings as well as earlier research on dredged sand, a simulated direct shear test model was created using the Discrete Element Method (DEM).

KEY WORDS: Colombo Port City, dredged sand, Direct shear test, Discrete Element Method, EDEM

1 INTRODUCTION

Colombo Port City Development Project (CPCDP) is the first mega coastal reclamation project in Sri Lanka, which is an extension of the central business district of Sri Lanka, Colombo.

There have been several geotechnical issues in line with the reclaimed land areas such liquefaction. To avoid such failures, ground improvements must be carried out up to the required degree of compaction using the site-specified improvement methods. The relative compaction can be assessed through the examination of the geotechnical properties of marine dredged sand.

The shear strength of soils is represented mainly by cohesion and friction angle. Mohr-Coulomb envelope is the most common representation of shear strength variation of soils. Linear Mohr-Coulomb envelope assumes constant friction angle and cohesion, but according to Terzaghi (1996), friction angle of coarse-grained soils vary due to confining pressure, relative density, mineralogy, particle crushing, particle size distribution and fine content.

Due to the difficulty in laboratory testing, time and cost, modelling has been carried out using computer-aided programs. Discrete Element Method (DEM) uses a set of discrete particles which represents the real material sizes and their shapes as stated by Hopkins et al. (1991). DEM simulates the mechanical behaviour of a system of a collection of differently shaped particles of different sizes. In this study, the variation of shear strength parameters of dredged sand with relative density was evaluated and non-linear stress variation with the increase of normal stress was assessed using a series of direct shear tests. Based on the results and using previous studies on dredged sand, a virtual direct shear test model was developed using the DEM.

2 METHODOLOGY

2.1 Laboratory Experiments

The construction of infrastructure in the Colombo Port City specifies different relative densities for different structures. Therefore, the variation of shear strength parameters with the relative densities and the confining pressure should be determined. So, the laboratory experiments were carried out to identify the geotechnical properties of dredged sand in the Colombo Port City Project. Table 1 shows basic properties of dredged sand in the Colombo Port City Project. (Ranbandara, et al (2020))

Table 1. Sand parameters of dredged sand in the Colombo Port City Project (Ranbandara, et al (2020))

Parameter	Value	Units
Minimum dry density of sand	1515.15	kg/m^3
Maximum dry density of sand	1818.50	kg/m^3
Specific gravity of sand	2.68	_

2.1.1 Direct shear test

The standard direct shear test (BS 1377-7: 1990 clause 4) was selected to determine the shear strength parameters of the dredged sand for different relative densities. A series of direct shear test was performed for oven dried sand samples of 105 0C to 110 0C under 90% and 97% relative densities and for normal stresses of 20, 50, 100, 200, 400 and 800 kPa to represent different loading conditions. For the direct shear test the square shear box of size 60mm x 60mm was used. A shearing rate of 0.5 mm/min was kept throughout the test series.

2.1.2 Sieve analysis test

Sieve analysis (BS 1377-2: 1990 clause 9.3) was carried out to determine the particle size distribution of the dredged sand. Basically, this test was performed before and after the direct shear test. During the direct shear test sand samples experienced shear stress as well as normal stress. Due to that shear stress and normal stress, crushing of sand particles could have occurred. So, to determine at which rate the particle crushing occurred to the sample after the direct shear test another sieve analysis test was carried out.

2.2 Development of a virtual Direct shear test model using DEM

It is time-consuming to perform laboratory tests manually and there may be more errors included in the results. So as a solution to that a virtual model will be useful to obtain shear strength parameters in a short period without much laboratory work. The virtual model was developed for direct shear test using Discrete Element Method (DEM). EDEM software was used for modelling the virtual direct shear test.

Percentage volume of the particles with different diameters were calculated based on the sieve analysis tests and input for the EDEM model as shown in Table 2. As the computation time drastically increases when the number of particles in the simulation is high, all the particles were enlarged by 10 times and Since the particles are very small, all the particles were modelled as spheres. Also particles less than 0.75 mm were not included in the model due to computational malfunctions.

Table 2. Particle size distribution

Particle name	Sieve size (mm)	Particle radius (mm)	Volume percentage
D1	2.00	10.00	2.06 %
D2	0.85	4.25	18.77 %
D3	0.60	3.00	20.71 %
D4	0.43	2.13	21.33 %
D5	0.25	1.25	25.01 %
D6	0.15	0.75	12.12 %

Series of virtual direct shear test simulations with applied normal stresses of 50, 100, 200, 400, and 800 kPa were carried out to achieve the objective of determining the shear strength variations of reclaimed sand using a virtual direct shear test for different relative densities. Figure 1 shows the model after the shearing process.

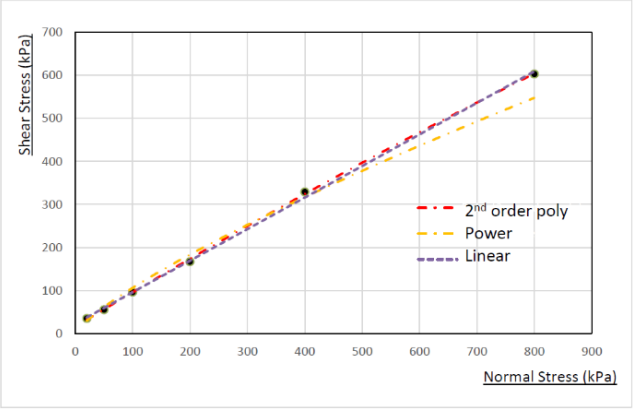

Fig. 1 EDEM direct shear test model after shearing

3 RESULTS AND DISCUSSION

3.1 Direct Shear Test

Fig.2 and Fig.3 illustrates the variation of shear stress with shear displacements for 90% and 97% degree of compactions respectively.

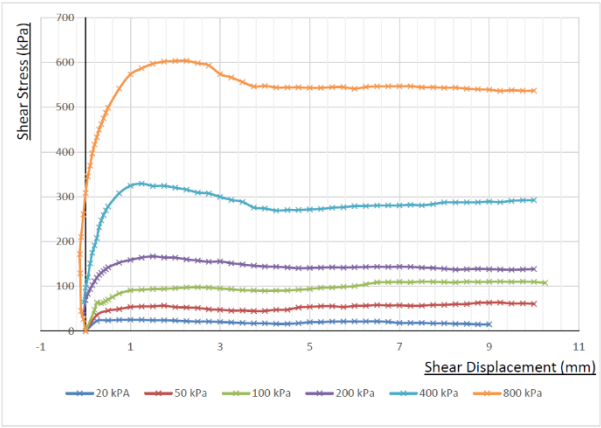

Fig.2 Variation of shear stress versus shear displacement for 90% Relative density

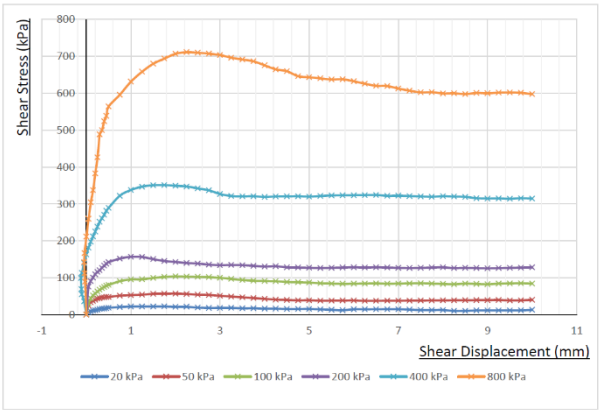

Fig.3 Variation of normal displacement versus shear displacement for 97% Relative density

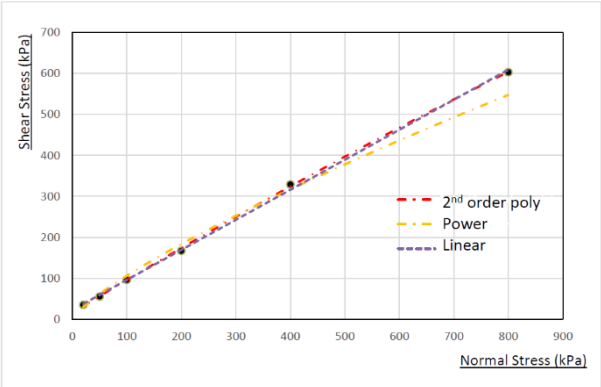

Fig.4 Linear and nonlinear failure envelopes for 90% Relative density

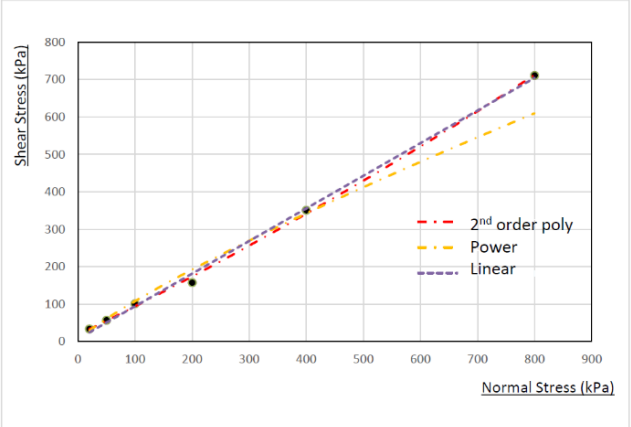

Fig.5 Linear and nonlinear failure envelopes for 97% Relative density

The shear strength parameters are tending to vary linearly for low normal stresses and then become nonlinearly with the increment of applied normal stress for relative densities 90% and 97% as shown in Fig.4 and Fig.5. Therefore, power and second-order polynomial curve fit were utilized to describe the non-linear fluctuation. The sand grains from Port City may be crushed during shear and hence dilatancy reduces. Equations resulted for 90% relative density and 97% relative density can be seen in Table 3 and Table 4.

Table 3. Failure envelope equations for 90% Relative density

Envelope	Equation	R^2
Linear	Y=0.7332x+22.481	0.9990
2nd order polynomial	$Y=-0.0002x^2+0.9056x$	0.9989
Power	$Y=2.8095x^{0.7888}$	0.9959

Table 4. Failure envelope equations for 97% Relative density

Envelope	Equation	R^2
Linear	0.8718x+6.5781	0.9975
2nd order polynomial	$0.00004x^2+0.8575x$	0.9981
Power	$2.3128x^{0.834}$	0.9890

The resulted peak and ultimate friction angles for Colombo port city dredged sand for different degree of compactions are listed in the Table 5.

Table 5. Variation of peak and ultimate friction angles with the relative density

Relative Density	Peak Friction angle (°)	Ultimate Friction angle (°)
90	36.03	33.62
95	39.07	34.45
97	41.24	37.1

3.2 Sieve Analysis

The particle size distribution obtained for the initial sand sample is shown in Fig.6 Table 6 exaggerates the values obtained for the initially carried out sieve analysis tests and the average values.

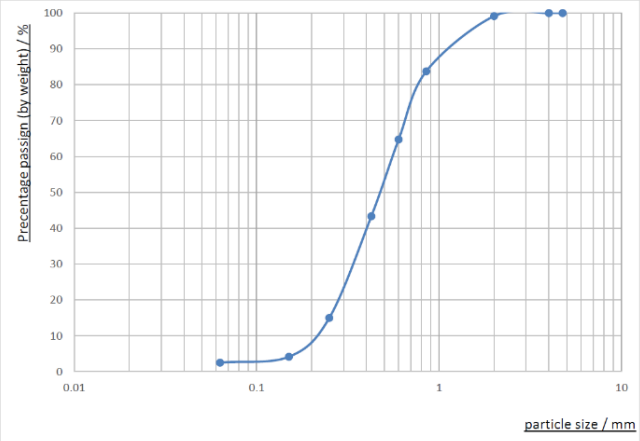

Fig.6 Particle size distribution curve

Table 6. Results of sieve analysis tests

Parameter	Test 1	Test 2	Test 3	Average
Fineness modulus	4.87	5.1	5.17	5.05
D_{10}	0.22	0.24	0.24	0.23
D_{30}	0.28	0.3	0.31	0.3
D_{50}	0.35	0.38	0.39	0.37
D_{60}	0.48	0.54	0.55	0.52
C_u	2.5	2.58	2.67	2.58
C_c	0.55	0.62	0.64	0.6

Upon completion of the direct shear tests, sieve analysis tests were carried out to check the degree of the particle crushing. It was noticed that the crushing has occurred for the samples with normal stresses larger than 100 kPa. Fig.7 presents the variation of particle size distribution before and after compaction process for 97% relative density.

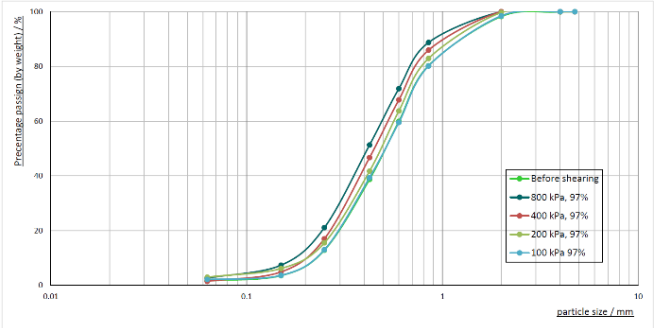

Fig.7 Variation of particle size distribution before and after compaction process for 97% relative density.

3.3 EDEM Model

Since direct test results cannot be obtained from EDEM, first the total force acting on the bottom box with time was analysed and the shear stress was calculated via the total force. Fig.8 compares the variation of shear stress with the shear displacement for the EDEM results and the laboratory results without application of a correlation.

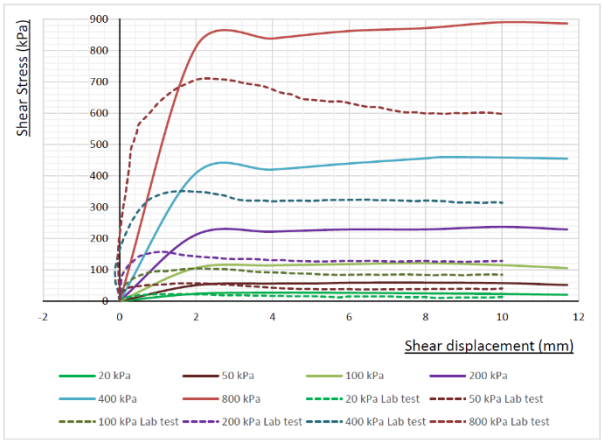

Fig.8 Variation of shear stress with the shear displacement for the EDEM results and the laboratory results.

To find the correlation function, the ultimate shear stress derived from the laboratory experiments and the DEM model was plotted as a linear function. Using a linear function with zero intercept, a correlation function was obtained and the corrected results are shown in Fig.10.

$$\tau_{corrected} = 0.6743\tau_{simulation} \quad (1)$$

where $\tau_{corrected}$ is the corrected ultimate shear stress and $\tau_{simulation}$ is the ultimate shear stress obtained from the EDEM simulation.

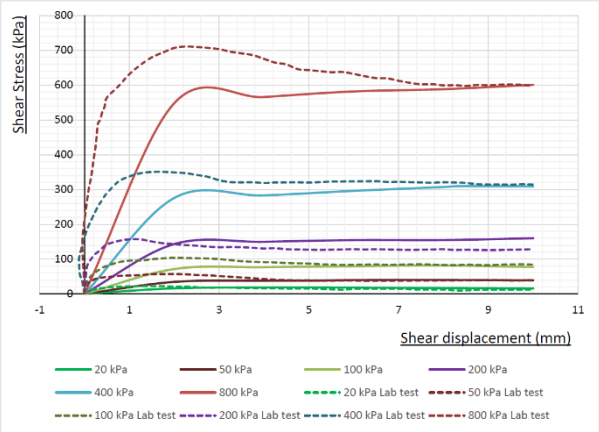

Fig.10 Variation of corrected shear stress of the DEM model and shear stress from the laboratory experiments with the shear displacement

Table 7 summarize the results secant friction angles obtained for different relative densities and from the EDEM model.

Table 7. Summarized secant friction angles

Relative Density	Peak Friction angle (°)	Ultimate Friction angle (°)
90	36.03	33.62
95	39.07	34.45
97	41.24	37.10
EDEM Model	46.47	37.16

4 CONCLUSIONS

- When direct shear tests were performed for the compacted sand samples, further crushing of the particles were seen. From 20 kPa to 100 kPa, there is no crushing occurred during the shearing.
- With the increment of normal load from 200 kPa, a significant amount of particle crushing has occurred while the shearing process has been carried out.
- Shear strength increment with the increasing of normal stresses up to 100 kPa can be described as a linear variation for both the sand samples with 90% and 97% relative densities.
- The linear relationships cannot be used to represent the variation of shear strength with higher normal stresses.
- Secant friction angle increases with the increase of relative density.
- By increasing the degree of compaction shear strength of the dredged sand can be increased.
- Since the change of friction angle is nonlinear, it is more suitable to use the nonlinear variation of secant friction angle for high load carrying geotechnical designs.
- Results obtained from the EDEM software are reasonably acceptable when comparing with the laboratory experimental results for low normal stresses.
- Since the variation of shear stress with shear displacement has similar pattern compared to the laboratory results, a correction factor is applied for the EDEM results.

ACKNOWLADEGEMENT

We would like to express our gratitude and appreciation to the panel members of the Geotechnical Engineering research section, Dr. S. K. Navarathnarajah and Dr. M. C. M. Nasvi, and to Dr. K.K. Wijesundara, the main coordinator of this course for supporting us. We would like to extend our thanks to, Eng. P.G.G.M. Ranbandara for providing us with the data and experiment test results needed to complete the research and make it a successful project. Finally, to thank to those who supported us in completing this research successfully.

REFERENCES

Chang, C., Cerato, A. and Lutenegger, A., (2010). Modelling the scale effect of granular media for strength and bearing capacity. *International Journal of Pavement Engineering*, 11(5), pp.343-353.

Chang, M.F., Yu, G., Na, Y.M. and Choa, V., (2006). Evaluation of relative density profiles of sand fill at a reclaimed site. *Canadian geotechnical journal*, 43(9), pp.903-914.

Hosseini, S.M.R. and Jesmani, M., (2016). Effect of normal stress and relative compaction on secant friction angle of sands. *Turkish Journal of Engineering and Environmental Sciences*, 38(3), pp.382-391.

Kotrocz, K., Mouazen, A.M. and Kerényi, G. (2016). Numerical simulation of soil–cone penetrometer interaction using discrete element method. *Computers and Electronics in Agriculture*, 125, pp.63–73. doi:10.1016/j.compag.2016.04.023.

Maksimovic, M. (1991). Nonlinear failure envelope for coarse grained soils. *International Journal of Rock Mechanics and Mining Sciences & Geomechanics Abstracts*, 28(6), p.A339. doi:10.1016/0148-9062(91)91201-2.

McManus K. and Cunrinovski M. (2021). Module 3. Identification, assessment and mitigation of liquefaction hazards, *Earthquake geotechnical engineering practice*, Ministry if business, Innovation & Employment. pp. 35-37

McManus K. and Cunrinovski M. (2021). Module 5. Ground improvement of soils prone to liquefaction, *Earthquake geotechnical engineering practice*, Ministry if business, Innovation & Employment. pp. 3-7

Ranbandara, P.G.G.M., Thilakarathne, R.U., Athapaththu, A.M.R.G., Kurukulasooriya, L.C. and Gonaduwage, B.P. (2020). Examination on Geotechnical Properties of Marine Dredge Sand of Colombo Port City

Terzaghi, K., Peck, R.B. and Mesri, G., (1996). Soil mechanics in engineering practice. John Wiley & Sons. pp.146 – 158.

Yang, G. and Wang, X., (2012). Discrete element modeling for granular materials. *Electronic Journal of Geotechnical Engineering*, 17, pp. 2463-2474.

Triaxial mechanical behaviour of blended fly ash-rice husk ash based geopolymer well cement under different curing temperatures

E.A.D.D. Vivek, W.M.N.L. Wanasinghe and M.C.M Nasvi

Department of Civil Engineering, University of Peradeniya, Sri Lanka

ABSTRACT: This study investigates the potential use of geopolymers prepared using class F fly ash and rice husk ash as an alternative material to ordinary Portland cement (OPC) for CO_2 sequestration wells. Geopolymer samples were prepared and subjected them to heat-curing at four different temperatures (30, 40, 60, and 80°C) and two curing periods (7 and 28 days) to investigate the effect of curing temperature on the mechanical behaviour of the geopolymers. To study the properties of the geopolymers, uniaxial compressive strength was performed. Tri-axial behaviour was analysed using COMSOL multiphysics software at various confining pressures (5-25 MPa) and the model was validated using uni-axial test results. The findings indicate that geopolymers derived from fly ash and rice husk ash have the potential to be a viable OPC replacement for CO_2 sequestration wells.

KEY WORDS: Geopolymer, Fly ash, Rice husk ash, Well cement, Triaxial

1 INTRODUCTION

The greenhouse effect, which is created by gases such as carbon dioxide, methane, nitrous oxide, water vapor, and fluorinated gases, is currently a serious concern. Human activities have contributed to the problem by increasing the amount of CO_2 in the atmosphere. With a target efficiency of 90%, carbon capture and storage (CCS) is the most effective technique of decreasing CO_2 emissions. Carbon dioxide is captured from power plants or industrial operations, transported, and stored deep underground in sequestration wells or depleted oil and gas reserves. CO_2 is naturally present in the atmosphere and contributes for 64% of human-caused greenhouse gas emissions (Bertier et al., 2006). Human activities have had an impact on the carbon cycle, reducing the ability of natural sinks such as trees and soils to capture and store CO_2.

Aarany et al. (2017) discovered that ordinary Portland cement (OPC) weakens and degrades with time in CO_2 rich environments due to increased temperature and pressure with depth (30 ^{0}C/km) in the earth. Geopolymer is offered as a cleaner and more sustainable alternative to OPC, created by alkaline activation of alumina and silica-rich materials such as fly ash and slag, which emit no CO_2 during production. This study considers a blended fly ash-rice husk ash geopolymer as an alternative for CO_2 sequestration wells. Prior research has shown that geopolymer has lower axial deformation than OPC and demonstrates equivalent strength increase under active lateral confinement. However, there is a lack of research on the tri-axial behaviour of blended fly ash-rice husk ash geopolymer under different curing temperatures.

2 RESEARCH SIGNIFICANCE

Many studies have been conducted to study the mechanical properties of geopolymer at various temperatures. No research has been undertaken to far to investigate the effect of temperature on the tri-axial mechanical behaviour of blended fly ash-rice husk ash geopolymer. The aim of this research is to investigate the effect of temperature, curing time and confining pressure on the tri-axial mechanical behaviour of geopolymer.

This study used both experimental and numerical methods, which are addressed in depth in the sections that follow. During the experimental phase, the unconfined compressive strength (UCS) of geopolymer samples was determined at various temperature and salinity combinations. Using a computational model, the acquired data were used to validate

the uniaxial stress-strain behaviour of geopolymer. The numerical model was extended after validation to simulate the tri-axial mechanical behaviour of geopolymer. It should be noted that laboratory-based tri-axial experiments were not carried out due to the existing laboratory setup at the Department of Civil Engineering, University of Peradeniya, Sri Lanka's incapacity to fail samples under high confining pressures.

3 EXPERIMENTAL WORK

3.1 *Materials*

Samples of low calcium-based fly ash (Ca < 10%) (ASTM Class F) and rice husk ash (RHA) were obtained from the Lakwijaya coal power station in Norochcholai, Puttalam, Sri Lanka, and local rice mills in the Divulapitiya district of Sri Lanka, respectively. The RHA sample chosen for this investigation has a low unburnt carbon percentage and a high amorphous content, which provides more reactive SiO_2 for the alkali activation process. Compositions of the FA and RHA used are presented in Table 1. Despite earlier literature recommending a particle size of at least 80% below 45 m for best strength, the selected RHA was ground into fine particles and sieved to achieve particles 75 m and lower to minimize practical challenges during the grinding process for industry applications.

Table 1 – Composition of Class F fly Ash and Rice Husk Ash.

Constituents	Percentage Composition/wt.%	
	Fly ash	Rice husk ash
SiO_2	45.10	91.55
Al_2O_3	33.22	0.42
SiO_2 + Al2O3	78.33	91.97
Fe_2O_3	3.33	0.47
CaO	9.26	1.25
P_2O_5	1.30	1.43
TiO_2	2.08	0.04
MgO	2.27	1.28
K_2O	0.74	2.87
SO_3	0.56	0.21
MnO	0.06	0.23
Na_2O	1.07	0.00

3.2 *Mix design*

An optimized reference mix design based on activator modulus (AM) was used to determine the proportions of each material to be mixed in order to gain the desired strength parameters. This mix design with the following ratios were maintained as it has been found to be the optimum mix for RHA blended geopolymer to achieve higher strength as per Sarah et al (2021).

The ratio of fly ash to RHA used was 9:1, meaning that 90% of the mixture was made up of fly ash, while 10% was RHA. It has determined that the optimal amount of RHA to use in this geopolymer product is 10%. Sarah et al (2021) found that the optimum activator modulus for 10% RHA is 1.375. Activator modulus was maintained at 1.375 while Na_2O percentage fixed at 15%. Mix design is presented in Table 2.

$$AM = \frac{SiO_2 \text{ in the alkaline solution}}{Na_2O \text{ in the alkaline solution}} \quad (1)$$

$$Na_2O \text{ dosage} = \frac{Na_2O \text{ in the alkaline solution}}{\text{Mass of fly ash}} \quad (2)$$

Table 2 – Reference Mix Design using Absolute Volume Method for AM=1.375

Constituent	Mass ratio of materials
Fly ash	0.9
Rice husk ash	0.1
Sodium silicate	0.702
Sodium hydroxide	0.157
Water/solid ratio	0.371

3.3 *Specimen preparation, curing and testing*

To prepare the samples, dry fly ash samples were initially mixed together with RHA samples that had been ground and sieved using 75 µm, for around 5 minutes using a mixer, according to the optimal mix proportions that had been obtained by Sarah et al (2021) as 10% of RHA and 90% of FA. After being mixed properly, the mixture was treated with alkaline activator to accelerate the hydration process. Although the activator solution had initially been proposed to be prepared 24 hours prior to the preparation of the cement samples in order for the chemicals to thoroughly react with each other, no significant strength increment was observed throughout

the course of trial tests. Hence, in this study, the alkaline activator solution was made ready just before the geopolymer cement mix was prepared. The activator solution, fly ash, and rice husk ash were thoroughly mixed for 8 minutes using a mechanical mixer to prepare the geopolymer paste. Immediately after mixing, the paste was placed in the PVC moulds of 54 mm diameter and 108 mm height in approximately 3 equal layers. Each layer was vibrated using a vibration table for 2 minutes to remove the trapped air bubbles. A total of 48 samples were prepared, and Fig. 1 shows the moulds used in casting.

Fig. 1 PVC Moulds

Then the samples were heat cured under four different curing temperatures (30 ^{0}C, 40 ^{0}C, 60 ^{0}C, 80 ^{0}C) and 2 different curing periods (7 and 28 days). Three samples were tested for each condition in order to get the précised results. Heat curing was done for 24 hours and then samples were demoulded and the samples were covered with a polythene to prevent the excessive loss of moisture.

4 NUMERICAL WORK

4.1 *Model development*

COMSOL Multi-physics simulation software used to analyse the tri-axial compressive strength. The structural mechanics module was used. The simulation process involves setting units for physical quantities, selecting the geometry, setting material properties, selecting mesh options, deciding on boundary conditions and loading criteria, and running the model to obtain results. The input parameters for the specific model used in our project were UCS values obtained from experiments, Young's modulus of samples, Poisson's ratio of samples, density of samples, UT and BCS were derived from UCS values.

The 2-D axisymmetric geometry refers to the shape of the sample that is being modeled. An axisymmetric geometry is one where the object has rotational symmetry around an axis. In this case, only half of the sample was modeled as the system is symmetric.

The boundary conditions are the conditions that are applied to the edges of the model. These conditions can include things such as displacement, temperature, pressure, and more. Fig. 2 shows the specific conditions that were used in this particular model.

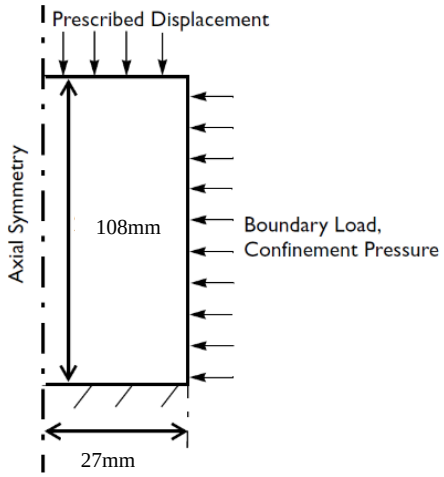

Fig. 2 Dimensions and Boundary Conditions for Numerical Model

To model the effect of confinement pressure on the mechanical behavior of the sample, a confinement pressure was applied to the right vertical boundary, and a parametric sweep was used to vary the pressure as 0, 5, 10, 15, 20, 25MPa. The left vertical boundary was set to have axial symmetry, to reflect the real-life scenario in which the sample was symmetric around its axis. To simulate the loading on the sample, the top boundary was set to a prescribed displacement that gradually increases in steps of 0.05, using an auxiliary continuation sweep. The lower horizontal boundary was fixed to simulate the rigid and perfectly rough base on which the sample was supported during the experiments. Fig. 3 shows the assumed mapped mesh and it illustrates a good quality mesh which perfectly fits the modeled geometry. The parameters of the mapped mesh are given in Table 3.

4.2 *Model validation and extension*

In this study, the model was validated by comparing the model results to experimental data obtained from uni-axial compression test. The stress-strain

curve values, which represent the relationship between the applied stress and the resulting deformation of a material, were used as a reference for validation. This process was carried out to confirm the reliability of the new model. After the validation of model, the same model was further extended to investigate the tri-axial mechanical behaviour of geopolymer.

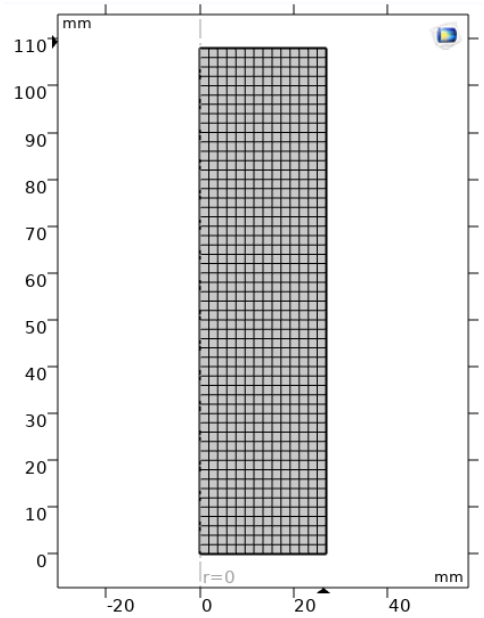

Fig. 3 Assumed Mapped Mesh

Table 3 – Meshing Parameters

Parameter	Value
Element size	1.92 x 1.92mm
Number of rectangular elements	784
Number of nodes	855

5 RESULTS AND DISCUSSION

5.1 *Experimental results on the mechanical behaviour of Geopolymer under uni-axial stress condition*

Fig. 4 shows the variation of UCS with the curing temperature for curing periods of 7 and 28 days. According to Fig. 4, UCS shows an increasing trend with the increasing curing temperature for all temperatures. In addition, the UCS values also increase with the curing period. Higher curing temperatures accelerate the chemical reactions within the geopolymer mixture and lead to better crystallization and allows rapid dissolution of Si and Al from the source material, which improves the chemical reactions (Nasvi et al., 2012). At lower temperatures, the dissolution of Si and Al from the source materials takes place at a reduced pace and the geopolymer gel develops at a lower rate. The amount of precursors dissolved are insufficient for polymerization. Hence the compressive strength shows minimum values at lower curing temperatures. Elevating the curing temperature is associated with the increased dissolution of Si and Al and accelerated formation of a hard structure at the early stages of geopolymerization. The gel continues to grow while filling the larger pores (macro pores) available in the geopolymer matrix by significantly increasing the mesopore volume (Sindhunata et al., 2006, Mo Bing-hui et al., 2014), thus allowing an increasing trend in the uniaxial compressive strength values with the curing temperature.

The strength of geopolymers increases with increasing curing period due to continued polymerization reactions. These reactions involve the formation of chemical bonds between the alumino-silicate molecules, which leads to the formation of a more rigid and stable structure. Additionally, as the curing period increases, the amount of water present in the mixture decreases, leading to a higher degree of polymerization and a more dense structure.

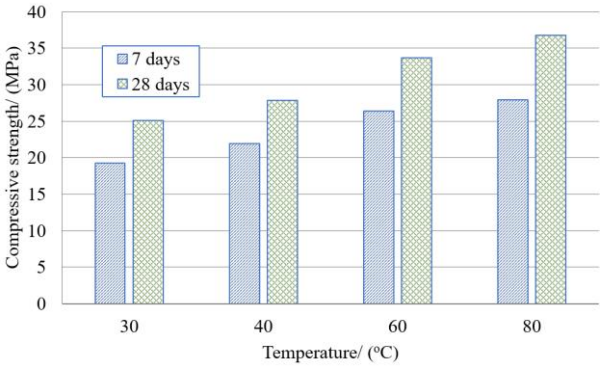

Fig. 4 Variation of UCS with Curing Temperature and Curing Period

5.2 *Numerical results*

The stress-strain behaviour of the specimens was analysed by constructing stress-strain curves, as shown in Fig. 5.

The comparison between the model predictions and the experimental results was carried out, which revealed a high degree of correlation between the two.

As illustrated in Fig. 5, it is clear that the experimental and modeled stress-strain curves are in agreement with one another up to the yield point, where the material reaches its maximum strength before deformation. That indicates, the model is able to accurately predict the mechanical behaviour of the geopolymer specimens. The stress-strain curves displayed typical characteristics of a brittle material, with no strain hardening observed beyond the yield point. This implies that the material does not exhibit any further resistance to deformation after reaching its maximum strength, thus it is brittle. The model assumed perfectly plastic behaviour beyond the yield point.

Based on the comparison between the model predictions and the experimental results, it can be deduced that the numerical model developed in this study is valid for the analysed material and experimental conditions. This implies that the model can be used with confidence to make predictions about the mechanical behaviour of the material under different loads and loading conditions. As such, the model can be extended to investigate the tri-axial mechanical behaviour of geopolymer, which will provide a more complete understanding of the material's behaviour under different loading conditions.

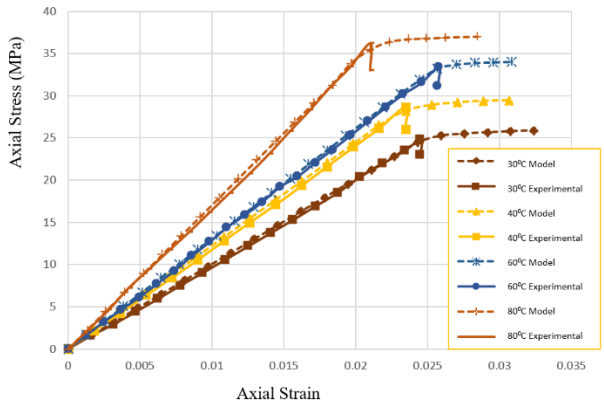

Fig. 5 Overall Comparison of Axial Stress and Strain Curves of Geopolymer Cured at Different Curing Temperature

5.3 *Effect of curing temperature and curing period on mechanical behaviour of blended fly ash-rice husk ash geopolymer*

The relationship between resulting strength and various confining pressures for geopolymer samples cured at 60^{0}C is illustrated in Fig. 6. It is clear that as the confining pressure increases, there is a corresponding increase in the failure stress of the geopolymer samples.

The reason for that, pores present in geopolymer paste act as a source of weakness in the microstructure, resulting in lower mechanical strength. However, as confinement level increases, these pores tend to close, thereby reducing permeability and void proportion, leading to an increase in mechanical strength (Nasvi et al., 2013). The highest resulting strength is achieved at the highest level of confinement of 25 MPa. As shown in Fig. 6 it can be seen that, for a given temperature, failure strength percentage increment is higher at lower confinement levels, and the resulting stress percentage increment is comparatively lower at higher confinements. According to the Fig. 7, resulting strength increases by 54.8% for confining pressure increment from 0-10 MPa and by 11.5% for a pressure increment from 10-25 MPa.

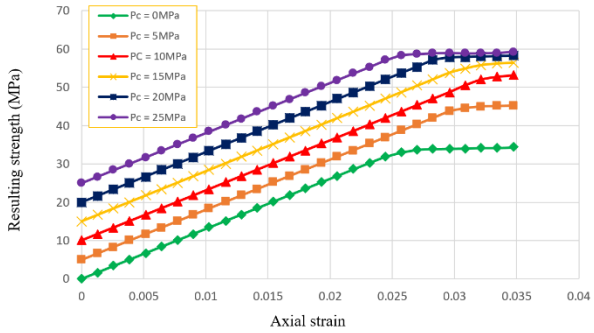

Fig. 6 Variation of Resulting Strength with Different Confining Pressure for Geopolymer Cured at 60 ^{0}C for 28 days.

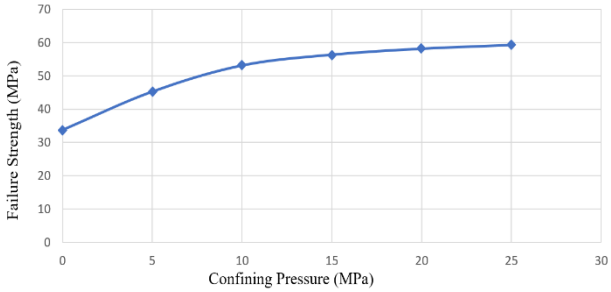

Fig. 7 Variation of Failure Strength with Confining Pressures for Geopolymer cured at 60 ^{0}C for 28 days.

At high pressure levels, the external confining pressure is the dominant factor influencing the behaviour of geopolymer, rather than the resulting strength. This is evidenced by the fact that, as shown in Fig. 8, at high levels of confinement, the rate of strength gain is minimal and there is no corresponding increase in deviatoric stress, which is calculated by subtracting confining pressure from resulting strength. As the confining pressure increases, deviatoric stress should be increased, however, this trend does not hold true when the pressure surpasses

15MPa. It can be clearly seen that the deviatoric stress increases up to 10MPa and then decreases beyond 10MPa.

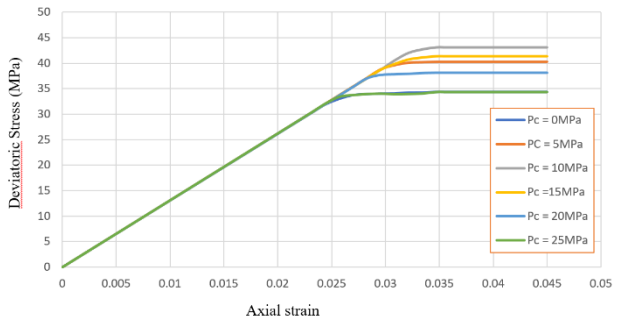

Fig. 8 Deviatoric stress variations of geopolymer cured at 60 ^{0} for 28 days.

Fig. 9 and Fig. 10 show the relationship between the failure strength and curing temperature for geopolymer cured for 7 days and 28 days. According to Fig. 9 and Fig. 10, when the curing temperature increases, the failure strength also increases. This can be seen by the rise in failure strength of about 9.1 % when the curing temperature is between 30 ^{0}C to 40 ^{0}C and a further increase of about 69.1 % when the curing temperature is increasing from 40 ^{0}C to 80 ^{0}C for 28 days cured samples. However, for 7 days cured samples it shows from 30 ^{0}C to 40 ^{0}C temperature failure strength is decreasing or remain similar and from 40 ^{0}C to 80 ^{0}C failure strength increases. At a particular confinement, failure stress increases with the curing temperature. This is due to the favourable effect of increasing temperature on the geopolymerization reaction.

Furthermore, the confinement pressure increases, the failure strength also increases. However, the increase in failure strength is greater when the confinement pressure is lower compared to when the confinement pressure is higher. This is clearly demonstrated in the Fig. 9 and Fig. 10 where the variation of failure strength at lower confinement levels is higher compared to the variation of failure strength at higher confinement levels. It can also be seen that, the variation of failure strength at higher confinement levels (20MPa and 25MPa) is almost similar. It can be inferred that increasing the curing temperature and confinement pressure will result in an increase in failure strength. increment from 10-25 MPa.

Fig. 11, Fig. 12, Fig. 13 illustrate the variation of failure strength of geopolymers with both curing temperature and curing period for different confining stress levels. It can be seen that the failure strength increases with the increase in both curing temperature and the curing period. Longer curing times improve the polymerization process, which is the process by which the polymer is formed. This process results in higher compressive strength. However, the increase in strength due to the curing temperature is greater than the increase in strength due to the curing period. Average percentage increase of compressive strength due to increase of curing temperature is 32% while the average percentage increase due to increase of curing period is 14%. This is due to the favourable effect of temperature on the geopolymerization reaction more than compared to effect of curing period.

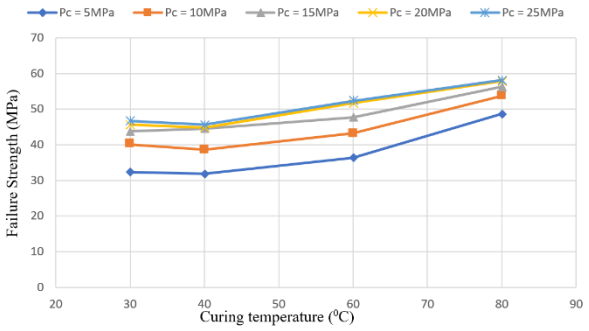

Fig. 9 Variation of Failure Strength with Curing Temperature for Geopolymer Cured for 7 Days.

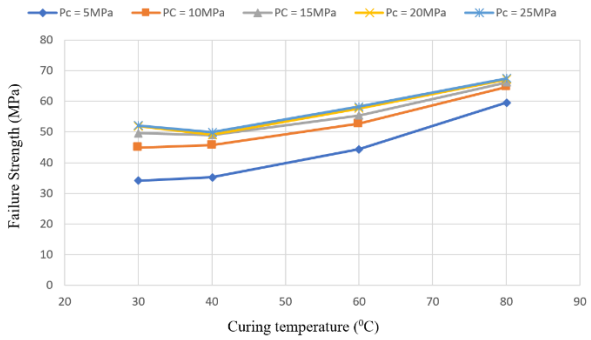

Fig. 10 Variation of Failure Strength with Curing Temperature for Geopolymer Cured for 28 Days.

According to Rangan et al. (2010), the rate of increase in strength is rapid up to 24 hours of curing time. Beyond 24 hours, the gain in strength is only moderate. This suggests that the majority of the strength gain occurs in the early stages of curing, and the gain becomes slower as the curing time increases.

It can be seen that, when confining pressure increasing from 0MPa to 10MPa, the rate of increase in compressive strength is 108% while increasing from 0MPa to 25MPa is 142%. This is because the higher confining pressure leads to more significant grain rearrangement, leading to a higher degree of compaction and greater inter-grain contact forces. As a result, the resistance to compression is increased, leading to a higher strength increase. The observed rate of increase in compressive strength when the confining pressure increases from 10 MPa to 25 MPa is 16.35%. This is because the specimen has already undergone significant grain rearrangement and compaction during the initial increase in confining pressure, and the further increase in pressure has a diminishing effect on the strength increase.

Cement used in the well must have a compressive strength between 20MPa and 50 MPa to provide thermal insulation and prevent mechanical fracturing (Balinee et al. 2018). The maximum strength that can be achieved by geopolymers under these conditions is approximately 68 MPa, which is higher than the maximum strength that can be achieved by the OPC currently used in well cementing. Therefore, geopolymers may be a good alternative to ordinary Portland cement (OPC) in sequestration wells because of their superior mechanical behaviour under tri-axial conditions.

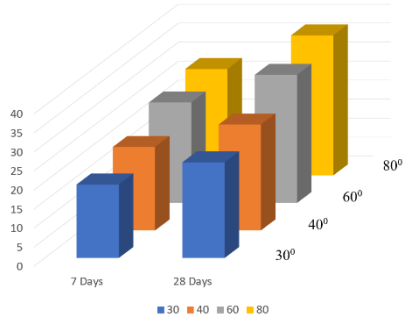

Fig. 11 Variation of Failure Strength with Curing Temperature and curing period, for Pc= 0MPa.

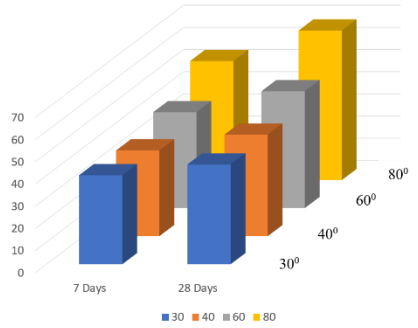

Fig. 12 Variation of Failure Strength with Curing Temperature and curing period, for Pc= 10MPa.

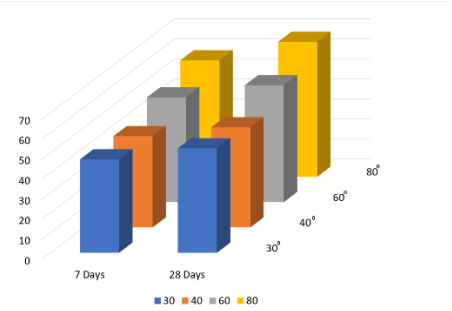

Fig. 13 Variation of Failure Strength with Curing Temperature and curing period, for Pc= 25MPa.

6 CONCLUSIONS

The study was conducted to investigate the effect of temperature on the tri-axial mechanical behaviour of blended fly ash-rice husk ash geopolymer. The experiment involved conducting laboratory tests for four different temperatures (30 °C, 40 °C, 60 °C 80 °C) and two different curing periods (7 days, 28 days) to determine the uniaxial stress-strain behaviour of geopolymer. A numerical model was then developed and validated using the experimental data. The model was used to simulate the triaxial mechanical behaviour of geopolymer under varying levels of confinement (0, 5, 10, 15, 20, 25 MPa).

- The results showed that the unconfined compressive strength (UCS) of geopolymer increased with both curing temperature and curing period. The study also found that the failure strength increased with the level of confinement at a given temperature, due to the reduced permeability and proportionate pore voids that result from the application of confinement.
- The study revealed that the combined effect of temperature and curing period provided excellent mechanical behavior at elevated curing temperatures with active confinements. Therefore, geopolymer could be a suitable replacement for OPC-based well cement in CO2 sequestration wells.
- In conclusion, the study showed that the triaxial mechanical behavior of geopolymer was influenced by both temperature and curing period. The results indicated that the UCS and failure strength of geopolymer increased with the temperature, curing period and with the level of confinement. The findings suggest that geopolymer has the potential to be a reliable and effective alternative to OPC-based well cement in CO2 sequestration

wells, particularly at elevated curing temperatures with active confinements

7 REFERENCES

Balinee, B., Disaanth, P. and Nasvi, M.C.M. (2018). Comparison of Salinity Dependent Mechanical Behaviours of Geopolymer and OPC: An Application to CCS and Oil / Gas Wells. Engineer: Journal of the Institution of Engineers, Sri Lanka, 51(3), p.13. doi:https://doi.org/10.4038/engineer.v51i3.7301.

Bertier, P., Swennen, R., Laenen, B., Lagrou, D., Dreesen, R., 2006. Experimental identification of CO2-water-rock interactions caused by sequestration of CO2 in Westphalian and Buntsandstein sandstones of the Campine Basin (NE Belgium). J. Geochem. Explor. 89, 10e14.

Fernando, S., Nasvi, M.C.M., Gunasekara, C., Law, D.W., Setunge, S. and Dissanayake, R. (2021). Systematic Review on Alkali-Activated Binders Blended with Rice Husk Ash. Journal of Materials in Civil Engineering, 33(9), p.04021229. doi:https://doi.org/10.1061/(asce)mt.1943-5533.0003825.

Lloyd, N. and Rangan, V. (2010). Geopolymer Concrete with Fly Ash. [online] espace.curtin.edu.au. Available at: https://espace.curtin.edu.au/handle/20.500.11937/3540 [Accessed 11 Mar. 2023].

Mo, B., Zhu, H., Cui, X., He, Y. and Gong, S. (2014). Effect of curing temperature on geopolymerization of metakaolin-based geopolymers. Applied Clay Science, [online] 99, pp.144–148. doi:https://doi.org/10.1016/j.clay.2014.06.024.

Nasvi, M.C.M., Ranjith, P.G. and Sanjayan, J. (2013). The permeability of geopolymer at down-hole stress conditions: Application for carbon dioxide sequestration wells. Applied Energy, 102, pp.1391–1398. doi:https://doi.org/10.1016/j.apenergy.2012.09.004.

Nasvi, M.M.C., Gamage, R.P. and Jay, S. (2011). Geopolymer as well cement and the variation of its mechanical behavior with curing temperature. Greenhouse Gases: Science and Technology, 2(1), pp.46–58. doi:https://doi.org/10.1002/ghg.39.

Sindhunata, van Deventer, J.S.J., Lukey, G.C. and Xu, H. (2006). Effect of Curing Temperature and Silicate Concentration on Fly-Ash-Based Geopolymerization. Industrial & Engineering Chemistry Research, 45(10), pp.3559–3568. doi:https://doi.org/10.1021/ie051251p.

Subaha, A., Aarany, V. and Nasvi, M.C.M. (2017). The Combined Effect of Temperature and Salinity on the Mechanical Behaviour of Well Cement. Engineer: Journal of the Institution of Engineers, Sri Lanka, 50(1), p.1. doi:https://doi.org/10.4038/engineer.v50i1.7239.

Comparison of shear strength parameters of jointed rocks

M.P.M.G.L.S. Bandara, L.T. Nanayakkara and A.M.R.G. Athapaththu
Department of Civil Engineering, University of Peradeniya, Sri Lanka

ABSTRACT: Assessing the shear strength parameters of jointed rock masses is crucial for geotechnical projects, including slope stability, foundations, underground caverns, and tunnels. This study adopted various methods, including rock mass classification systems and empirical equations, to determine the shear strength parameters of jointed rock masses in the central province of Sri Lanka. Results showed that the RMR system and tilt test yielded similar values for the internal friction angles, while the Q system tended to predict slightly higher values. The RMR system and empirical equations proposed by Aydan and Kawamoto (2001) and Sen and Sadagah (2002) were used to determine the cohesion of rock masses. The self-fabricated apparatus for the tilt test and Barton comb profiler were used in this research and it has created a good background for future researchers in this geotechnical field. However, this study had limitations, such as a small sample size and a focus on metamorphic rocks in the central province of Sri Lanka.

KEYWORDS: Geotechnical engineering, Jointed rock masses, Shear strength parameters, Sri Lanka

1 INTRODUCTION

The shear strength of jointed rock masses is a critical factor that is taken into consideration in the design of engineering constructions such as slope stability, foundations, underground caverns, and tunnels. A more thorough understanding of the shear strength response of jointed rock masses can lead to more realistic approaches to design being developed. While large-scale testing is the most accurate method for determining shear strength parameters, it is both time and expense-intensive and is therefore not always practical. As a result, rock mass classification systems and empirical formulas are often used as alternatives. In this study, a comparison is made between the shear strength parameters determined by rock mass classification and empirical relationships in order to determine which method is more appropriate for estimating the shear strength response of jointed metamorphic rocks in Sri Lanka.

The shear strength parameters of jointed rock masses can be determined using a variety of approaches, including large-scale testing, back-calculation, rock mass classification systems, and empirical criterion. Large-scale testing, which requires a lengthy set of laboratory experiments, is both time and expense-intensive, therefore rock mass classification systems and empirical formulas are the best alternatives. The widely distributed rocks in Sri Lanka are high-grade metamorphic rocks. Comparison between the shear strength parameters determined by rock mass classifications and empirical relationships has a significant effect on the analysis and design of the civil engineering constructions to select more appropriate methods to estimate the shear strength response of jointed metamorphic rocks. Researchers, geotechnical engineers, and geologists have proposed empirical equations to characterize the shear strength response of rocks. Coulomb (1773) introduced a shear strength model for rock materials that vary with the normal stress, friction angle(Φ), and cohesion(c). Patton (1966) concluded that surface roughness has a significant impact on the shear strength of discontinuity surfaces and developed an empirical formula to describe the shear strength response of the discontinuity surface. Barton (1973) proposed an empirical relationship to estimate the peak friction angle by incorporating the surface roughness parameter and the joint wall strength as a function of the normal stress. Ghani Rafek et al. (2012) have established a polynomial equation to estimate peak friction angles of fresh and slightly weathered Schist and Granite. In addition to the empirical equations mentioned above, rock mass classification systems such as Rock Mass Rating (RMR) by Bieniawski (1973), Q-system (Barton et al.,1974), and Slope Stability Probability Classification (SSPC) by Hack (1998) are another approaches to estimate the shear strength parameters of jointed rock masses.

2 MATERIALS AND METHOD

In this study, rock slopes were selected in hilly terrain, in Sri Lanka. The selection of the locations was done considering the disparity in geological characteristics, lithology, and degree of weathering. 10 rock slopes were selected along B492- Mahaweli Raja Mawatha. Fig. 1 shows the study area for this study.

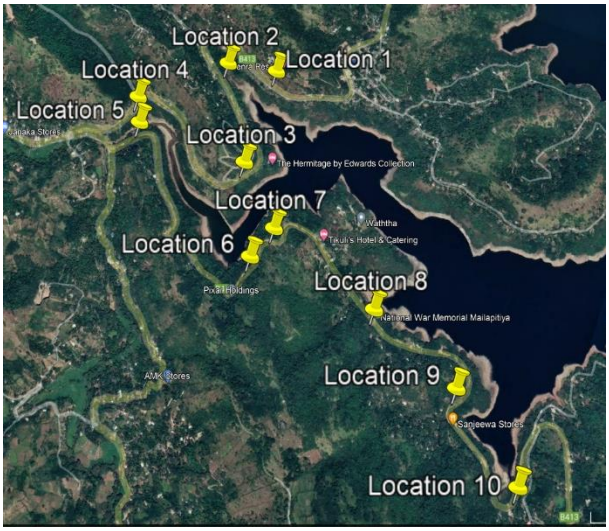

Fig. 1 Study area

The methodology of this study can be interpreted under main 3 phases. Under phase 1 of the methodology, suitable empirical equations, and rock mass classification systems to conduct this study was selected from the available literature works. Identifying the shear strength parameters used in selected approaches and searching for the available methods to determine was carried out under phase 2. Collecting of required data from visual inspection and in-situ tests at selected 10 different sites was conducted under phase 3.

The rebound hammer test, direct measurements in the field, and visual inspection were the methods used in this study to collect the required data from the 10 selected sites. In addition, rock blocks containing natural discontinuity planes were collected from the different test sites and carefully separated into two blocks (upper and lower blocks) along the natural discontinuities. The surface roughness of these planes was measured using a self-fabricated comb profiler. Fig. 2 shows the self-fabricated Barton's comb profiler used in this study.

Fig. 2 Self-fabricated 15cm Barton's comb profiler

Self-fabricated tilt test apparatus was used to determine the peak friction angle of samples with a single common discontinuity. Self-fabricated apparatus consists of a tilting table, four-foot screws, and a hand-operating device to control and maintain the angle of tilt. Fig 3. Shows using self-fabricated tilt testing apparatus to determine the peak friction angles of rock samples.

Fig. 3 Self-fabricated tilt test apparatus to determine the peak friction angle.

Collected samples were cut and prepared to get square or rectangular shapes that satisfy the ISRM testing procedure and dimensions. Samples were cut in the laboratory with a 60cm diameter, diamond-tipped, water-lubricated saw. Samples were cut into rectangular/square samples which satisfy the length-to-thickness ratio and width-to-thickness ratio. Recommended minimum length-to-thickness

ratio and width-to-thickness ratio are 6 and 4. (Alejano et al.,2018). Self-fabricated hand-operating tilt testing apparatus, modelled after Priest (1993) was employed to measure the peak friction angle of these joint planes. The rock blocks containing upper and lower blocks were positioned in the tilt testing apparatus. The rock blocks were inclined from a horizontal position until the upper block slides and the angle of inclination was measured with a clinometer. The tilting operation was performed carefully with a slower rate between 5° – 10°/min. The tilt test was conducted four times for each sample to reduce possible errors during inclination measurements.

Data required to determine the shear strength parameters using rock mass classification systems were collected during the field visits to the selected 10 sites. Weathering grades of rocks and joint surfaces were identified through expert guidance and visual inspection. Spacing of discontinuities, Discontinuity length (Persistence), Separation (Aperture), and Average Joint Spacing was measured and recorded at the sites in prepared data collection sheets. Fig. 4 shows the direct measurements and visual inspection at a selected site.

Fig. 4 Direct measurements and visual inspection at a selected site

3 RESULTS AND DISCUSSION

In this study, various methods were used to determine the shear strength parameters of jointed rock masses in the central province of Sri Lanka. The methods included the RMR system, Q system, empirical equations, and tilt test.

Following empirical equations were used in this study to calculate the shear strength parameters of jointed rocks.

$$\phi_m = \tan^{-1}\left(\frac{J_r}{J_a} J_w\right) \quad (01)$$

$$\phi_m = 20\,\sigma_{cm}^{0.25} \quad (02)$$

$$\phi_m = 20 + 0.5RMR \quad (03)$$

$$\phi_m = 25(1 + 0.001RMR) \quad (04)$$

$$\varphi_m = 1.5\,RMR \quad (05)$$

$$\phi_r = \left(\phi_b - 20^\circ\right) + 20^\circ\left(\frac{r}{R}\right) \quad (06)$$

$$C_m = \left(\frac{RQD}{J_n}\right)\left(\frac{1}{SRF}\right)\left(\frac{\sigma_{ci}}{100}\right) \quad (07)$$

$$C_m = 3.65\,RMR \quad (08)$$

Where,

C_m is the Cohesion of The Undisturbed Rock Mass

Φ_m is the Friction Angle of The Mass

Φ_r is the Residual Friction Angle of The Mass

Φ_b is the Basic friction angle

RQD is the Rock Quality Designation

J_n is the Joint Set Number

J_r is the Joint Roughness Number

J_a is the Joint Alteration Number

J_w is the Joint Water Reduction Factor

σ_{ci} is the Uniaxial Compressive Strength of Intact Rock Material

SRF is the Stress Reduction Factor

R is the Schmidt rebound number for wet, weathered fracture surfaces

r is the Schmidt rebound number on dry, weathered sawn surfaces

Table 1. Internal friction angles of jointed rock masses determined selected methods for the 10 locations

Site	Joint Set	RMR System Φ_m (^{0})	Eq (1) Φ_m (^{0})	Eq (2) Φ_m (^{0})	Eq (3) Φ_m (^{0})	Eq 4&5 Φ_m (^{0})	Eq (6) Φ_m (^{0})	Tilt test Φ_m (^{0})	Avg Φ_m (^{0})
1	J1	35-45	52.9	60.8	56.5	43.3	38.7	35.0	40
	J2	35-45	41.3		55.0	42.5		43.0	
	J3	35-45	52.9		53.5	41.8		42.6	
2	J1	35-45	52.9	39.7	53.5	43.0	36.2	38.0	37
	J2	35-45	52.9		53.5	43.0		36.0	
3	J1	35-45	44.7	51.5	54.0	42.0	38.4	36.6	40
	J2	35-45	44.7		54.0	42.0		43.0	
4	J1	35-45	45.0	57.4	52.0	40.3	37.8	39.4	40
	J2	35-45	45.0		53.5	41.0		41.0	
5	J1	35-45	33.4	44.0	52.0	41.0	33.5	36.2	35
	J2	35-45	33.4		55.5	42.8		33.4	
6	J1	35-45	44.7	37.2	57.0	43.5	36.6	39.8	40
	J2	35-45	33.4		51.0	40.5		40.2	
7	J1	35-45	33.4	48.1	50.5	40.3	39.4	40.4	41
	J2	35-45	33.4		50.5	40.3		40.6	
8	J1	35-45	56.3	48.6	50.0	40.0	37.5	35.2	36
	J2	35-45	45.0		51.5	40.8		35.8	
9	J1	35-45	36.9	47.0	53.0	41.5	39.8	39.8	39
	J2	35-45	36.9		52.0	41.0		37.4	
10	J1	35-45	52.9	54.3	56.0	43.0	37.1	38.4	37
	J2	35-45	52.9		56.0	43.0		35.8	

Table 2. Cohesion values were determined using selected methods for the 10 locations.

Location	RMR system C_m (MPa)	Eq. (08) C_m (MPa)	Eq.(07) C_m (MPa)
1	0.3-0.4	0.27	1.77
	0.3-0.4	0.26	
	0.3-0.4	0.24	
2	0.3-0.4	0.24	0.85
	0.3-0.4	0.24	
3	0.3-0.4	0.25	4.22
	0.3-0.4	0.25	
4	0.3-0.4	0.23	1.95
	0.3-0.4	0.24	
5	0.3-0.4	0.23	1.79
	0.3-0.4	0.26	
6	0.3-0.4	0.27	0.74
	0.3-0.4	0.23	
7	0.3-0.4	0.22	3.28
	0.3-0.4	0.22	
8	0.3-0.4	0.22	3.40
	0.3-0.4	0.23	
9	0.3-0.4	0.24	1.06
	0.3-0.4	0.23	
10	0.3-0.4	0.26	5.35
	0.3-0.4	0.26	

Table 1 shows the Internal friction angles of jointed rock masses determined by selected methods for the 10 locations. The RMR system was used to predict the friction angles of the rock masses, with a range of values between 35-45 degrees for all joint sets. The Q system was used to determine the friction angles, which ranged from 33.4-63.4 degrees for different joint sets. Additionally, the Q system was used to determine the residual friction angle, which ranged from 45.0 - 63.4 degrees for different joint sets.

Empirical equations were also used to determine the friction angles of the rock masses. The first equation, proposed by Aydan et. al (1993), and the second equation proposed by Aydan and Kawamoto, are shown as empirical equations 1 and 2 in Table 1. The results obtained from the tilt test are also presented in Table 1 as tilt test.

Table 2 shows cohesion values of jointed rock masses were also determined using various methods. The RMR system was used to predict the cohesion values, which range from 0.3-0.4 MPa for all joint sets. An empirical equation proposed by Aydan and Kawamoto (2001) was used to determine the cohesion values. Another empirical equation suggested by Sen and Sadagah (2002) was also used to determine the cohesion values, which range from 0.22-0.27 MPa.It is important to note that this study had several limitations. The study was limited to metamorphic rocks in the central province of Sri Lanka and no chemical or mineralogical testing was conducted. Additionally, the sample size for the study was small, with only 10 locations being analyzed. These limitations should be taken into consideration when interpreting the results of the study.

In summary, the methods used in this study include the RMR system, Q system, empirical equations, and tilt test to determine the shear strength parameters of jointed rock masses in the central province of Sri Lanka. The results obtained from these methods are presented in Table 1, which includes the friction angles for the 10 locations

analyzed. However, it is important to note that this study had several limitations and further research is needed to fully understand the shear strength parameters of rock masses in other regions and types of rocks.

A comparison of the results obtained from the different methods shows that the Q system and the empirical equations proposed by Aydan et. al (1993) and Aydan and Kawamoto generally predict similar values for the friction angles of the rock masses. The RMR system and tilt test, on the other hand, tend to predict slightly lower values. For example, the friction angles obtained from the RMR system predict a range of values between 35-45 degrees for all joint sets, while the friction angles obtained from the Q system range from 33.4-63.4 degrees for different joint sets. The empirical equations proposed by Aydan et. al (1993) and Aydan and Kawamoto also predict similar values for the friction angles, with values ranging from 39.7-60.8 degrees and 53.5-57.0 degrees respectively. The tilt test results also predict lower values, with values ranging from 34.8-40.5 degrees.

The above comparison of results shows that there are variations in the values obtained from the different methods. These variations could be due to the limitations of the study, such as the small sample size and the focus on metamorphic rocks in the central province of Sri Lanka. However, further research is needed to fully understand the variations in the values obtained from the different methods and to determine the applicability of these methods in other regions and types of rocks.

A comparison of the cohesion values obtained from the RMR system and the empirical equations proposed by Aydan and Kawamoto (2001) and Sen and Sadagah (2002) is presented in Table 2. The RMR system predicts cohesion values in the range of 0.3-0.4 MPa for all joint sets. On the other hand, the empirical equation proposed by Aydan and Kawamoto (2001) predicts cohesion values in the range of 0.74 - 4.22 MPa. The empirical equation proposed by Sen and Sadagah (2002) predicts cohesion values in the range of 0.22-0.27 MPa.The comparison of the cohesion values obtained from the different methods shows that there are significant variations in the values predicted by the RMR system, the empirical equation proposed by Aydan and Kawamoto (2001) and the empirical equation proposed by Sen and Sadagah (2002). The RMR system predicts much lower cohesion values compared to the other two methods. The empirical equation proposed by Aydan and Kawamoto (2001) predicts relatively higher values of cohesion compared to the other two methods. The empirical equation proposed by Sen and Sadagah (2002) predicts values that are relatively similar to the values predicted by the RMR system. It is important to note that these variations in the cohesion values predicted by the different methods may be due to the different assumptions and simplifications made in each method. Additionally, the limitations of the study, such as the limited sample size and the lack of chemical and mineralogical testing, may also contribute to the variations in the results. Despite these variations, the results of this study provide valuable insights into the cohesion values of jointed rock masses in the central province of Sri Lanka. The results suggest that further research is needed to better understand the cohesion values of rock masses in other regions and types of rocks, as well as the potential benefits of incorporating chemical and mineralogical testing in future studies.

4 CONCLUSIONS

The objective of this study was to determine the shear strength parameters of jointed rock masses in the central province of Sri Lanka using rock mass classification systems and empirical equations. The RMR system, Q system, empirical equations, and tilt test were used to determine the internal friction angles and cohesion values for the 10 selected locations.

The results of this study show that the RMR system, empirical equations, and tilt test give comparable and reasonable results for the shear strength parameters of jointed rock masses in the selected area. The RMR system and the empirical equations, which are based on the RMR system, take into account the geometrical properties of the rock mass, which is an important factor in determining the shear strength parameters. The Q system, on the other hand, does not take into account the geometrical properties of the rock mass and may not be as appropriate for estimating the shear strength response of jointed metamorphic rocks in Sri Lanka.

5 RECOMMENDATIONS

To further improve the understanding of the shear strength parameters of jointed rock masses in Sri Lanka, it is recommended that: Future studies include a larger sample size and a wider range of rock types to ensure more comprehensive results. Chemical and mineralogical testing should be conducted to better understand the properties of the rock masses. The self-fabricated tilt test apparatus and Barton comb profiler developed in this study can be used as a starting point for future researchers in the geotechnical field.

It is important to acknowledge that the limitations in the methodology adopted and the data obtained and analyzed have an impact on the conclusions drawn from this study. However, the results obtained in this study provide a good starting point for future research on the shear strength parameters of jointed rock masses in Sri Lanka.

ACKNOWLEDGMENTS

We are thankful to Dr. S.K. Navaratnarajah, Senior lecturer, Department of Civil Engineering, University of Peradeniya, and Dr. M.C.M Nasvi, Senior lecturer, Department of Civil Engineering, University of Peradeniya for assessing our progress and for the comments to improve our project.

REFERENCES

Aydan, Akagi, T. and Kawamoto, T. (1993). The squeezing potential of rocks around tunnels; Theory and prediction. *Rock Mechanics and Rock Engineering*, 26(2), pp.137–163. doi:https://doi.org/10.1007/bf01023620.

Aydan, Ö., Ulusay, R. and Tokashiki, N. (2013). A New Rock Mass Quality Rating System: Rock Mass Quality Rating (RMQR) and Its Application to the Estimation of Geomechanical Characteristics of Rock Masses. *Rock Mechanics and Rock Engineering*, 47(4), pp.1255–1276. doi:https://doi.org/10.1007/s00603-013-0462-z.

Barton, N. (2002). Some new Q-value correlations to assist in site characterisation and tunnel design. *International Journal of Rock Mechanics and Mining Sciences*, 39(2), pp.185–216. doi:10.1016/s1365-1609(02)00011-4.

Barton, N. (2013). Shear strength criteria for rock, rock joints, rockfill and rock masses: Problems and some solutions. *Journal of Rock Mechanics and Geotechnical Engineering*, 5(4), pp.249–261. doi:10.1016/j.jrmge.2013.05.00

Bhasin, R. and Grimstad, E. (1996). The use of stress-strength relationships in the assessment of tunnel stability. *Tunnelling and Underground Space Technology*, 11(1), pp.93–98. doi:10.1016/0886-7798(95)00047-x.

Bieniawski, Z.T. (1978). Determining rock mass deformability: experience from case histories. *International Journal of Rock Mechanics and Mining Sciences & Geomechanics Abstracts*, 15(5), pp.237–247. doi:10.1016/0148-9062(78)90956-7.

Ghani, R.A., Goh, T.L., Hariri, A.M. and Baizura, Y.N. (2011). Field and Laboratory-based Approach for the Determination of Friction Angle of Geological Discontinuities of Malaysian Granites. *ASEAN Journal on Science and Technology for Development*, 28(2), p.151. doi:10.29037/ajstd.41.

Gokceoglu, C., Sonmez, H. and Kayabasi, A. (2003). Predicting the deformation moduli of rock masses. *International Journal of Rock Mechanics and Mining Sciences*, 40(5), pp.701–710. doi:10.1016/s1365-1609(03)00062-5.

International society for rock mechanics commission on standardization of laboratory and field tests. (1978). *International Journal of Rock Mechanics and Mining Sciences & Geomechanics Abstracts*, 15(6), pp.319–368. doi:10.1016/0148-9062(78)91472-9.

Kayabasi, A., Gokceoglu, C. and Ercanoglu, M. (2003). Estimating the deformation modulus of rock masses: a comparative study. *International Journal of Rock Mechanics and Mining Sciences*, 40(1), pp.55–63. doi:10.1016/s1365-1609(02)00112-0.

Palmström, A. and Singh, R. (2001). The deformation modulus of rock masses — comparisons between in situ tests and indirect estimates. *Tunnelling and Underground Space Technology*, 16(2), pp.115–131. doi:10.1016/s0886-7798(01)00038-4.

Prassetyo, S.H., Gutierrez, M. and Barton, N. (2017). Nonlinear shear behavior of rock joints using a linearized implementation of the Barton–Bandis model. *Journal of Rock Mechanics and Geotechnical Engineering*, 9(4), pp.671–682. doi:10.1016/j.jrmge.2017.01.006.

Priest, S.D. and Hudson, J.A. (1976). Discontinuity spacings in rock. *International Journal of Rock Mechanics and Mining Sciences & Geomechanics Abstracts*, 13(5), pp.135–148. doi:https://doi.org/10.1016/0148-9062(76)90818-4.

Şen, Z. and Sadagah, B.H. (2002). *Mathematical Geology*, 34(7), pp.845–855. doi:https://doi.org/10.1023/a:1020928727867.

Serasa, A.S., Goh, T.L., Rafek, A.G., Hussin, A., Lee, K.E. and Mohamed, T.R. (2017). *Peak friction angle estimation from joint roughness coefficient of discontinuities of limestone in peninsular Malaysia. Sains Malaysiana*, [online] 46(2), pp.181–188. doi:10.17576/jsm-2017-4602-01.

Single, B., Goel, R.K., Mehrotra, V.K., Garg, S.K. and Allu, M.R. (1998). Effect of intermediate principal stress on strength of anisotropic rock mass. *Tunnelling and Underground Space Technology*, 13(1), pp.71–79. doi:10.1016/s0886-7798(98)00023-6.

Stability analysis of road embankment constructed by treating marginal soils with geopolymer based stabilizers.

S. Selvarajah, T. Sooriyakumar and M.C.M Nasvi

Department of Civil Engineering, University of Peradeniya, Sri Lanka

ABSTRACT: This study aims to analyse the stability of the embankment constructed using marginal embankment materials treated with fly ash based geopolymers (FA-GP). Under experimental work, fly ash based geopolymer stabilized soil (FA-GP-SS) was prepared by mixing marginal soil with 30% of geopolymer paste, 8M NaOH when ratio of Na_2SiO_3/ NaOH were 2.5. For fly ash-rice husk ask based geopolymer stabilized soil (FA-RHA-GP-SS), 60% of fly ash was replaced by rice husk ash. Series of experiments were conducted to obtain the engineering properties of raw soil and stabilized soil. Under numerical study, PLAXIS 2D and GeoStudio were used to simulate the slope stability of the embankment at different height (4 m, 6 m, and 8 m) and slope (30^0, 45^0,60^0 and 75^0). Based on findings, Factor of safety (FOS) values obtained from PLAXIS 2D and Slope/W software were consistent. The FOS values of the embankment constructed using stabilised mixes (FA-GP-SS and FA-RHA-GP-SS) were higher than the FOA values of the embankment constructed using raw soil. Of the two stabilised mixes, FA-GP-SS performs better compared to FA-RHA-GP-SS. On the whole, geopolymer based stabilisers can be used to enhance the marginal soils for embankment construction.

KEY WORDS: Embankment, Fly ash, Rice husk ash, Stabilized soil.

1 INTRODUCTION

Embankments are among the most ancient forms of civil engineering structures but are still among the most relevant ones. They are widely used in road construction. Embankment used in Sri Lanka should meet the specification provided in RDA guide (ICTAD SCA/5 (2009)**.** There is a shortage in suitable embankment materials in vicinity of the construction site, and as a result, good quality embankment materials are hauled from long distances with high cost. Treating the marginal soils in the vicinity of the project site is one of the best options to reduce the energy, time and cost related to the long hauling distances. Marginal soil can be stabilized to modify the soil engineering properties by various means including mechanical, chemical or biological means. Chemical soil stabilization is becoming increasingly popular method for improving the engineering properties of soil. Additionally, chemical stabilization is often cost-effective compared to other methods. Cement and lime are commonly used stabilizers.

Power generation produces large amount of FA and become available as by product of coal-based power station. Soil stabilization with RHA is mostly recommended method for rice-producing regions where RHA is accessible at low cost. Muntohar, (2009) concluded that lack of cementitious properties of RHA doesn't allow it to be used solely in the soil stabilization. Geopolymer is a type of inorganic polymer which can be produced from a variety of raw materials such as fly ash, slag, clay, and other industrial by-products. It is commonly made of alkali-activated aluminosilicate materials and produce low CO_2 emission and energy consumption. In addition to all the positive environmental effects, geopolymers also provide good mechanical performances in some applications. Mixing of geopolymer within the soil matrix promotes enhanced unconfined compressive strength (Phummiphan et al., 2016).

There are limited studies focusing on the stability analysis of embankments constructed by treating marginal embankment materials with GP based stabilizers (Fly ash based geopolymer stabilized soil (FA-GP-SS) and Flyash-Rice husk ash based geopolymer stabilized soil (FA-RHA-GP-SS)). In this research, feasibility of using FA-GP and FA-RHA-GP to stabilize embankment material, which is not suitable at its natural condition, were analysed. This study contains experimental and numerical works. Slope stability of embankment was analysed using PLAXIS 2D and GeoStudio in numerical study.

2 MATERIALS

Undisturbed and disturbed two different marginal soil samples which do not satisfy the RDA requirement for the embankment material was collected at two locations from the borrow pit of the iRoad project area, Naula, Sri Lanka. Table 1 shows liquid limit (LL), plastic limit (PL), maximum dry density (MDD) and 4 days soaked CBR at 95% MDD(CBR_4days) for Location 1 and 2 (L1 and L2) comparing with RDA requirement.

Table 1: Properties of L1 and 2 comparing with RDA requirement.

Property	**RDA requirement**		**L1**	**L2**
	Type I	Type II		
LL **(%)**	≤50	≤55	50.5	39.8
PL **(%)**	≤25	≤25	23	28
MDD **(kg/m^3)**	≥1600	≥1500	1906	1785
CBR_4days **(modified) (%)**	≥7	≥5	1	2

Type of FA used for our project is ASTM class F FA and it was collected from Lakvijaya coal power plant, Norochcholai, Sri Lanka. Rice husk ash samples were collected from the rice mills in Divulapitiya, Negombo, Sri Lanka.

3 METHODOLOGY

3.1Experimental work

Particle size analysis (BS 1377 -2:1990), Atterberg limit test(BS 1377 -2:1990), Modified proctor compaction test(BS 1377 -4:1990),)Unconfined compressive strength (UCS)test (BS 1377 -7:1990), California bearing ratio (CBR)test(BS 1377 -4:1990), Falling head permeability test(BS 1377 -5:1990) and Triaxial test(BS 1377 -8:1990) were conducted to determine the index properties of raw soil obtained from two locations.

PL of L2 and CBR value of both locations did not meet RDA requirement according to the Table 1. L2 was selected as critical soil for stabilization.

It has been found that 30% geopolymer paste, 8M NaOH, 2.5 Na_2SiO_3/NaOH and 2 FA/Alkali activators are the optimum composition of FA-GP mix (Arul et al., (2016); Mustafa et al., (2013); Dungca et al., (2017)). It has also been found that replacement of 60% FA by RHA reflects higher strength (Poltue et al., 2019; Dungca and Ephrem, 2017). FA-GP-SS and FA-RHA-GP-SS were prepared in proportion mentioned above. Cohesion and friction angle values of raw soil, FA-GP-SS and FA-RHA-GP-SS were obtained from relevant literature (Kumar et al., 2014; Raj et al., 2016) and other geotechnical properties of two stabilizer system were determined from a series of experiments.

3.2 Numerical study

Embankment section was adopted from the literature (Khan and Abbas, 2014) as shown in Fig. 1. Model geometry used in GeoStudio and PLAXIS 2D are shown in Fig 2 and 3.

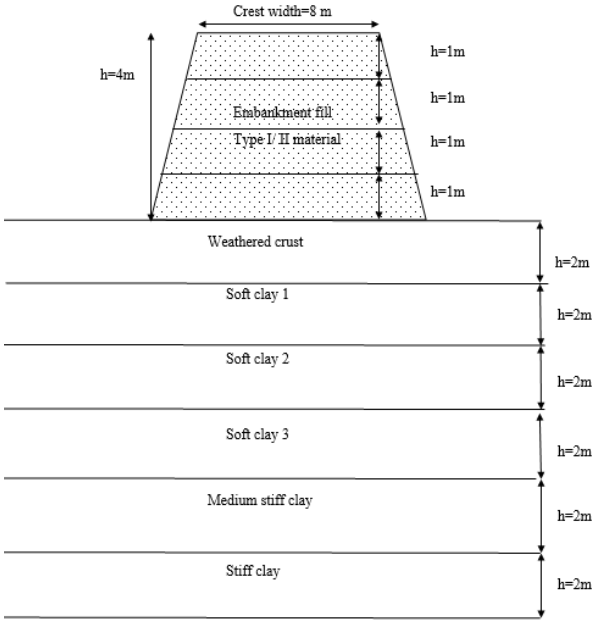

Fig. 1: Embankment section with 4 m height and 30^0 slope.

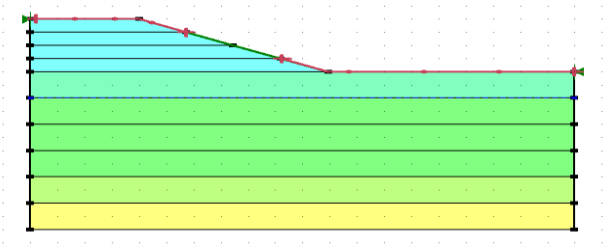

Fig 2: Model geometry used in GeoStudio.

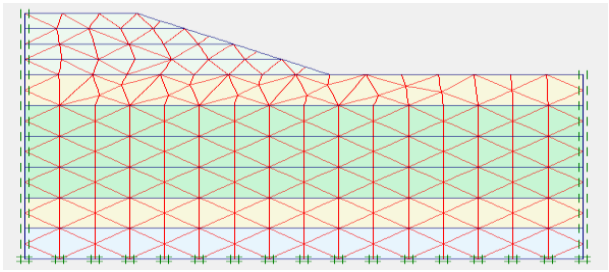

Fig 3: Model geometry used in PLAXIS 2D

Embankment with 30^0 slope and 4 m height was considered in preliminary analysis. A parametric study was conducted by changing the embankment height and slope angle and the corresponding factor of safety (FOS) values were obtained from Slope/W software and PLAXIS 2D software. Height of the embankment were changed to 6m, 8m and 10m. For each height, Slope angle was modified as 45^0 60^0 and 75^0. For the numerical study, subsoil properties obtained from literature (Chaiaput et al.,2012) is shown in Table 2.

Table 2: Properties of subsoil layer

	Weathered crust	Soft clay 1	Soft clay 2	Soft clay 3	Medium stiff clay	Stiff clay
Model	MCM	SSM	SSM	SSM	MCM	MCM
Material behavior	Undrained	Undrained	Undrained	Undrained	Undrained	Undrained
γsat (kN/m³)	17	15	15	15	17	19
γdry (kN/m³)	15	13	13	13	15	17
E (kN/m²)	3000				5000	9000
kx (m/day)	0.002	0.0008	0.0008	0.0008	0.0004	0.004
Ky (m/day)	0.001	0.0004	0.0004	0.0004	0.0002	0.002
c (kN/m²)	10	3	3	3	10	30
Φ (degree)	23	23	23	23	25	26
ν	0.25				0.25	0.25
λ *		0.14	0.14	0.14		
K *		0.028	0.028	0.028		
OCR		1.55	1.4	1.3		

In Slope/W, stability was checked using ordinary method (OM), bishop simplified method (BSM), Jambu simplified method (JSM), spencer simplified method (SSM) and mogernstern price method (M-PM). PLAXIS 2D 8.6 software was utilized to conduct the Finite Element Method (FEM) analysis. FOS was determined using the phi-c reduction method in PLAXIS 2D.

4. RESULTS AND DISCUSSION

4.1 Experimental results

Atterberg limit values of raw soil, FA-GP-SS and FA-RHA-GP-SS are shown in Table 3. Plasticity characteristics of the soil decreases with addition of FA-GP. The decrease in LL is attributed to the increase in water holding capacity and indicates the increase in shearing strength. Increase in the soil workability may be the reason for variation in PI (Jafer et al.,2017).

Compaction curves for raw soil, FA-GP-SS and FA-RHA-GP-SS are shown in Fig. 4. MDD decreases with addition of FA-GP due to presence of carbon content and lower specific gravity. Increase in OMC illustrates the need of hydration reaction for cementitious FA and to release the capillary tension from the greater expose surface of the finer FA particle. When 60% of FA is replaced by RHA, MDD decreases further due to comparatively low specific gravity. As RHA has finer particles, more surface area needs more water content to provide well lubrication. Pozzolanic reaction of RHA-GP also attributes increase in OMC (Sarkar et al.,2015).

Table 3: Atterberg limits values

Property	**Raw soil**	**FA-GP-SS**	**FA-RHA-GP-SS**
LL (%)	39.8	32.6	27.5
PL (%)	28	24.5	22.5
PI	11.8	8.1	5

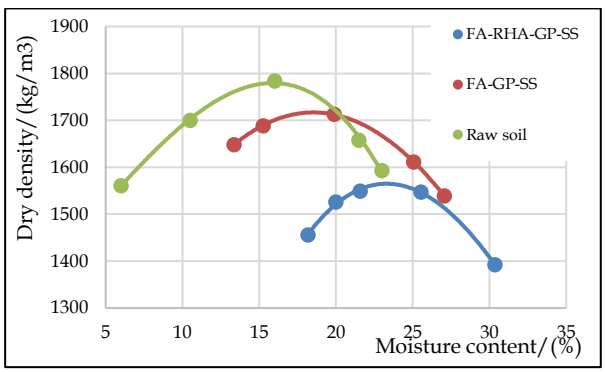

Fig. 4: Compaction test results

The 4days soaked CBR values at 95% MDD of the soil were significantly improved with the

addition of FA-GP as well as with the incorporation of RHA, resulting in CBR values of 8 and 7, respectively, compared to the raw soil which had a CBR value of 2. These results shows that addition of FA-GP the CBR value, possibly due to cation exchange in the soil mix, which results in the replacement of sodium ions with calcium ions in the fly ash. This exchange reduces soil settlement, thereby increasing the CBR value (Rajak and Sujitkumar pal, 2015). Formation of cementitious compounds between the RHA and CaO contained in the soil may increase CBR in FA-RHA-GP-SS. Furthermore, the CBR value of the soil with the FA-RHA-GP-SS mix is lower than that of the FA-GP-SS mix, but it is still higher than that of the raw soil.

Average Unconfined Compressive Strength (UCS) values for FA-GP-SS and FA-RHA-GP-SS were 1523 kPa and 1103 kPa, respectively. Whereas average CBR for raw soil was 259kPa as shown in Fig. 5. As FA contains high silica and alumina content, it forms silica and alumina hydrates which develops the strength in the geopolymerization. The addition of FA-GP without replacement of RHA resulted in a higher compressive strength value compared FA-RHA-GP-SS.

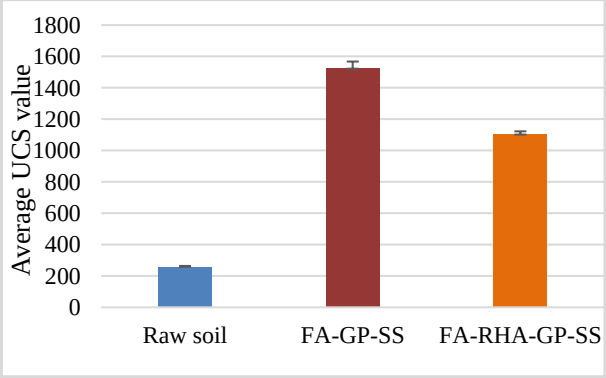

Fig. 5: Average UCS values

When FA-GP and FA-RHA-GP were added to raw soil, permeability decreases as shown in Fig. 6. Pozzolanic material (FA and RHA) tends to absorb the vacant space in the pore composition and significantly cuts down the permeability. Increase in cementitious content may also be a reason for decline in permeability.

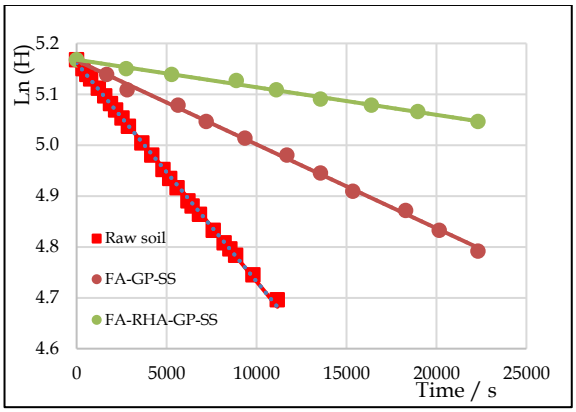

Fig. 6: Permeability curves

FA-GP-SS and FA-RHA-GP-SS resulted in Type I materials, as per the RDA requirement. Hence, constructing a homogeneous embankment using either FA-GP-SS or FA-RHA-GP-SS mixtures would be feasible.

4.2 Numerical results

4.2.1 Slope/W results

Critical slip surface for raw soil at height of 4 m and slope of 30^0 is shown in Fig. 7. The MPM method covers both force and moment requirements of the static equilibrium. That's why it is extensively used in slope stability evaluation. MPM was selected as the best method for comparison of Factor of Safety (FOS) values with PLAXIS 2D results (Ayob et al.,2019).

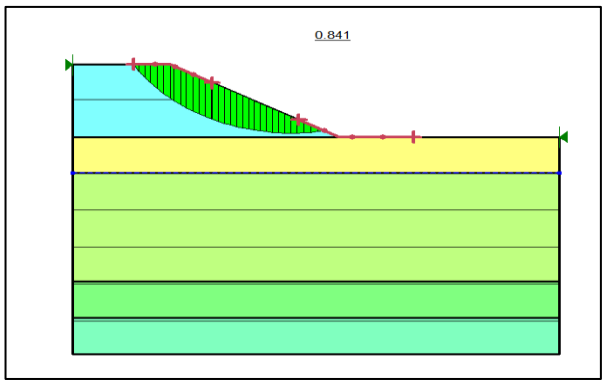

Fig. 7: Critical slip surface for raw soil at height of 4 m and slope of 30^0

4.2.2 PLAXIS 2D results

The deformed mesh and critical slip surface of the embankment with FA-GP-SS (4m height and 30^0 slope) are illustrated in Figs. 8 and 9, respectively. Table 3 presents the FOS values obtained for raw soil, FA-GP-SS, and FA-RHA-GP-SS at a height of

4 m and different angles, as calculated using PLAXIS 2D and Slope/W.

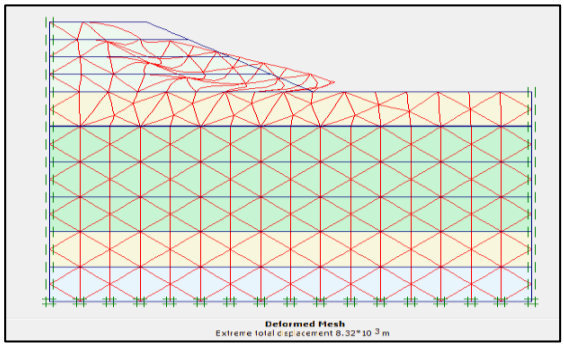

Fig. 8: Deformed mesh for the embankment with FA-GP-SS (4 m height and 30^0 slope)

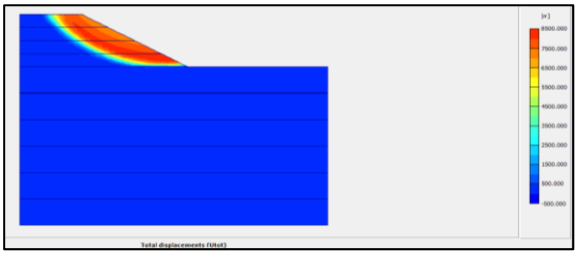

Fig. 9: Critical slip surface for the embankment with FA-GP-SS (4 m height and 30^0 slope)

Table 3: FOS values for raw soil, FA-GP-SS, and FA-RHA-GP-SS at a height of 4 m and different angles.

Slope	**For embankment height of 4 m**		
		Slope/W	PLAXIS
30^0	Raw soil	0.841	0.749
	FA-GP-SS	2.926	2.833
	FA-RHA-GP-SS	2.024	1.927
45^0	Raw soil	0.622	0.524
	FA-GP-SS	2.722	2.629
	FA-RHA-GP-SS	1.822	1.723
60^0	Raw soil	0.522	0.425
	FA-GP-SS	2.622	2.523
	FA-RHA-GP-SS	1.722	1.628
75^0	Raw soil	0.518	0.426
	FA-GP-SS	2.576	2.483
	FA-RHA-GP-SS	1.718	1.623

Table 4: FOS values for raw soil, FA-GP-SS, and FA-RHA-GP-SS at different height and 30^0 slope.

Height	**For embankment height of 30^0**		
		Slope/W	PLAXIS
4 m	Raw soil	0.841	0.749
	FA-GP-SS	2.926	2.833
	FA-RHA-GP-SS	2.024	1.927
6 m	Raw soil	0.716	0.621
	FA-GP-SS	2.816	2.723
	FA-RHA-GP-SS	1.915	1.816
8 m	Raw soil	0.630	0.535
	FA-GP-SS	2.731	2.634
	FA-RHA-GP-SS	1.832	1.737

FOS values obtained from both software were found to be consistent. It was observed that increasing the height and slope resulted in a reduction of FOS for raw soil, FA-GP-SS, and FA-RHA-GP-SS. The slope/W ratio was found to be insufficient in fully considering the stress-strain relationship of the soil. For the analysis of geotechnical problems, Plaxis2D was employed as a powerful and user-friendly finite element package (Ayob et al., 2019).

To compare the strength improvement achieved by both mixes, we considered the PLAXIS results. Based on the FOS values obtained at different height and slopes, it can be concluded that both stabilizer mixes can be used as embankment materials since the FOS values were greater than 1. However, the FA-GP-SS performed better than FA-RHA-GP-SS.

5. CONCLUSION

Experimental and numerical study was conducted to analyse the slope stability of embankments constructed using geopolymer stabilizers, with the aid of GeoStudio and PLAXIS 2D software. During this study, critical soil was identified and used to prepare the FA-GP-SS and FA-RHA-GP-SS. At the initial stages, a series of laboratory experiments were performed, followed by the development and analysis of a numerical model using PLAXIS 2D and Slope/W software. Based on the outcomes of this study, the following conclusions can be drawn.

- The addition of FA-GP and FA-RHA-GP to marginal soil resulted in 3.2% and 9.5% reduction respectively in MDD compared to the raw soil, as both additives have lower

specific gravity. Additionally, a comparison of the raw soil with the FA-GP-SS and FA-RHA-GP-SS revealed that the pozzolanic reaction and higher hydration needs increased the OMC of the two mixes.

- UCS increment for FA-GP-SS and FA-RHA-GP-SS as 488% and 325% respectively with respect to raw soil indicates an improvement in strength. This improvement may be attributed to geopolymerization and the formation of cementitious compounds.
- The CBR values obtained were 8 and 7 for FA-GP-SS and FA-RHA-GP-SS, respectively. It was observed that the addition of both mixes resulted in an increase in the CBR value, which may be attributed to cation exchange in the geopolymer and the formation of cementitious content. In contrast, the raw soil had a CBR value of 2, highlighting the effectiveness of the geopolymer mixes in improving the strength of the soil.
- When compared to the raw soil, a decline in permeability values was observed upon the addition of FA-GP and FA-RHA-GP. This decrease in permeability may be attributed to the formation of cementitious content.
- By comparing the FOS values obtained using PLAXIS 2D and Slope/W, we found that the results were consistent in both software. Furthermore, it was observed that an increase in height and slope led to a reduction in the strength of the raw soil, as well as the FA-GP-SS and FA-RHA-GP-SS mixtures.
- Overall, both the FA-GP-SS and FA-RHA-GP-SS can be utilized in the construction of homogeneous embankments, as indicated by FOS values greater than 1. Range of FOS values at considered height and slope, for FA-GP-SS and FA-RHA-GP-SS are 2-3 and 1-2 respectively. However, it should be noted that FA-GP-SS performed better than the FA-RHA-GP-SS.

6. ACKNOWLEDGEMENT

The successful completion of our research study was made possible by the generous support and assistance of several individuals. Foremost, we are highly indebted to our supervisor Dr. M. C. M. Nasvi for his valuable guidance and constant supervision in progressing this endeavour. Additionally, we would also like to acknowledge the department of civil engineering for providing both the encouragement necessary for conducting the research project and for access to the laboratory facilities. Finally, we extend our heartfelt thanks and appreciation to all the individuals within and outside the faculty who have willingly offered their assistance and expertise.

7. REFERENCES

Ayob, M., Kasa, A., Sulaiman, M.S., Devi, N. (2019). Slope Stability Evaluations Using Limit Equilibrium and Finite Element Methods. International Journal of Advanced Science and Technology, 28(18):27-43

Hassnen Jafer, William Athertonb, Monower Sadiqueb, Felicite Ruddockb and Edward Loffillb. (2017). Stabilisation of soft soil using binary blending of high calc, ium fly ash and palm oil fuel ash

Jonathan R. Dungca and Edward Ephrem T. Codilla. (2017). FLY-ASH-BASED GEOPOLYMER AS STABILIZER FOR SILTY SAND EMBANKMENT MATERIALS. International Journal of GEOMATE, June 2018 Vol.14, Issue 46, pp.143-149

Kumar, D., Kumar, N., Gupta, A. (2014). Geotechnical Properties of Fly Ash and Bottom Ash Mixtures in Different Proportions.International Journal of Science and Research (IJSR) Europe, 3(9):1487-1494.

Muntohar, A.S., (2002). Utilization of Uncontrolled Burnt Rice Husk Ash in Soil Improvement. Civil Engineering Dimension, 4(2):100-105.

Phummiphan, I.; Horpibulsuk, S.; Sukmak, P.; Chinkulkijniwat, A.; Arulrajah, A.; Shen, S.-L. (2016). Stabilisation of marginal lateritic soil using high calcium fly ash-based geopolymer. Road Mater. Pavement Des. 17, 877–891

Rathan Raj R; Banupriya S;Dharani R.(2016). Stabilization of soil using Rice Husk Ash.

S.Chaiput,D.T.Bergado, S.Artidteang.(2012). FEM 2D Numerical simulation reinforced embankment on soft ground by limited life geosynthetics (LLGS).

Teerapruet Poltue; Apichat Suddepong; Suksun Horpibulsuk; Wisanukhon Samingthong; Arul Arulraj and Ahmad Safuan A.Rashid.(2019). Strength development of recycled concrete aggregate stabilized with fly ash-rice husk ash based geopolymer as pavement base material.

Sujit Kumar Pal, Tarun Kumar Rajak, Laxmikant Yadu and Sandeep Kumar Chouksey. (2017). Strength Characteristics of Fly Ash Stabilized Soil Embankment and Stability Analysis UsingNumerical Modelling